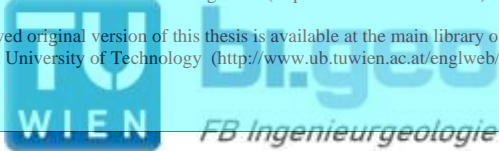


Die approbierte Originalversion dieser Dissertation ist an der Hauptbibliothek der Technischen Universität Wien aufgestellt (<http://www.ub.tuwien.ac.at>).

The approved original version of this thesis is available at the main library of the Vienna University of Technology (<http://www.ub.tuwien.ac.at/englweb/>).



## **Doctoral Thesis**

# **PREDICTION OF TUNNEL BORING MACHINE PERFORMANCE USING MACHINE AND ROCK MASS DATA**

**Submitted in satisfaction of the requirements for the degree of Doctor of Science in Civil  
Engineering of the Vienna University of Technology, Faculty of Civil Engineering**

## **Dissertation**

# **VORHERSAGE DER LEISTUNG VON TUNNELBOHRMASCHINEN MITTELS MASCHINENDATEN UND GEBIRGSPARAMETERN**

**Ausgeführt zum Zwecke der Erlangung des akademischen Grades eines  
Doktors der technischen Wissenschaften  
eingereicht an der Technischen Universität Wien, Fakultät für Bauingenieurwesen  
von**

**Ghulam Dastgir, M.S.  
Matrikelnummer 0827994  
Karlsplatz 13/220-1, A-1040 Wien**

**Gutachter: O.Univ.Prof. Dr. Ewald Tentschert  
E203-Institut für Geotechnik, ForschungsbereichIngenieurgeologie  
Karlsplatz 13/220-1, A-1040 Wien**

**Gutachter: O.Univ.Prof. Dipl.-Ing. Dr.techn. Hans Georg Jodl  
E234 - Institut für interdisziplinäres Bauprozessmanagement  
Karlsplatz 13/234-2, A-1040 Wien**

**Wien, May 2012**

# Dedication

Dedicated to my late parents.

# Acknowledgment

In the name of Allah, the Most Gracious and the Most Merciful, all praises to Allah for the strengths and His blessings in completing this research work. My first and most earnest acknowledgment must go to my first supervisor Prof. Dipl. -Ing. Dr. techn. Rainer Poisel. I cannot forget his very kind response when I was looking for my PhD supervisor. His support, both technical and moral, gave me the courage to complete my higher studies at the Institute of Geotechnical (Department of Engineering Geology) at the Vienna University of Technology (TU Wien). Having difficulty in appropriate words selection for him I can only say that he has been instrumental in ensuring my academic, professional, and moral well being ever since. I would like to express my profound gratitude to my supervisor Prof. Dipl. -Ing. Dr. techn. Ewald Tenschert whose overwhelming help, support and guidance were present throughout my studies. I would like to express my gratitude to honorable O.Univ.Prof. Dipl.-Ing. Dr.techn. Hans Georg Jodl, Institute of Interdisciplinary Construction Process Management of the Vienna University of Technology for his second opinion on my thesis. I am greatly indebted to Univ.Prof. Dipl.-Ing. Dr.techn. Andreas Kolbitsch for his support. The author also pays his thanks to Ao.Univ.Prof. Mag. Dr. Andreas Rohatsch and Assistant Prof. Dipl.-Ing. Dr.techn Alexander Preh, for the provision of technical and software support whenever it was needed during full length of research work. I cannot forget the valuable scientific discussion with Kurt am Tinkhof and Prof. Dr. Rudolf Heuer. I am also deeply grateful to our secretary Christine Cerny and Dipl.-Ing. Victor Navas-Basantes, who remained very helpful and kind throughout my stay here in this institute. I am grateful for the financial support for three years that I have received during my doctoral studies from the Austrian Society for Geo-mechanics (ÖGG) and Higher Education Commission (HEC) of Pakistan for funding my research for last year. I personally honor Prof. Dr. Atta-ur-Rahman, the former Chairman of Higher Education Commission (HEC), for his valuable contributions for the higher education in Pakistan. Last, but far from least, I want to express my deep appreciations for my wife Dr. Qurat ul Ain who managed her PhD work in parallel with the fulfillment of all the responsibilities of our kids and home in an excellent way. I have no words to express my feelings for the contribution from my chubby daughter Sijjal Fatima and lovely son Alyaan Ali for making me smile whenever I fed up.

# Abstract

Performance of the tunnel boring machine (TBM) and its prediction by different methods has been a hot issue since the first TBM was developed. For the sake of safe and sound transport, improvement of hydro-power, mining, for civil and many other tunneling projects, TBMs are quite frequently used. TBM parameters and rock mass properties, which heavily influence machine performance, should be known or estimated before TBM-type is chosen and start of excavation. By applying linear regression analysis, Fuzzy logic tools and a special MATLAB code on actual field data collected from seven TBM driven tunnels (Hieflau expansion tunnel, Queen water tunnel, Vereina, Hemerwald, Maen, Pieve and Varzo tunnel), an attempt was made to provide prediction of rock mass class, rock fracture class, penetration rate and advance rate. For detailed analysis of TBM performance, machine parameters (thrust, machine rpm, torque, power etc.), machine types and specification, rock mass properties (UCS, discontinuity in rock mass, RMC, RFC, RMR, etc.) were analyzed by 3-D surface plotting using the statistical software R. Correlations between machine parameters and rock mass properties, which effectively influence prediction models, are presented as well.

In the Hieflau expansion tunnel advance rate linearly decreases with increase of thrust due to high dependence of machine advance rate upon rock strength. For the Hieflau expansion tunnel three types of data (TBM, rock mass and seismic data, e.g., amplitude, pseudo velocity, etc.) were coupled and simultaneously analyzed by plotting 3-D surfaces. No appreciable correlation between seismic data (amplitude and pseudo velocity), rock mass properties and machine parameters could be found. Tool wear as a function of TBM operational parameters was analyzed, it revealed that tool wear is minimum when applied thrust is moderate and that tool wear is high when thrust is too low or too high. An empirical linear model for advance rate was predicted with a high accuracy. On the other hand, in the Hemerwald tunnel thrust and advance rate have the same correlation as in the Hieflau. A significant correlation between machine parameters and rock mass properties was found. An empirical linear equation with great accuracy was achieved to predict advance rate as a function of different rock mass properties and machine parameters.

After analyzing the data from seven tunnel sites, based on rock strength, fracture class, behavior of thrust versus advance rate, seven case histories have been divided into two major groups. Group one consists of Hieflau, Hemerwald, Maen and Pieve tunnel.

Rock mass strata mainly comprise of Limestone, Schistose-Gneiss, Micaschists and Meta-granite. For group one rock strength ranges from 162-226 MPa, which contains high strength rocks. In this group advance rate decreases linearly with increase of thrust. This is due to very high strength, presence of less joints and very low fracture class. For high strength rocks a prediction model for advance rate may be used with slight variations from case to case. On the other hand, group two comprises Queen water tunnel, Vereina and Varzo tunnel. Rock mass strata mainly consists of Micaschists and Gneiss. Rock strength varies between 55-162 MPa, which is low to medium strength rocks. In group two advance rate linearly increases with increase of TBM thrust. The reason is low rock strength, presence of medium to high frequency of joints and a high rock fracture class. For the low strength rocks, another advance rate prediction model is suggested.

# Kurzfassung

Die Vorhersage der Vortriebsleistung von TBMs ist eine wichtige Fragestellung seit dem Beginn des Einsatzes von TBMs für den kontinuierlichen Vortrieb. Der Einsatz von Tunnelbohrmaschinen gewinnt aufgrund seiner Effizienz gegenüber dem konventionellen Vortrieb auch zunehmend an Bedeutung. Die Maschinendaten und die geotechnischen Gebirgsparameter haben einen signifikanten Einfluss auf die Vortriebsleistung und sollten daher bereits bei der Wahl der TBM, d.h. vor Baubeginn, abgeschätzt werden.

Mit Hilfe der Methode der linearen Regression, der Fuzzy Logic und eines speziell entwickelten Matlab-Programms wurden die gesammelten Daten von sieben Tunnelbohrprojekten (Hieflau, etc.) analysiert und eine Vorhersage der Gebirgszerlegung, der Vortriebsrate sowie der Penetrationsrate versucht. Mit Hilfe der Statistiksoftware „R“ wurde eine detaillierte statistische Analyse und eine Gegenüberstellung der Maschinenparameter (Anpresskraft, Umdrehung, Drehmoment, etc.) und der Gebirgsparameter (einaxiale Druckfestigkeit, des Zerlegungsgrads des Gebirges, etc.) durchgeführt. Es wurden Zusammenhänge zwischen den Maschinendaten und den Gebirgsparametern die für ein Vorhersagemodell entscheidend sind abgeleitet.

Beim Erweiterungsstollen Hieflau sinkt die Vortriebsrate mit Zunahme des Anpressdrucks infolge der hohen Anhängigkeit der Vortriebsrate von der Gesteinsfestigkeit. In Hieflau wurden drei Klassen von Daten miteinander in Beziehung gesetzt und mit Hilfe dreidimensionaler Diagramme (Oberflächen) analysiert: Maschinendaten, Daten zur Beschreibung des Gebirges und seismische Daten.

Dabei wurden keine verwertbaren Zusammenhänge zwischen seismischen Daten (amplitude und pseudogeschwindigkeit), Maschinenparametern und Gebirgsparametern gefunden. Die Analyse des Verschleißes der Meisel, Lager und Hydraulik im Vergleich mit den aufgezeichneten Vortriebsdaten hat gezeigt, dass der Werkzeugverschleiß bei einem moderaten Anpresskraft zu einem Minimum wird und bei einem geringen- oder hohen Anpresskraft der Werkzeugverschleiß ein Maximum erreicht. Die Vortriebsgeschwindigkeit wurde mit Hilfe eines linear empirischen Modells mit hoher Genauigkeit vorhergesagt.

Beim Hemerwald Tunnel wurden zwischen Vortriebsgeschwindigkeit und Anpresskraft dieselben Korrelationen beobachtet als beim Fallbeispiel Hieflau. Die Analyse zeigt einen signifikanten Zusammenhang zwischen den aufgezeichneten Maschinenparametern und den Gebirgskennwerten.

Insgesamt wurden die Daten von sieben Tunneln in Bezug auf die Gebirgsfestigkeit, die Gebirgszerlegung und den Zusammenhang zwischen Anpressdruck und Vortriebsgeschwindigkeit ausgewertet. Die sieben untersuchten Fallbeispiele können in zwei Gruppen unterteilt werden.

Die erste Gruppe beinhaltet die Tunnel Hieflau, Hemerwald, Maen and Pieve. Die vorherrschenden Gesteine der ersten Gruppe sind Kalksteine, Schiefer, Gneise und Granite und ihre einaxiale Druckfestigkeit variiert zwischen 162 und 226 MPa. Bei dieser Gruppe nimmt die Vortriebsgeschwindigkeit mit zunehmender Anpresskraft ab. Die Analyse hat gezeigt, dass die Ursache für dieses Verhalten in der hohen Gesteinsfestigkeit und der geringen Gebirgszerlegung zu finden ist. Bei hoher Gesteinsfestigkeit kann das entwickelte Vorhersagemodell für die Vortriebsgeschwindigkeit mit nur geringen Variationen von Fall zu Fall angewendet werden.

Die zweite Gruppe beinhaltet den Queen water, den Vereina und den Varzo Tunnel. Hier sind die vorherrschenden Gesteine Schiefer und Gneise mit einer einaxialen Druckfestigkeit zwischen 55 und 162 MPa und hoher Gebirgszerlegung, diese Fälle repräsentieren ein geringfestes bis mittelfestes Gebirge. Bei dieser Gruppe nimmt die Vortriebsgeschwindigkeit mit zunehmender Anpresskraft zu. Bei Gesteinen mit geringer Festigkeit muss das entwickelte Vorhersagemodell nicht ohne weitere Anpassungen benutzt werden.

# Contents

<b>1</b>	<b>Introduction</b>	<b>1</b>
1.1	Overview of the Dissertation . . . . .	2
1.2	History of Tunnel Boring Machines (TBMs.) . . . . .	2
1.2.1	Different Types of TBM . . . . .	3
1.2.1.1	Gripper Machine . . . . .	3
1.2.1.2	Single Shield Machine . . . . .	4
1.2.1.3	Double Shield Machine . . . . .	5
1.2.1.4	Mix Shield Machine . . . . .	6
1.2.1.5	Slurry Machine . . . . .	7
1.2.1.6	Earth Pressure Balance Machine . . . . .	8
1.2.1.7	Auger Boring Machine (ABM) . . . . .	9
1.3	The New Austrian Tunnelling Method (NATM) . . . . .	10
1.4	TBM Tool Wear . . . . .	10
1.5	Methods/Tools Used for Investigation . . . . .	10
1.6	Previous Work . . . . .	11
1.6.1	Samuel 1984 . . . . .	11
1.6.2	Gehring 2009 . . . . .	11
1.6.3	Gong et al 2006 . . . . .	12
1.6.4	Balci 2009 . . . . .	13
1.6.5	Ribacchi et al 2004 . . . . .	14
1.6.6	Cardu 2009 . . . . .	15
1.6.7	Poisel et al 1999 . . . . .	15
1.6.8	M. Berti et al 2002 . . . . .	16
1.6.9	Saffet Yagiz 2007 . . . . .	17
<b>2</b>	<b>Methods/Tools Description</b>	<b>18</b>
2.1	Methods/Tools Used for Investigation . . . . .	18
2.1.1	Kaleida Graph . . . . .	18
2.1.2	Fuzzy Logic Tools . . . . .	20
2.1.3	Math-Lab Code . . . . .	22
2.1.4	Statistical Software “R” . . . . .	22



2.1.4.1	R and Statics . . . . .	23
2.1.4.2	Graphical Procedures . . . . .	23
2.1.5	Statistical Modeling with “SPSS19” . . . . .	24
2.1.5.1	Data . . . . .	24
2.1.5.2	Assumptions . . . . .	24
2.1.5.3	Procedure . . . . .	24
2.1.5.4	Automatic Linear Modeling . . . . .	25
2.1.6	Partial and Bi-variate Correlations . . . . .	28
<b>3</b>	<b>Case Descriptions</b>	<b>30</b>
3.1	Hieflau Power Plant (Expansion Tunnel) . . . . .	30
3.1.1	Description of the Hieflau Project . . . . .	31
3.1.2	Hieflau Headrace Tunnel Geology . . . . .	32
3.2	Queens Water Tunnel . . . . .	34
3.3	Vereina Tunnel . . . . .	37
3.4	Hemerwald Tunnel . . . . .	39
3.5	Tunnels in the Italian Alps (Maen, Pieve and Varzo Tunnel) . . . . .	44
<b>4</b>	<b>TBM Data Analysis</b>	<b>47</b>
4.1	Hieflau . . . . .	47
4.1.1	Hieflau Seismic Data . . . . .	47
4.1.2	Data Analysis with Excel . . . . .	48
4.1.3	3-D Data Analysis with “R” . . . . .	50
4.1.4	Tools/Cutter Wear . . . . .	53
4.1.5	Statistical Modeling with SPSS-19 . . . . .	54
4.1.5.1	Frequency Distribution of Parameters . . . . .	55
4.1.5.2	Prediction Model Summary and Coefficients . . . . .	57
4.1.5.3	Partial and Bi-Variant Correlation . . . . .	62
4.1.6	Conclusions . . . . .	64
4.2	Queens Water Tunnel . . . . .	65
4.2.1	2-D Analysis, Rate of Penetration (ROP) . . . . .	65
4.2.2	3-D Analysis, Rate of Penetration (ROP) . . . . .	68
4.2.3	Statistical Modeling . . . . .	70
4.2.3.1	Frequency Distribution of Different Parameters . . . . .	71
4.2.3.2	ROP Regression Analysis . . . . .	72
4.2.3.3	Rock Fractured Class (RFC) . . . . .	76
4.2.3.4	Partial and Bi-Variant Correlations . . . . .	77
4.2.4	Conclusions . . . . .	78
4.3	Vereina tunnel . . . . .	79
4.3.1	Data Analysis by Microsoft Excel . . . . .	79

4.3.2	Data Analysis and RMC Prediction by Fuzzy Logic Tools . . . . .	82
4.3.2.1	Tunnel Section from 3000- <i>TM</i> to 4000- <i>TM</i> . . . . .	83
4.3.2.2	Section Tunnel Meters 9,000 <i>m</i> to 10,000 <i>m</i> . . . . .	86
4.3.3	3-D Analysis with “R” . . . . .	88
4.3.4	Statistical Modeling with IBM SPSS 19 . . . . .	89
4.3.4.1	Penetration Rate Prediction Model . . . . .	91
4.3.4.2	Prediction Models for RMC and RFC . . . . .	93
4.3.4.3	Correlation and Correlation Coefficient . . . . .	98
4.3.5	Conclusions . . . . .	98
4.4	Hemerwald Tunnel . . . . .	99
4.4.1	Preparation for Excel Data Sheets . . . . .	99
4.4.2	Rock Mass Data . . . . .	100
4.4.2.1	2-D Data Analysis with Microsoft Excel . . . . .	100
4.4.2.2	3-D Analysis with “R” . . . . .	101
4.4.2.3	Prediction Model With Fuzzy Logic . . . . .	104
4.4.2.4	Statistical Modeling with SPSS . . . . .	106
4.4.2.5	Correlation and Correlation Coefficient . . . . .	109
4.4.3	Muskowit-Granite-Gneis . . . . .	110
4.4.3.1	2-D Data Analysis with Microsoft Excel . . . . .	110
4.4.3.2	3-D Data Analysis With “R” . . . . .	112
4.4.3.3	Statistical Modeling With SPSS19 . . . . .	112
4.4.3.4	Correlation and Correlation Coefficients . . . . .	115
4.4.4	Mica-Schist . . . . .	116
4.4.4.1	Data Analysis with Excel . . . . .	116
4.4.4.2	Fuzzy Logic RMC Prediction Model . . . . .	119
4.4.4.3	3-D Analysis with “R” . . . . .	119
4.4.5	Schistose-Gneis . . . . .	120
4.4.5.1	Data Analysis with Excel . . . . .	120
4.4.5.2	Fuzzy RMC Model . . . . .	122
4.4.5.3	3-D Surface Plot and Analysis With “R” . . . . .	122
4.4.6	Mica-schist+Schistose-Gneis . . . . .	124
4.4.6.1	Data Analysis with Excel . . . . .	124
4.4.7	Conclusions . . . . .	125
4.5	Tunnels (Maen, Pieve and Varzo) in the Italian Alps . . . . .	126
4.5.1	Maen Tunnel . . . . .	126
4.5.1.1	Data Analysis by Excel . . . . .	127
4.5.1.2	Data Analysis With Fuzzy Logic . . . . .	129
4.5.1.3	Data Analysis by Statistical Software “R” . . . . .	131
4.5.1.4	Statistical Modeling with SPSS 19 . . . . .	132

4.5.1.5	Correlation and Correlation Coefficients . . . . .	142
4.5.2	Pieve Vergonate Tunnel . . . . .	143
4.5.2.1	2-D Analysis by Excel . . . . .	144
4.5.2.2	Fuzzy Logic Prediction Model . . . . .	146
4.5.2.3	3-D Analysis with “R” . . . . .	147
4.5.2.4	Statistical Modeling with SPSS (Pieve) . . . . .	148
4.5.2.5	Correlation and Correlation Coefficient . . . . .	151
4.5.3	Varzo Tunnel . . . . .	152
4.5.3.1	2-D Data Analysis with Excel . . . . .	153
4.5.3.2	RMC Prediction Model by Fuzzy Logic Varzo Tunnel . . .	155
4.5.3.3	3-D Analysis with “R” . . . . .	156
4.5.3.4	Statistical Modeling with SPSS, Varzo Tunnel . . . . .	159
4.5.3.5	Bi-variant Correlations and Correlation Coefficient . . . .	162
4.5.4	Conclusions . . . . .	163
<b>5</b>	<b>Discussion and Conclusions</b>	<b>165</b>
5.1	Comparison Between Case Histories . . . . .	165
5.2	Discussion . . . . .	166
5.3	Conclusions . . . . .	169
	<b>Bibliography</b>	<b>171</b>

# Chapter 1

## Introduction

Performance of the tunnel boring machine (TBM) and its prediction by different methods has been a hot issue since the first TBM was built. For safe and sound transport, improvement of hydro-power, mining, civil and many other tunneling projects, TBMs are quite frequently used. There is a constant and growing demand in the mining industry for rapid excavation to develop new ore bodies faster in order to reduce overall development cost. TBM which has been developed in recent years, has revolutionized the tunnelling industry by making tunnelling safer and economical for creating underground space and opening the possibility of creating tunnels where it was not feasible before [1]. These machines are used to excavate tunnels through a variety of different rock types. They can be used to bore through hard rock or sand or almost anything in between. These boring machines are used as an alternative to drill and blast (D and B) methods. TBM has the advantages of not disturbing surrounding soil or rock producing a smooth tunnel wall [2]. This significantly reduces the cost of lining the tunnel, and makes them suitable to use in built-up areas, suitable to use in heavily urbanized areas. It is also a complete single unit moving factory.

In this thesis, in order to set forth a more accurate and detailed control system and estimation models for the TBM machine, analysis of machine and rock mass data from seven tunnel sites were done. Main aim of this research work is to improve the existing prediction models and to provide a tool-box for the TBM tunnelling industry (underwrites, project owners, consultants, contractors, manufacturers, researchers etc.) which can be used through all phases of a project. It consists of optimizing the TBM performance, keeping the machine utilization maximum, lowest possible tool wear and prediction about the rock mass class and possible effect of the ground water. Seismic data collected by Geo-physic department of TU Wien was coupled with TBM and rock mass data of Hieflau tunnel, that resulted into another outcome of prediction models for TBM before the start of actual excavation. The correlations between machine parameters thrust, advance rate, torque and rock parameters, unconfined compressive strength (UCS), rock mass class (RMC) or rock mass rating (RMR) are found using real field data from many tunnel sites

excavated by TBM.

## 1.1 Overview of the Dissertation

This thesis basically consists of five chapters. Chapter 1 includes introduction, purpose and structure of the dissertation. In chapter 2, the tools and methods that are used for analysis, are briefly described with examples and graphical user interface (GUI). Chapter 3 contains basic data and history of tunnel sites from where the data was acquired, with the help of photographs taken from relevant websites of Robbins, Herrenknecht etc. Chapter 4 comprises core work done, includes analysis and results of data taken from these sites. Last chapter five includes discussions and conclusions.

## 1.2 History of Tunnel Boring Machines (TBMs.)

The first successful tunnelling shield which is normally regarded as the precursor of the tunnel boring machine was developed by Sir Marc Isambard Brunel to excavate the Rotherhithe tunnel under the Thames in 1825.

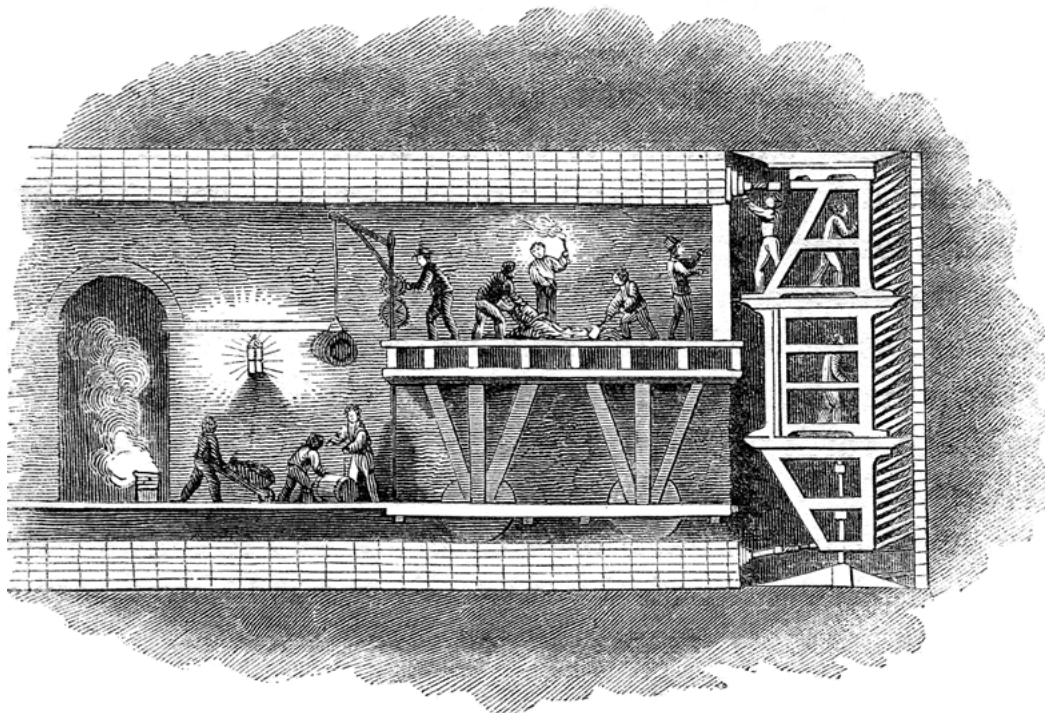


Figure 1.1: First tunnelling shield [1].

However, this was only the invention of the shield concept and did not involve the construction of a complete tunnel boring machine, the digging still was done by standard excavation methods using miners to dig under the shield and behind them brick layers

built the lining Fig. 1.1. Although the concept was successful, eventually it was not an easy project [1].

The first boring machine was Henri-Joseph Maus' Mountain Slicer. It was commissioned by the King of Sardinia in 1845 to dig the Fréjus Rail Tunnel between France and Italy through the Alps, Maus had built it in 1846 in an arms factory near Turin [3]. In 1851 Charles Wilson invented a boring machine with disc type cutters. Another machine was built for boring the English Channel tunnel between England and France in 1865. Use of the TBM is very old and common in underground excavations, like transport tunnels and high pressure water tunnels for hydro power plants [4]. In the United States, the first boring machine was used in 1853 during the construction of the Hoosac Tunnel which was made of cast iron, it was known as Wilson's Patented Stone-Cutting Machine, after inventor Charles Wilson [5]. It drilled 10 feet into the rock before breaking down. The tunnel was eventually completed more than 20 years later by using less ambitious methods [6]. One need to move on nearly 100 years when James S. Robbins built a machine to dig through what was the most difficult shale to excavate at that time, the Pierre Shale. Robbins built a machine that was able to cut 160 feet in 24 hours in the shale, which was ten times faster than any other digging speed at that time.

## **1.2.1 Different Types of TBM**

The description of the types of TBM are inferred from what type of soil is being excavated.

### **1.2.1.1 Gripper Machine**

Essential to the functioning of Gripper TBMs are their drilling, bracing, support and safety systems. The drilling system, i.e. the cutter-head is fitted with cutter rings (disks). In this process the disks roll over the tunnel face, thereby loosening the native rock. The excavated rock or chips (commonly known), is collected in muck bucket lips (openings in the cutter-head) and discharged via hoppers onto a conveyor belt. The tunnelling performance of a Gripper TBM depends essentially on the time required to install rock supporting devices. Same safety measures are used as those in conventional tunnel building, rock anchors, meshes and shotcrete together with the segments characteristic of TBMs and the steel beam supports which are particularly suitable for this purpose.

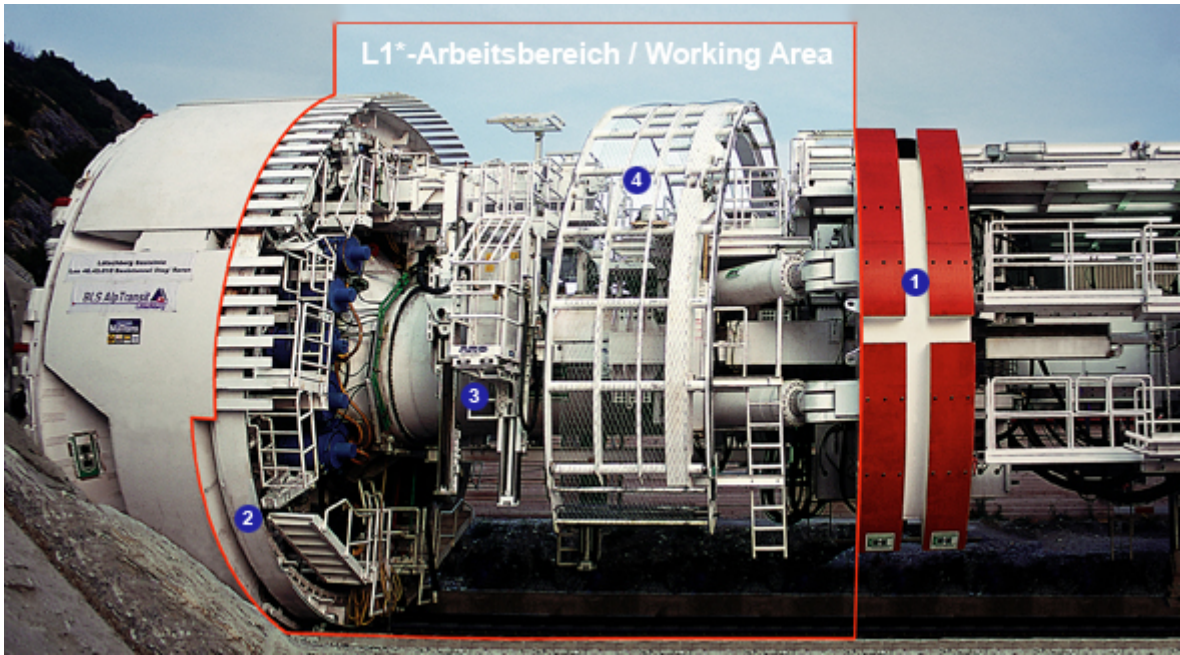


Figure 1.2: Gripper machine [7].

The Gripper machine enables comprehensive rock support measures to be taken even right behind the cutter-head Fig. 1.2, in the so-called L1 work area (1), Ring erectors (2), anchor drilling devices (3) or wire-mesh erectors (4) for example, can be provided for installing the steel supports. Shotcrete is applied and segments are installed in backup area.

### 1.2.1.2 Single Shield Machine

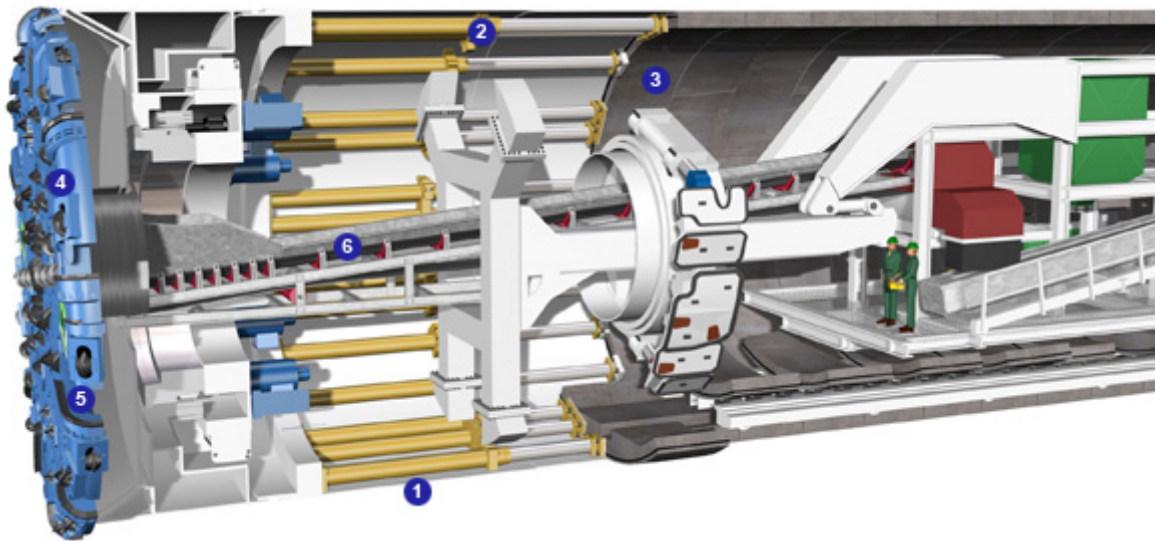


Figure 1.3: Single shield machine [7].

The single shield TBM Fig. 1.3 belongs to a category of machines which are fitted with an open shield. Tunnelling machines described as open shields are machines without a closed system for pressure compensation at the tunnel face. In other words, no excavation chamber has been defined. TBMs fitted with a shield are used on brittle rock formations or soft rock. They have a very wide range of applications on hard rock. Protected by the shield (1), a cylindrical tapered steel structure, the machine extends and drives forward the tunnel practically automatically. In order to drive the tunnel forward, the single shield TBM uses the hydraulic thrust cylinders (2) on the last segment ring (3) installed. The cutting wheel (4) is fitted with hard rock disks, which roll across the tunnel face cutting notches in it. These notches dislodge fairly large chips of rock. Muck bucket lips (5), which are positioned at some distance behind the disks, carry the extracted rock behind the cutting wheel. The excavated material is brought to the surface by conveyers (6). In addition to many other parameters, the torque depends largely on the degree of penetration of the disks and their contact pressure [7].

### 1.2.1.3 Double Shield Machine

Double shields machines are amongst the most technically sophisticated tunnel boring machines used in tunnelling operations. Combining the Gripper principle and the installation of the segments in one perfectly coordinated process, double shields can easily be adapted to the particular geological conditions of any tunnel route [7].

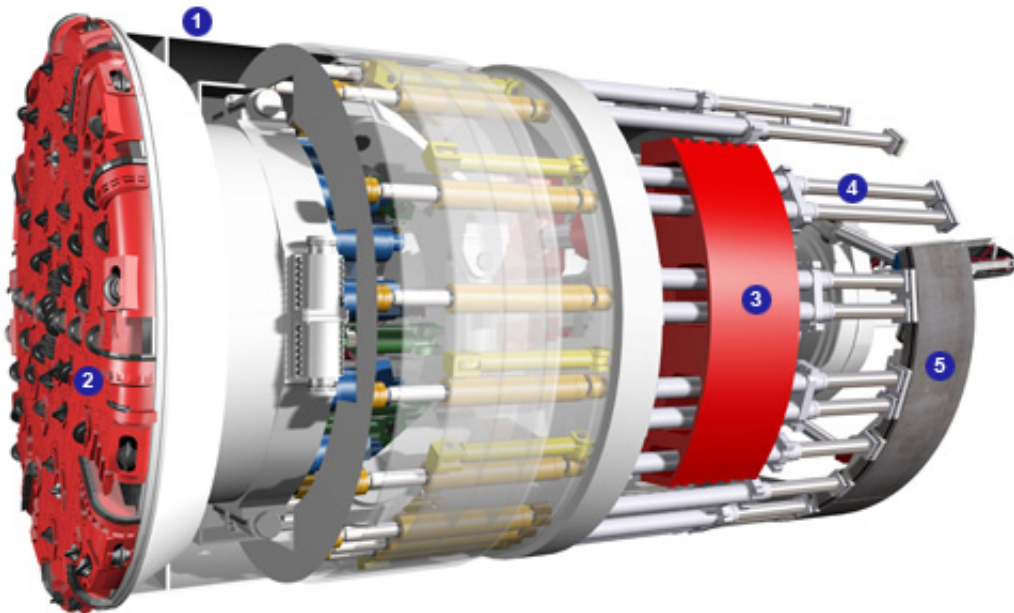


Figure 1.4: Double shield TBM [7].

This type of machine is thus ideally suited for drilling long tunnels in hard rock where geological fault zones occur. The double shield TBM owes its name to its special design, whose main feature Fig. 1.4 is an extendable front shield (1) in the front part of



the machine, which allows the cutter-head (2) to be extended. Reaction forces (torque, axial and longitudinal forces) arising during drilling are conducted into the rock by the extended gripper shoes (3), which are located in the middle section of the tunnel boring machine. Since these forces have been dissipated, the lining segments (5) can be installed during tunnelling, ensuring high tunnelling performance. This is not possible using the conventional method. On completion of a thrust stroke, the gripper shoes are retracted and the rear section of the machine is pushed against the front shield by the auxiliary thrust cylinders (4). This changeover phase only lasts a few minutes and then the next section of tunnel can be drilled. However, continuous drilling like this can be carried out only in undisturbed sections of rock because the gripper shoes need the surrounding rock as an anchorage. When the double shield reaches a section of rock containing fault zones, the telescopic front shield is retracted. The entire boring machine is then driven forward for drilling only by the auxiliary thrust cylinders (4), which are supported on the tunnel lining (5). This type of tunnelling is referred to as "discontinuous" since in this process, as with a conventional shield, tunnelling with the thrust cylinders is not possible until a segment ring has been installed (Fig. 1.4).

**1.2.1.4 Mix Shield Machine**

This machine is used as a mix-shield where gravelly geological conditions indicate an unstable tunnel face or mixed geological conditions.

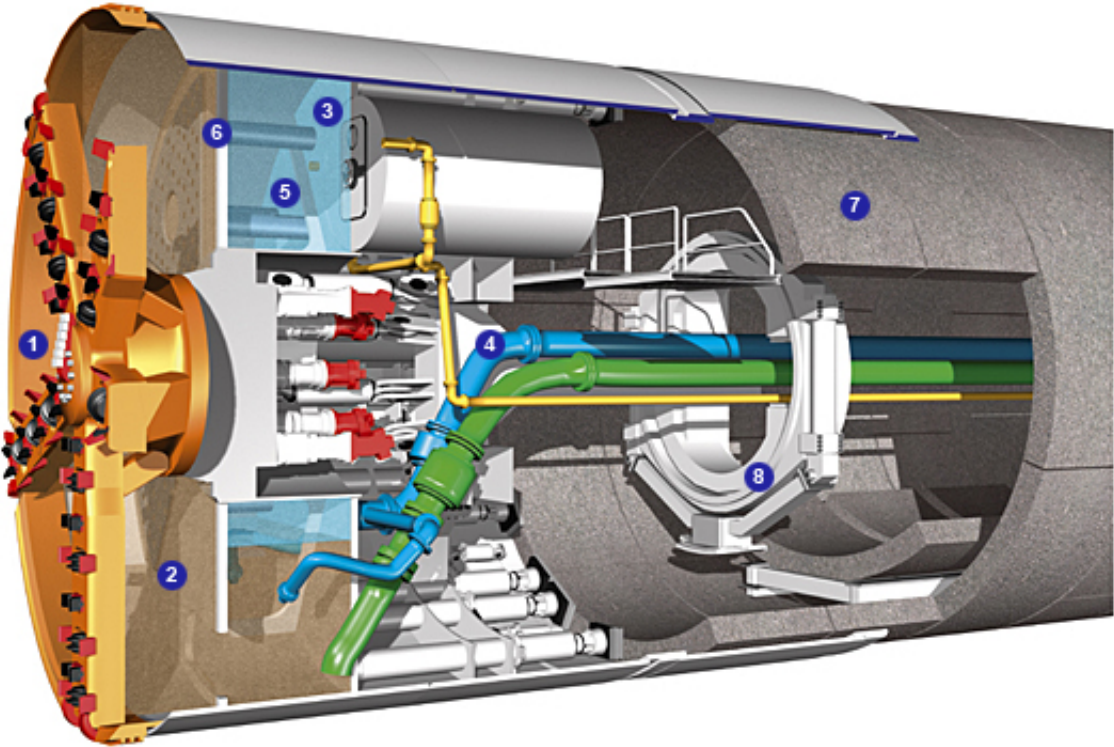


Figure 1.5: Mix-shield TBM [7].

At the tunnel face the soil is loosened all over by the cutting wheel (1) rotating in the bentonite suspension. The soil then mixes with the bentonite suspension. The area of the shield in which the cutting wheel rotates is known as the excavation chamber (2) and is separated by the pressure bulk head (3) from the section of the shield under atmospheric pressure Fig. 1.5. The bentonite suspension supplied by the feed line (4) is applied in the excavation chamber via an air bubble (5) at a pressure equaling the native soil and water pressure, thus preventing an uncontrolled penetration of the soil or a loss of stability at the tunnel face. The support pressure in the excavation chamber is not controlled directly by the suspension pressure but by a compressible air cushion (5). For this reason excavation chamber behind the cutting wheel is separated from the pressure bulk head by a so-called submerged wall (6). The area of the submerged wall and pressure bulk head is known as the pressure or working chamber. The tunnels are normally lined with steel reinforced lining segments (7), which are positioned under atmospheric pressure conditions by means of erectors (8) in the area of the shield behind the pressure bulk head and then bolted in place. Mortar is continuously forced into the remaining gap between the lining segments outer side and the excavation diameter through injection openings in the tail skin or openings directly in the segments (Fig. 1.5).

**1.2.1.5 Slurry Machine**

Slurry machine is used for soils usually of varying hardness. Excavated soil is mixed with slurry to create positive face pressure required to sustain the excavation. This is known as a closed machine. The system for the removal of the soil involves pumping the soil mixed with slurry to plant located outside the tunnel that separates the slurry from the muck allowing its recirculation [1].

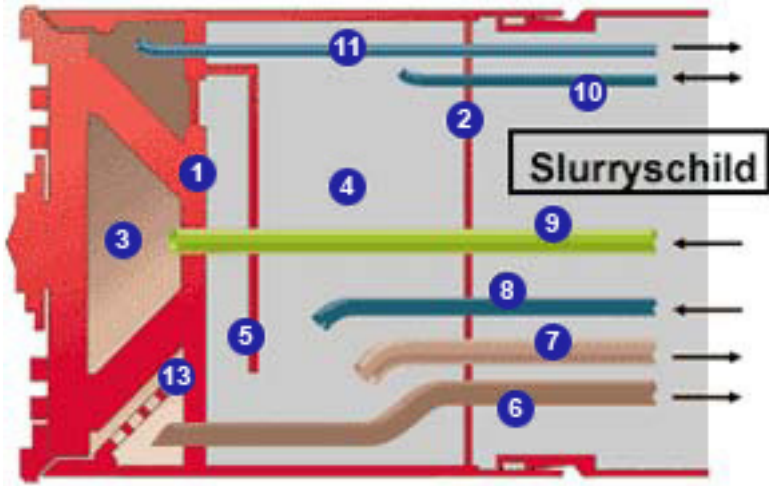


Figure 1.6: Slurry machine [7].

The machine is used as a mix-shield where gravelly geological conditions indicate

an unstable tunnel face or mixed geological conditions. In this mode the extraction chamber is completely filled with suspension, while the pressure chamber (4) Fig. 1.6, situated after the dive wall (1), the suspension is supported by the air pressure cushion (12) and the pressure bulkhead (2). The air pressure is automatically controlled by an air regulating equipment (10+11) to avoid blow outs and base failures at the tunnel face. The pressure compensation between the extraction chamber (3) and the suspension in the pressure chamber after the dive wall is implanted via the communicating pipe (5). The supply conduit (9) delivers the suspension into the extraction chamber. The suspension is removed by the slurry conduit (6) from the extraction chamber behind the suction rack (13). An accumulation of sediments below the communicating pipe is avoided by a constant flush above the supply conduit (8) and the conveyor conduit (7) in the pressure chamber.

### 1.2.1.6 Earth Pressure Balance Machine

This is a closed machine and is used usually for softer fairly cohesive soils. In this case the positive face pressure is created by the excavated ground that is kept under pressure in the chamber by controlled removal through the rotation of the screw conveyor. Muck is thereafter removed by a conveyor belt or skips [1].

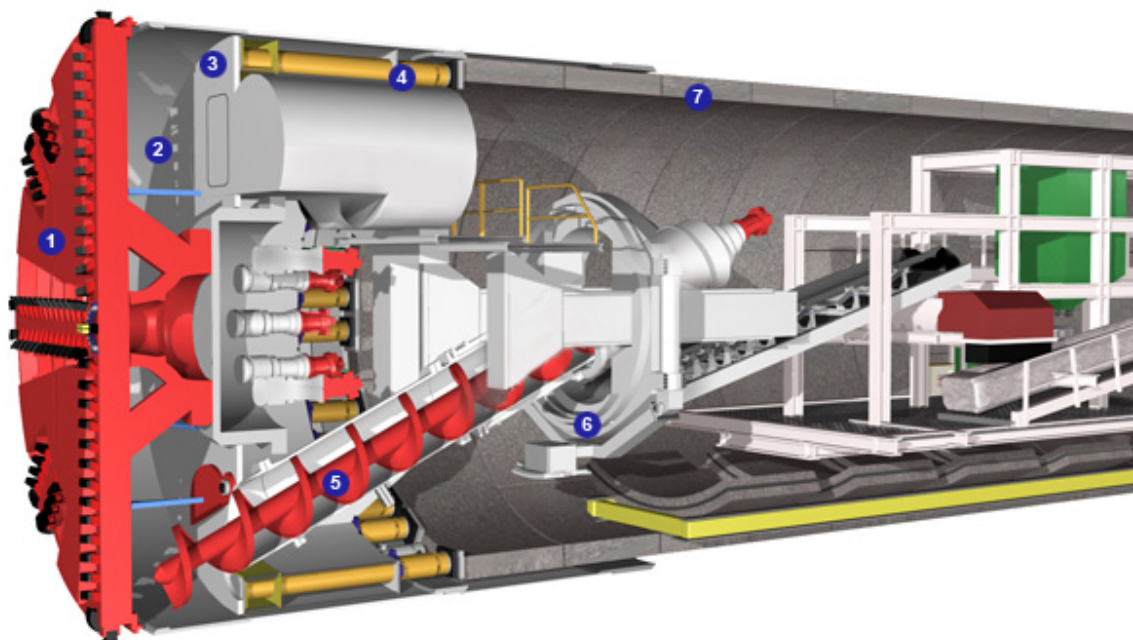


Figure 1.7: Earth pressure balance machine [7].

Where shield excavation is carried out in non stable soils, a loss in stability of the tunnel face is prevented by creating a support pressure. With earth pressure balance machine (EPBM), Fig. 1.7 the cohesive soil loosened by the cutting wheel (1) serves to support the tunnel face, unlike other shields which are dependent on a secondary support

medium. Area of the shield in which the cutting wheel rotates is known as an excavation chamber (2) and is separated from the section of the shield under atmospheric pressure by the pressure bulk head (3). Soil is loosened by the cutters on the cutting wheel, falls through the openings of the cutting wheel into the excavation chamber and mixes with the plastic soil already there. Uncontrolled penetration of the soil from the tunnel face into the excavation chamber is prevented because the force of the thrust cylinders (4) is transmitted from the pressure bulk head onto the soil. A state of equilibrium is reached when the soil in the excavation chamber cannot be compacted any further by the native earth and water pressure. The excavated material is removed from the excavation chamber by an auger conveyor (5). The amount of material removed is controlled by the speed of the auger and the cross-section of the opening of the upper auger conveyor driver. The auger conveyor conveys the excavated material to the first of a series of conveyor belts. Excavated material is conveyed on these belts to the so-called reversible conveyor from which the transportation gantries in the backup areas are loaded when the conveyor belt is put into reverse. The tunnels are normally lined with steel reinforced lining segments (7), which are positioned under atmospheric pressure conditions by means of erectors (6) in the area of the shield behind the pressure bulkhead and then temporarily bolted in place. Mortar is continuously forced into the remaining gap between the segments outer side and the rock through injection openings in the tail skin or openings directly in the segments [7].

#### 1.2.1.7 Auger Boring Machine (ABM)



Figure 1.8: Auger boring machine [8].

An Auger Boring Machine (ABM) Fig. 1.8 is used to bore horizontally through soil or rock with a cutting head and auger. Majority of ABMs are used to install pipe casing under railroads, highways, airport runways, creeks or any area of ground that cannot be open cut or disturbed in any way. Initially the ABM is set up in the starting pit on a predetermined length of track. A backing plate, usually steel or reinforced concrete

block, is installed in the wall opposite of the boring to withstand the thrust exerted by the boring machine. The machine bores through the earth with a cutting head and the jacking force is provided by the hydraulic thrust. The pipe casing and auger sections are added as the machine advances. Soil is removed from the auger through the casing to a door located on the side of the machine [8].

### **1.3 The New Austrian Tunnelling Method (NATM)**

The New Austrian Tunnelling methods (NATM) were developed between 1957 and 1965 in Austria [9]. It was given its name in Salzburg in 1962 to distinguish it from old Austrian tunneling approach. The main contributors to the development of NATM were Ladislaus V. Rabcewicz, Leopold Müller and Franz Pacher. The main idea is to use the geological stress of the surrounding rock mass to stabilize the tunnel itself. The NATM was originally applied for tunnels in rock in the 1970s, however, this tunnelling method was carried out more and more also in soft rock with low overburden and in urban areas. Because of the outstanding importance of the shotcrete (sprayed concrete) for the application of this method the denotation "Sprayed Concrete Lining Method" or simply "Shotcrete Method" is mainly used in Germany [10].

### **1.4 TBM Tool Wear**

Tool (TBM cutter) wear is another important factor which play rigorous role in machine utilization and tunnelling cost. Effort was made to get a correlation between thrust and cutter wear and advance rate of TBM and to minimize the tool wear. Data from many TBM driven tunnels were gathered and analyzed for above mentioned goals. This part of research showed that tool wear was least when TBM diameter is high and machine is operated at moderate thrust. Only Hieflau data has been analysed for tool wear analysis, as no other data for tool wear from any other site have been available.

### **1.5 Methods/Tools Used for Investigation**

Fuzzy logic, Origin 8.1, Microsoft excel, Kaleida graphs, statistical software "R", Math-Lab, and a commercially available software packages IBM SPSS19 were used to analyse actual field data, collected from five tunnel sites. Full details and description of these tools or methods is presented in chapter 3.

## 1.6 Previous Work

Lot of work is already done regarding TBM performance. Here few specific research works are presented, which are closely related to this research work.

### 1.6.1 Samuel 1984

This paper shows the results of 2 tests conducted for boreability, one in vesicular basalt and other in non-vesicular basalt. The results and analysis of the paper shows that, the geological defects will produce varying effects depending on the size of cutter used and the penetration of disc cutter. This effect of penetration is particularly great in highly porous and highly faulted rock. Since a higher penetration by the cutter would be able to take more advantage of the structural weakness, than if the penetration is less than the typical dimension of the holes or faults in the rock. Higher advance rate could be achieved by using a higher head speed for boring, provided that the condition of the disc cutters does not deteriorate. Consequently, all other things being equal, it would appear to be better to operate the machine at moderate propel pressure so as to achieve higher advance rate [11].

### 1.6.2 Gehring 2009

The paper states that, with same machine, tool and rock parameters the penetration can be assumed to be directly proportional to the specific excavated volume over most of the range of application. This value is mainly used for practical reasons and is itself inversely proportional to the tool wear. The correlation between effective thrust force and penetration is found to be approximately linear for a certain machine assuming comparable rock conditions. This linearity does not show below a critical penetration and above a certain maximum penetration. This maximum penetration is defined by the shape of the cutting edge of the discs and the state of cutter wear and can be approximately in a range between 11 to 15  $mm/rev$ . Larger diameters permit higher head speed and higher advance rate. Also the life time of cutters was found to increase with diameter Fig. 1.10. Gehring K. also introduced a formula for TBM excavation, given below [12]:

$$V_{S-rpm} = V_S \cdot \frac{50}{D_B \cdot R_{B-i}} [m^3/cutter] \quad (1.1)$$

where:

$V_{S-rpm}$  specific excavated volume at a certain cutter head speed [ $m^3/cutter$ ];

$V_S$  specific excavated volume at nominal cutter head speed [ $m^3/cutter$ ];

$R_{B-i}$  actual cutter head speed [ $min^{-1}$ ].

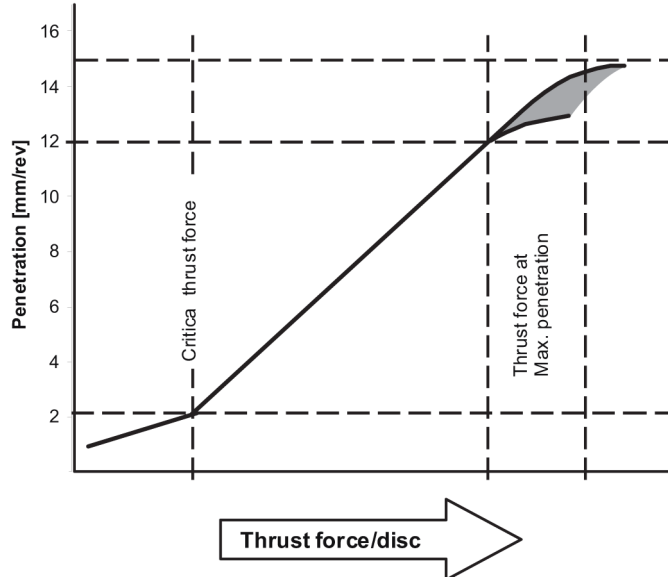


Figure 1.9: Thrust versus penetration [12].

### 1.6.3 Gong et al 2006

Results showed that a critical point exists in the penetration curves. The penetration per revolution increases rapidly with increasing thrust per cutter when it is higher than the critical value. When the thrust is greater than the critical value, the muck becomes well-graded. The muck shape analysis results also showed with the increase of the thrust, the chip shape changes from flat to elongated and flat. Boreability index at the critical point of penetration of  $1 \text{ mm/rev}$ , defined as the specific rock mass boreability index is proposed to evaluate rock mass boreability. It decreases with increasing thrust per cutter. This is due to a change in the efficiency of the cutting action at the cutter head. Borg (1988) and Bruland (1998) found that a critical thrust must be applied to overcome the rocks inherent resistance against breaking. Below this critical thrust value almost no penetration rate can be achieved and above this value the penetration rate increases rapidly with the increase of thrust force. Therefore, the previously defined boreability index calculated by the TBM performance data can not accurately represent the rock mass boreability. Only when the thrust force remains same, the calculated boreability index can demonstrate the different rock mass conditions. It was concluded that with the increase of the thrust force per cutter, the penetration per revolution increases Fig. 1.10. For example, the rock strength of granite in *T05* penetration test is  $172.9 \text{ MPa}$  and its specific rock mass boreability index is  $208 \text{ kN/cutter/mm/rev}$ , while the rock strength of granite-gneiss in Buchi's test is close to  $250 \text{ MPa}$  and its specific rock mass boreability index is only  $120.67 \text{ kN/cutter/mm/rev}$  (Büchi, 2004). The specific rock mass boreability index remains a constant in the same rock mass condition if the same TBM is used, and does not change at different operating thrust forces. With increasing torque and thrust per cutter, the

penetration per revolution increases. The correlation between the thrust per cutter and the penetration also shows that there exists a critical value in the correlation curve [13].

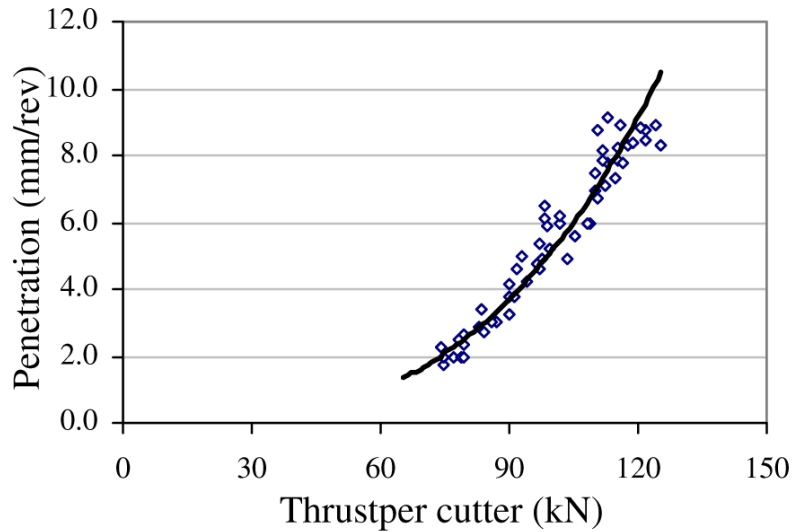


Figure 1.10: Thrust versus penetration [13].

#### 1.6.4 Balci 2009

A case study in Kozyatagi-Kadikoy metro tunnel, Turkey. This paper presents determination of some design parameters and performance prediction of a TBM carried out using full-scale rock cutting tests.

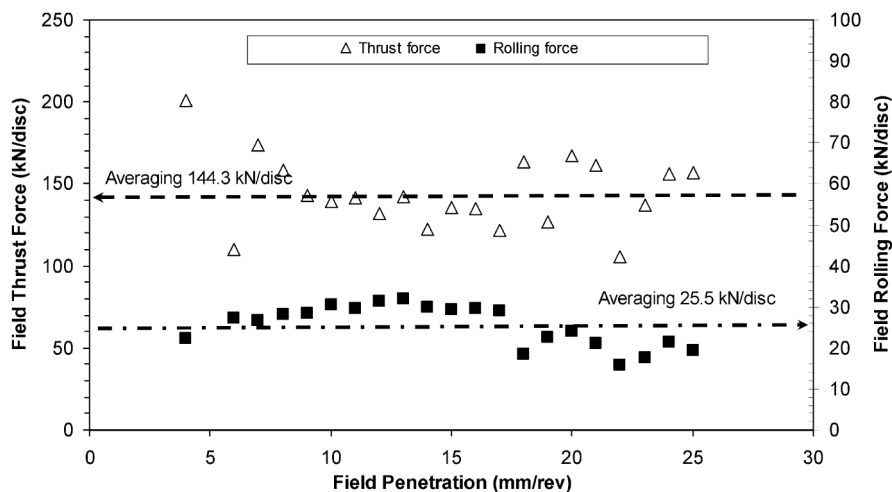


Figure 1.11: Relationship between thrust and penetration [14].

Contrary to the basic rock cutting mechanics and rock cutting tests realized in the laboratory on intact rock, the field thrust and rolling force do not show any increase or relationships with penetration in the field. This is mainly due to the highly fractured characteristic of the rock formation excavated. Thrust force for a specific penetration is higher in the field than in the laboratory test results, probably due to high frictional



forces between shield and highly fractured or almost loose rock formation accumulated in front of the cutter-head. This causes an increase in torque, power and specific energy requirements compared to the laboratory test results. In most cases, small size of the muck causes specific energy to increase. This is well explained by Fig. 1.11 coarseness index values obtained by sieve analysis of the muck from the laboratory experiments and the field.

### 1.6.5 Ribacchi et al 2004

This paper analyzed the influence of rock mass quality on the performance of TBM in a high strength and low fracture density rock. An increase in penetration with thrust is observed in specific tests carried out on the same face or under the same rock conditions, sometimes with a well defined knee for a critical value of the thrust. However the values determined during normal machine operation often show a reverse correlation (Grandori et al., 1995). This behavior is possibly due to the fact that the machine operator tries to improve the low penetration rate in very hard rock by pushing the thrust near or above the recommended level, whereas he reduces the thrust when the penetration rate  $V_p$  is considered to be acceptable [15]. The data obtained for the Varzo tunnel do not show a marked relationship between applied thrust and penetration rate, if the data corresponding to the learning phase are excluded, only a slight increase in the thrust at decreasing penetration rates is observed.

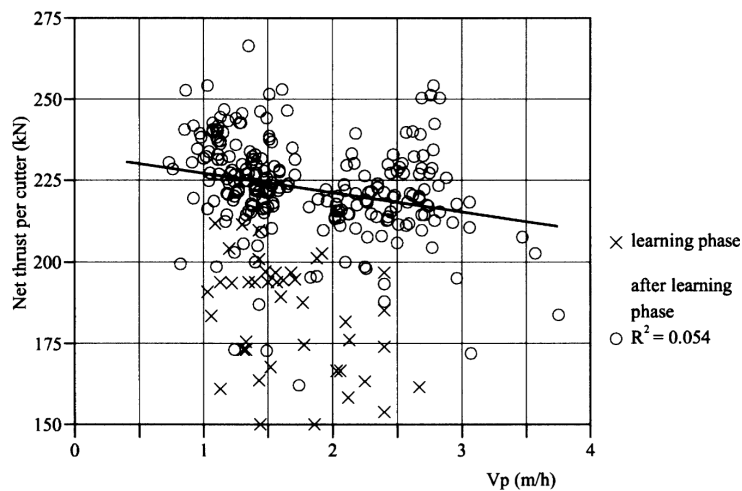


Figure 1.12: Thrust versus advance rate [15].

This hypothesis is supported by the penetration data for a tunnel in granitic rock analyzed by Mogana et al. (1998), it was found that spacing accounted for about 26% of the total variance of the penetration rate (a much lower value than in the Varzo tunnel), whereas the inclusion of various other rock mass characteristics (e.g. compressive strength, joint quality) brought the coefficient of correlation  $R^2$  to 0.53 and 0.62 respectively for the penetration rate and the scaled penetration rate. The influence of thrust on penetration

does not emerge clearly from the excavation data. When boreability indexes including thrust are adopted, such as V (in which the penetration rate is scaled with respect to the thrust per cutter), correlations with the quality indexes of the rock mass show only a slight improvement. As in other rocks masses characterized by low machinability, a weak negative correlation between thrust and penetration rate was found for the Varzo tunnel. This behavior may be determined by the operator’s conduct who tries to push the thrust to the limit of admissible values, or even beyond, when the penetration rate is deemed to be unsatisfactory.

**1.6.6 Cardu 2009**

In this study, an analysis has been carried out on about 587 m of a service tunnel, excavated by a TBM in a flysch formation. Some relationships have been highlighted between the excavation specific energy, net advance rate, thrust on the cutter-head and the rock mass rating. TBM performance predictive law has been also applied verifying a scarce gap between the predicted and actual values of the net advance rate Fig. 1.13. Resulted relationship between excavation specific energy and RMR can help the choice of the TBM for a specific tunnel or the estimation of the net advance rate using a specific machine.

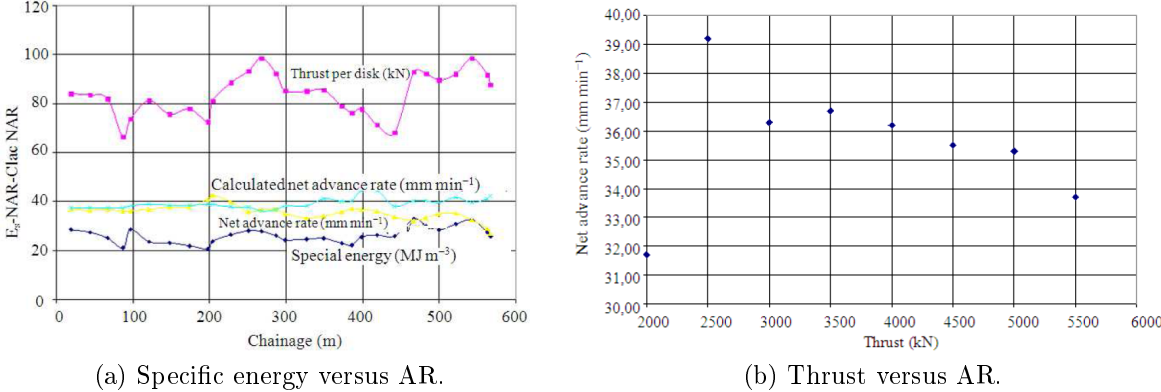


Figure 1.13: Applied thrust versus net advance rate [16].

**1.6.7 Poisel et al 1999**

The investigations showed that it is possible to assess rock mass class (RMC) evaluating machine data. By this it would be possible to establish an overall rule base accounting for the complete complex system. Poisel R. et al. suggested Fuzzy rule base for prediction of rock mass class (RMC) and apply it to different rock mass data from Schwarzach, Vereina and Evinos tunnels Fig. 1.14.

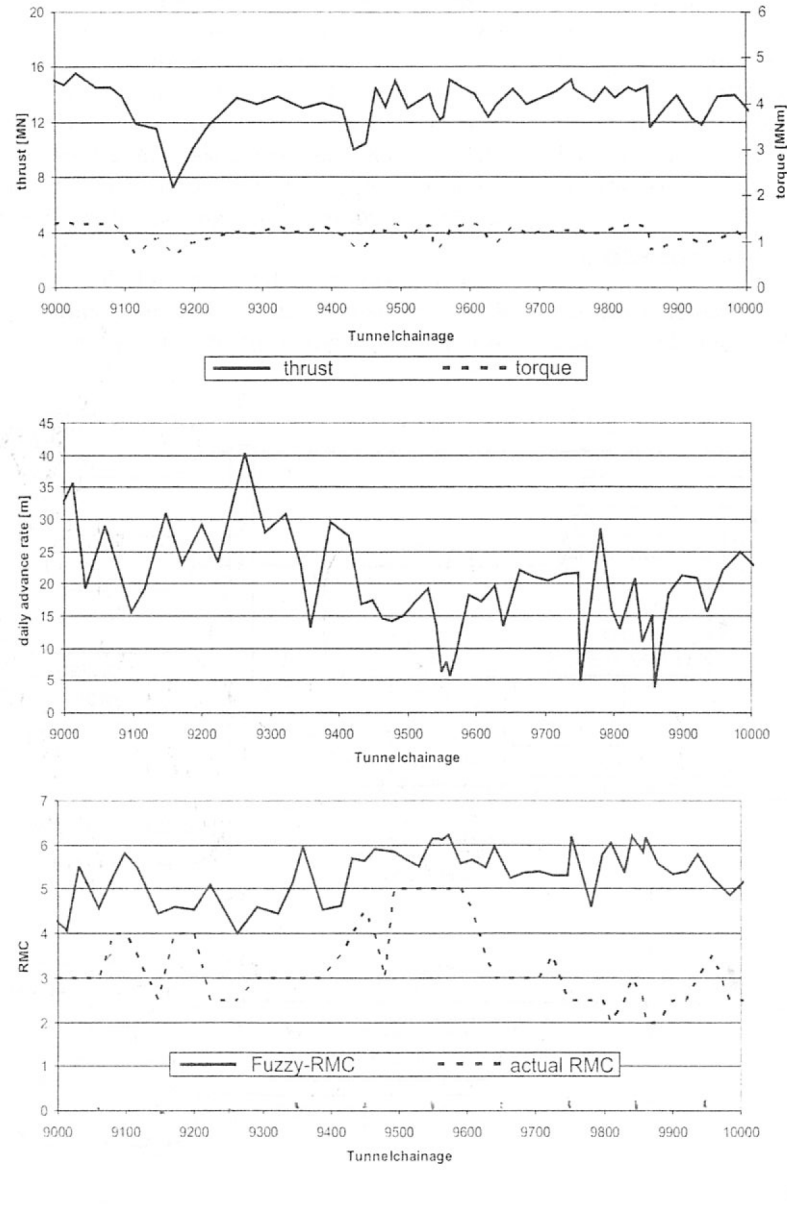


Figure 1.14: Rock mass class predicted by Fuzzy logic [17].

At the moment there is no investigations available how to evaluate water and structure orientation best [17].

### 1.6.8 M. Berti et al 2002

A lot of analysis on three tunnels (Maen, Pieve and Varzo in Italian Alps) data, including histogram plot, 2-D correlations between rock mass rating (RMR), thrust, penetration rate, Q-value, utilization coefficient and UCS Fig. 1.15. A reliable estimation of excavation rates is needed for time planning, cost control and choice of excavation method in order to make tunnel boring economic in comparison with the classical drill and blasting method. As a consequence, great efforts have been made to correlate TBM performance

with rock mass and machine parameters, either through empirical approach or physically based theories.

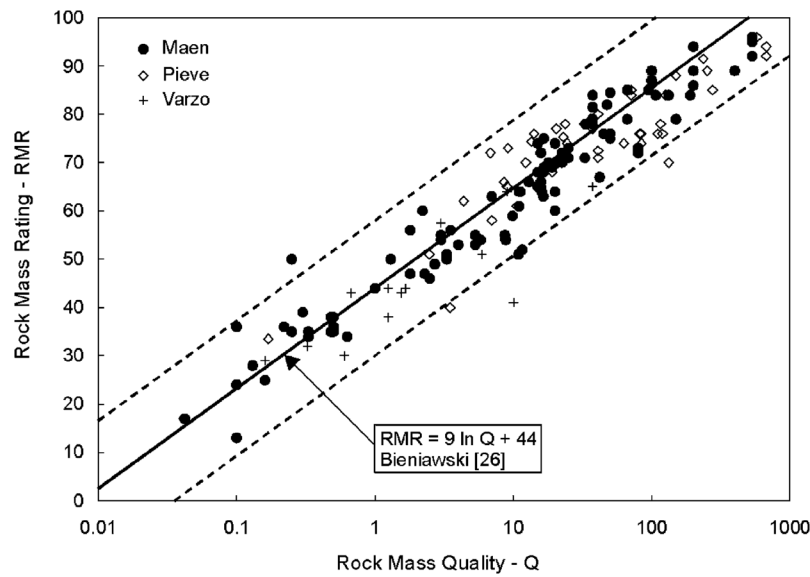


Figure 1.15: RMR versus rock mass quality [18].

### 1.6.9 Saffet Yagiz 2007

Data from the tunnel excavated in predominantly fractured igneous and metamorphic rock were used to achieve TBM performance predictive equation as a function of engineering rock properties. TBM performance requires the estimation of penetration rate (ROP), the ratio of excavated distance to the operating time during continuous excavation phase

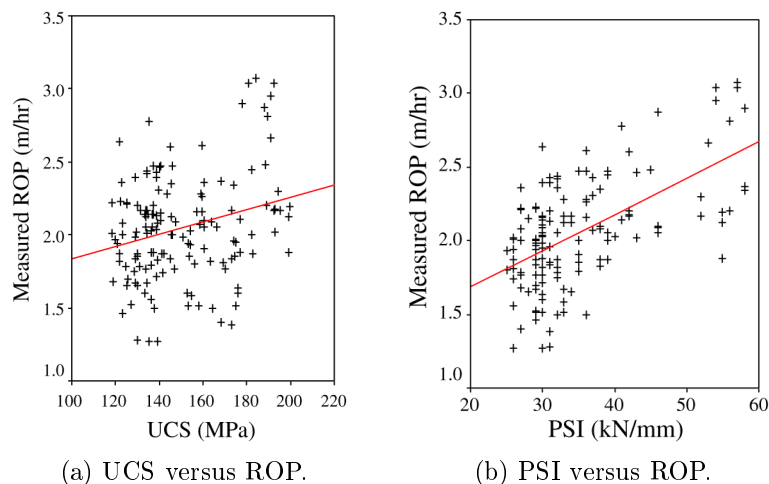


Figure 1.16: ROP versus PSI and UCS [19].

and advance rate (AR), the ratio of both mined and supported actual distance to the total time Fig. 1.16. In fact, most of the predictive models are concerned with the estimation of ROP [19].

# Chapter 2

## Methods/Tools Description

### 2.1 Methods/Tools Used for Investigation

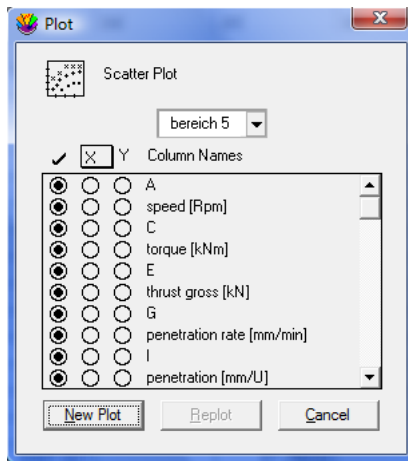
#### 2.1.1 Kaleida Graph

Kaleida graph works just like Excel, but there are more option and applications for curve fitting, 3-D plotting, linear regression and statistical modeling. Kaleida needs not any extra code or subroutine, it works with import and export of data from and to the excel file. In this software there are so many options for curve fitting and also it can perform matrix operations. Now, let's create a plot using the example data.

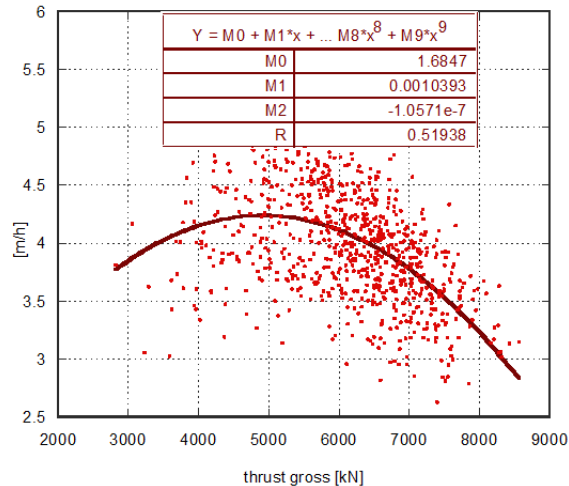
- Choose Gallery > Linear > Scatter.

This will display the Variable Selection dialog. Notice that the name of the data file and its column titles are displayed in this dialog.

- Select Time as the X variable and Test 1 as the Y variable by clicking the appropriate buttons.
- Click New Plot to create a Scatter plot.



(a) Graphical user interface for Kaleida.



(b) Kaleida graph scattered plot.

Figure 2.1: Kaleida GUI and scattered plot.

Figure 2.1a shows what your Variable Selection dialog should look like at this point and Fig. 2.1b shows an output scattered plot and polynomial curve fit.

The X variable you selected is the independent variable and the Y variable is the dependent variable. By default, the X variable is plotted on the horizontal axis and the Y variable is plotted on the vertical axis. The title of the plot is taken from the name of the data window. The X and Y axis titles are taken from the column titles of the variables being plotted. The Y variable title is also used in the legend. Now that the graph has been created, it can be modified very easily. For example, let's change how the data is represented on the plot. You will use the Plot Style dialog to change the marker type, size, and color.

- Triple-click the marker displayed in the legend (or choose Plot > Plot Style).
  - Select a different marker to represent the variable on the plot. The markers are displayed on the left side of the dialog. The first six markers in the left column are transparent; all of the others are opaque.
  - Change the value in the Marker Size field to 18 and select a different color from the color palette.
  - Click OK and the plot will be redrawn to reflect the changes that have been made.
- Now we will use the Identify tool ( ) from the toolbox to display the coordinates of the data.
- Select the Identify tool by either clicking it or pressing I on your keyboard.
  - Once the tool is selected, click one of the data points. The X and Y coordinates are displayed in the upper-left corner of the plot window [20].
  - Reselect Linear from the Curve Fit menu. A Curve Fit Selections dialog appears with a drop-down arrow under View.

- Click the drop-down arrow and choose Copy Curve Fit to Data Window from the pop-up menu.
- Click OK to return to the plot window.

## 2.1.2 Fuzzy Logic Tools

Fuzzy logic tools are used to evaluate the machine data (thrust, torque, power, machine velocity and advance rate), which was collected during the tunnel excavation process and is used to predict the behavior of surrounding rock and interaction between rock mass properties and machine parameters (Fig. 2.2).

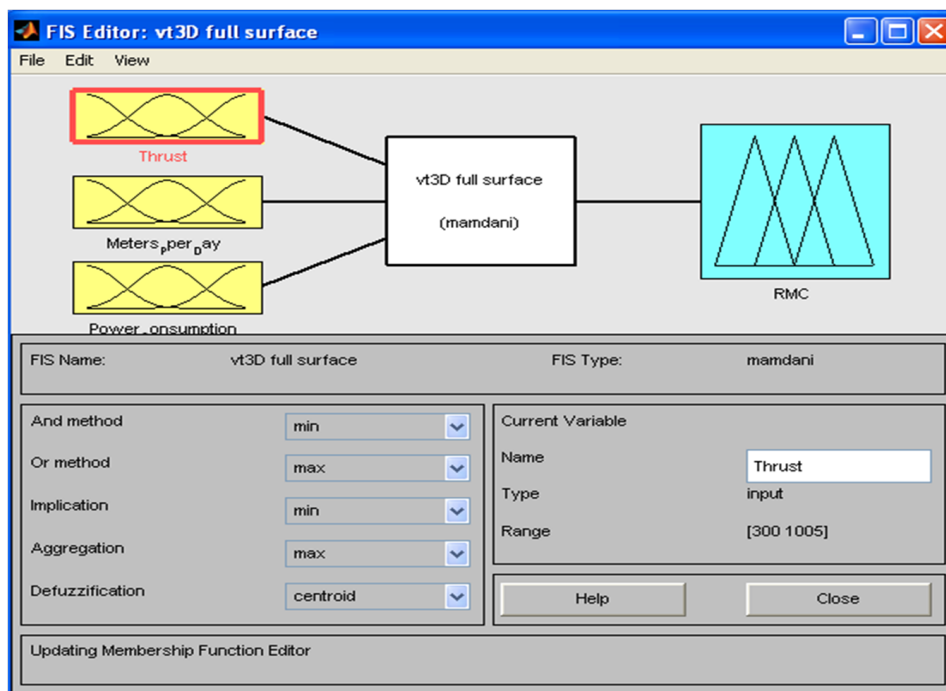


Figure 2.2: Fuzzy logic tools [21].

Fuzzy logic tools Fig. 2.3 are used to predict the rock mass classification (RMC), keeping the machine parameters (thrust, advance rate and machine power) as input variables and RMC as output variables. In between the input and output variables, a rule base Fig. 2.4 was developed that govern the process of prediction. This rule base consists of membership functions with 'AND', 'OR' rules and range of the variables. The output is in the form of 3-D surface Fig. 2.5 having two or three input and one output variable. However if one or more variables like rock strength, are uncertain in input, then output is definitely uncertain.

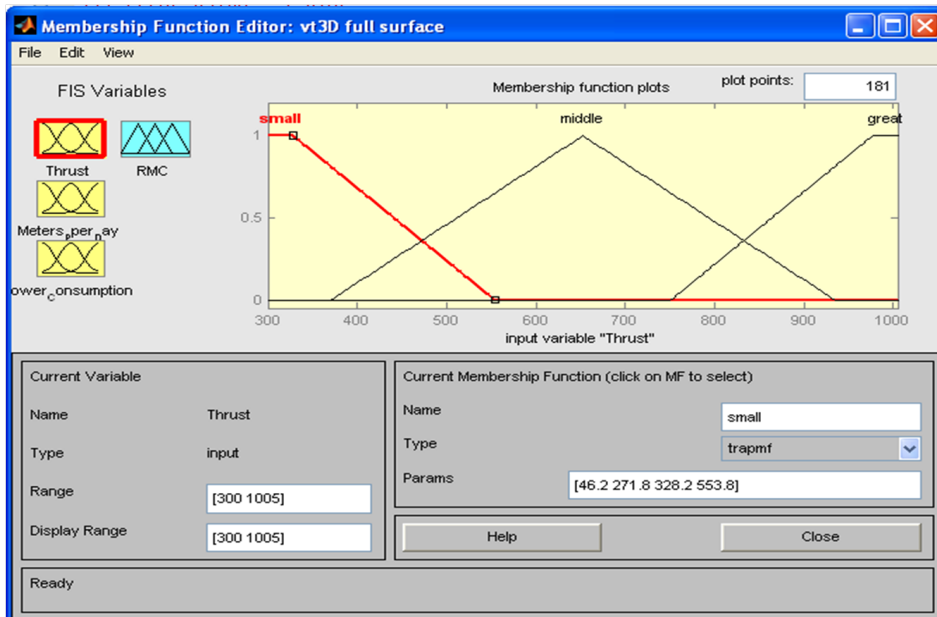


Figure 2.3: Fuzzy logic tools.

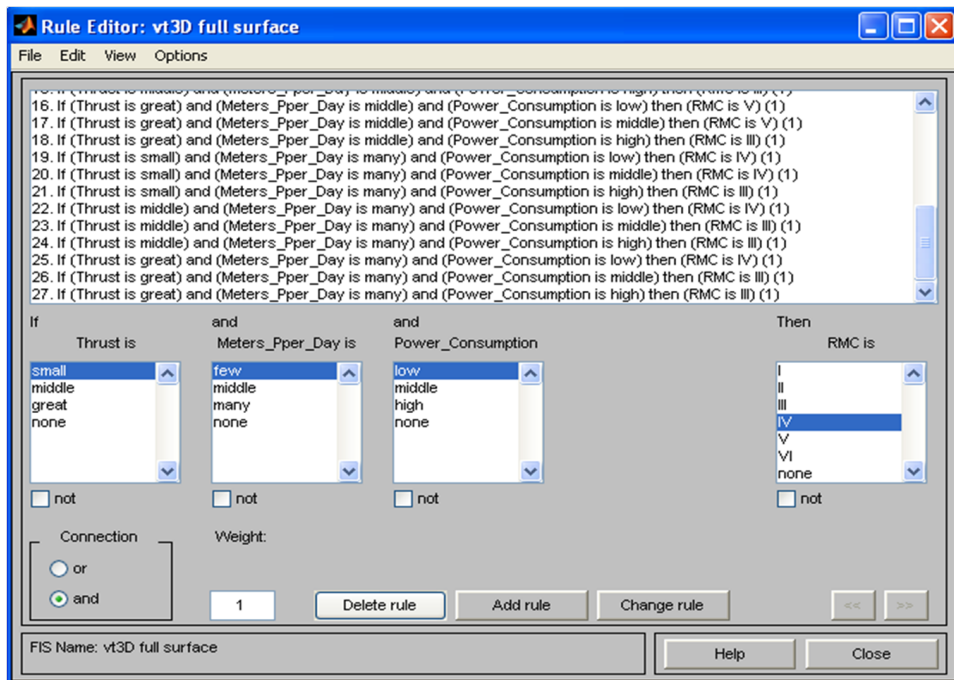


Figure 2.4: Fuzzy rule base.



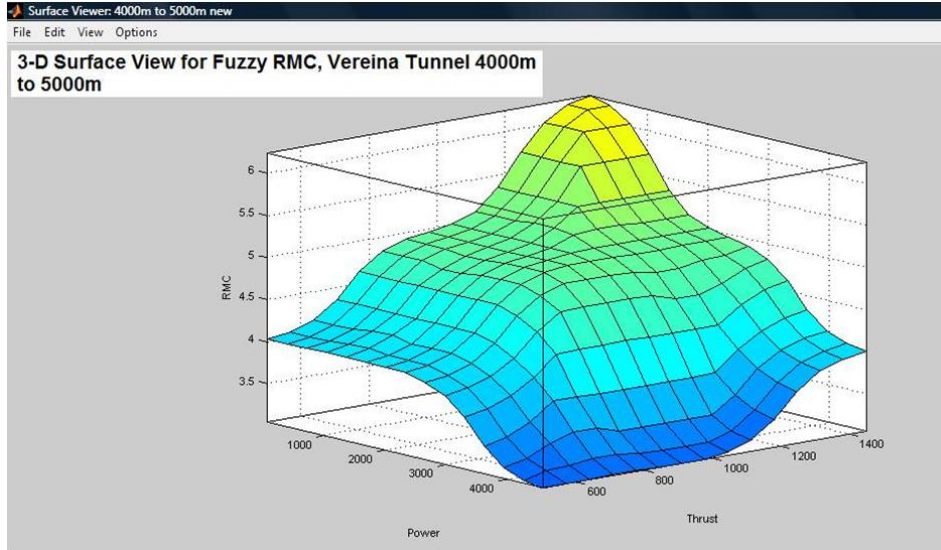


Figure 2.5: Fuzzy 3-D surface.

### 2.1.3 Math-Lab Code

For a comprehensive and flexible model prediction for rate of penetration (ROP) and rock mass class (RMC) and rock fracture class (RFC), a sub-routine program in Math-Lab has been developed that reads the data from excel file and grade it into sub-classes (low, middle, high etc) and then according to pre-defined rule base, perform a specific action using IF-THEN rules to all input machine parameters and gives a output variable (RMC). Also output variable is plotted in 3-D surface against the three input variables. This process was repeated by replacing the input variables by seismic parameters (amplitude pseudo velocity etc) instead of TBM parameters. It is far better than Fuzzy logic prediction model, as out put is in numeric form unlike the 3-D surface in Fuzzy. Moreover it has a capacity to perform analysis for input and output variables more than one. This code takes excel data as input, check each element of each row one by one, decide its group (low, medium, high) i.e where to put it according to a predefined rule-base. When position of each element in a single row is decided, then according to “IF-THEN” rule (already set) for all three or four input variables, value of out-put variable is decided. In this way every element in the data is taken into account and it gives rise to a corresponding out-put. All out-put values are printed/displayed in last column. Code can also be modified to print 2-D charts and 3-D surfaces. Code is flexible to receive unlimited amount of data entries, no restriction on number of input and even out put variables.

### 2.1.4 Statistical Software “R”

Many 3-D surfaces were generated using “R”. For better comparison and analysis of different variables 3-D surface generated by “R” are very helpful to see the behavior of rock and machine parameters. To produce the 3-D surfaces and other graphs, a R-code (Algorithm

2.1), written by Peter Filzmoser (TU Wien) has been used. This code uses R-syntax 'scatter plot' for 3-D surface and dm.smooth, grid and axis for line plot functions. Code takes data from excel file saved in "comma separated version" (CSV), and perform necessary action on input data as per code instruction and plot a 3-D surface and line plots for different variables.

#### 2.1.4.1 R and Statics

Many people use R as a statistics system. Basically it is an environment within which many classical and modern statistical techniques have been implemented. A few of these are built into the base R environment, but many are supplied as packages. Most classical statistics and much of the latest methodology is available for use with R, but users may need to be prepared to do a little work to find it. R will give copious output from a regression or discriminant analysis, this will give minimal output and store the results in a fit object for subsequent interrogation by further R functions [22]. R can perform some regression analysis, variance, generalized linear modeling and curve fitting. But its not as simple as excel or other mathematical tools, user has to write code for every single order to perform. R provides an interlocking suite of facilities that make fitting statistical models very simple [23].

#### 2.1.4.2 Graphical Procedures

Graphical presentation of results in 3-D surfaces were plotted by using a subroutine code. Code is listed below as algorithm 2.1.

---

**Algorithm 2.1** Algorithm for R software.

---

```
# PF, 25.4.2012
# Daten einlesen:
MGG <- read.csv("G:/Vereina tunnel1/Vereina4R1.csv",dec="," ,sep=";")
attach(MGG)
library(Rcmdr)
scatter3d(RMC, Penetration_mph, RFC,
sphere.size=1,threshold=0.01,point.col="orange",
fit=c("smooth"), df.smooth=15,bg="white", axis.scales=TRUE, grid=TRUE,
ellipsoid=FALSE,surface.col="blue",residuals=0.1)
```

---

Graphical facilities are an important and extremely versatile component of the R environment. It is possible to use the facilities to display a wide variety of statistical graphs and also to build entirely new types of graphs. Here "R" is used for scattered 3-D graphs, written by Peter Filzmoser, Department of Statistics and Probability Theory TU Wien 2.1.

## 2.1.5 Statistical Modeling with “SPSS19”

Commercial software packages SPSS are very helpful to plot frequency distribution with  $R^2$  values, linear and quadratic correlations between rock and machine (TBM) parameter, regression coefficients and finally a statistical model to predict ROP, RMR and RMC values. Comparison of all these models with other model obtained from Fuzzy logic, Math-Lab code, and “R” have been performed in the second last chapter . Linear regression analysis estimates the coefficients of a linear equation, involving one or more independent variables, that best predict the value of the dependent variable. SPSS is useful for situations in which one want to predict the presence or absence of a characteristic or outcome based on values of a set of predictor variables. It is similar to a linear regression model but is suited to models where the dependent variable is dichotomous. Logistic regression coefficients can be used to estimate odd ratios for each of the independent variables in the model [24].

### 2.1.5.1 Data

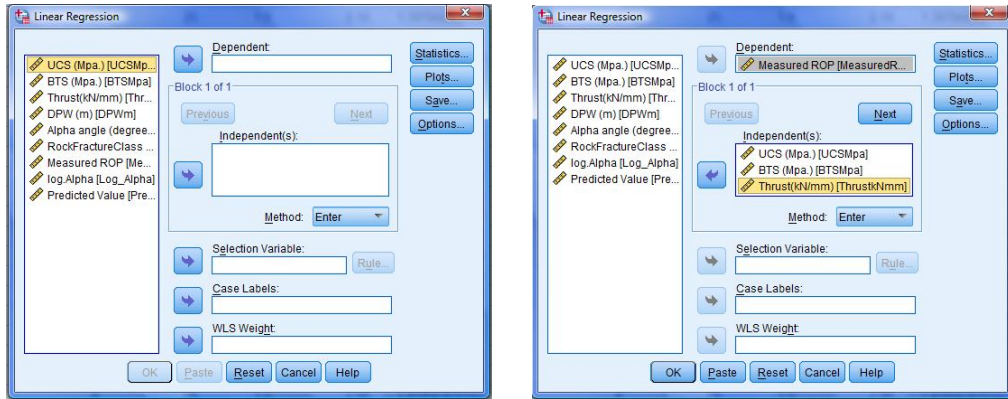
The dependent and independent variables should be quantitative. Categorical variables such as religion, major field of study, or region of residence, need to be recoded to binary (dummy) variables or other types of contrast variables.

### 2.1.5.2 Assumptions

For each value of the independent variable, the distribution of the dependent variable must be normal. The variance of the distribution of the dependent variable should be constant for all values of the independent variable. The relationship between the dependent variable and each independent variable should be linear, and all observations should be independent. The significance levels have to be less than 0.05 for the parameter to be statistically significant [24].

### 2.1.5.3 Procedure

To open the Linear Regression dialog box, from the menus choose  $\rightarrow$  *Analyze*  $\rightarrow$  *Regression*  $\rightarrow$  *Linear*. Select more than one variable for the Independent (s) list, if you want to obtain a multiple linear regression [24]. You can specify more than one list, or “block” of variables, using the Next and Previous buttons to display the different lists. Up to nine blocks can be specified Figs. 2.6-2.7.



(a) Linear model for regression.

(b) Linear variable input

Figure 2.6: Linear regression method description.

Variables Entered/Removed <sup>b</sup>				Model Summary				
Model	Variables Entered	Variables Removed	Method	Model	R	R Square	Adjusted R Square	Std. Error of the Estimate
1	log.?, UCS (Mpa.), Thrust (kN/mm)	.	Enter	1	.711 <sup>a</sup>	.505	.495	.25646

a. Predictors: (Constant), log.?, UCS (Mpa.), Thrust(kN/mm)

a. All requested variables entered.  
b. Dependent Variable: Measured ROP

ANOVA <sup>b</sup>						
Model		Sum of Squares	df	Mean Square	F	Sig.
1	Regression	9.858	3	3.286	49.963	.000 <sup>a</sup>
	Residual	9.668	147	.066		
	Total	19.527	150			

a. Predictors: (Constant), log.?, UCS (Mpa.), Thrust(kN/mm)  
b. Dependent Variable: Measured ROP

Coefficients <sup>a</sup>						
Model		Unstandardized Coefficients		Standardized Coefficients	t	Sig.
		B	Std. Error	Beta		
1	(Constant)	.790	.175		4.509	.000
	UCS (Mpa.)	-.003	.001	-.198	-2.654	.009
	Thrust(kN/mm)	.031	.003	.727	9.713	.000
	log.?	.428	.064	.391	6.727	.000

a. Dependent Variable: Measured ROP

Figure 2.7: SPSS model coefficients.

#### 2.1.5.4 Automatic Linear Modeling

In this section detailed method for performing automatic linear modeling is described Figs. 2.8-2.11. Assumptions are same as for "Linear Regression Modeling". But variable input and brief case history and method used for analysis is described. Total of five tunnel sites are taken into account and data analysis that is carried out is separated from already done work.

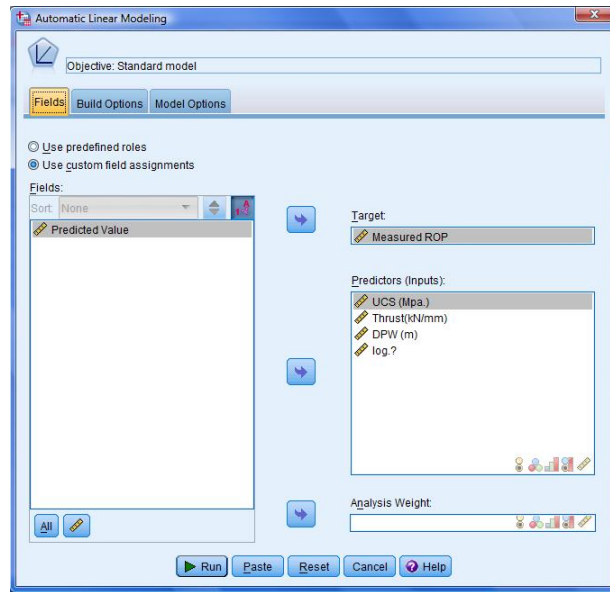


Figure 2.8: Automatic linear modeling.

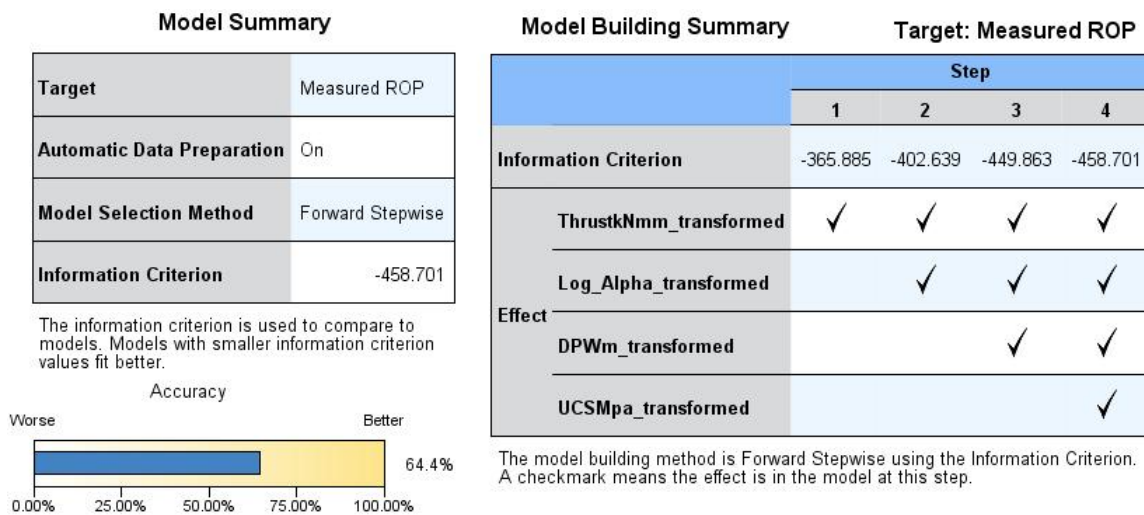


Figure 2.9: Model summary.

Procedure for automatic linear modeling is very simple. Select input variables and output variable as target to be predict. Go to model options and set model procedure as step-forward and check out model output save option. Then press the run button, model summary, model effects, coefficients are displaced on output file. model summary shows the method of model selection e.g step-forward, target variable and accuracy of the model. Using coefficients, a linear prediction model can be formulated as shown in Eq. 2.1.

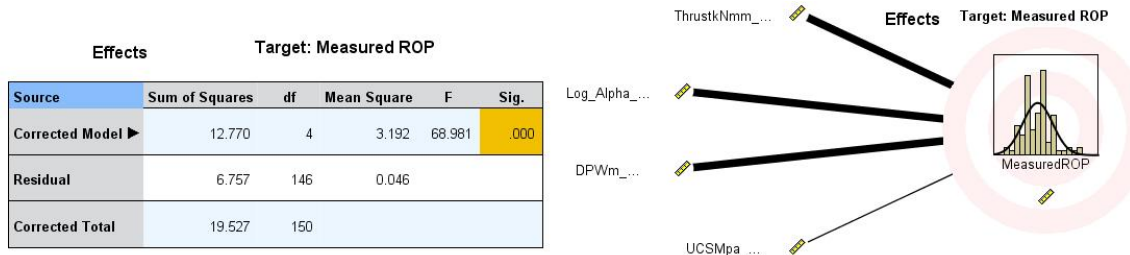


Figure 2.10: Effects of input parameters.

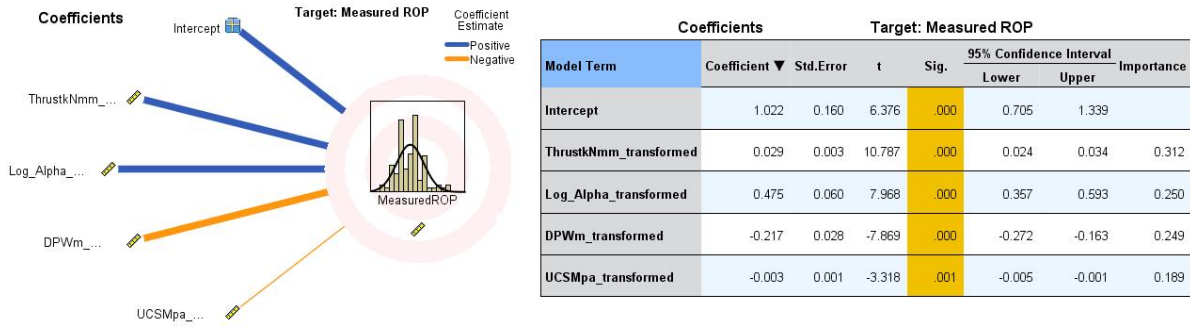


Figure 2.11: Table of coefficients.

Finally predicted values obtained from Eq. 2.1 can be plotted in the form of scattered and line plot as shown in Figs. 2.12 and 2.13 respectively.

$$ROP(m/h) = 1.022 + 0.029Thrust + 0.475Log(\alpha) - 0.217DPW - 0.003UCS \quad (2.1)$$

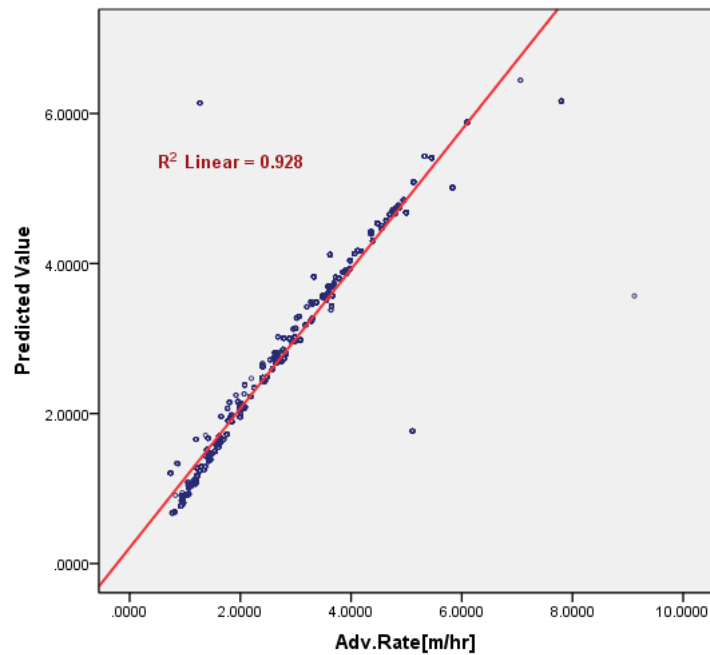


Figure 2.12: Scattered plot between actual and SPSS predicted value.

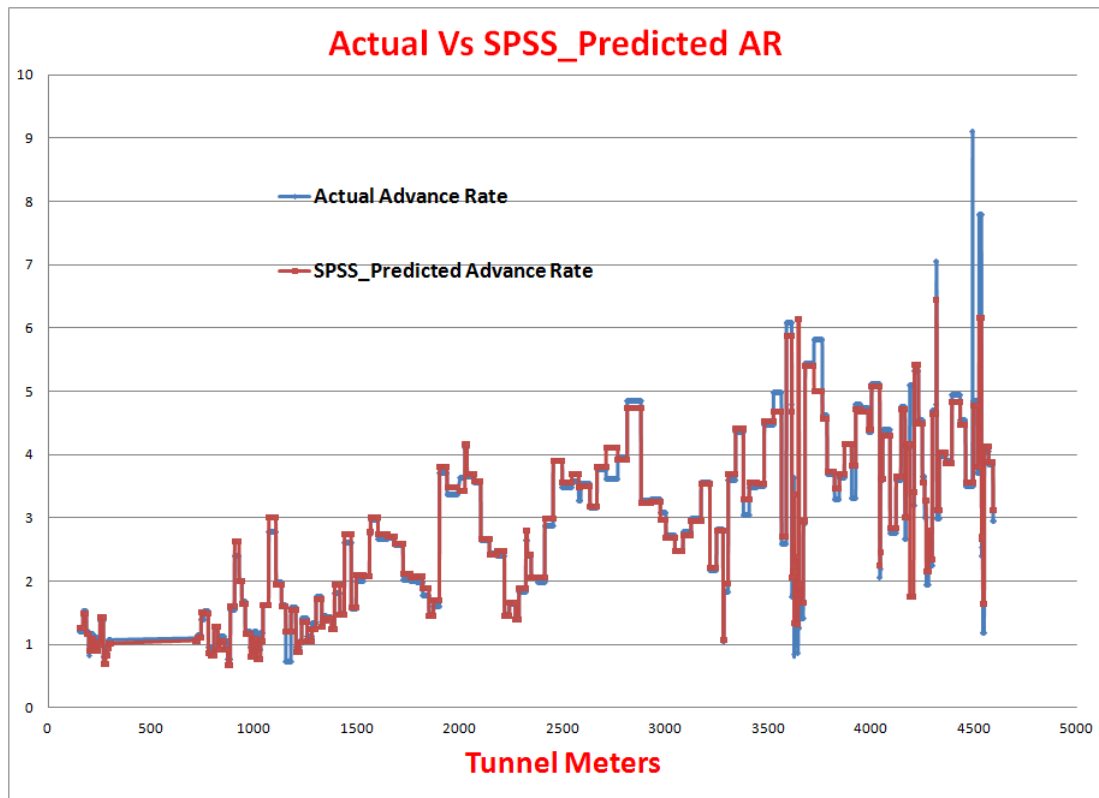


Figure 2.13: SPSS predicted AR line plot.

### 2.1.6 Partial and Bi-variate Correlations

In Bi-variate correlations, the relationship between two variables is measured. The degree of relationship table 2.1 (how closely they are related) could be either positive or negative.

**Correlations**

		Thrust[M.Pa]	Power [kw]	Adv.Rate [m/hr]
Thrust[M.Pa]	Pearson Correlation	1	-.112 <sup>**</sup>	-.740 <sup>**</sup>
	Sig. (2-tailed)		.000	.000
	N	4021	4013	4021
Power [kw]	Pearson Correlation	-.112 <sup>**</sup>	1	.532 <sup>**</sup>
	Sig. (2-tailed)	.000		.000
	N	4013	4013	4013
Adv.Rate[m/hr]	Pearson Correlation	-.740 <sup>**</sup>	.532 <sup>**</sup>	1
	Sig. (2-tailed)	.000	.000	
	N	4021	4013	4021

\*\* . Correlation is significant at the 0.01 level (2-tailed).

Table 2.1: Bi-variant correlation.

Pearson correlation coefficient shows linear interdependence between two parameters,

when frequency distributions of both interlinked variables are normal. The maximum number could be either +1 (positive) or -1 (negative). This number is the correlation coefficient. A zero correlation indicates no relationship and value close to +1 shows strong positive correlation [25]. The Bi-variate correlations procedure computes Pearson's correlation coefficient, Spearman's rho, and Kendall's tau-b with their significance levels Fig. 2.14. Correlations measure how variables or rank orders are related. Before calculating a correlation coefficient, screen your data for outliers and evidence of a linear relationship. Pearson's correlation coefficient is a measure of linear association. Two variables can be perfectly related, but if the relationship is not linear, Pearson's correlation coefficient is not an appropriate statistic for measuring their association. Spearman's and Kendall's correlation coefficients indicate degree of linear relationship between two variables, when frequency distributions of both interlinked variables are not perfect linear.

**Correlations**

			Thrust[MPa]	Adv.Rate [m/hr]
Kendall's tau_b	Thrust[MPa]	Correlation Coefficient	1.000	-.510**
		Sig. (2-tailed)	.	.000
		N	4189	4188
	Adv.Rate[m/hr]	Correlation Coefficient	-.510**	1.000
		Sig. (2-tailed)	.000	.
		N	4188	4188
Spearman's rho	Thrust[MPa]	Correlation Coefficient	1.000	-.692**
		Sig. (2-tailed)	.	.000
		N	4189	4188
	Adv.Rate[m/hr]	Correlation Coefficient	-.692**	1.000
		Sig. (2-tailed)	.000	.
		N	4188	4188

\*\* . Correlation is significant at the 0.01 level (2-tailed).

Figure 2.14: Spearman's and Kendall's correlation coefficients.

Partial correlation measures the degree of relationship between two random variables, with the effect of a set of controlling random variables removed. In fact, the first-order partial correlation is nothing else than a difference between a correlation and the product of the removable correlations divided by the product of the coefficients of alienation of the removable correlations. The Partial correlations procedure computes partial correlation coefficients that describe the linear relationship between two variables while controlling for the effects of one or more additional variables [25]. Pearson correlation coefficients are referred to the data, that is normally distributed and if the data sets are randomly distributed then, Spearman and Kendall correlation coefficients are determined.



# Chapter 3

## Case Descriptions

### 3.1 Hieflau Power Plant (Expansion Tunnel)

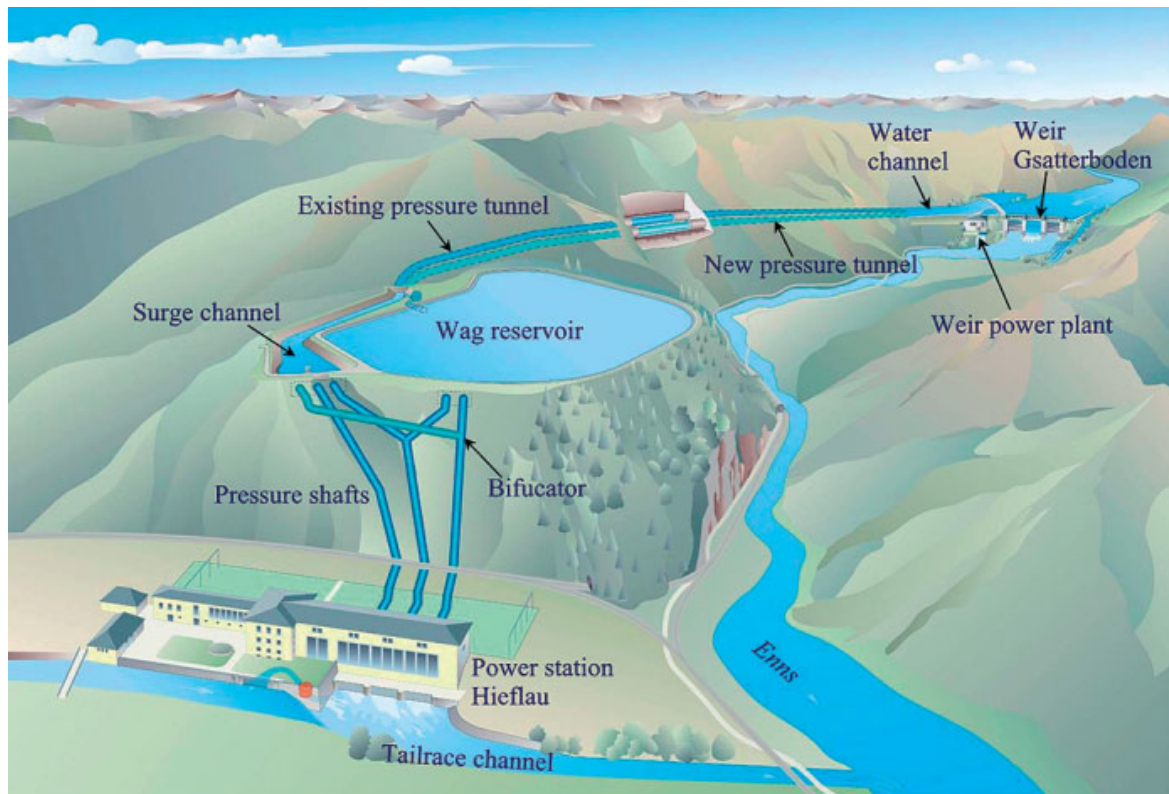


Figure 3.1: Hieflau expansion tunnel layout [26].

The Hieflau, 63 MW diversion HPP (hydro power plant), located along the river Enns in Styria, enhanced the power supply in a first stage about 50 years ago by construction of a reservoir (Wag storage) for daily storage. The next stage of the enhancement project Fig. 3.1 started in 2005 by carrying out a feasibility study, followed by site investigations and elaboration of an upgraded scheme. Environmental aspects play an important role due to the vicinity to the Gesäuse National Park and some particular ecological requirements

had to be especially considered in the upgraded scheme [26]. The Hieflau power plant expansion includes an increase in discharge water volume from  $60 \text{ m}^3/\text{sec.}$  to  $90 \text{ m}^3/\text{sec.}$  The planned changes will increase the standard capacity of the power plant, which began operation in 1955, by approximately  $70 \text{ GWh/year}$ . In addition to the necessary adaptation and renovation of the inlet and outlet structures, the newly built motive water tunnel will be the centerpiece of the expansion [27]. Technical data of the Hieflau TBM is displayed in table 3.1.

1	Excavation Diameter	6.18 <i>m</i>
2	Disc cutters, back loading	17 <i>in</i>
3	Number of cutting discs	43
4	Max. recommended average cutter load	267 <i>kN</i>
5	Max. cutter-head thrust	11.481 <i>kN</i>
6	Max. power rating per main drive unit	180 <i>kW</i>
7	Number of main drive units	8
8	Cutter-head drive	1440 <i>kW</i>
9	Cutter-head speed	0–8 <i>rpm</i>
10	Max. Torque at speed range	3440 <i>kNm</i> at the rate of 0–4 <i>rpm</i>
11	Torque at max. power rating (max. speed)	1720 at the rate of 8 <i>rpm</i>
12	Breakout torque (0–5 Hz, max. 60 s)	4470 <i>kNm</i>
13	Max. Hydraulic system pressure	345 <i>bar</i>
14	Stroke of main thrust cylinder	1.320 <i>mm</i>
15	Primary voltage	16 <i>kV</i>
16	Secondary voltage	660, 400, 110 <i>V</i>
17	Frequency (power supply)	50/60 <i>Hz</i>
18	TBM conveyor belt width	762 <i>mm</i>
19	Max. conveyor speed	3 <i>m/s</i>
20	Machine weight	500 <i>t</i>

Table 3.1: Technical data of the Hieflau TBM.

The new motive water tunnel has an interior diameter of 5.6 *m*. In the continuously-driven sections, lining was done with reinforced concrete tubbing where cyclical driving is used, the lining are cast-in-place concrete shell [27].

### 3.1.1 Description of the Hieflau Project

Head-race tunnel for the Hieflau hydro-power station.

Hard rock double shield:*TBM* , *RobbinsDS – TBM – Model194 – 272 – 2*

No. of disc cutters: 43

Tunnel length: 4918*m*

Drill and blast excavation X-section: 34.0 – 42.0*m*<sup>2</sup>, Length: 810 *m*

**TECHNICAL DATA** Average advance rate: 27.5*m/day*

Best advance rate:  $52.3m/day$

Lining: Parallel-System mono-shell segment ( $w = 20cm$ )

### 3.1.2 Hieflau Headrace Tunnel Geology

The project area lies in the eastern part of the limestone Gesäuseberge Alps south of the Enns valley, which is partially narrowed as a gorge. The stratification of the rock shows a typical triadic limestone alpine sequence of strata, with Ramsau dolomite over Raibler beds and saddle-stone Dolomite down to large stretches of the predominant saddle-stone limestone Fig. 3.2. The alignment of the second tunnel runs parallel and in a distance of not more than  $30\text{ m}$  to the existing one. Most information about the geological conditions along this route is derived from the mapping of the first pressure tunnel.

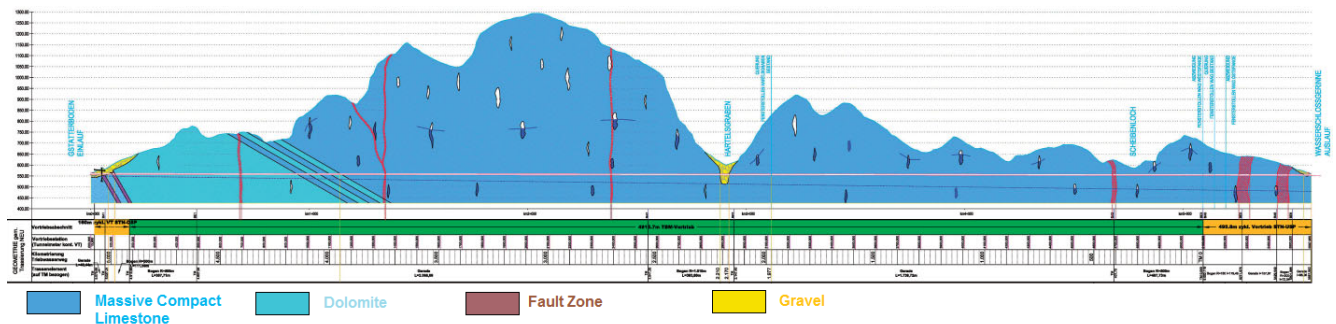


Figure 3.2: Geology of Hieflau headrace tunnel [26].

Additionally some site investigations were carried out to gain a well mapped basis about the geology of the new headrace tunnel [28]. The large part of the TBM tunnel is excavated in good rock conditions, predominantly Limestone and Dolomite. In Limestone some small fault zones and some local karstic cavities with diameters up to  $0.5\text{ m}$  are predicted.



(a) Hieflau expansion tunnel [29].



(b) Segmental lining system [26].

Figure 3.3: The Hieflau hydro power project, TBM and lining segments.

Doppelschild - TBM Robbins 194-272-2, Ø6,18m									
Tagesbericht Data Logger Import									
Datum		10/19/2008							
Bericht Nr.		188							
1	2	3	4	5	6	7	8	9	
ÖBA									
Date	Time	Approx. Chainage	TBM					Perlkies	Leistung TBM
			CHD Speed	CHD Torque	CHD Thrust Gross	Penetration Rate	Penetration		
[tt.mm.jjjj]	[hh:ss:mm]	[m]	[Rpm]	[kNm]	[kN]	[mm/min]	[mm/U]	[m <sup>2</sup> ]	[kW]
10/19/2008	0	35.95	6.91	1.802	10.340	114	17	32.402	0
	0	3335.06	7.25	1.259	8.199	53	7	[U]	0
	0	3355.89	7.49	1.875	10.670	120	18	4.696	0
	0	3319.94	0.58	73	330	6	1	0.000	0
10/19/2008	08:00:00	3,319.94	7.29	1,699	9,460			0.000	
10/19/2008	08:00:10	3,319.95	7.30	1,699	9,350	72.00	10	0.000	
10/19/2008	08:00:20	3,319.96	7.20	1,724	9,680	60.00	8	0.000	
10/19/2008	08:00:30	3,319.97	7.32	1,187	8,800	48.00	7	0.000	
10/19/2008	08:00:40	3,319.97	7.27	1,763	9,350	66.00	9	0.000	
10/19/2008	08:00:50	3,319.98	7.30	1,492	8,910	42.00	6	0.000	
10/19/2008	08:01:00	3,319.99	7.28	1,578	9,130	48.00	7	0.000	
10/19/2008	08:01:10	3,320.00	7.31	1,256	8,690	42.00	6	0.000	
10/19/2008	08:01:20	3,320.01	7.31	1,342	8,250	84.00	11	0.000	
10/19/2008	08:01:30	3,320.02	7.30	1,385	8,360	54.00	7	0.000	
10/19/2008	08:01:40	3,320.03	7.28	1,496	8,800	36.00	5	0.000	
10/19/2008	08:01:50	3,320.04	7.31	1,393	8,030	48.00	7	0.000	
10/19/2008	08:02:00	3,320.04	7.32	1,264	8,030	66.00	9	0.000	
10/19/2008	08:02:10	3,320.05	7.26	1,600	8,580	48.00	7	0.000	
10/19/2008	08:02:20	3,320.06	6.89	1,772	9,460	66.00	10	0.000	
10/19/2008	08:02:30	3,320.07	7.34	882	7,260	36.00	5	0.000	
10/19/2008	08:02:40	3,320.08	7.30	937	7,150	42.00	6	0.000	
10/19/2008	08:02:50	3,320.09	7.30	869	6,930	30.00	4	0.000	
10/19/2008	08:03:00	3,320.10	7.27	1,359	8,250	42.00	6	0.000	
10/19/2008	08:03:10	3,320.10	7.28	1,458	8,800	66.00	9	0.000	
10/19/2008	08:03:20	3,320.11	7.30	1,170	7,920	24.00	3	0.014	
10/19/2008	08:03:30	3,320.12	7.32	1,320	8,140	66.00	9	0.021	
10/19/2008	08:03:40	3,320.13	7.31	1,458	8,800	60.00	8	0.014	
10/19/2008	08:03:50	3,320.14	7.31	1,531	8,910	60.00	8	0.014	
10/19/2008	08:04:00	3,320.15	7.32	1,548	9,020	66.00	9	0.014	
10/19/2008	08:04:10	3,320.16	7.29	1,651	9,240	54.00	7	0.021	
10/19/2008	08:04:21	3,320.17	7.32	1,608	9,680	60.00	8	0.014	
10/19/2008	08:04:31	3,320.17	7.29	1,604	9,350	54.00	7	0.014	
10/19/2008	08:04:41	3,320.18	7.29	1,591	9,680	72.00	10	0.021	
10/19/2008	08:04:51	3,320.19	7.29	1,501	9,570	54.00	7	0.014	

Table 3.2: Hieflau TBM data logger [27].

The challenge of the TBM-drive is the crossing of a 40 m wide section in soft ground conditions (Hartelsgraben). Within this zone loose rock boulders Fig. 3.3, bedded in

a matrix of fine materials such as sand and clay were observed. In view to the hydrogeological condition water in flow of 2 l/s were predicted in the related section. TBM data were recorded automatically in the form of excel sheet at the time of excavation as listed in table 3.2. In this thesis data from Prof. Dr. Rainer Poisel in excel format is received. It is stated here clearly that a Master Thesis by Viktoria Ostermann is written on this Hieflau power project. Already work done by Ostermann includes:

- Correlations between all TBM parameters and Rock parameters e.g. Thrust vs Advance Rate, Thrust vs Rock Fracture Class (RFC) etc.
- Box plots for all parameters
- Determination coefficients
- Scatter diagram
- 3-D analysis, for machine velocity, torque, thrust, power, advance rate and degree of disintegration (RFC)
- Statistical analysis using software “R”

But, Ostermann had written in her thesis abstract that “ No significant relationship between the TBM data and the different rock types could be determined”. In this dissertation extended analysis by using Fuzzy logic, Math-Lab code and a commercially available software SPSS19 is done. Good results are obtained that will be presented in coming chapter.

## 3.2 Queens Water Tunnel

New York City Tunnel no. 3 is Fig. 3.4 one of the most complex and intricate engineering projects in the world. Constructed by the New York City Department of Environmental Protection (DEP), the tunnel will eventually span 60 miles and is expected to be complete by 2020. The total cost of the project was expected to be about US \$6 billions [30]. The size and length of the tunnel, its sophisticated control system, the placement of its valves in special chambers and the depth of excavation, represent state-of-the-art technology. While city tunnel no. 3 will not replace city tunnels no. 1 and no. 2, it will enhance and improve the adequacy and dependability of the water supply system and improve service and pressure to outlying areas of the city. It will also allow the DEP to shut down, inspect and repair city tunnels nos. 1 and 2 for the first time since they were activated in 1917 and 1936 respectively [30]. The Queens Water Tunnel 3, stage 2 is intended to improve fresh water distribution throughout the City of New York, USA. The tunnel being about 7.5 km long and 7 m in diameter was excavated beneath Brooklyn and Queens at an

average depth of 200 m below the sea level in West-Central Queens County with using a high power TBM. Construction of stage 2, is greatly accelerated by a mechanical rock excavation technology [31].



Figure 3.4: Queen water tunnel [32].

A tunnel boring machine (TBM), which has been lowered in sections and assembled at the bottom of the shaft, will chip off sections of bedrock through the continuous rotation of a series of steel cutting tools (cutters) mounted on a large-diameter, full-circular, welded steel cutter head. The machine body of a TBM, which can be as long as 50 feet, is mounted behind the cutter head. It contains the drive motors and other electrical, mechanical and hydraulic equipment that provide the necessary thrust and torque that is transmitted to the cutters through the cutter head. The TBM, also known as “The Mole”, replaces the conventional drilling and blasting methods used during the construction of Stage 1. It is expected that the improved technology will allow tunnel workers to excavate at an average of 50 feet/day at a diameter of 23 feet more than twice the rate previously in water tunnel construction through drilling and blasting methods [33]. Another

important advantage to using the TBM is it bores into the rock, there is less damage at the point of excavation and no noise at the surface to disturb surrounding communities.

1	TBM diameter	7.06 <i>m</i> (23 <i>ft</i> 2 <i>in</i> )
2	Diameter range	6.50 <i>m</i> to 8.50 <i>m</i>
3	Cutter size	482.6 <i>mm</i> (19 <i>in</i> )
4	TBM model	Robbins 235 – 282 <i>HP</i> (High Performance)
5	TBM type	Open
6	Max. Cutter load capacity	311 <i>kN</i>
7	Number of cutters	50
8	Cutter-head Thrust	15,550 <i>kN</i>
9	Cutter-head power	3150 <i>kW</i> (4220 <i>hp</i> )
10	Cutter-head Torque	3624 <i>kNm</i>
11	Cutter-head Speed	8.3 <i>rpm</i>
12	TBM weight	610 <i>metric tons</i>

Table 3.3: Specification of TBM for Queens water tunnel [34].

Underground fabrication of the high performance, open type hard rock TBM diameter of 23' commenced by September 1996, after a year of on-site utility and equipment installation. Specifications of TBM for Queens water tunnel are listed in table 3.3.



Figure 3.5: TBM for Queens water tunnel [31], [33].

The TBM, which had been shipped from Chesterfield, England in June 1996 and delivered in 28 truckloads of assemblies and parts, was designed and engineered by the Robbins-Atlas-Copco Company. Since the inception of mining northeastward from the Maspeth (Shaft 19B) in late October 1996 and completion in October 1999, five miles of tunnel have been excavated, producing a 23' – 2''- wide, sub horizontal fresh bore hole through this deeply eroded crystalline portion of the Appalachian mountain chain [33]. Geological condition can be quantified as frequency and orientation of discontinuity in rock mass as well as main regional/global geological structures such as faults and

shear zones encountered in the field. Further, intact rock properties including strength and brittleness should also be considered for performance analysis in mechanical tunnels. Charles Merguerian, “Brittle Faults of the Queens Tunnel Complex, NYC Water Tunnel ” and Saffet Yagiz, “Utilizing rock mass properties for predicting TBM performance in hard rock condition”, have done a lot of work on the data of the Fig. 3.5. Specially Yagiz 2007 draw frequency distribution graph for unconfined compressive strength (UCS), punch slope index (PSI),  $\alpha$  angle, distance between plane of weakness (DPW) and rate of penetration (ROP), along with this, he plotted 2-D correlation of ROP with all rock properties. Moreover Yagiz formulated an empirical model for ROP and compared it with measured ROP values [33]. In this thesis data from Saffet Yagiz 2007 research paper is taken and analyzed for prediction of ROP using all rock properties. Moreover a statistical model for ROP and rock fracture class (RFC) was developed and compared with Hieflau, Vereina, Hemerwald and the Italian Alps tunnel data.

### 3.3 Vereina Tunnel

The Vereina tunnel (Fig. 3.6) is 19050 *m* long with an overburden amounting up to as much as 1500 *m*. The tunnel is essentially single track. In the middle and at both ends approx. 2 *km* long twin track and triple track sections allow trains to pass each other. The drive was carried out by drill and blast in the twin and triple track sections with cross sections from 70 – 85 *m*<sup>2</sup> resp 135 *m*<sup>2</sup> and in the single track section at the south side (with a cross section of 39 – 42 *m*<sup>2</sup>) and by TBM in the single track section at the north side (cross section of 46 *m*<sup>2</sup>) (Fig. 3.7). Two-thirds of the entire length of the tunnel are located in the Silvretta crystalline, an old crystalline complex which was minor affected by the alpine folding and which mainly comprises gneiss and amphibolites the latter being extremely hard and tough rocks. All these formations are bedded horizontally or sub-horizontally, like the sedimentary formations lying underneath.





Figure 3.6: Vereina tunnel east portal [35].

The Vereina tunnel was designed and built with a monocoque shotcrete lining, which was applied for the first time in this manner in a open TBM (Figs. 3.7-3.8) . At the time of the construction of the Vereina tunnel (1993 – 1999) considerable developments had been made since the time of the construction of the Furka Base Tunnel yielding steel arches, epoxi-resin glass fiber reinforced rock-bolts and wet mix sprayed concrete, thus resulting in remarkable higher qualities (like  $60 \text{ N/mm}^2$  unconfined compressive strength for sprayed concrete after 28 days) and extended durability. The temperatures were again fairly low with  $28^\circ\text{C}$  at the maximum. Technical data for this TBM is listed in table 3.4 and statistical analysis done by Viktoria Ostermann, Fuzzy logic rock mass classification (RMC) by Poisel et al. The author received Vereina tunnel data as excel format from Prof. Dr. Rainer Poisel and tried to analyze all data using Excel, Origin Pro 8, Kaleida graph, Math-Lab tools like Fuzzy logic and Math-Lab code. Moreover statistical modeling was carried out using software packages “IBM – SPSS19”.

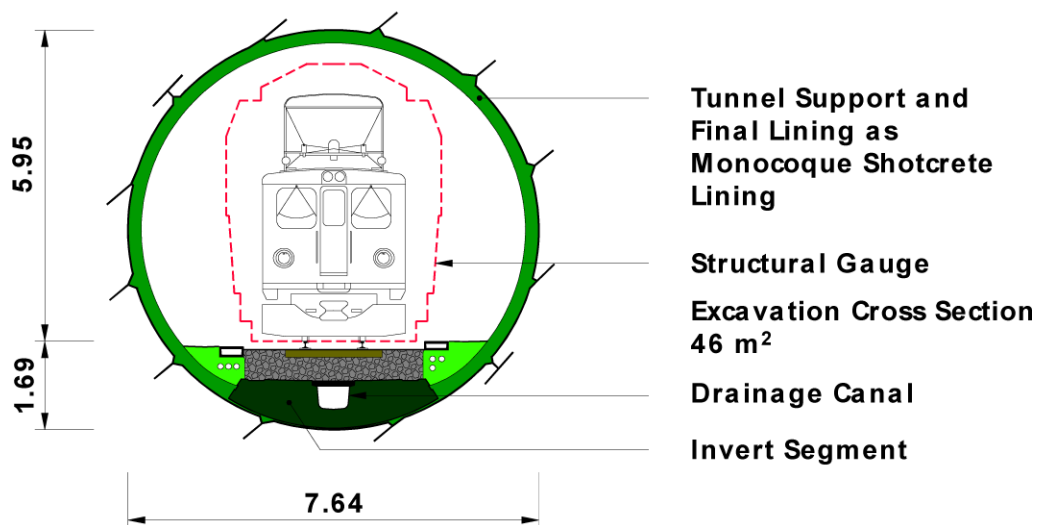


Figure 3.7: Vereina tunnel X-section [36].

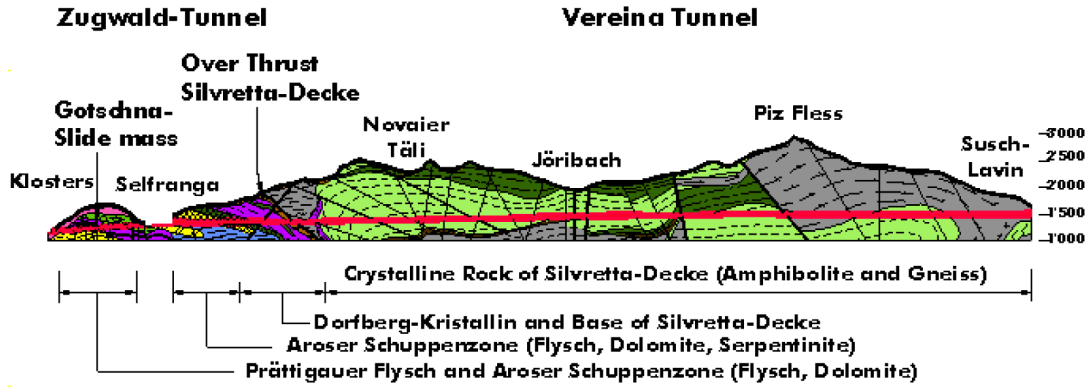


Figure 3.8: Geological longitudinal X-section of Vereina tunnel [36].

1	TBM diameter	7.64 m
2	Number of cutter	51
3	Diameter of cutter	191 m
4	Maximum individual cutter load	311 kN
5	Cutter-head operating thrust	17.105 kN
6	Maximum Operating Thrust	22.934 kN
7	Maximum Hydraulic Pressure	345 bar
8	Number of Drive motors	10
9	Power/Drive Motor	300kW
10	Total Cutter-head Power	3000 kW
11	Cutter-head Speed	0 – 4.63 rpm
12	Number of Thrust Cylinders	4
13	Primary Voltage	10,000 V
14	Secondary Voltage	690/380 V
15	Conveyor Belt Capacity	1,100 $\frac{m^3}{hr}$

Table 3.4: Vereina TBM technical data.

### 3.4 Hemerwald Tunnel

Hemerwald tunnel (Fig. 3.9) is 4720 m long pressure tunnel excavated by Tiroler Water Power Company. Leading from a highly situated (1900 m) side valley to the Penstock leading to the Inn valley at sea level 645 m. Maximum overburden was 1250 m. It was built by using Robbins Series 120 TBM. Technical data of the Hemerwald tunnel TBM are listed in table 3.5.



Figure 3.9: Hemerwald tunnel TBM [courtesy, Ewald Tentschert].

1	TBM diameter	3.90 m
2	Cutter-head	Cutter-Disc 14"
3	No. of cutters	32cutters, 2.68 cutters/m <sup>2</sup>
4	Installed Power	4 × 125 HP= 500 HP
5	Power Supply	6000 Volts
6	RPM	5.6 rpm Constant
7	Maximum peak out put	595 hp
8	Normal Operating power	452 hp
9	Maximum Thrust of the TBM	421.4 kN
10	Maximum Power Consumption of the TBM	339.63 kW

Table 3.5: Technical data of Hemerwald tunnel TBM.

**Rock mass data:** Muscovite granite gneiss: 47.11%

Schist gneiss: 47.38%

Micaschists: 4.53

Granodiorite: 0.98%

Rock mass class (RMC) data

I . 69.1%

II . 21%

III . 3.2%

IV . 2.16%

V . 1.55%

- VI . 2.34%
- VII . 0.15%
- VIII. — — —

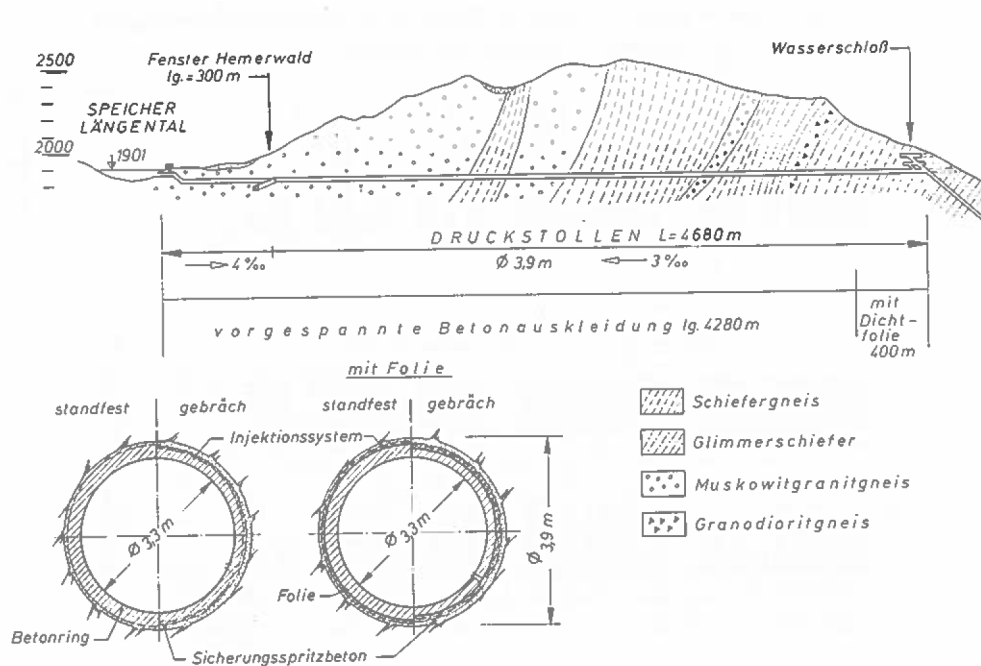


Figure 3.10: Geological profile and X-section of Hemerwald tunnel [?].

Geological profile and cross section view of the Hemerwald tunnel is displayed in Fig. 3.10. Data from this tunnel is received in the form of hard copy from Prof. Ewald Tentschert as shown in Figs. 3.11 and 3.12. No previous work is available online on the Hemerwald tunnel. Excel sheets from hard copy and logging data graphs were prepared and analyzed for 2-D and 3-D surface analysis in this thesis. Finally statistical models were established for RMC and advance rate using a statistical software SPSS19. Then separate excel data files were prepared for different types of rocks and analysed for Hemerwald tunnel.

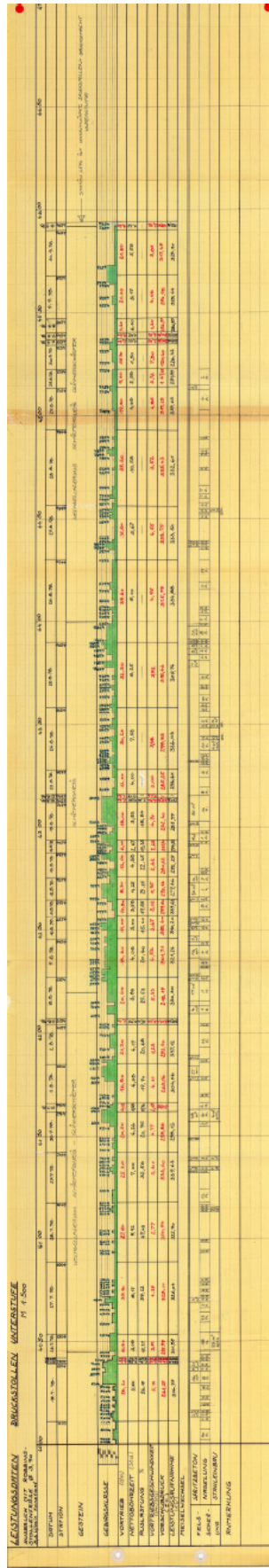


Figure 3.11: Original data file.

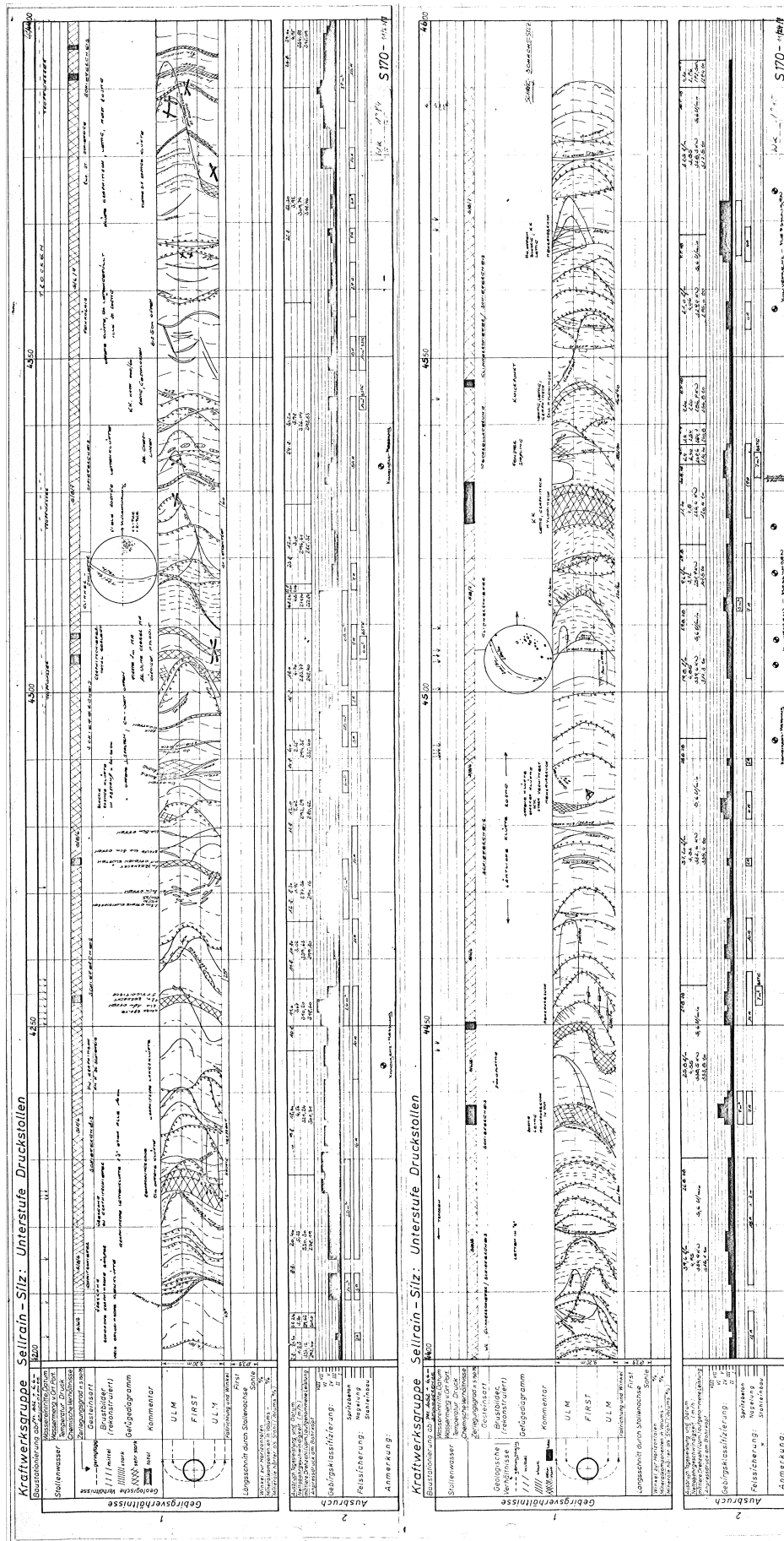


Figure 3.12: Tunnel log map.

### 3.5 Tunnels in the Italian Alps (Maen, Pieve and Varzo Tunnel)

Three tunnels (Maen, Pieve and Varzo) for hydraulic purposes were excavated by tunnel-boring-machines in mostly hard metamorphic rocks in Northern Italy (Fig. 3.13). A total of 14 km of tunnel was surveyed almost continually, yielding over 700 sets of data featuring rock mass characteristics and TBM performance. Technical data for these three tunnel is listed in table. 3.6. The empirical relations between rock mass rating and penetration rate clearly show that TBM performance reaches a maximum in the rock mass rating (RMR) range 40 → 70 while slower penetration is experienced in both too bad and too good rock masses . However different rocks gives different penetrations for the same RMR, the use of Bieniawski's classification for predictive purpose is only possible provided one uses a normalized RMR index with reference to the basic factors affecting TBM tunneling. Comparison of actual penetrations with those predicted by the Innaurato and Barton models shows poor agreement.

Description	Maen	Pieve	Varzo
Total tunnel length (m)	1750	9600	6600
Tot. excavation time (days)	413	809	468
Surveyed section length(m)	1750	6400	5800
Excavation diameter (m)	4.20	4.05	4.05
Tunnel slope (°)	24 – 35	≈ 0	≈ 0
TBM model	Wirth 340/420 E	Robbins1111-234-3	Robbins 1214-240/1
TBM type	Open	Double Shield	Double Shield
Number of cutters	36	27	27
Cutter spacing (mm)	66	75	75
Cutter diameter (in)	17	17	17
Maximum Thrust (kN)	7920	4602	8827
Boring stroke (m)	1.5	0.63	0.63
Cutter-head curvature	Domed	Flat	Flat
Cutter-head RPM	5.5 – 11	11.3	4.5 – 8.9

Table 3.6: Description of three tunnels and TBM technical data.

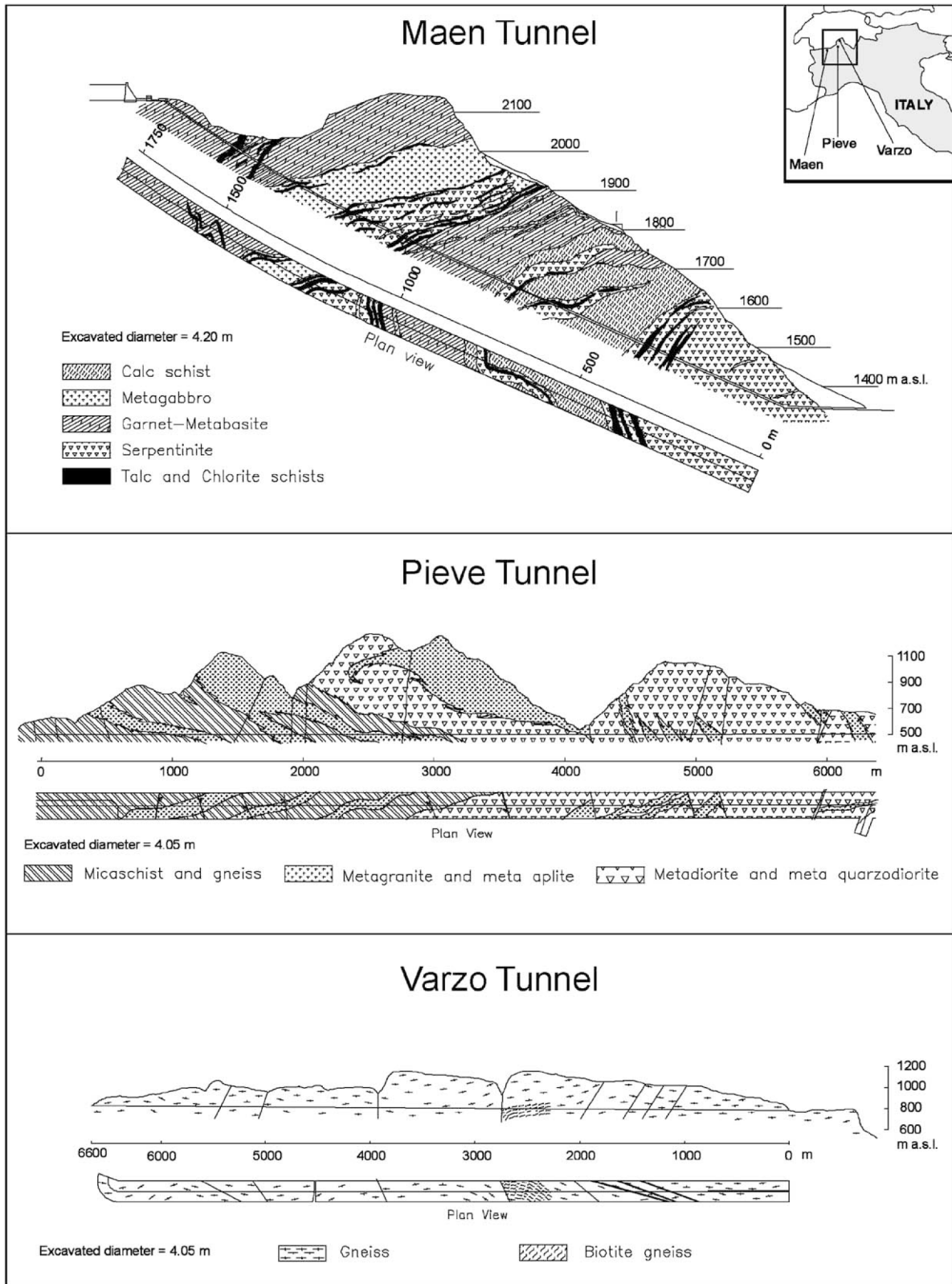


Figure 3.13: Maen-Pieve-Varzo layout [37].

M. Berti et al 2002, have done already a lot of analysis on these three tunnel data, including histogram plot, 2-D correlations between rock mass rating (RMR), thrust, penetration rate, Q-value, utilization coefficient and UCS. They also establish an empirical



correlation between penetration rate and RMR and then compared it with all available models. They conclude that penetration rate strongly dependent on rock type and quality of rock mass. In this research work data for these three tunnels from M. Berti by email is received and analyzed for all machine and rock parameters. A Fuzzy logic model and a Math-Lab code was written to predict the advance rate and RMR. Comparison of the results with existing data from Hieflau, Hemerwald, Vereina and Queens tunnel sites is done. Moreover, a statistical model is established for RMC, RMR and penetration rate using a commercially available software SPSS-19.

# Chapter 4

## TBM Data Analysis

### 4.1 Hieflau

#### 4.1.1 Hieflau Seismic Data

Seismic data for a section (Tunnel meters 137-2794) of Hieflau tunnel were recorded by Werner Chatwal et al. (TU Wien). TBM cutter-head was used as primary signal source.

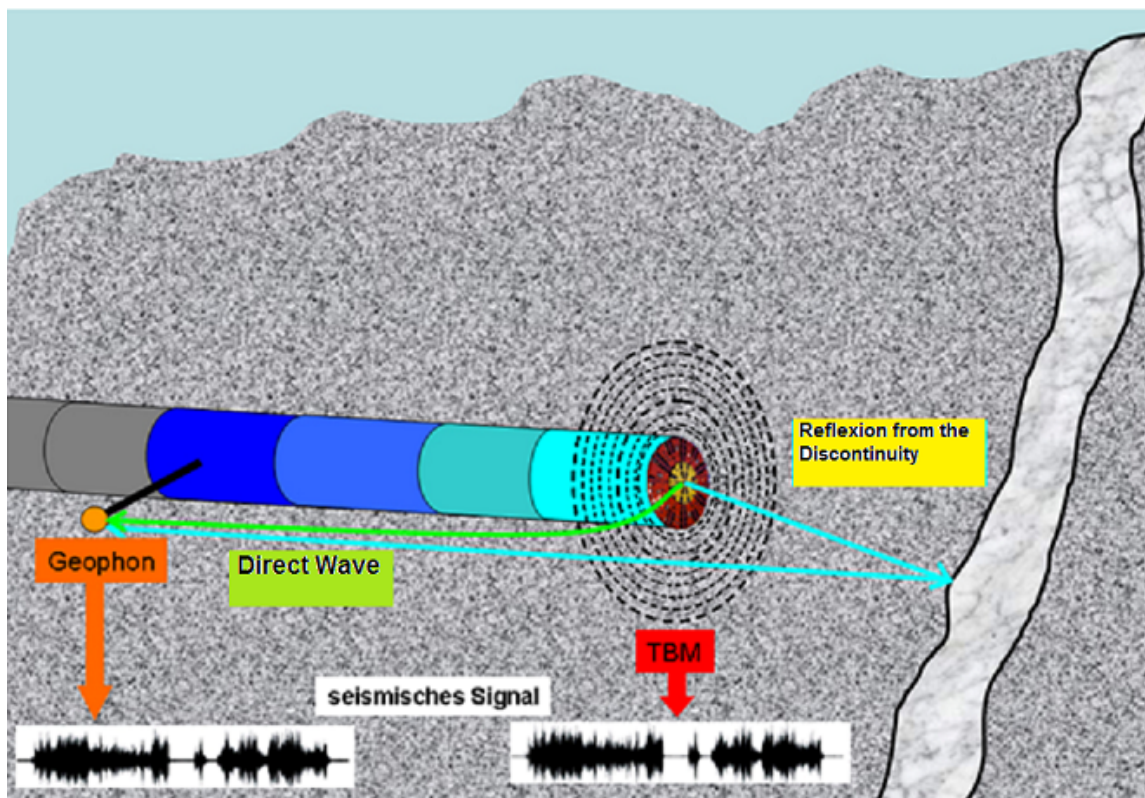


Figure 4.1: Seismic data recording procedure [38].

The signal is recorded directly on the machine disc cutters (for example: at the main cavity of the cutting head). This very interesting development is tunnel seismic while

drilling (TSWD), which has been derived from other seismic techniques using the seismic waves generated by the cutting head as a signal. The quasi-continuous signal generated by the cutting head in operation can be transformed to a normal seismogram by the use of a pilot signal measured directly at the source (cutting head). This technique can be adapted to the exploration ahead of a tunnel face. Conventional seismic traces are extracted from the recordings by the use of a pilot signal recorded near the cutting head of the TBM. The bandwidth of the seismic signals is  $> 200$  Hz, a high signal to noise ratio is achieved, and excellent conventional seismic traces are extracted. Method layout is described in Fig. 4.1. “Amplitude of ersteinsatz” is amplitude of the direct wave transmitted by source (TBM cutter-head), where as “amplitude of reflexion” is amplitude of reflected wave, transmitted from source and recorded after reflected from discontinuity. “Pseudo velocity” is a fake or false velocity of the seismic waves in the rock mass, which ranges from 2900 m/s to 5300 m/s for Hieflau tunnel [38]. Pseudo velocity mainly depends upon rock mass density and rock strength, more dense rock rock propagate more pseudo velocity.

### 4.1.2 Data Analysis with Excel

Hieflau tunnel data were coupled with seismic data recorded ahead of tunnel face during the excavation of the tunnel. Different correlations have been plotted between thrust and amplitude of reflexion, amplitude of ersteinsatz and pseudo velocity.

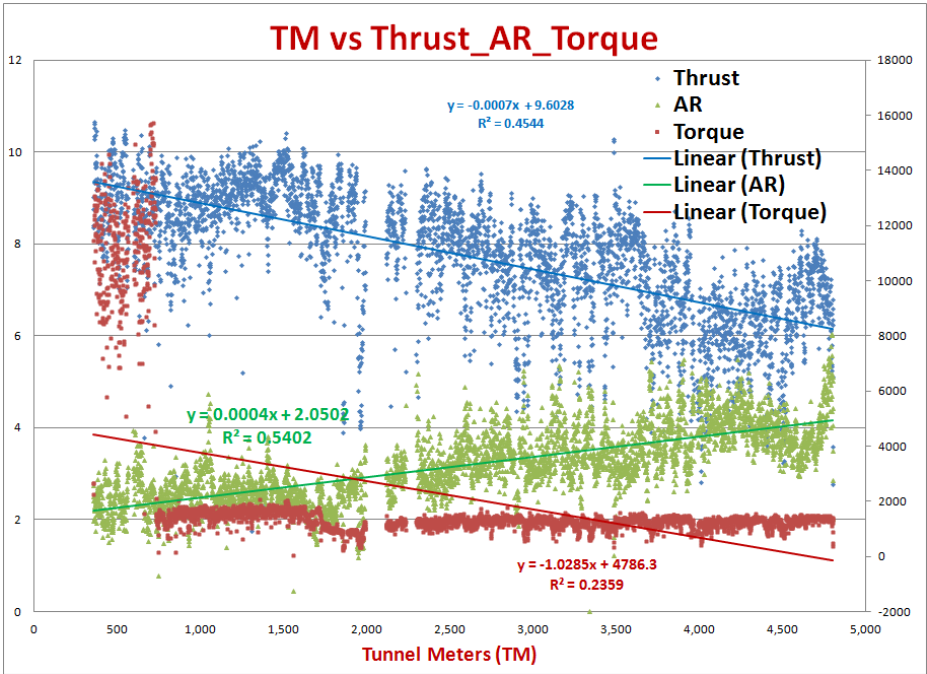
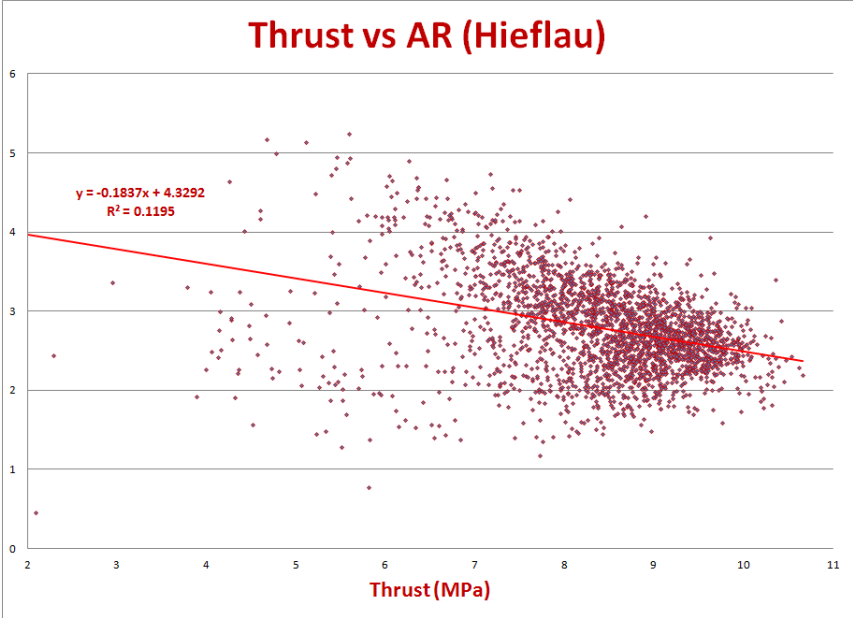


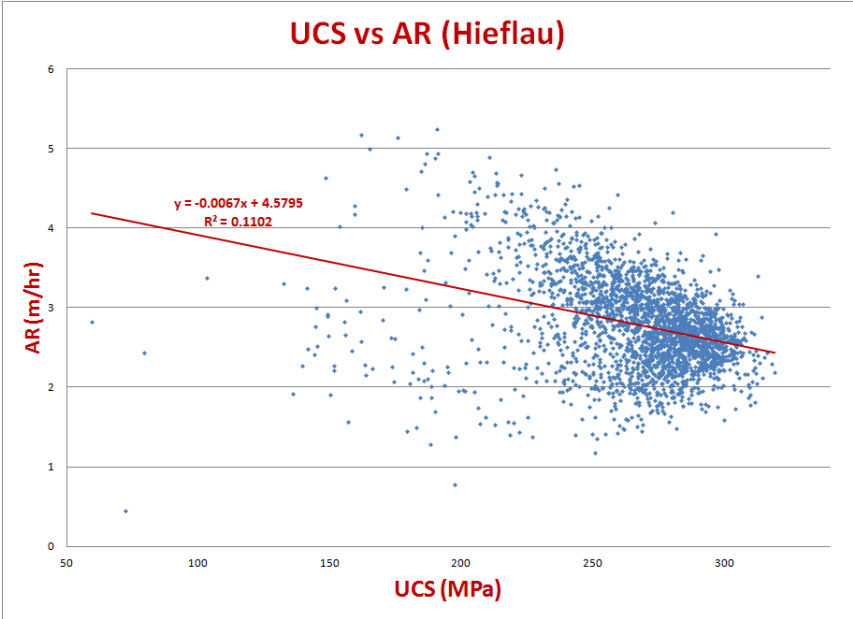
Figure 4.2: Chainage versus thrust, torque and AR.

Figure 4.2 shows trend of different variables along with chainage, it is clear that thrust and torque values are linearly decreasing with chainage, while advance rate is

linearly increased. Figs. 4.3(a,b) shows trend of AR against thrust and UCS respectively, UCS values are predicted after assuming a normal frequency distribution of UCS. Linear decreasing of advance rate in both cases, shows that AR is entirely dependent upon rock strength.



(a) Thrust versus AR.



(b) UCS versus AR.

Figure 4.3: 2-D graphs for TM, thrust, AR and torque.

In Fig. 4.4 thrust is plotted against amplitude of reflexion and ersteinsatz. Amplitude of ersteinsatz is almost independent of thrust, while amplitude of reflexion values are low at high thrust. Both trend lines show a maximum data point frequency at maximum thrust frequency.

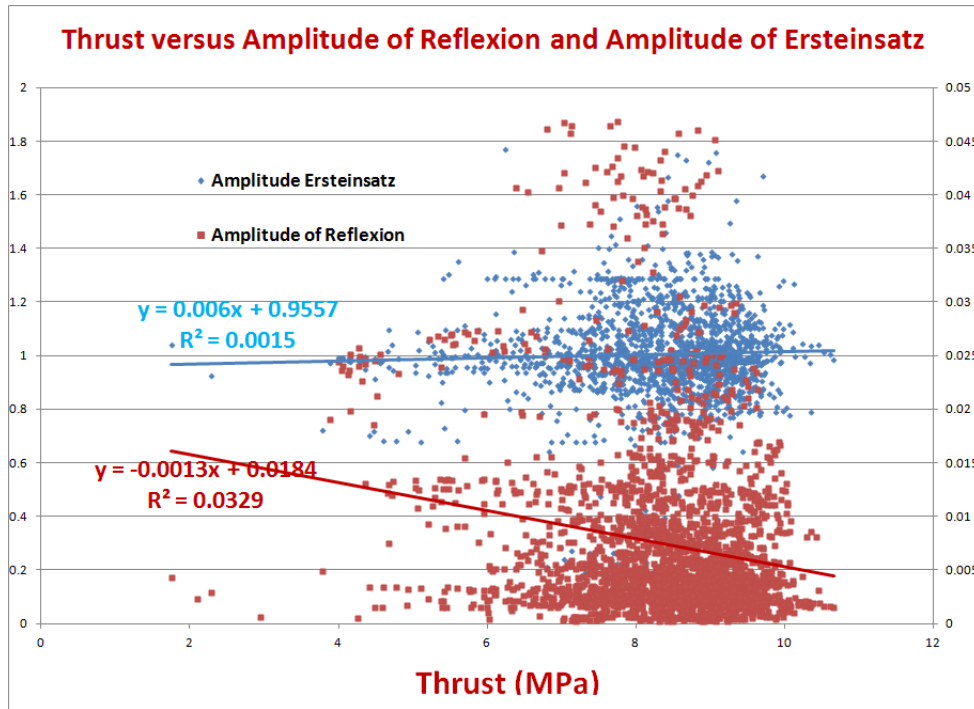
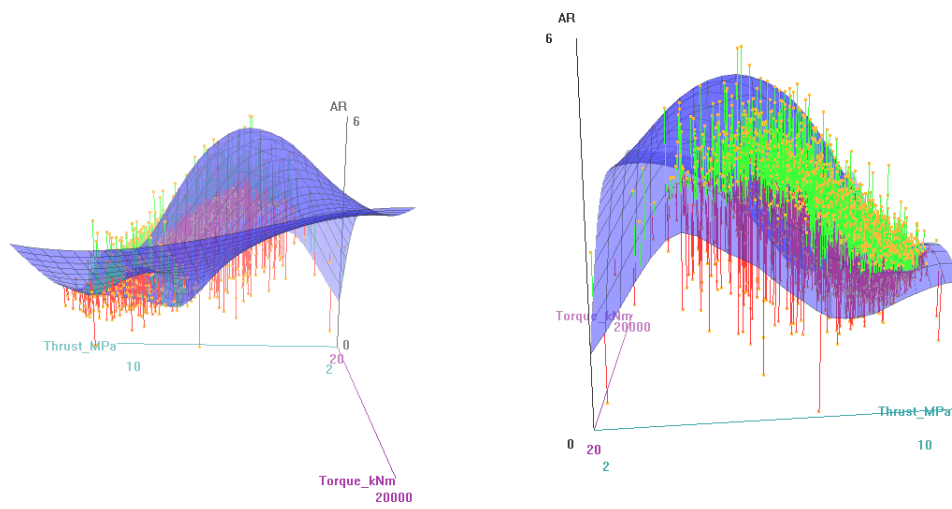


Figure 4.4: Thrust versus amplitude of ersteinsatz and reflexion.

### 4.1.3 3-D Data Analysis with “R”

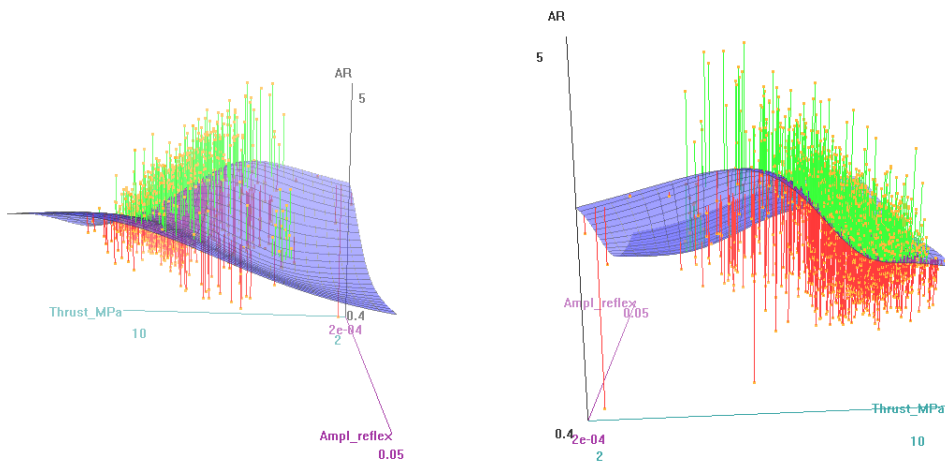
Figures 4.5(a,b) shows variation of AR versus thrust at low and high torque. At high torque, AR is linear to thrust, while at low thrust the relation is entirely complex like a sinusoidal wave, which reflect the effect of torque on chip formation and advance rate. This shows the reason behind the phenomenon of application of high torque motors in TBM.



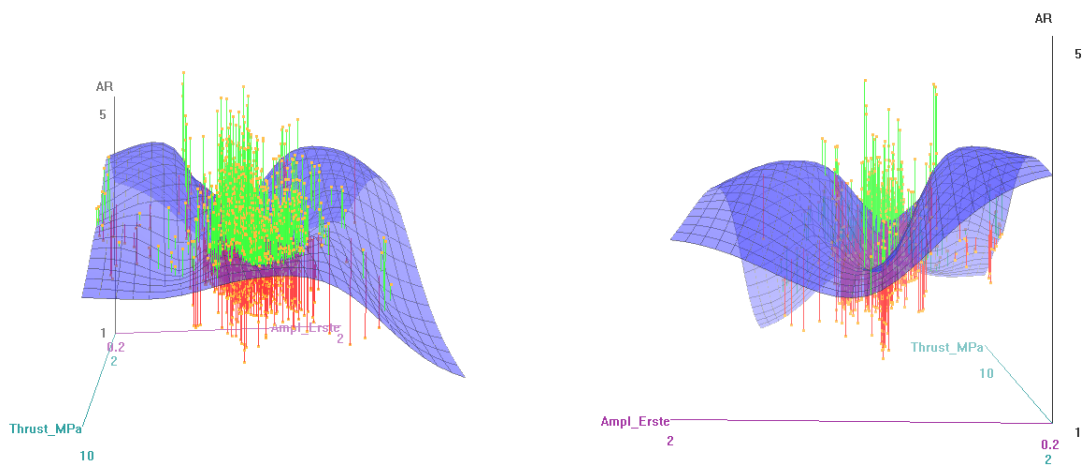
(a) Thrust versus AR at high torque.

(b) Thrust versus AR at low torque.

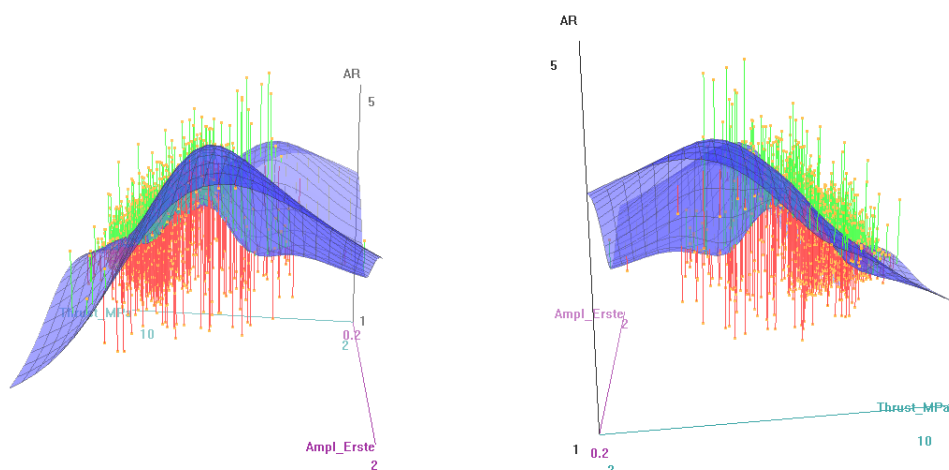
Figure 4.5: 3-D surfaces.



(a) Thrust versus AR at high amplitude of reflexion. (b) Thrust versus AR at low Amplitude of reflexion.



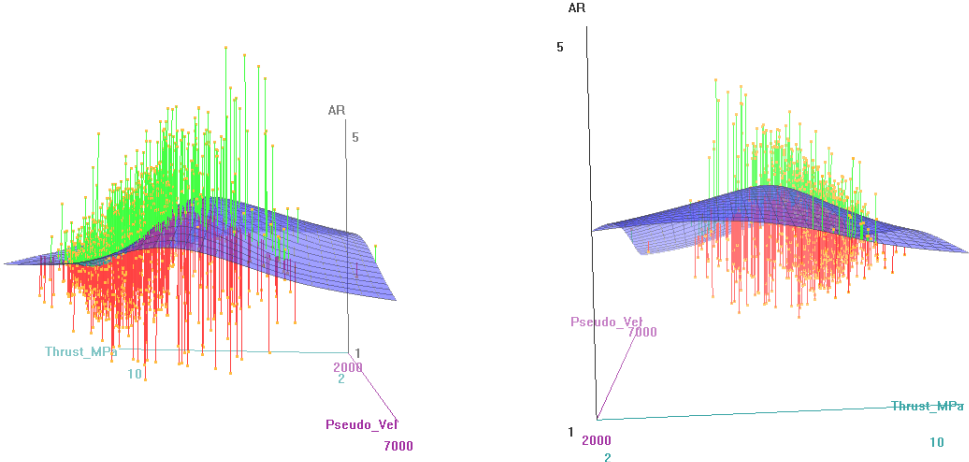
(c) Amplitude of ersteinsatz versus AR at high thrust. (d) Amplitude of ersteinsatz versus AR at low thrust.



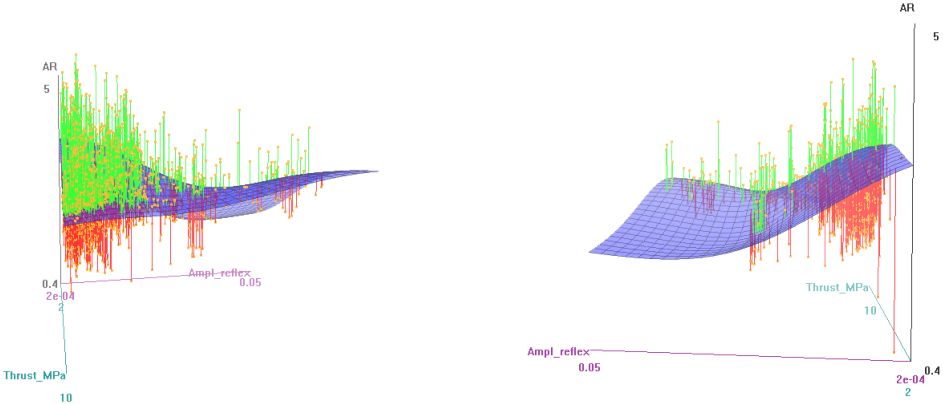
(e) Thrust versus AR at high amplitude of ersteinsatz. (f) Thrust versus AR at low amplitude of ersteinsatz.

Figure 4.6: 3-D surfaces.

As at low torque, tool wear is maximum and TBM cannot achieve more AR only with applying more thrust. That is why high torque motors are used in TBM. Figures 4.6(a,b) show thrust versus AR at low and high amplitude of reflexion. Again at high amplitude values, the AR is linearly increasing with thrust contrary to low amplitude of reflexion. Reason may be as more torque produces more amplitude of reflexion and at high amplitude of reflexion, more advance rate is observed.



(a) Thrust versus AR at high pseudo velocity. (b) Thrust versus AR at low pseudo velocity.



(c) Amplitude of reflexion versus AR at high thrust. (d) Amplitude of reflexion versus AR at low thrust.

Figure 4.7: 3-D surfaces.

Figures 4.6(c,d) shows variation of AR with respect to amplitude of erestizeit at low and high thrust. In both cases, at high and low thrust, AR curve has a depression at maximum value of amplitude of reflexion, which shows here a region of very challenging rock properties that creates a hindrance for TBM to get more AR with more thrust. Figures 4.6(e,f) shows AR versus thrust at low and high amplitude of erestizeit that revealed AR in both cases increases up to a maximum value of 4.5 *m/hr* then decrease with the same rate as it increased. But here we see that decline for AR, even increasing

thrust is started where the amplitude is max. This shows a major influence of AR upon rock strength.

Figures 4.7(a,b) shows AR and thrust dependency upon each other at low and high pseudo velocity. It is clear from the surface plot that in both cases trend is same, showing that AR and thrust behaviour is independent of pseudo velocity. Fig. 4.7(c,d) shows AR versus amplitude of reflex at low and high thrust. It is obvious that AR decreases when there is more amplitude of reflex. Amplitude of reflexion is more when rock strength is high, therefore in high strength rock, at same TBM thrust values, AR reduces.

### 4.1.4 Tools/Cutter Wear

Disc cutter wear in mechanized tunneling has a strong influence on cost and performance in hard rock tunnelling and soil mechanics. Cutter wear is affected by several parameters. Cutter consumption estimates are most effective if based on most recent experiences and recent experimental data related to rock properties. These estimates are highly influenced by advance rates, rock strengths, and types of cutters immersed in abrasive ground. Data from the Hieflau pressure tunnel were analyzed for cutter wear.

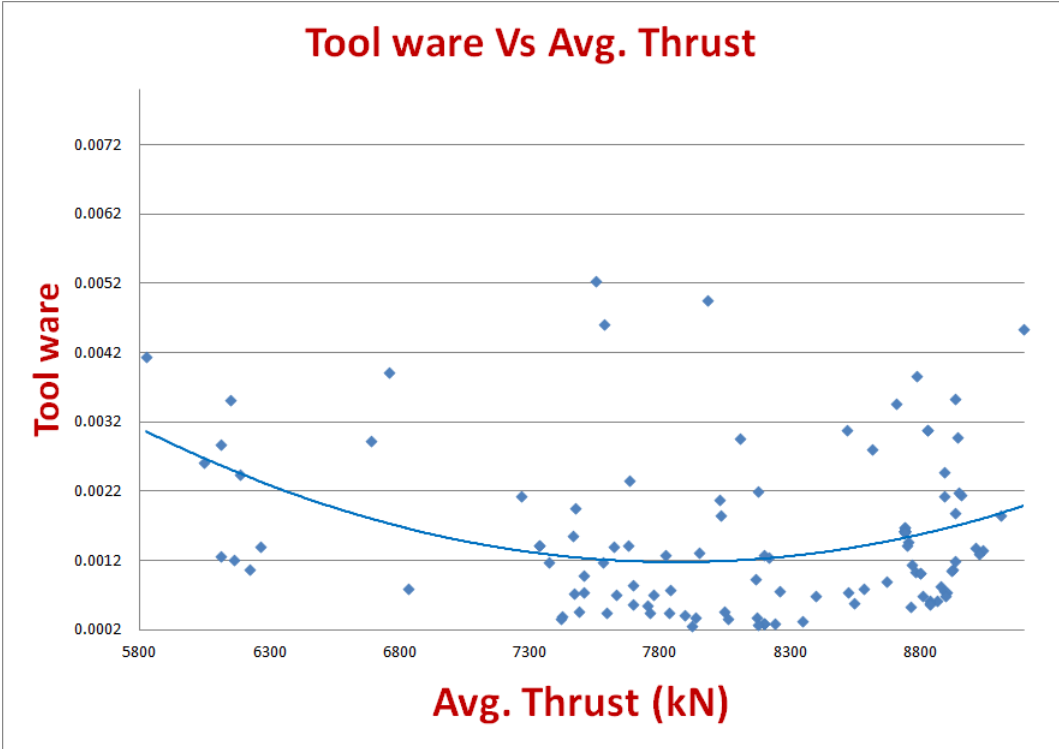


Figure 4.8: Thrust versus tool wear.

Figure 4.8 shows cutters per chainage (cutter consumption or tool ware) against average thrust. It is clear that cutter consumption is decreased with increase of average thrust. This may be due to low thrust values, magnitude of thrust is insufficient for chip formation and energy transferred to rock is too low and dissipated as heat.



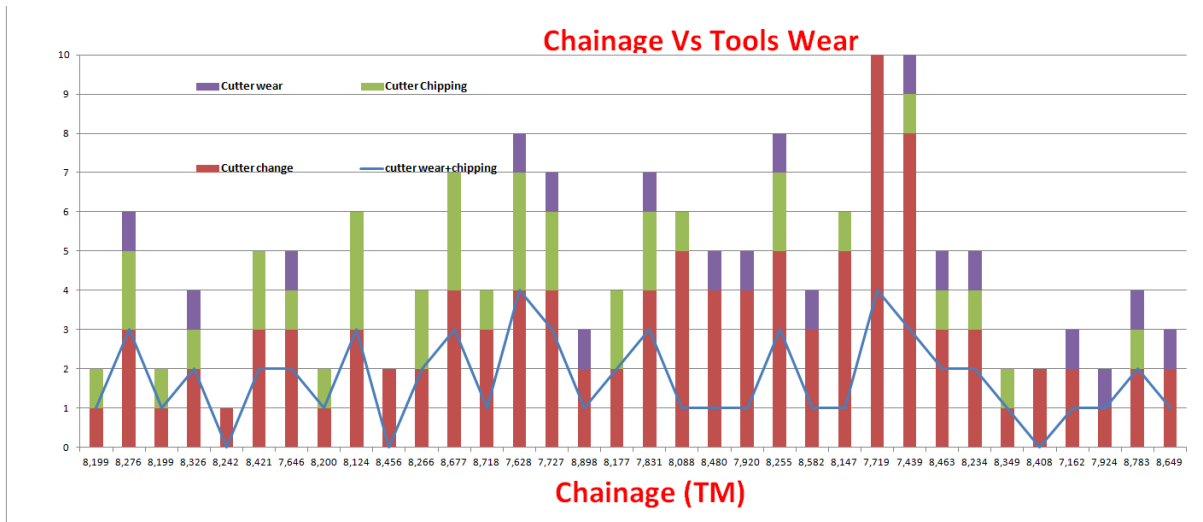


Figure 4.9: Chainage versus tool wear.

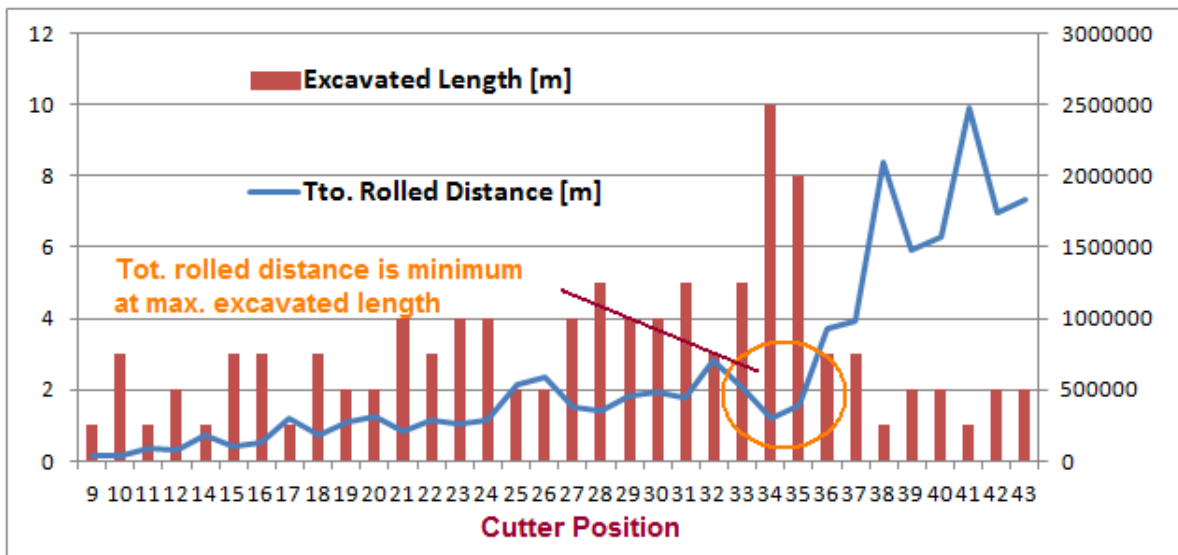


Figure 4.10: Tool wear.

Figures 4.9 and 4.10 shows different parameters changing with TM. It is clear from these figures that maximum number of cutter change appeared at TM-7719 and one of the two peaks for cutter wear plus chipping is also lying on the same TM. More cutter wear and chipping is responsible for more cutter changes. Total rolled distance is minimum at maximum excavated length, reason may be due to specific damage and location of cutter numbers 34-35.

#### 4.1.5 Statistical Modeling with SPSS-19

Statistical software SPSS-19 was used to analyze statistically the Hieflau data. Data is divided into three classes.

1. Machine + Rock Mass + Seismic data
2. Machine +Rock Mass data
3. Machine + Seismic data

Here analysis was carried out separately for each data class and results were compared in last section.

Relation of Property with AR	Empirical Equation	Corr. Coeff. $R^2$
AR vs Thrust	$AR = 5.9875 - 0.3617Thrust$	0.419
AR vs UCS	$AR = 4.579 - 0.0067UCS$	0.1102
AR vs Torque	$AR = 3.35 - 7 * 10^5Torque$	0.0702
AR vs Amp_ Reflex	$AR = 2.76 + 4.086Ampl_{Reflex}$	0.0039
AR vs Amp_ Erst	$AR = 2.957 - 0.0957Ampl_{Erst}$	0.0008
AR vs Pseudo_ Vel	$AR = 3.592 - 0.0001Pseu_{Vel}$	0.0264

Table 4.1: Rock mass plus machine and seismic data versus AR.

Table 4.1 lists linear relationship and coefficient of correlation  $R^2$  for linear curve fitting. From above table it is clear that only thrust and advance rate have a good linear correlation with  $R^2 = 0.419$ . All other parameters are more or less are linearly correlated with AR but with very poor correlation.

#### 4.1.5.1 Frequency Distribution of Parameters

Here the frequency distribution of all input and output variables are given to visualize their importance and eligibility as an input parameter for the multidimensional analysis and prediction models.

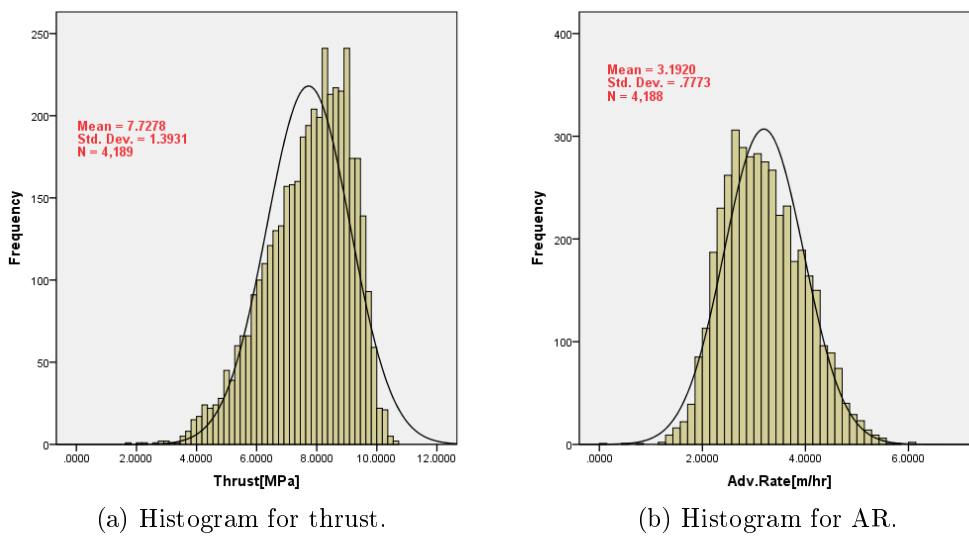
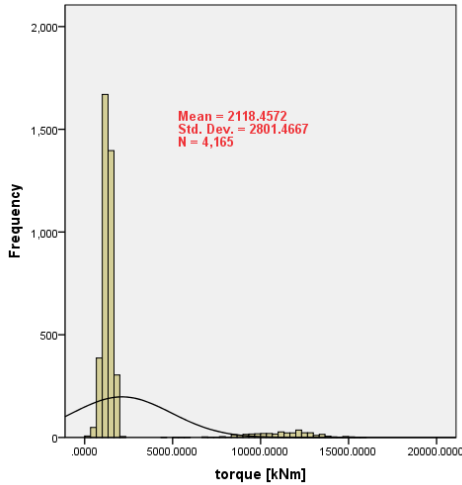
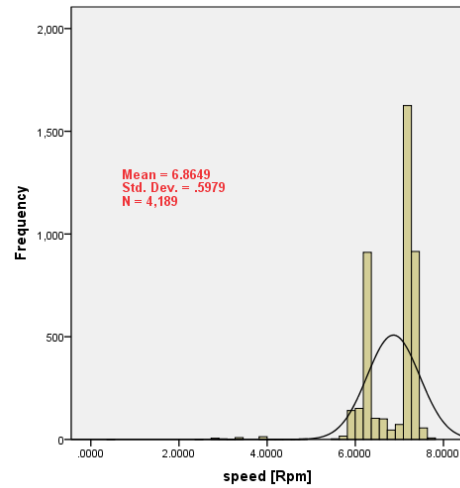


Figure 4.11: Histograms of TBM data 1.



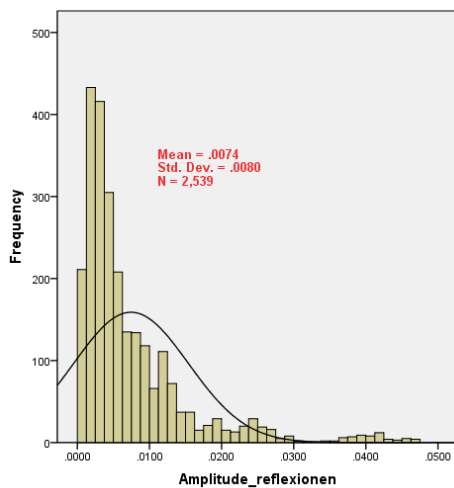
(a) Histogram for torque.



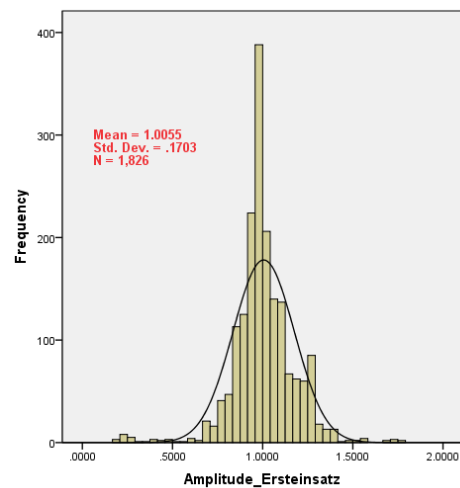
(b) Histogram for RPM.

Figure 4.12: Histograms of TBM data 2.

Figures 4.11 - 4.14 shows frequency distributions of machine variables and seismic data. Here in Figs. 4.11(a,b) we see that a perfect normal distribution in thrust and advance rate, whereas torque and TBM speed data is skewed left and skewed right respectively. Figures 4.13 and 4.14 shows seismic data frequency distribution, here only amplitude of erestzeit has a perfect normal frequency distribution, where as all other seismic data is scattered, except Fig. 4.12b where except one point, remaining frequency distribution is perfect normal.

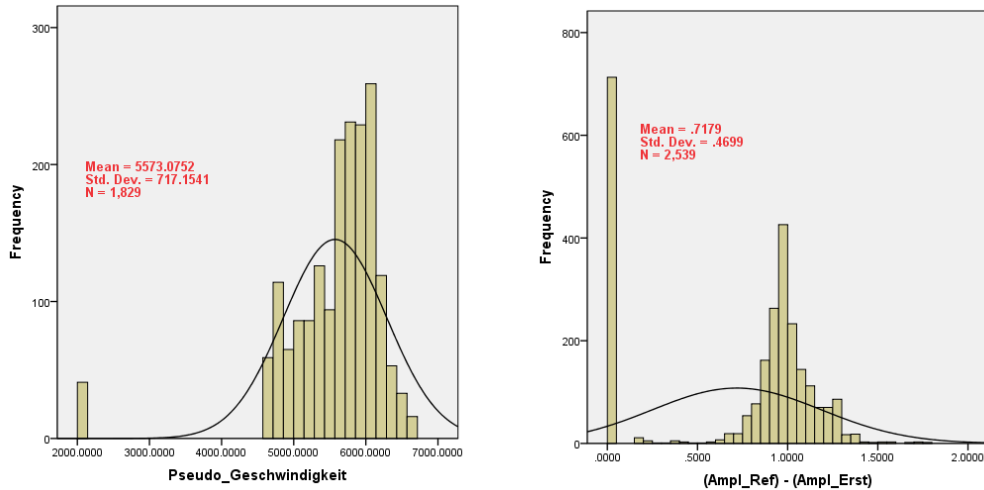


(a) Histogram for amplitude of reflexion.



(b) Histogram for amplitude of erestsatz.

Figure 4.13: Histograms of seismic data 1.



(a) Histogram for pseudo velocity. (b) Histogram for difference of amplitudes.

Figure 4.14: Histogram of seismic data 2.

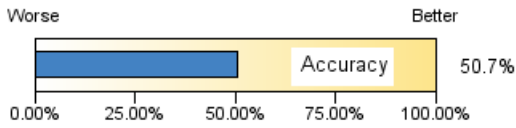
#### 4.1.5.2 Prediction Model Summary and Coefficients

Tables 4.2(a,b) shows model summaries for mix data (TBM+Seismic+Rock mass data) and TBM-Rock mass data. In mix data, AR prediction model has an accuracy of 50.7%, where for the TBM-Rock mass data accuracy is 48%. In both cases forward stepwise method is used and AR is target value in both cases. Tables 4.3 (a,b) shows predictor importance and number of input parameters used for the prediction model. In mix data AR model, five input parameters are used, that include all machine, rock mass and seismic data properties and thrust is most important parameter that strongly affect the model output. Torque is least import parameter here and can be neglected in the model calculations.

**Model Summary**

<b>Target</b>	Adv.Rate[m/hr]
<b>Automatic Data Preparation</b>	On
<b>Model Selection Method</b>	Forward Stepwise
<b>Information Criterion</b>	-5,064.407

The information criterion is used to compare to models. Models with smaller information criterion values fit better.

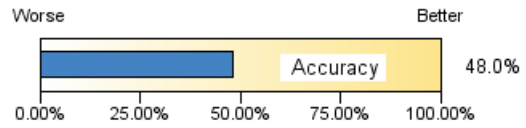


(a) TBM, rock mass and seismic data.

**Model Summary**

<b>Target</b>	Adv.Rate[m/hr]
<b>Automatic Data Preparation</b>	On
<b>Model Selection Method</b>	Forward Stepwise
<b>Information Criterion</b>	-4,843.854

The information criterion is used to compare to models. Models with smaller information criterion values fit better.



(b) TBM and rock mass data.

Relation of Property with AR	Empirical Equation	Corr. Coeff. R
AR vs Thrust	$AR = -0.3617Thrust + 5.9875$	0.647
AR vs Machine Torque	$AR = 7 \times 10^{-5} Torque + 3.35$	0.265
AR vs UCS	$AR = 0.0067UCS + 4.579$	0.332
AR vs Amp. <sub>Reflex</sub>	$AR = 0.04.086Amp_{reflex} + 2.76$	0.062
AR vs Amp. <sub>Erest</sub>	$AR = 0.0957Amp_{erest} + 0.2.957$	0.028
AR vs Pseudo <sub>Vel</sub>	$AR = 0.0001 Pseudo_{vel} + 3.592$	0.163

(c) Linear relation between output and input parameters.

Table 4.2: Model summaries.

Table 4.3 indicates that only machine parameters are used to predict AR, where again thrust is most important and torque is least important parameters but torque cannot be neglected here as number of input parameters are too small. Table 4.2c shows linear relationship between all input parameters and target variable (AR). Using these equations, SPSS-19 software has predicted the target variable with a reasonably good accuracy.

		Effects		Target: Adv.Rate[m/hr]		
Source	Sum of Squares	df	Mean Square	F	Sig.	Importance
Corrected Model ▼	1,283.890	5	256.778	861.706	.000	
ThrustMPa_transformed	479.251	1	479.251	1,608.290	.000	0.249
speedRpm_transformed	125.274	1	125.274	420.399	.000	0.198
Amplitude_reflexionen_transformed	48.322	1	48.322	162.161	.000	0.186
Pseudo_Geschwindigkeit_transformed	34.583	1	34.583	116.056	.000	0.184
torquekNm_transformed	24.548	1	24.548	82.380	.000	0.183
Residual	1,246.185	4,182	0.298			
Corrected Total	2,530.075	4,187				

(a) Effects for TBM, rock mass and seismic data.

		Effects		Target: Adv.Rate[m/hr]		
Source	Sum of Squares	df	Mean Square	F	Sig.	Importance
Corrected Model ▼	1,215.244	3	405.081	1,289.034	.000	
ThrustMPa_transformed	480.353	1	480.353	1,528.561	.000	0.395
speedRpm_transformed	111.715	1	111.715	355.496	.000	0.314
torquekNm_transformed	12.818	1	12.818	40.788	.000	0.292
Residual	1,314.830	4,184	0.314			
Corrected Total	2,530.075	4,187				

(b) Effects for TBM and rock mass data.

Table 4.3: Model effects.

Coefficients				Target: Adv.Rate[m/hr]			
Model Term	Coefficient ▼	Std.Error	t	Sig.	95% Confidence Interval		Importance
					Lower	Upper	
Intercept	4.508	0.228	19.783	.000	4.061	4.955	
ThrustMPa_transformed	-0.293	0.007	-40.103	.000	-0.307	-0.278	0.249
speedRpm_transformed	0.396	0.019	20.504	.000	0.358	0.434	0.198
Amplitude_reflexionen_transformed	-23.493	1.845	-12.734	.000	-27.110	-19.876	0.186
Pseudo_Geschwindigkeit_transformed	-0.000	0.000	-10.773	.000	-0.000	-0.000	0.184
torquekNm_transformed	-0.000	0.000	-9.076	.000	-0.000	-0.000	0.183

(a) Coefficients for TBM, rock mass and seismic data.

Coefficients				Target: Adv.Rate[m/hr]			
Model Term	Coefficient ▼	Std.Error	t	Sig.	95% Confidence Interval		Importance
					Lower	Upper	
Intercept	2.986	0.168	17.793	.000	2.657	3.315	
ThrustMPa_transformed	-0.292	0.007	-39.097	.000	-0.306	-0.277	0.395
speedRpm_transformed	0.365	0.019	18.855	.000	0.327	0.403	0.314
torquekNm_transformed	-0.000	0.000	-6.387	.000	-0.000	-0.000	0.292

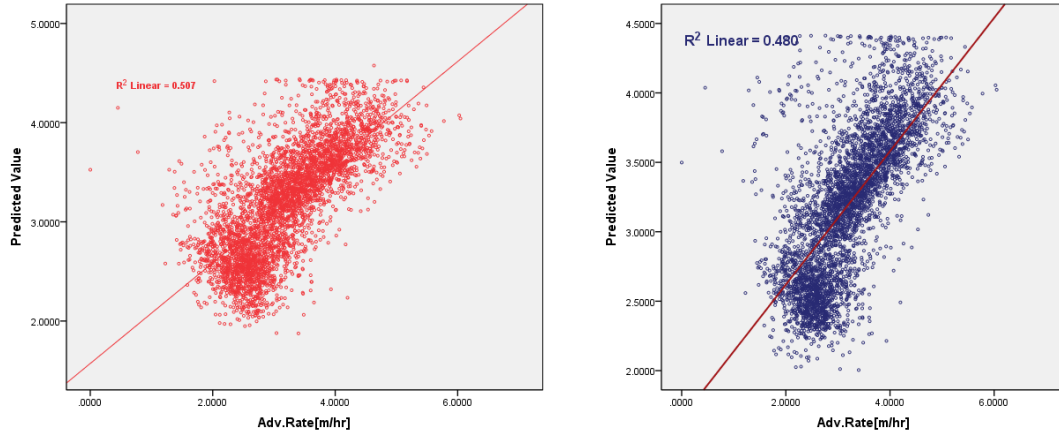
(b) TBM and rock mass data.

Table 4.4: Model effects.

From table 4.4(a,b) coefficients for the AR prediction models are collected to form empirical linear models. Eq. 4.1 shows AR prediction model for TBM+Rock Mass+Seismic (Mix data), with a  $R^2 = 0.507$  and Eq. 4.2 shows the same models for TBM and rock mass data, with a  $R^2 = 0.48$ . This indicates that with increasing input parameters prediction improves.

$$AR(m/h) = 4.51 - 0.293Thrust + 0.396rpm - 23.49Amp_{ref} - 0.001Torq - 0.001Psed_{vel} \quad (4.1)$$

$$AR(m/h) = 2.996 - 0.292Thrust + 0.365RPM - 0.001Torque \quad (4.2)$$



(a) AR model for TBM, rock mass and seismic data. (b) AR model for TBM and rock mass data.

Figure 4.15: AR regression models.

Prediction models scattered plots with  $R^2 = 0.48$  and  $R^2 = 0.48$  respectively Figs. 4.15(a,b), shows reasonably good accuracy. Figure 4.16 shows comparison between actual and predicted values of AR and a curve fit to the predicted values. Actual and predicted values are in good match and predicted values of AR almost 90% coincide with actual ones.

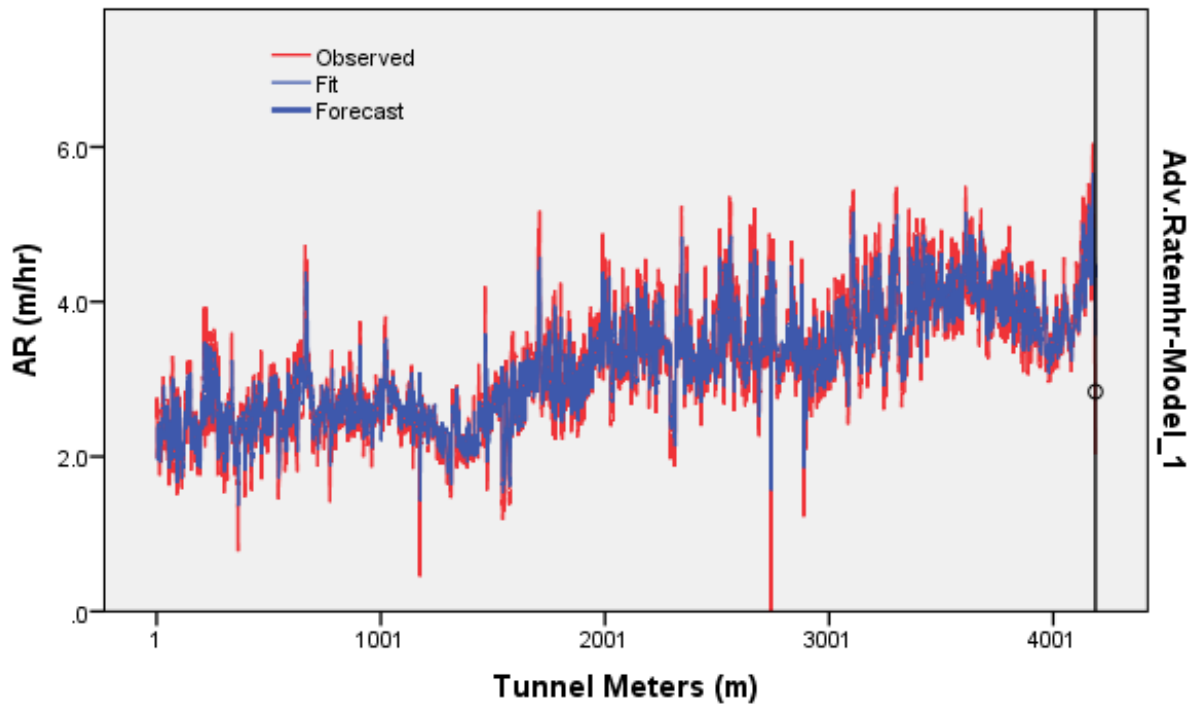


Figure 4.16: AR model comparison.



### 4.1.5.3 Partial and Bi-Variant Correlation

Machine and seismic data variables are analysed for partial and bi-variant correlation using SPSS-19.

**Correlations**

Control Variables			Thrust[MPa]	torque [kNm]	speed [Rpm]	Adv.Rate [m/hr]
-none <sup>a</sup>	Thrust[MPa]	Correlation	1.000	.304	-.427	-.647
		Significance (2-tailed)	.	.000	.000	.000
		df	0	4163	4187	4186
	torque [kNm]	Correlation	.304	1.000	-.152	-.268
		Significance (2-tailed)	.000	.	.000	.000
		df	4163	0	4163	4163
	speed [Rpm]	Correlation	-.427	-.152	1.000	.443
		Significance (2-tailed)	.000	.000	.	.000
		df	4187	4163	0	4186
	Adv.Rate[m/hr]	Correlation	-.647	-.268	.443	1.000
		Significance (2-tailed)	.000	.000	.000	.
		df	4186	4163	4186	0
Adv.Rate[m/hr]	Thrust[MPa]	Correlation	1.000	.177	-.206	
		Significance (2-tailed)	.	.000	.000	
		df	0	4162	4185	
	torque [kNm]	Correlation	.177	1.000	-.038	
		Significance (2-tailed)	.000	.	.014	
		df	4162	0	4162	
	speed [Rpm]	Correlation	-.206	-.038	1.000	
		Significance (2-tailed)	.000	.014	.	
		df	4185	4162	0	

a. Cells contain zero-order (Pearson) correlations.

(a) TBM data.

**Correlations**

Control Variables			Amplitude_reflexionen	Pseudo_Geschwindigkeit	Amplitude_Ersteinsatz	Adv.Rate [m/hr]
-none <sup>a</sup>	Amplitude_reflexionen	Correlation	1.000	-.505	-.353	.055
		Significance (2-tailed)	.	.000	.000	.005
		df	0	1827	1824	2537
	Pseudo_Geschwindigkeit	Correlation	-.505	1.000	.291	-.163
		Significance (2-tailed)	.000	.	.000	.000
		df	1827	0	1824	1827
	Amplitude_Ersteinsatz	Correlation	-.353	.291	1.000	-.028
		Significance (2-tailed)	.000	.000	.	.229
		df	1824	1824	0	1824
	Adv.Rate[m/hr]	Correlation	.055	-.163	-.028	1.000
		Significance (2-tailed)	.005	.000	.229	.
		df	2537	1827	1824	0
Adv.Rate[m/hr]	Amplitude_reflexionen	Correlation	1.000	-.504	-.352	
		Significance (2-tailed)	.	.000	.000	
		df	0	1826	1823	
	Pseudo_Geschwindigkeit	Correlation	-.504	1.000	.290	
		Significance (2-tailed)	.000	.	.000	
		df	1826	0	1823	
	Amplitude_Ersteinsatz	Correlation	-.352	.290	1.000	
		Significance (2-tailed)	.000	.000	.	
		df	1823	1823	0	

a. Cells contain zero-order (Pearson) correlations.

(b) Seismic data.

Table 4.5: Partial correlation coefficients.

Partial correlation measures the degree of relationship between two random variables, with the effect of a set of controlling random variables removed [39]. The Partial correlations procedure computes partial correlation coefficients that describe the linear relationship between two variables while controlling for the effects of one or more additional variables. Correlations are measures of linear association. Two variables can be perfectly related, but if the relationship is not linear, a correlation coefficient is not a proper statistic to measure their association. In bi-variate correlations, the relationship between two variables is measured. The degree of relationship (how closely they are related) could be either positive or negative. The maximum number could be either +1 (positive) or -1 (negative). This number is the correlation coefficient. A zero correlation indicates no relationship and value close to +1 shows strong positive correlation [25]. Table 4.5a shows that, there is a good correlation between thrust and advance rate ( $R^2 = -0.647$ ), and between machine speed and AR ( $R^2 = 0.443$ ). Negative correlation of ( $R^2 = -0.647$ ) between thrust and AR also verify the graph between them as shown in Fig. 4.1b. Table 4.5b shows correlation between AR and seismic data variables. It is clear from the table that there is no significant correlation between seismic data and AR.

Table 4.6 shows almost same results as shown in partial correlation between thrust and machine parameters. Table 4.7 shows a Bi-Variant correlation between thrust and seismic parameters, pseudo velocity have a partial correlation coefficient of ( $R^2 = -0.001$ ), amplitude erestizeit ( $R^2 = -0.039$ ) and amplitude reflexion have a correlation of ( $R^2 = 0.181$ ) only. These figures shows that, there is no significant partial correlation between thrust and rock mass seismic properties and there is no significant correlation between seismic data and AR.

<b>Correlations</b>					
		Thrust[MPa]	Adv.Rate [m/hr]	torque [kNm]	speed [Rpm]
Thrust[MPa]	Pearson Correlation	1	-.647 <sup>**</sup>	.304 <sup>**</sup>	-.427 <sup>**</sup>
	Sig. (2-tailed)		.000	.000	.000
	N	4189	4188	4165	4189
Adv.Rate[m/hr]	Pearson Correlation	-.647 <sup>**</sup>	1	-.268 <sup>**</sup>	.443 <sup>**</sup>
	Sig. (2-tailed)	.000		.000	.000
	N	4188	4188	4165	4188
torque [kNm]	Pearson Correlation	.304 <sup>**</sup>	-.268 <sup>**</sup>	1	-.152 <sup>**</sup>
	Sig. (2-tailed)	.000	.000		.000
	N	4165	4165	4165	4165
speed [Rpm]	Pearson Correlation	-.427 <sup>**</sup>	.443 <sup>**</sup>	-.152 <sup>**</sup>	1
	Sig. (2-tailed)	.000	.000	.000	
	N	4189	4188	4165	4189

\*\* . Correlation is significant at the 0.01 level (2-tailed).

Table 4.6: Bi-variant correlation coefficients.

Correlations					
		Thrust[MPa]	Amplitude_reflexionen	Pseudo_Geschwindigkeit	Amplitude_Ersteinsatz
Thrust[MPa]	Pearson Correlation	1	-.181**	-.001	.039
	Sig. (2-tailed)		.000	.980	.093
	N	4189	2539	1829	1826
Amplitude_reflexionen	Pearson Correlation	-.181**	1	-.505**	-.353**
	Sig. (2-tailed)	.000		.000	.000
	N	2539	2539	1829	1826
Pseudo_Geschwindigkeit	Pearson Correlation	-.001	-.505**	1	.291**
	Sig. (2-tailed)	.980	.000		.000
	N	1829	1829	1829	1826
Amplitude_Ersteinsatz	Pearson Correlation	.039	-.353**	.291**	1
	Sig. (2-tailed)	.093	.000	.000	
	N	1826	1826	1826	1826

\*\* . Correlation is significant at the 0.01 level (2-tailed).

Table 4.7: Bi-variant correlation coefficients.

#### 4.1.6 Conclusions

Worth mentioning of the drive is the successful passage of the challenging section at the Hartelsgraben as well as the crossing under the existing access gallery. The old tunnel was identified as a clear bottleneck in the headwaters system. Hard rock double shield TBM, Robbins DS-TBM-Model 194 – 272 – 2, was used to excavate the second tunnel 4819 m in length and interior diameter of 6.18 m, parallel to existing tunnel [26]. After detailed analysis of the data from Hieflau tunnel, it is concluded that, advance rate is inversely proportional to thrust and UCS, main reason for this is dependence of AR on rock strength. There is a good correlation between thrust and advance rate, and between machine speed and AR . There is no significant correlation between thrust and seismic parameters, between AR and seismic parameters. At low torque and low and high thrust, tool wear is maximum, TBM cannot achieve maximum AR only with increasing thrust. This is also included that moderate thrust values gives rise to maximum tool and cutter life. At maximum value of amplitude of reflexion, a depression in AR value is found, that shows rock brittleness and hardness as key parameters in TBM performance. After multidimensional analysis, advance rate linear regression prediction model formulated with the help of SPSS19 software, shows a good significance of the model. Also machine parameters have more influence on the model as compare to seismic data. Rock mass data are also normally distributed and useful for regression analysis, that is clearly used in analysis.

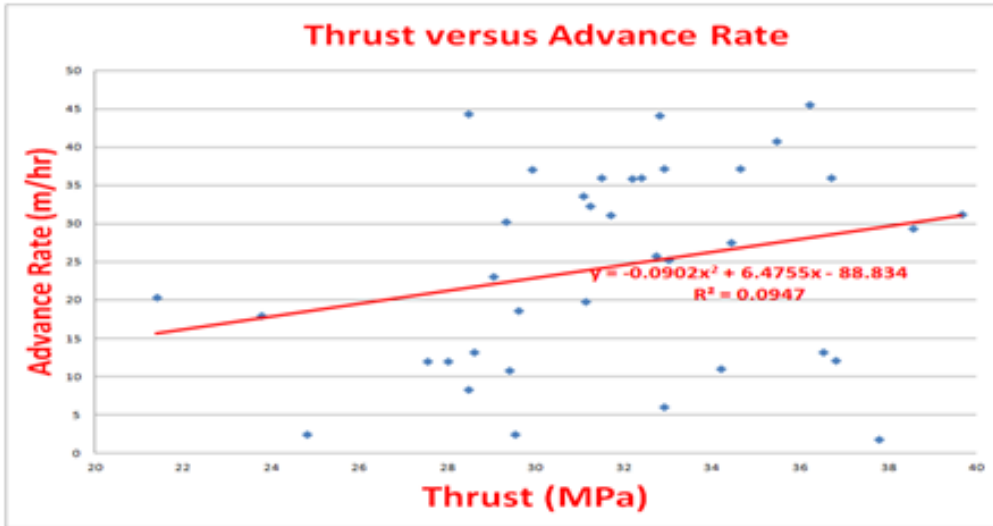
## 4.2 Queens Water Tunnel

Intensive studies have been carried out for estimating the TBM performance mostly based on intact rock properties to predict the TBM performance in jointed and faulted rock conditions. In this chapter TBM performance was more precisely related with machine and rock mass parameters. 2-D analysis was made using excel and Kaleida graphs. 3-D analysis was carried out by a statistical software “R”. Rock fractured class (RFC) was predicted using a Math-Lab code and by statistical modeling using a commercial software SPSS.

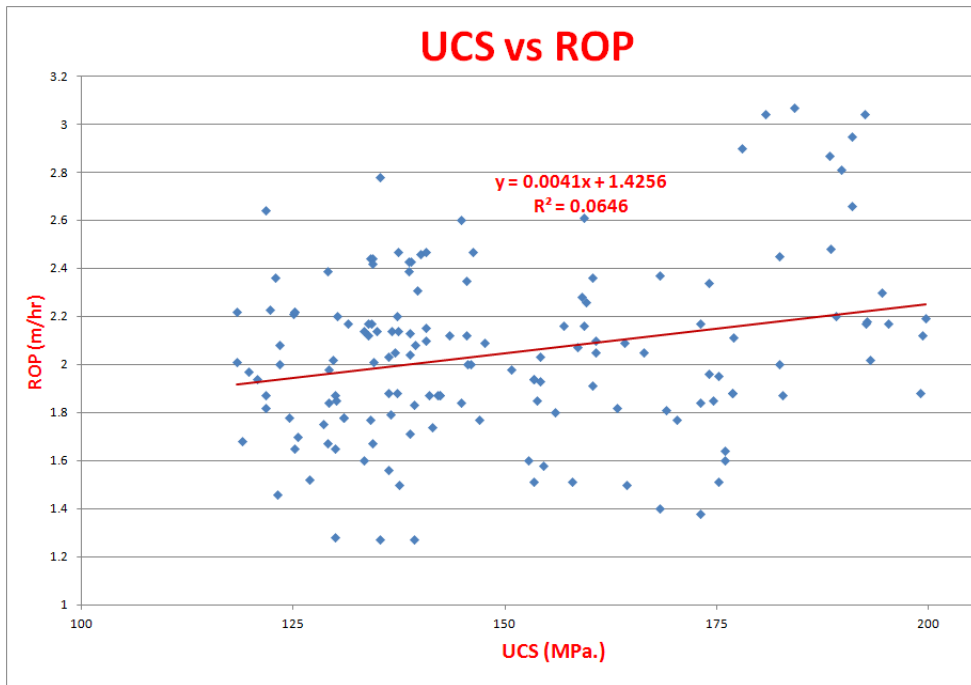
### 4.2.1 2-D Analysis, Rate of Penetration (ROP)

ROP was plotted against thrust of the machine Fig. 4.17a, it shows ROP increases with increase of thrust with a  $R^2 = 0.33$ . ROP have similar behaviour with UCS as in case of thrust (Fig. 4.17b). When we plot UCS vs thrust, it is clear from the graph that, again thrust has constant value with respect to UCS at low values, but at high values of  $UCS > 170 MPa$ , it drastically increases. The reason may be that up to a certain value of UCS cutters of the machine have low wear and good performance.

Figures 4.17(a,b) show AR trend against thrust and UCS, both trend are linear with respect to AR. Same trends are replicated in Figs. 4.18(a,b) for thrust versus UCS and rock fracture class versus AR. Both graph shows that thrust and UCS are closely related and their influence on advance rate is similar.

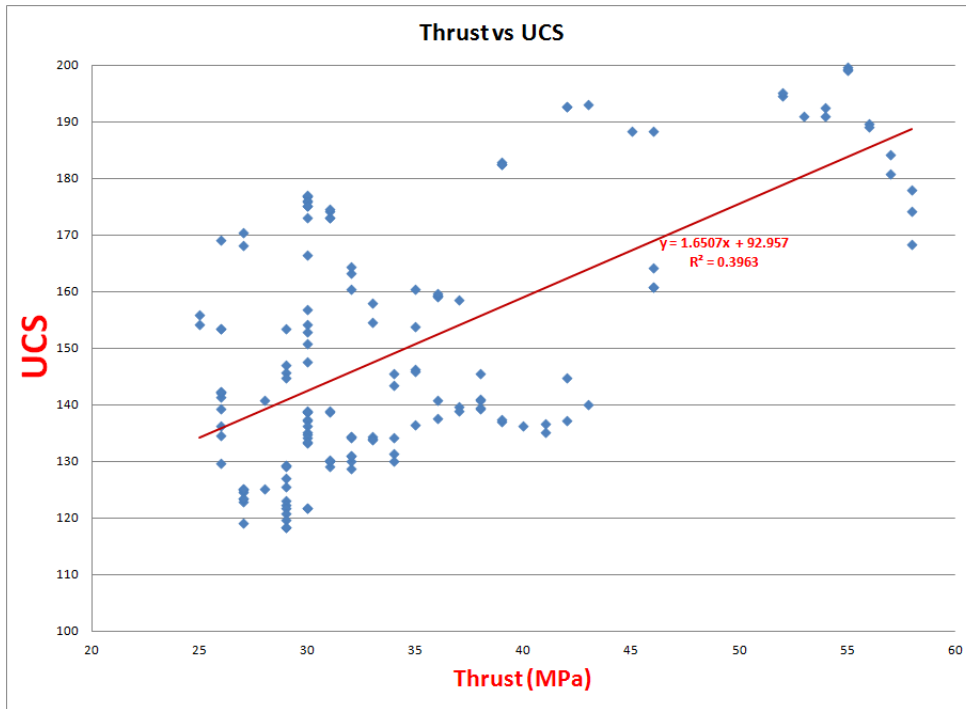


(a) Thrust versus AR.

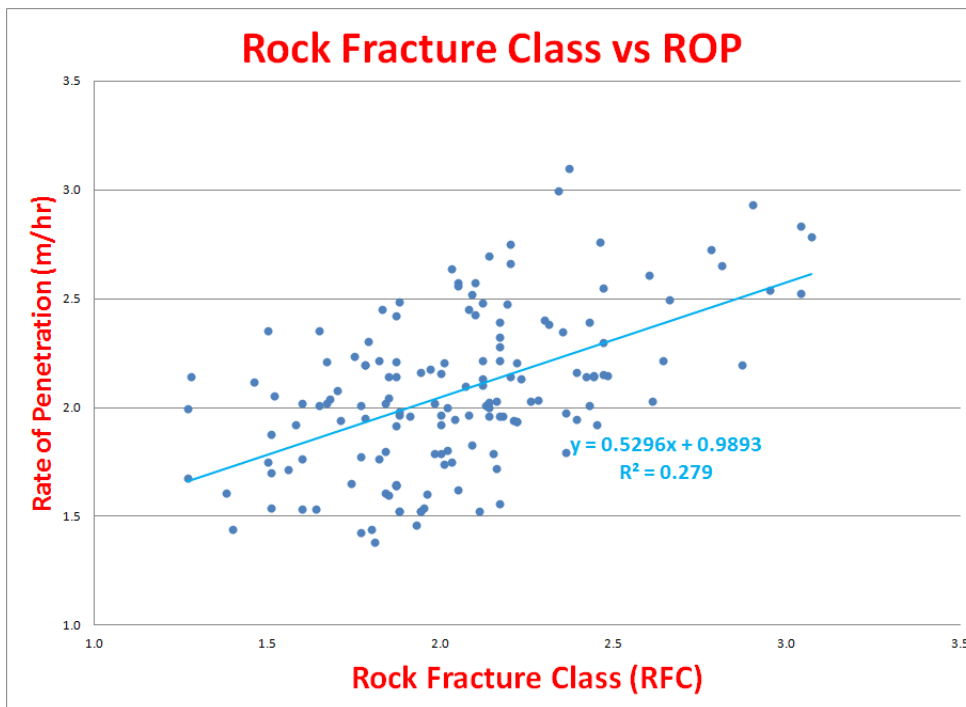


(b) UCS versus AR.

Figure 4.17: Thrust and UCS versus AR.



(a) Thrust versus AR.

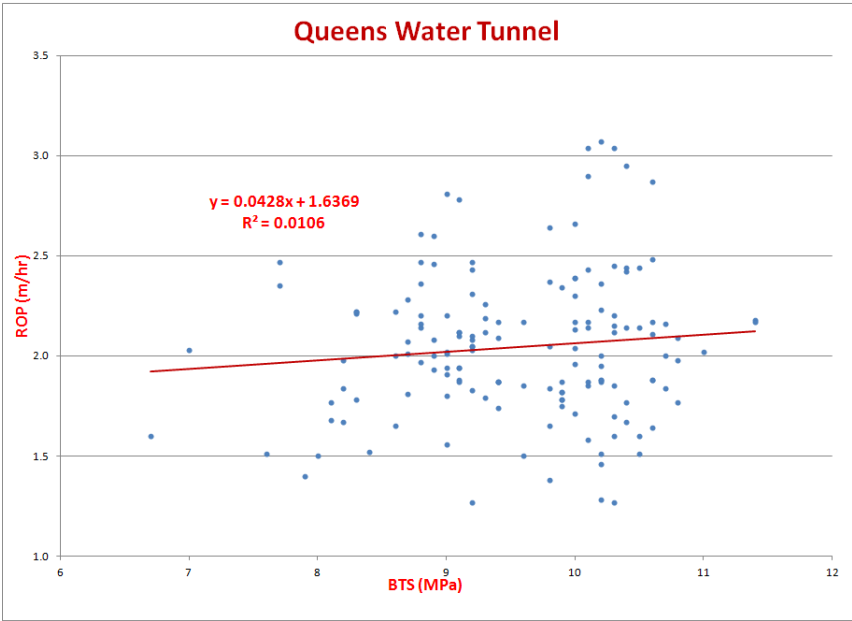


(b) RFC versus AR.

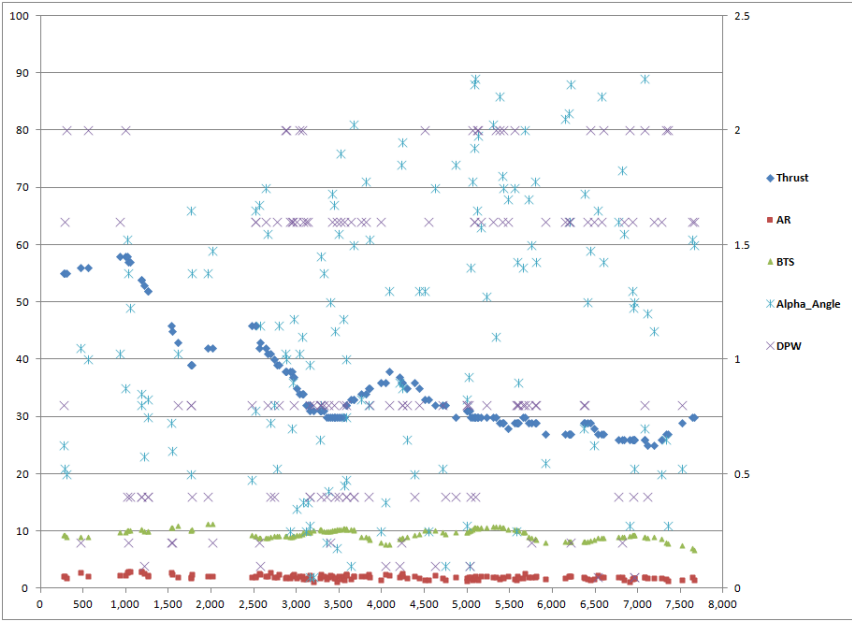
Figure 4.18: 2-D plots.

Figure 4.19a shows Brazilian Tensile Strength (BTS) versus AR, a linear increase in AR is observed with BTS with  $R^2 = 0.01$ . In Fig. 4.19b thrust, AR, BTS, distance between Planes of Weakness (DPW) and  $\alpha$  angle (alpha angle is the angle between tunnel axis and the planes of weakness) are plotted against tunnel meters. AR and BTS are almost constant throughout the length of chainage, while thrust goes down with some deviation

and  $\alpha$  angle and DPW are randomly distributed. From these 2-D graphs (Figs. 4.17-4.18), it can be concluded that AR and UCS can be predicted through linear regression modeling.



(a) BTS versus AR.



(b) TM versus thrust, AR, BTS, DPW and alpha angle.

Figure 4.19: 2-D plots.

### 4.2.2 3-D Analysis, Rate of Penetration (ROP)

A statistical software “R” was used to understand effects of UCS and BTS on advance rate with respect to machine thrust. These 3-D surfaces clearly describe the variation and dependence of one variable upon other, while third variable is kept constant at low

or high value.

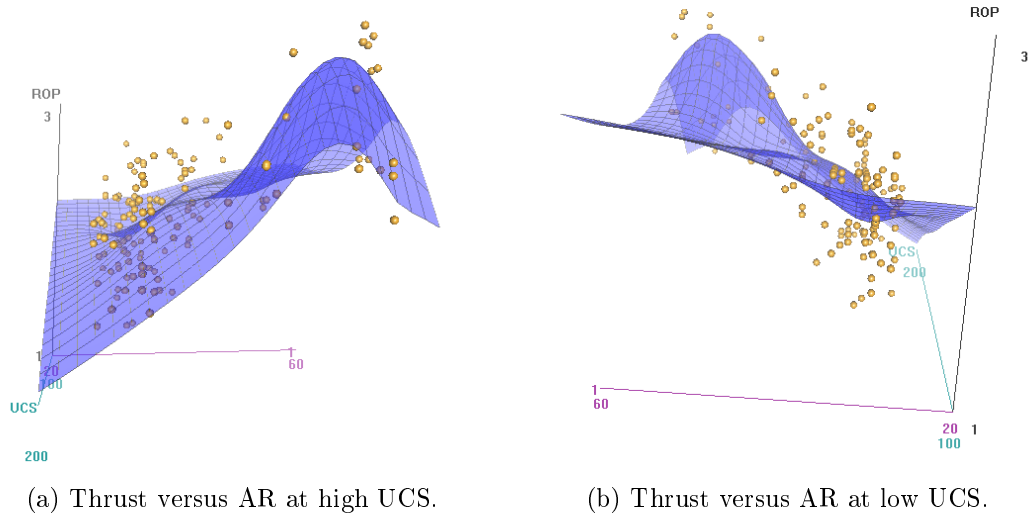


Figure 4.20: 3-D surfaces.

Figures 4.20(a,b) show AR variation with thrust at low and high UCS. At low UCS, AR increases linearly with thrust up to a certain limit, then goes down, while at high UCS, AR have a linear increase throughout the tunnel length. Figs. 4.21(a,b) show dependence of AR on UCS at high and low thrust. Interestingly, at high thrust values, ROP is decreasing linearly with UCS, then got a peak value of  $2.5 \text{ m/hr}$  at about  $200 \text{ MPa}$  and then tends to zero. At very low values of thrust, AR decreases linearly with UCS, clearly verifying the role of rock strength in machine advance.

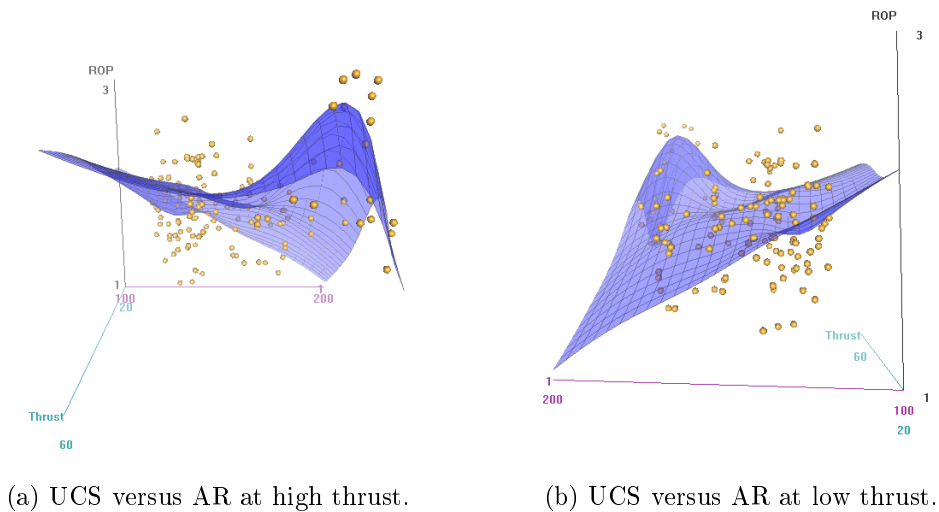


Figure 4.21: 3-D surfaces.



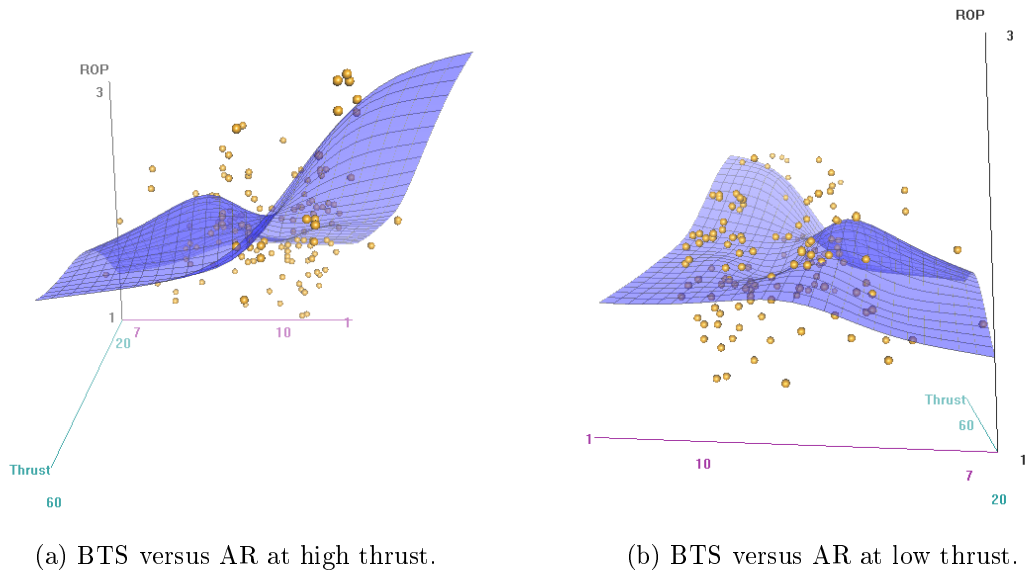


Figure 4.22: 3-D surfaces.

Figures 4.22(a,b) shows BTS relation with AR at high and low thrust. At high thrust, AR trend increases like a sinusoidal wave while on the other hand, AR remains constant with increase of BTS, at low thrust values. BTS have no influence on AR and thrust relation, as shown in Figs. 4.23(a,b).

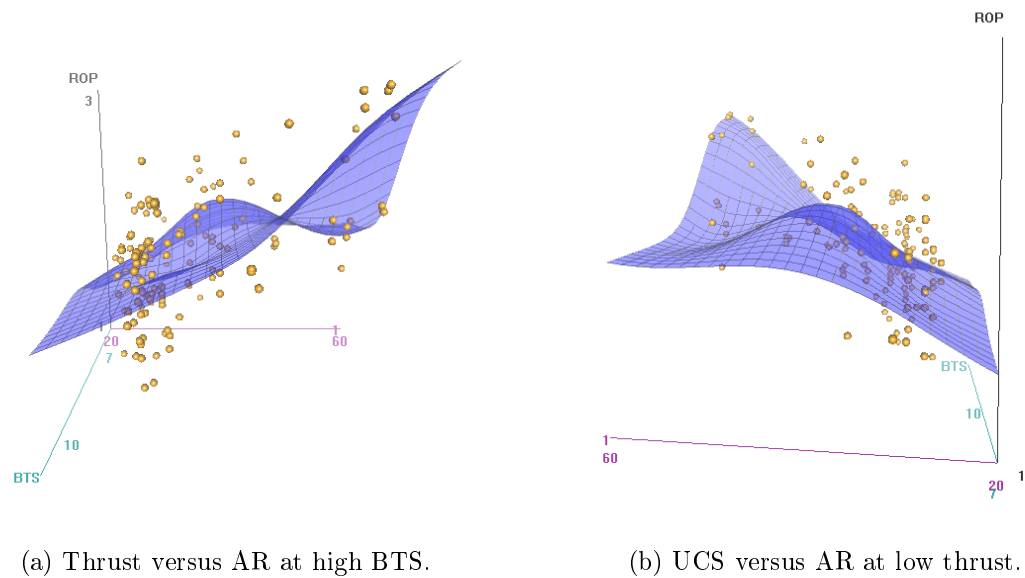


Figure 4.23: 3-D surfaces.

### 4.2.3 Statistical Modeling

SPSS-19 was used to model empirical equations for ROP and other parameters. After multidimensional analysis, different models are predicted using available data. Normal

frequency analysis, linear regression modeling and bi-variant correlation are formulated, plotted and compared with actual data.

4.2.3.1 Frequency Distribution of Different Parameters

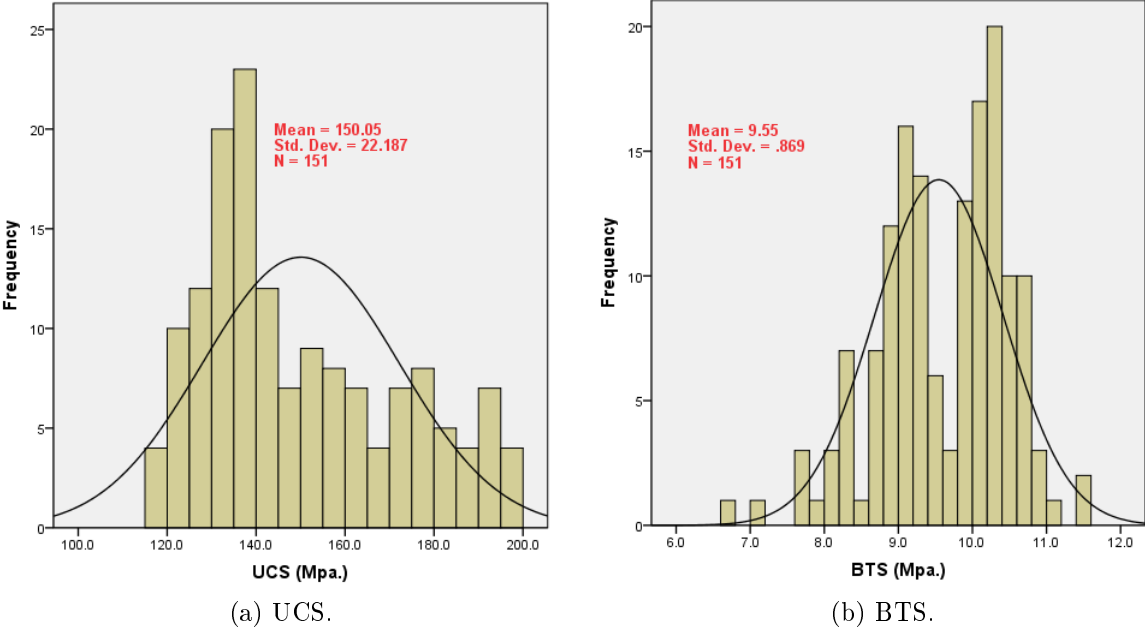


Figure 4.24: Histograms for UCS and BTS.

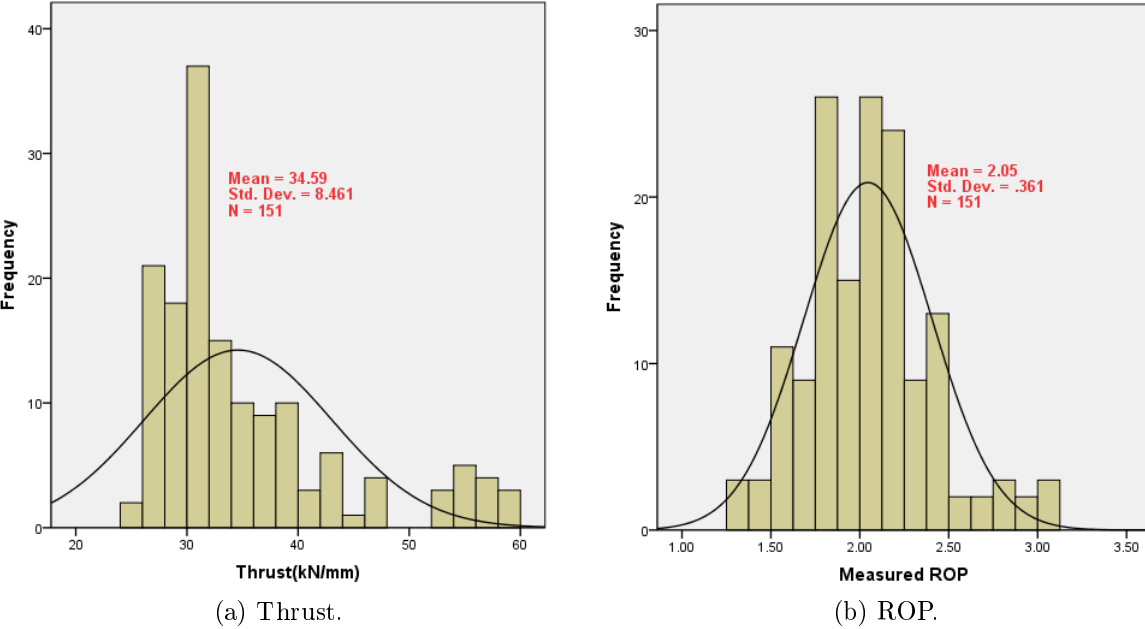


Figure 4.25: Histograms thrust and ROP.

Figures 4.24-4.26 show histograms of different variables. BTS and measured ROP has a good normal frequency distribution. While other parameters like thrust and UCS are left

skewed, DPW and alpha angle are randomly distributed.

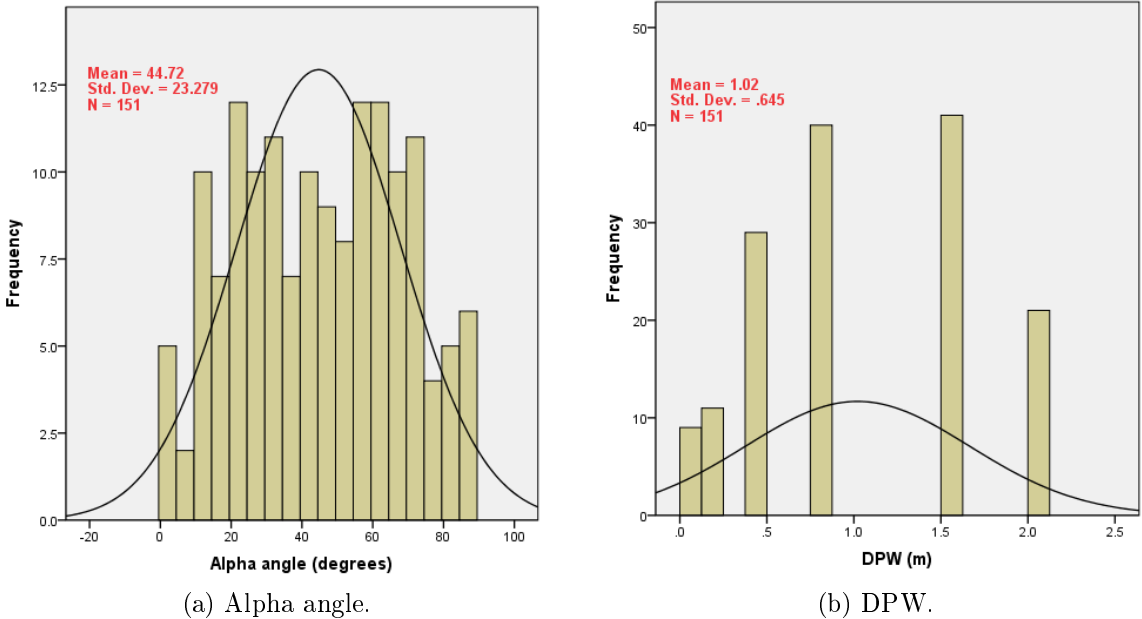


Figure 4.26: Histograms for alpha angle and DPW.

**4.2.3.2 ROP Regression Analysis**

Commercial software packages (IBM SPSS-19) for standard statistical analysis were used for stepwise, multiple variable regression analysis and statistical modeling using known parameters to model an unknown parameter. In order to obtain this model, multidimensional regression analysis were carried out for rock properties and machine parameters. Effect of each parameter separately on rate of penetration (ROP) was analyzed. Separate equation was developed for each rock parameter against the ROP, to see the weight and importance of that parameter in overall model.  $R^2$  values (linear and quadratic equations) of each equation were evaluated and compared for weight and importance of that variable. Model summary is shown in table 4.9, that elaborates model accuracy of 64.4%.

Relation of Property with AR	Empirical Equation	Corr. Coeff. R
AR vs Thrust	$AR = 0.0246 \text{Thrust} + 1.195$	0.577
AR vs BTS	$AR = 0.0428 \text{BTS} + 1.637$	0.13
AR vs UCS	$AR = 0.0041 \text{UCS} + 1.426$	0.24
AR vs $\text{Log}(\alpha)$	$AR = -0.579\alpha^2 + 2.784\alpha - 1.639$	0.485
AR vs DPW	$AR = -0.837 \text{DPW} + 2.73$	0.468

Table 4.8: Table of rock properties versus ROP.

### Model Summary

<b>Target</b>	Measured ROP
<b>Automatic Data Preparation</b>	On
<b>Model Selection Method</b>	Forward Stepwise
<b>Information Criterion</b>	-458.701

The information criterion is used to compare to models. Models with smaller information criterion values fit better.

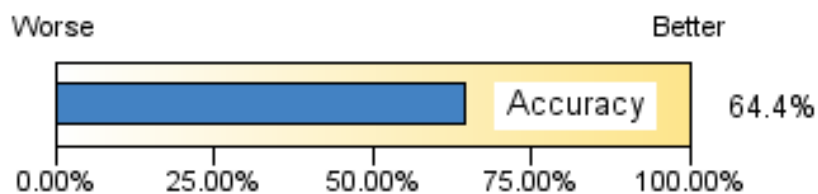


Table 4.9: AR model summary.

Effects		Target: Measured ROP				
Source	Sum of Squares	df	Mean Square	F	Sig.	Importance
Corrected Model ▼	12.770	4	3.192	68.981	.000	
ThrustkNmm_transformed	5.385	1	5.385	116.362	.000	0.312
Log_Alpha_transformed	2.938	1	2.938	63.493	.000	0.250
DPWm_transformed	2.865	1	2.865	61.916	.000	0.249
UCSMpa_transformed	0.510	1	0.510	11.010	.001	0.189
Residual	6.757	146	0.046			
Corrected Total	19.527	150				

(a) Parameters effects.

Coefficients		Target: Measured ROP					
Model Term	Coefficient ▼	Std.Error	t	Sig.	95% Confidence Interval		Importance
					Lower	Upper	
Intercept	1.022	0.160	6.376	.000	0.705	1.339	
ThrustkNmm_transformed	0.029	0.003	10.787	.000	0.024	0.034	0.312
Log_Alpha_transformed	0.475	0.060	7.968	.000	0.357	0.593	0.250
DPWm_transformed	-0.217	0.028	-7.869	.000	-0.272	-0.163	0.249
UCSMpa_transformed	-0.003	0.001	-3.318	.001	-0.005	-0.001	0.189

(b) Coefficient table for AR model.

Table 4.10: Effects and parameters of AR model.

After multidimensional analysis of the rock properties and machine parameters, different equations were developed and presented in table. 4.8. Finally a model for ROP was developed, using coefficient matrix (table 4.10b) as shown below in Eq. 4.3;

$$ROP(m/h) = 1.022 + 0.029Thrust + 0.475Log(\alpha) - 0.217DPW - 0.003UCS \quad (4.3)$$

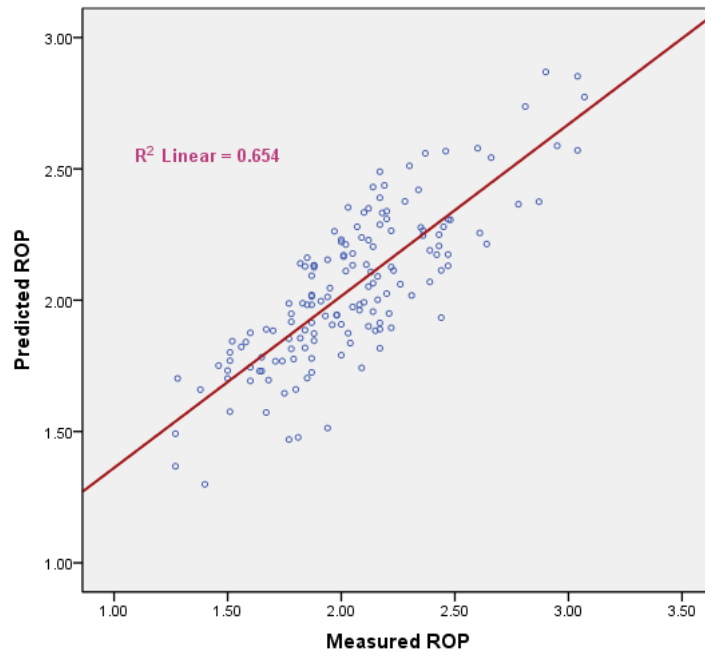


Figure 4.27: Predicted ROP model scattered plot.

Figure 4.27 displays scattered plot of predicted ROP and actual ROP, with  $R^2 = 0.654$ . Comparison between actual and SPSS ROP as a line plot is shown in Fig. 4.28. A reasonably good coincident showing the prediction power of SPSS model is observed.

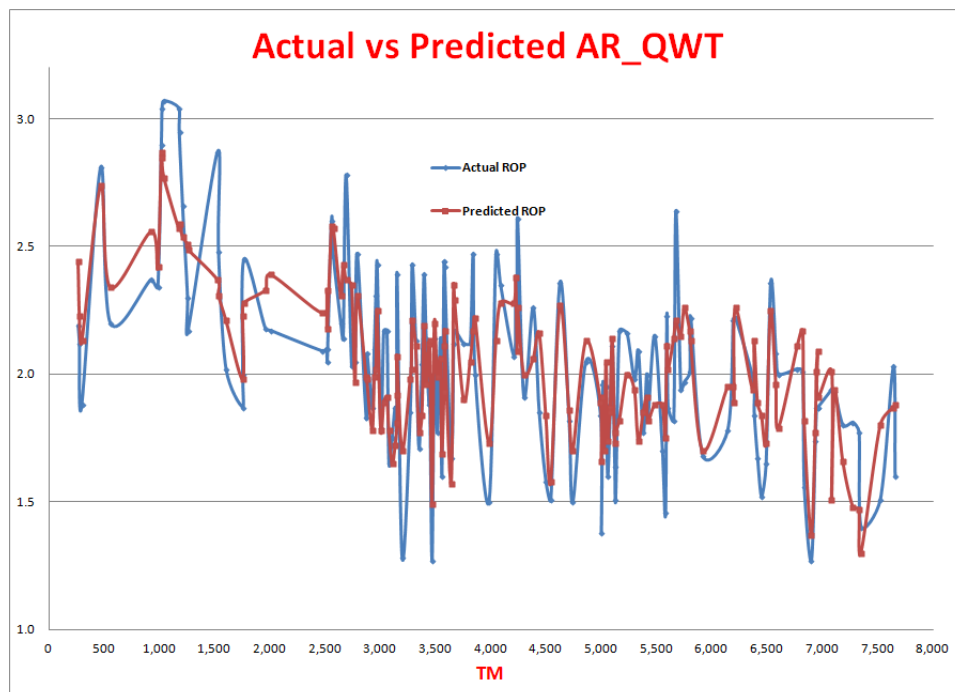


Figure 4.28: AR model comparison.

### 4.2.3.3 Rock Fractured Class (RFC)

After repeating same procedure as for ROP a model for RFC was formulated and shown in eq. 5.2. Model accuracy here is 57% and DPW is most important parameter among model predictors and ROP has the minimum influence on model prediction.

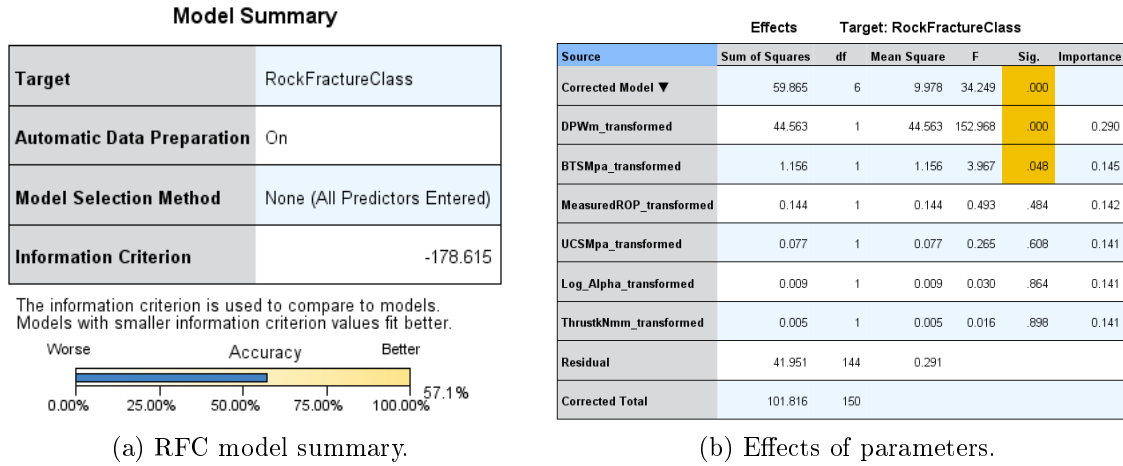


Table 4.11: RFC model summary and effects.

<b>Coefficients</b>		<b>Target: RockFractureClass</b>					
Model Term	Coefficient ▼	Std.Error	t	Sig.	95% Confidence Interval		Importance
					Lower	Upper	
<b>Intercept</b>	3.754	0.623	6.024	.000	2.522	4.986	
<b>DPWm_transformed</b>	-1.022	0.083	-12.368	.000	-1.186	-0.859	0.290
<b>BTSMpa_transformed</b>	-0.109	0.055	-1.992	.048	-0.217	-0.001	0.145
<b>MeasuredROP_transformed</b>	-0.146	0.208	-0.702	.484	-0.557	0.265	0.142
<b>UCSMpa_transformed</b>	-0.001	0.003	-0.515	.608	-0.007	0.004	0.141
<b>Log_Alpha_transformed</b>	-0.031	0.179	-0.172	.864	-0.385	0.324	0.141
<b>ThrustkNmm_transformed</b>	-0.001	0.009	-0.128	.898	-0.019	0.017	0.141

Table 4.12: RFC model coefficients.

$$RFC = 3.754 - 1.022DPW - 0.109BTS - 0.146ROP - 0.001UCS - 0.031Log(\alpha) - 0.001Thrust \quad (4.4)$$

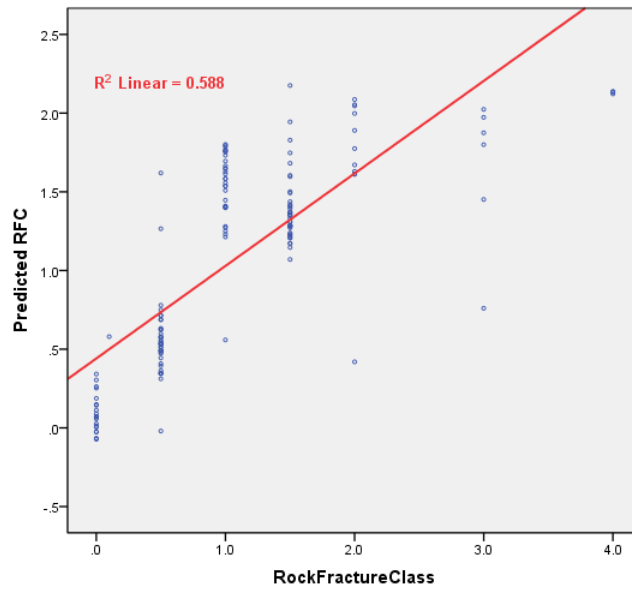


Figure 4.29: Predicted RFC model.

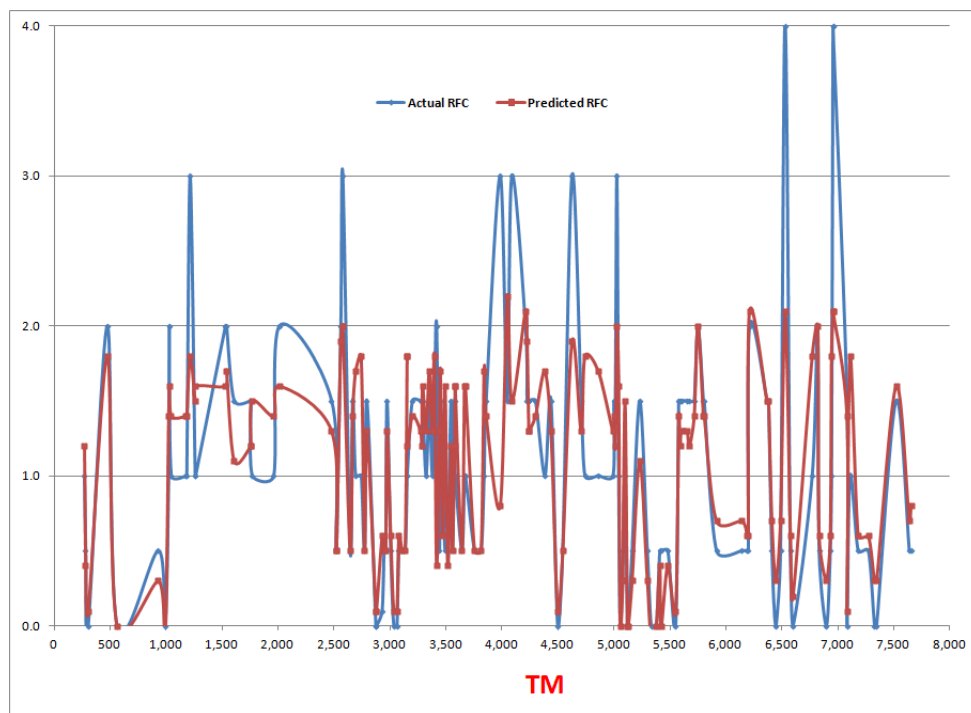


Figure 4.30: Comparison of RFC.

Scattered and line plot comparison of predicted and actual values Figs. 4.29 and 4.30 show medium accuracy of the model.

#### 4.2.3.4 Partial and Bi-Variant Correlations

Correlation measures the degree of relationship between two random variables, while the effect of a set of controlling random variables is removed. In fact, the first-order partial



correlation is a difference between a correlation and the product of the removable correlations divided by the product of the coefficients of alienation of the removable correlations [39]. The correlations procedure computes partial correlation coefficients that describe the linear relationship between two variables while controlling for the effects of one or more additional variables. Correlations are measures of linear association. Two variables can be perfectly related, but if the relationship is not linear, a correlation coefficient is not a proper statistic to measure their association. In Bi-variate correlations, the relationship between two variables is measured. The degree of relationship (how closely they are related) could be either positive or negative. The maximum number could be either +1 (positive) or -1 (negative). This number is the correlation coefficient. A zero correlation indicates no relationship and value close to +1 shows strong positive correlation [25].

		Correlations						
		UCS (Mpa.)	BTS (Mpa.)	Thrust (kN/mm)	DPW (m)	Alpha angle (degrees)	RockFracture Class	Measured ROP
UCS (Mpa.)	Pearson Correlation	1	.281**	.629**	-.116	-.089	-.002	.254**
	Sig. (2-tailed)		.000	.000	.157	.280	.985	.002
	N	151	151	151	151	151	151	151
BTS (Mpa.)	Pearson Correlation	.281**	1	.121	-.115	.025	-.037	.103
	Sig. (2-tailed)	.000		.139	.160	.764	.655	.207
	N	151	151	151	151	151	151	151
Thrust(kN/mm)	Pearson Correlation	.629**	.121	1	-.153	-.193*	.037	.577**
	Sig. (2-tailed)	.000	.139	.061	.017	.017	.652	.000
	N	151	151	151	151	151	151	151
DPW (m)	Pearson Correlation	-.116	-.115	-.153	1	.026	-.751**	-.469**
	Sig. (2-tailed)	.157	.160	.061		.749	.000	.000
	N	151	151	151	151	151	151	151
Alpha angle (degrees)	Pearson Correlation	-.089	.025	-.193*	.026	1	-.037	.213**
	Sig. (2-tailed)	.280	.764	.017	.749		.655	.009
	N	151	151	151	151	151	151	151
RockFractureClass	Pearson Correlation	-.002	-.037	.037	-.751**	-.037	1	.280**
	Sig. (2-tailed)	.985	.655	.652	.000	.655		.001
	N	151	151	151	151	151	151	151
Measured ROP	Pearson Correlation	.254**	.103	.577**	-.469**	.213**	.280**	1
	Sig. (2-tailed)	.002	.207	.000	.000	.009	.001	
	N	151	151	151	151	151	151	151

\*\* Correlation is significant at the 0.01 level (2-tailed).  
\* Correlation is significant at the 0.05 level (2-tailed).

Table 4.13: Bi-variant correlation.

Table 4.13 shows Bi-Variant correlation between machine and rock variables. It is clear from the table that, there is a good correlation between thrust and UCS ( $R^2 = 0.629$ ) and between thrust and AR ( $R^2 = 0.577$ ). Similarly a fair value of correlation ( $R^2 = 0.254$ ) exist between UCS and ROP. The best correlation is found between, DPW and RFC ( $R^2 = 0.751$ ). Overall values in tables shows that, in Queens water tunnel data, a reasonable correlation is found between machine and rock mass data.

#### 4.2.4 Conclusions

When rock mass have high UCS and low brittleness (BTS), then, obtained AR is relatively lower than expected. Maximum AR are observed as the alpha angle ranges from 50 – 65

degrees. As DPW ranges from about 20 – 40 *cm*, the obtained AR is also rather high. UCS plays a major role in TBM performance, at low UCS, AR has linear correlation with thrust, whereas at high USC, thrust make a curvi-linear correlation with AR. Advance rate (AR) prediction model has accuracy of 64.4% and AR linear regression model when plotted against the actual AR values gives a significant correlation ( $R^2 = 0.655$ ). Similarly a linear regression model for rock fracture class (RFC) was formulated and give accuracy of 57% and comparison of predicted and actual RFC values give  $R^2 = 0.588$ . Only one rock property i.e UCS is in good correlation with machine thrust ( $R^2 = 0.629$ ). Moreover machine thrust and AR have a positive linear correlation of  $R^2 = 0.577$ . Geological condition and rock mass characterization in the field should be investigated before selecting the TBM, since the machine specification including thrust, cutter-head power and both diameter and number of disc have influence on the ROP [33]. Hence geology and rock properties including orientation, condition and frequency of discontinuities together with rock strength and brittleness, provide the major control on the penetrability of tunnel boring machine.

### 4.3 Vereina tunnel

Vereina tunnel data consists of tunnel meters, thrust, torque, advance rate, petrography, fracture class, geological classes and tool wear. Data were segregated into different segments suitable for Microsoft excel, Fuzzy logic, statistical software “R”, Math-Lab code and IBM SPSS19. Rock fracture class (RFC) is sum of 5 – 6 rock geological parameters e.g fracture frequency, fracture spacing, orientation etc. Petrography deals with the systematic description of rocks. The term is sometimes loosely used as synonymous with "petrology", which, being the broad science of rocks, is concerned not only with precise description but also with understanding the origin (petrogenesis), modification (metamorphism), and ultimate decay of rocks [40], [41].

#### 4.3.1 Data Analysis by Microsoft Excel

Rock mass and TBM data are plotted against tunnel meters to see the variation and trend of individual parameter as chainage proceed ahead. It is clear from Fig. 4.31 that thrust and advance rate (AR) vary almost in the same pattern from 2000-*TM* to 5000-*TM*, then from 5000-*TM* to 10000-*TM* the relation is inverse i.e low ROP at relatively high thrust. From 10,000 – *TM* to end of 12,000 – *TM*, very low ROP is observed at high thrust, which may be due to relatively high rock strength and due to learning effect of the machine driver, who tried to push more thrust to achieve more ROP without knowing the effects of other parameters.

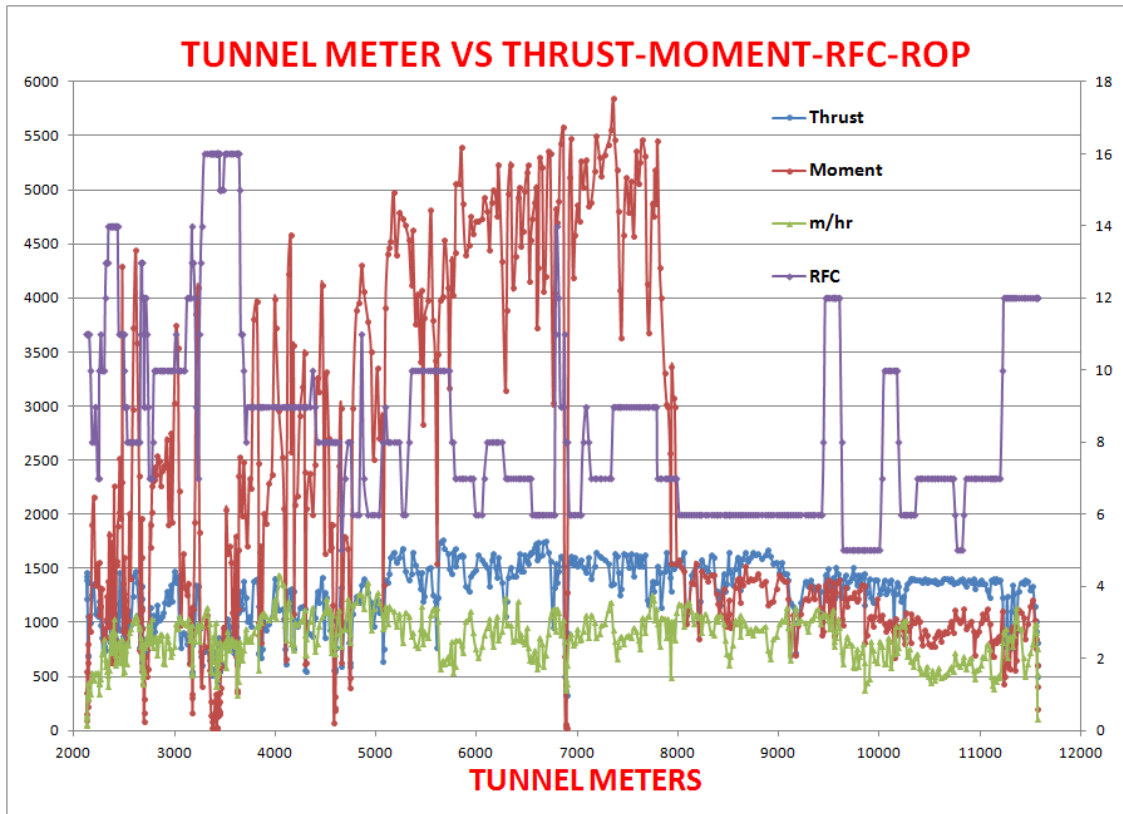
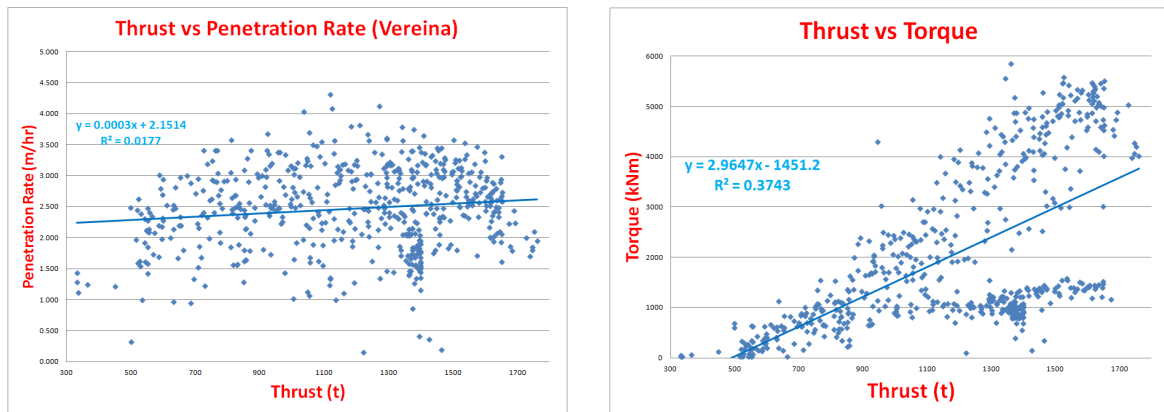


Figure 4.31: TM versus ROP, RMC, RFC and torque.



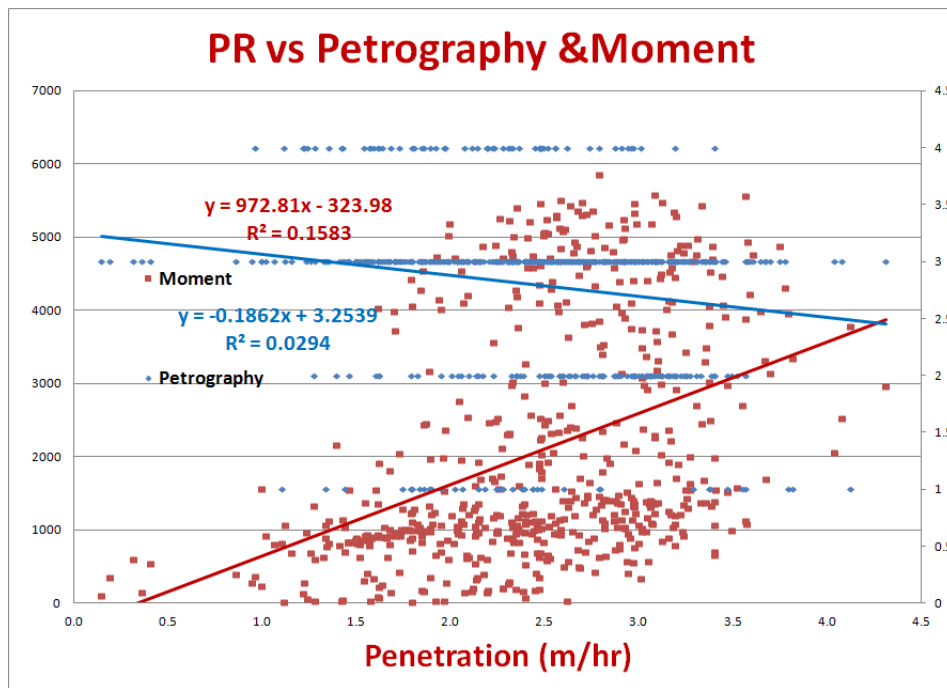
(a) Thrust versus PR.

(b) Thrust versus torque.

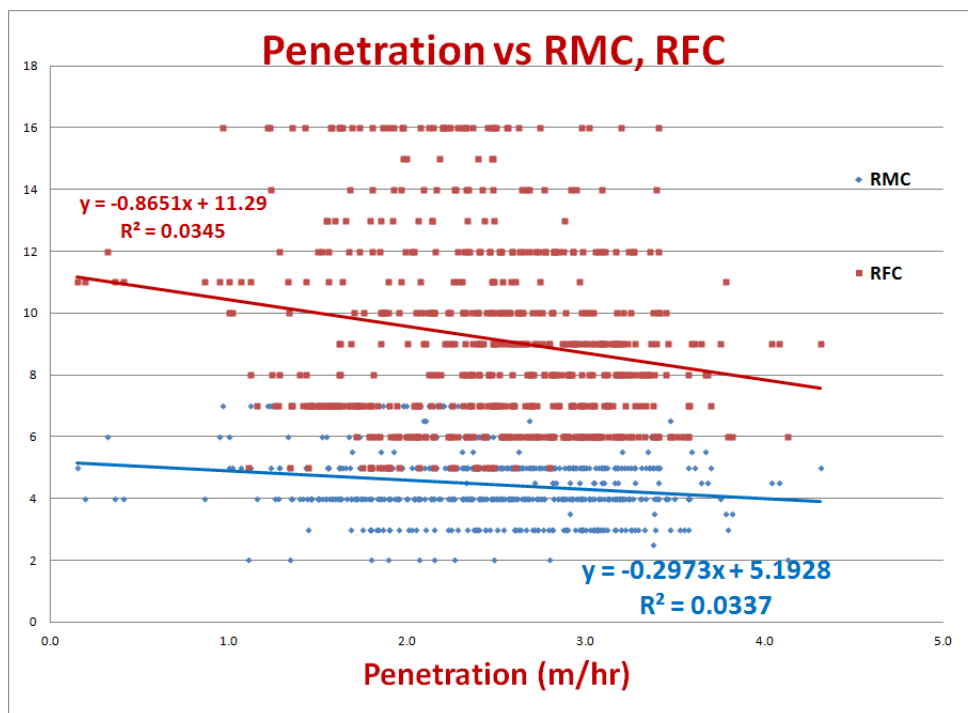
Figure 4.32: Thrust versus PR and torque.

Figure 4.32 shows relations between thrust and penetration and moment. Relation between thrust and ROP is very complicated. To illustrate it, a linear trend line is drawn by curve fit having  $R^2 = 0.018$ . Thrust and moment of machine also have same linear trend with  $R^2 = 0.38$ . It is clear from Figs. 4.33(a,b) that penetration is decreased with increase of all, RMC, RFC and petrography. On the other hand penetration increases with high values of torque. Figs. 4.34(a,b) clearly shows that RFC and RMC are inversely proportional to thrust, i.e. highly fractured rock can be easily excavated by TBM even

at moderate thrust.

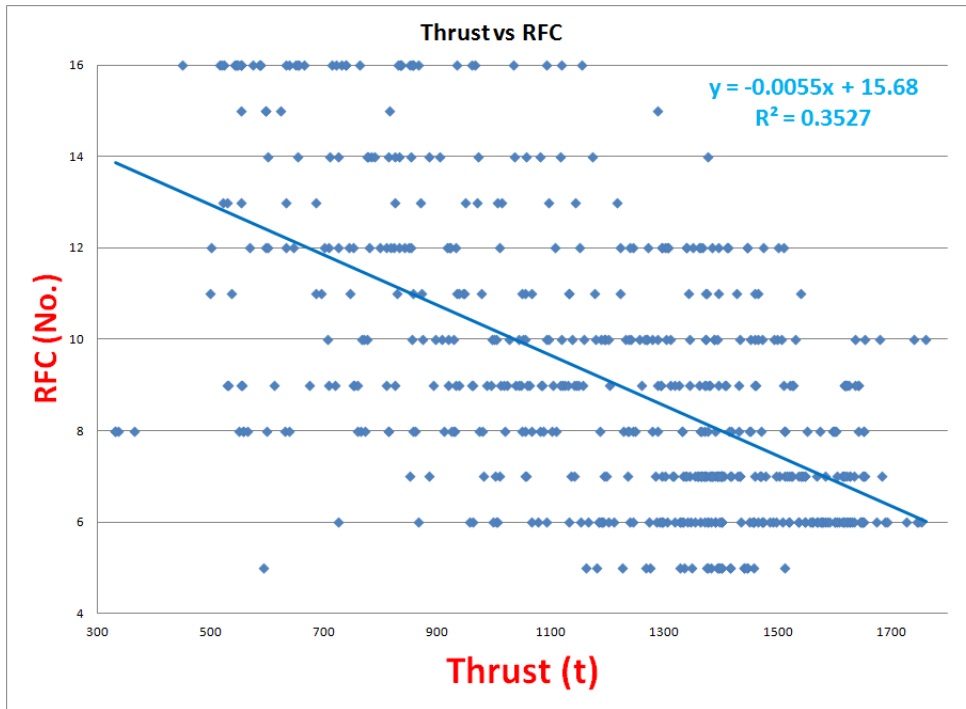


(a) PR versus torque and petrography.

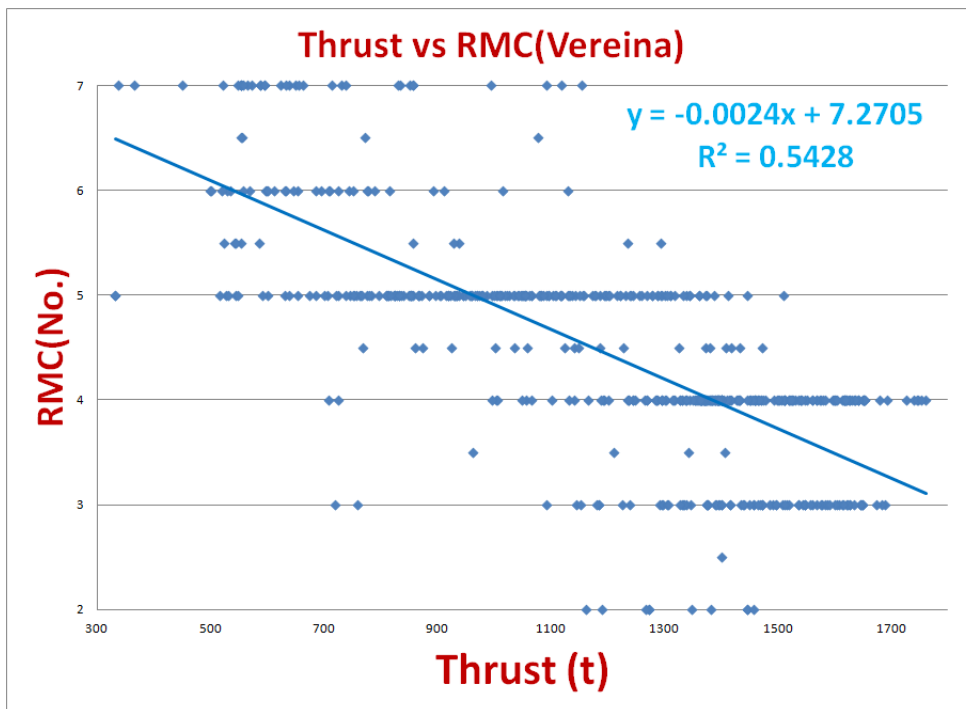


(b) PR versus RMC and RFC

Figure 4.33: Penetration versus RMC, RFC, torque and petrography.



(a) Thrust versus PR.



(b) Thrust versus Torque.

Figure 4.34: Thrust versus RMC and RFC.

### 4.3.2 Data Analysis and RMC Prediction by Fuzzy Logic Tools

For Fuzzy logic an input data file was prepared after filtering the data. Input data consists of three major parameters i.e. tunnel meters per day, cutter thrust and torque (power consumption), which acts as Fuzzy logic inputs and from these input rule base converts

them into a single output as rock mass class (RMC). An *I/O* subroutine for reading data from excels to Mat-Lab and then for plotting the results is written. This sub-routine can read data from any excel file how large it may be and can plot the data in required domain. Another *I/O* (input-output) routine is written, which perform Fuzzy logic operation (rule base) by taking three inputs and plot the output result as RMC. Then 3 – *D* surfaces were plotted for thrust, power and RMC for both data files.

Figure 4.35 shows a rule base table for Vereina tunnel. Rule base was compiled after a detailed study of relations between rock and machine parameters. After detailed analysis of data, the rule base is formed. But still here too much room for improvement in rule base is available by incorporating more variables like presence of water, overburden etc. as input variables, in rule base decision box.

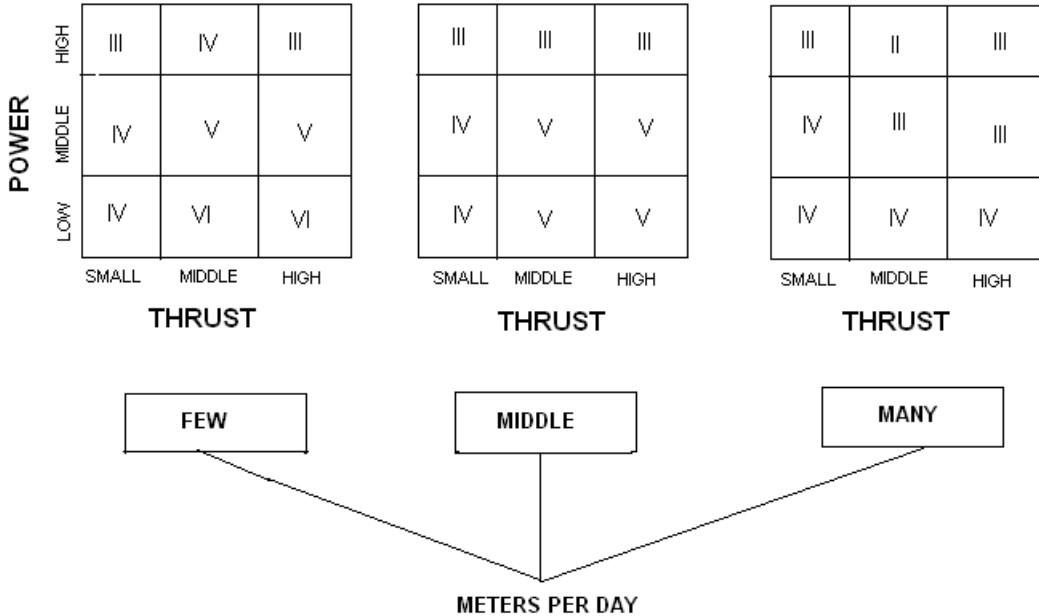


Figure 4.35: Fuzzy rule-base for Vereina tunnel data.

**4.3.2.1 Tunnel Section from 3000-TM to 4000-TM**

When we compare the results of RMC, calculated from Fuzzy logic with actual RMC, they are in good coincidence, i.e. the trend is same, except at three points (at 4313 m, 4634.7m and 4881.3m). When we see the 3 – *D* surface generated by Fuzzy tools (Fig. 4.36), at medium thrust and power consumption RMC is high value. This may be due to moderate strength rock ( $4 < RMC < 6$ ). TBM is more efficient and penetration is more at medium thrust and power consumption.

### Input/output subroutine for Vereina Tunnel 4000m-5000m

```
a=newfis('Vereina Tunnel');
a=addvar(a,'input','Thrust of the Cutter',[500 1350]);
a=addmf(a,'input',1,'small','trapmf',[425 700 750 900]);
a=addmf(a,'input',1,'middle','trimf',[750 925 1137]);
a=addmf(a,'input',1,'great','gaussmf',[925 1137 1250 1400]);
a=addvar(a,'input','Boring Meters per Day',[10 34]);
a=addmf(a,'input',2,'few','trapmf',[1 9 11 18]);
a=addmf(a,'input',2,'middle','trimf',[15 22.5 30]);
a=addmf(a,'input',2,'many','trapmf',[25 33 35 42]);
a=addvar(a,'input','Power Consumption',[70 4600]);
a=addmf(a,'input',3,'low','trapmf',[60 100 720 1200]);
a=addmf(a,'input',3,'middle','trimf',[1200 2335 3467]);
a=addmf(a,'input',3,'high','trapmf',[2335 3467 4500 4600]);
a=addvar(a,'output','RMC',[1 7]);
a=addmf(a,'output',1,'I','trapmf',[-1 0 1.2 2]);
a=addmf(a,'output',1,'II','trimf',[1 2 3]);
a=addmf(a,'output',1,'III','trimf',[2 3 4]);
a=addmf(a,'output',1,'IV','trimf',[3 4 5]);
a=addmf(a,'output',1,'V','trimf',[4 5 6]);
a=addmf(a,'output',1,'VI','trapmf',[5 5.8 8 8]);
ruleList=[ ...
1 1 1 5 1 1
2 1 1 6 1 1
3 1 1 6 1 1
1 1 2 4 1 1
1 1 3 3 1 1
2 1 2 5 1 1
2 1 3 4 1 1
3 1 2 5 1 1
3 1 3 3 1 1
1 2 1 4 1 1
2 2 1 5 1 1
3 2 1 5 1 1
1 2 2 4 1 1
2 2 2 4 1 1
3 2 2 4 1 1
1 2 3 3 1 1
2 2 3 3 1 1
3 2 3 3 1 1
1 3 1 4 1 1
2 3 1 4 1 1
3 3 1 4 1 1
1 3 2 4 1 1
2 3 2 3 1 1
3 3 2 3 1 1
1 3 3 3 1 1
2 3 3 2 1 1
3 3 3 3 1 1];
a=addrule(a,ruleList); gensurf(a)
```

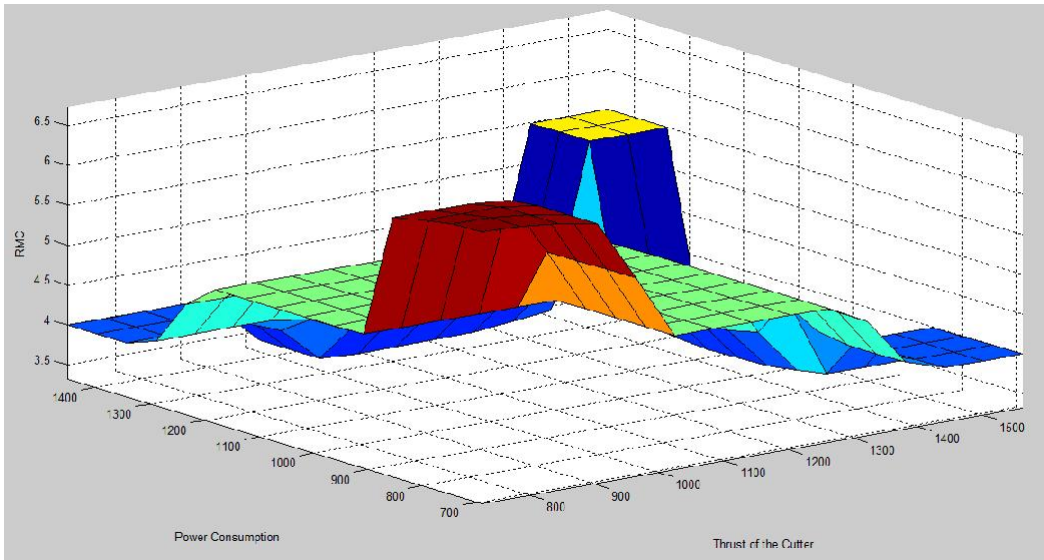


Figure 4.36: Fuzzy 3-D surface.

It is clear from the 3-D surface (Fig. 4.36) that high values of RMC correspond to moderate values of thrust and machine power. This clearly shows the effect of rock mass strength upon TBM performance and advance rate. Fig. 4.37 displays a comparison between actual and Fuzzy logic RMC. It is clear from the figure that, there is a good correlation and match between actual and Fuzzy values, hence this tool give a reasonably good prediction.

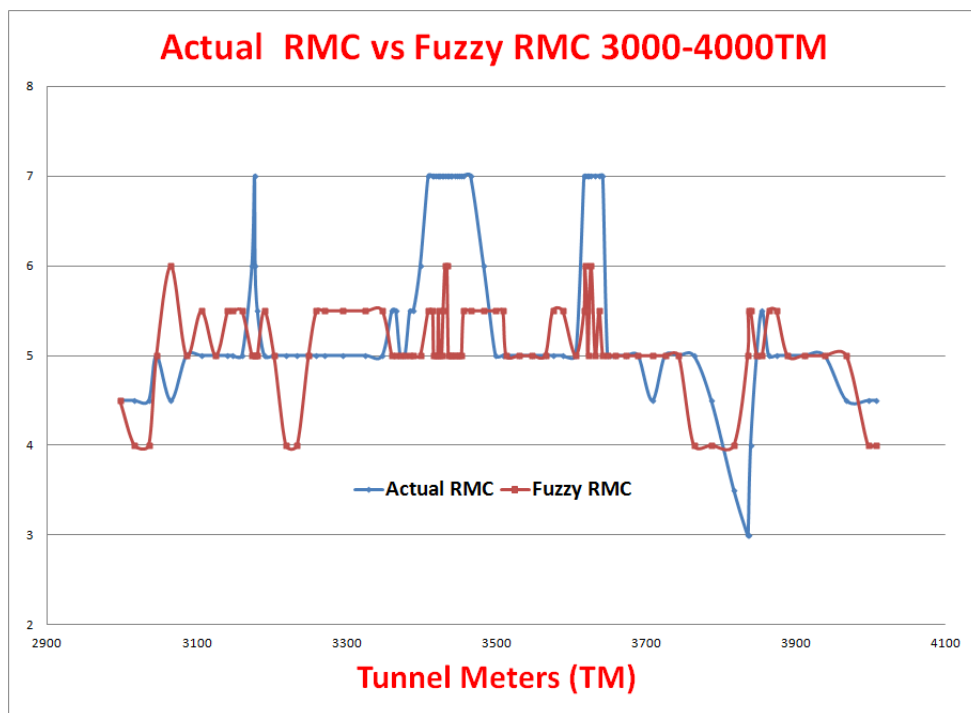
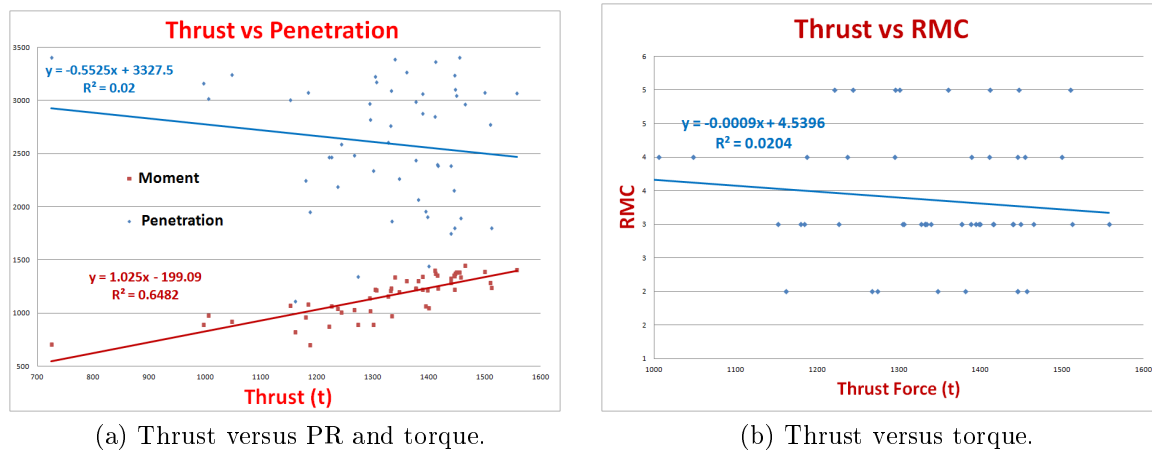


Figure 4.37: Comparison of actual and Fuzzy RMC.



#### 4.3.2.2 Section Tunnel Meters 9,000 m to 10,000 m

Tunnel section from 9,000 to 10,000 TM shows entirely different behavior as compared to section 3,000 to 4,000 TM. Thrust versus penetration has an inverse proportionality. This may be due to a high strength of rock. Moreover due to low rock fracture value here chip formation was difficult. More tool wear resulted low advance rate even on high thrust values. Machine thrust plotted against *RMC*, shows inverse proportionality, that means more thrust needed for strong and fractured rock. Thrust and torque are directly related in a linear correlation.



(a) Thrust versus PR and torque.

(b) Thrust versus torque.

Figure 4.38: Thrust versus penetration, RMC, torque 9000-10000 TM.

This section was also analyzed by Fuzzy logic. Separate subroutine was written for previous section after formulating the Fuzzy rule base. 3-D surface was generated for three parameters i.e thrust, RMC and power consumption of the TBM. 3-D surface (Fig. 4.39) shows more advance rate at low RMC and at medium and high values of thrust. Penetration is too low at low values of thrust and RMC.

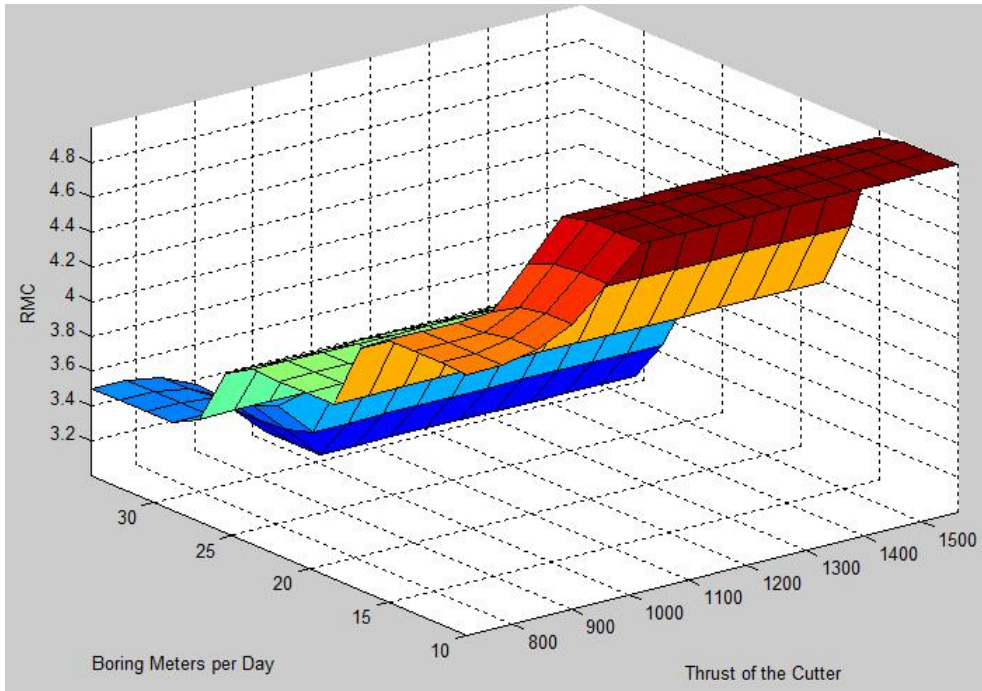


Figure 4.39: 3-D surface by Fuzzy logic.



Figure 4.40: Comparison of RMC.

RMC from Fuzzy logic and the actual are compared. Figure 4.40 shows both actual and predicted RMC follow the same trend but differ from each other. They have coincidence only on few points (at 9097m, 9463 m, 9542m and 9590 m). It can be extracted from the data results that Fuzzy logic can give good results if we take into account more parameters and re-formulate the rule base.

### 4.3.3 3-D Analysis with “R”

Statistical software “R” was used to draw a 3-D surfaces for different variables, which show the correlation and dependence of these variables on each other. Different views of these surfaces are shown to illustrate the interdependence of different parameters on each other.

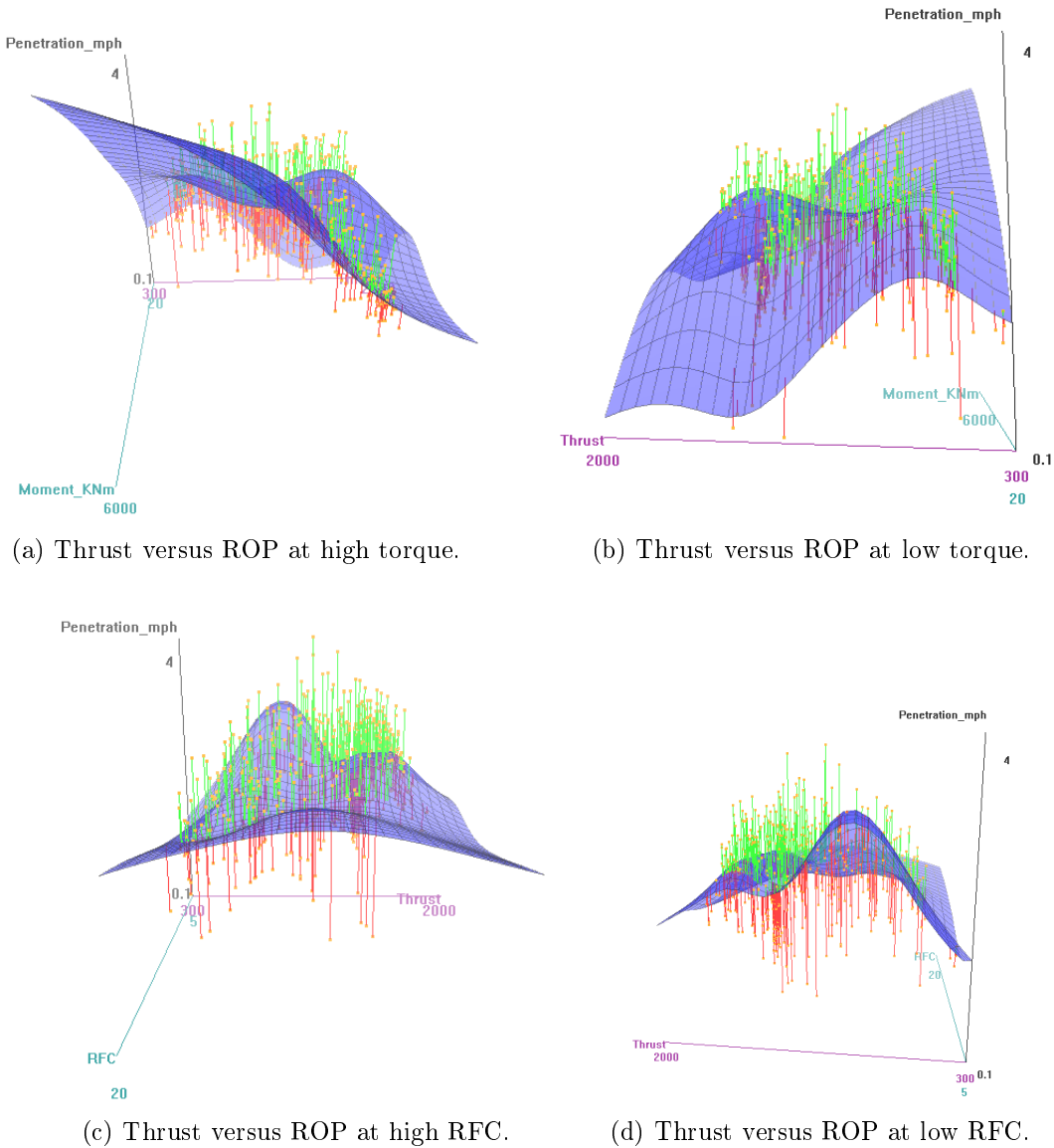


Figure 4.41: Thrust versus ROP at low and high torque.

From Figs. 4.41(a-d) it is clear that penetration is inversely proportional to thrust at high values of torque and same at low torque values, at low RFC advance rate is almost constant. At low RFC, penetration is maximum at medium thrust, showing the effect of rock fracture class upon TBM performance. Where as in Figs. 4.42(a,b,c,d), penetration when plotted against thrust at high and low RMC, shows at high rock mass class, ROP is again maximum at moderate thrust, while at low RMC, penetration looks

almost independent of RMC. At both high and low petrography, penetration is maximum at moderate thrust values. It can be concluded that TBM efficiency in terms of penetration and tool wear, is max when machine applied thrust values are of medium range. Overall RFC and torque has a little effect on ROP and thrust relation.

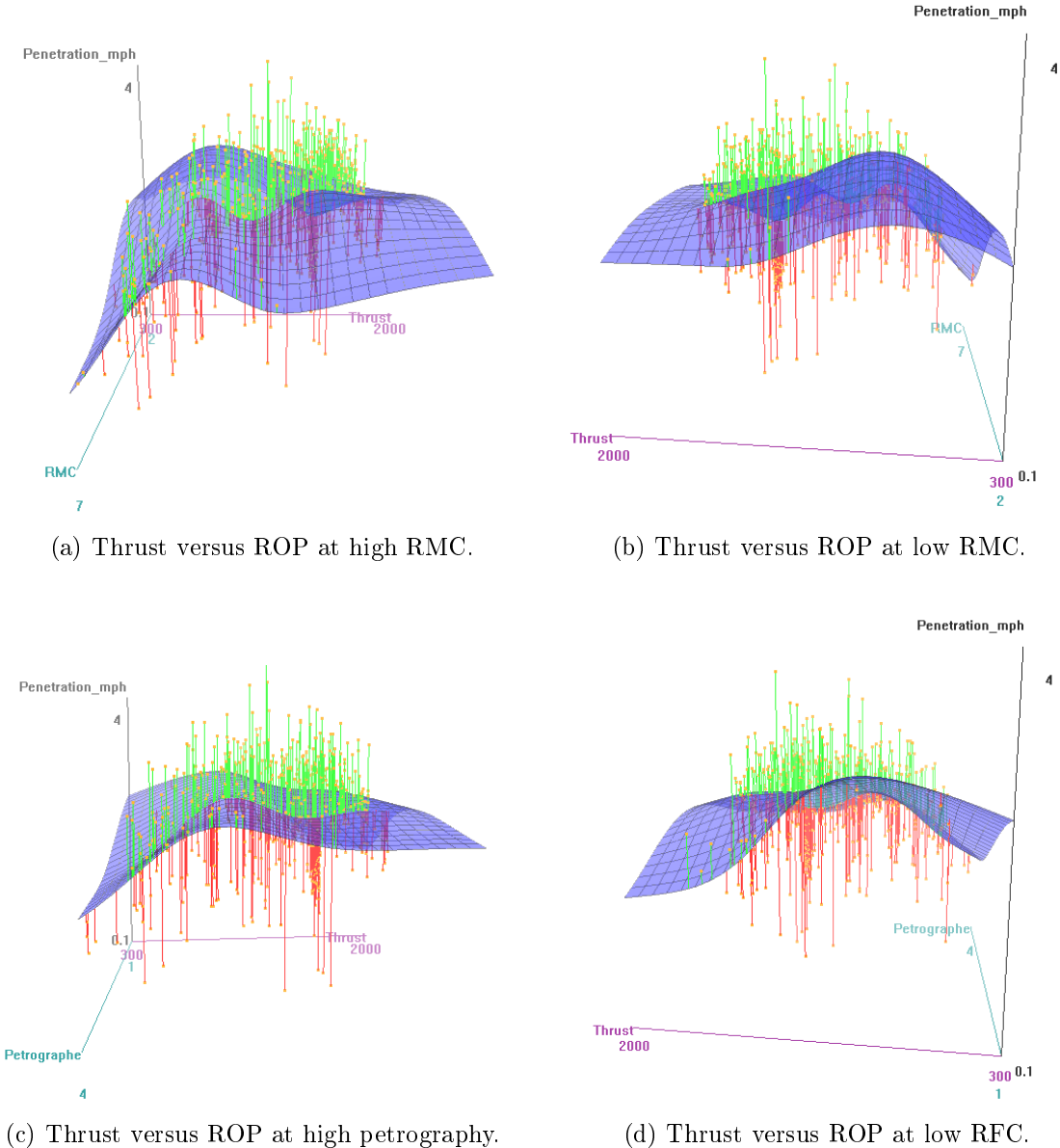


Figure 4.42: Thrust versus ROP at high and low RMC.

### 4.3.4 Statistical Modeling with IBM SPSS 19

After multidimensional analysis, different models are predicted using available data. Normal frequency analysis shows the following results. Penetration and rock fractured classification show a good normal distribution with very low standard deviation, on the other hand torque and RFC don't follow any normal distribution. Model selection method was

“forward stepwise” and default combining method was “mean” at 95% confidence level.

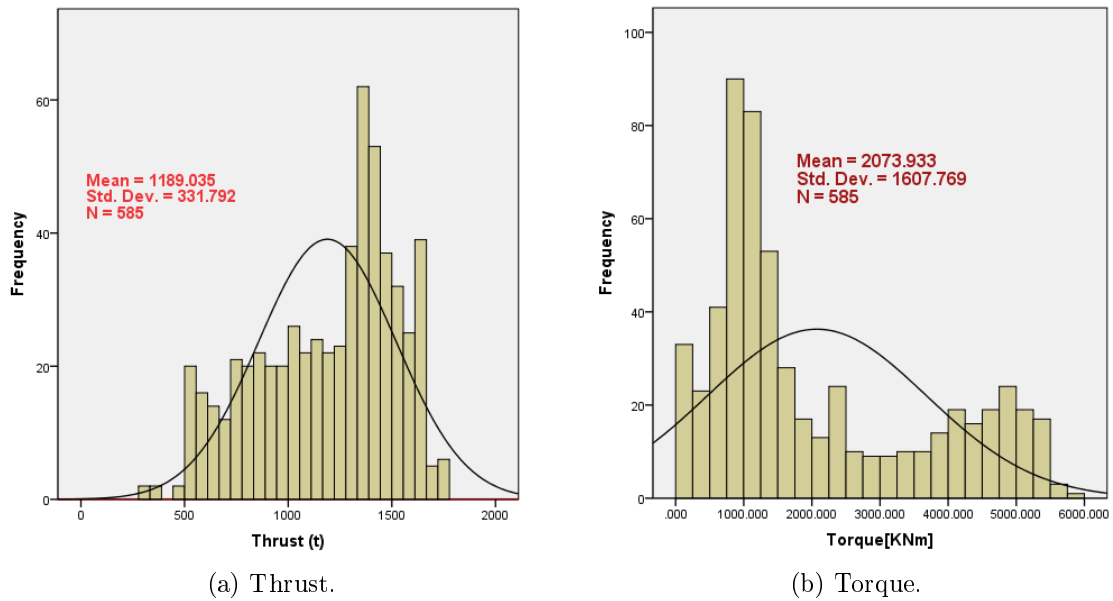


Figure 4.43: Histograms for thrust and torque.

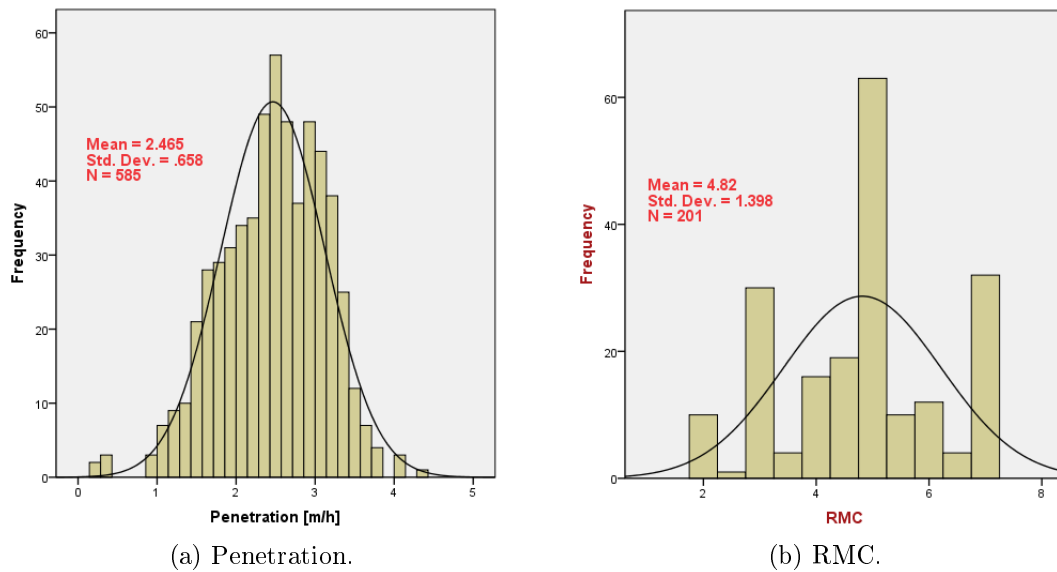


Figure 4.44: Histograms for ROP and RMC.

Figures 4.43 and 4.44 shows frequency distribution of different variables. Only single variable penetration rate (ROP) has a perfect normal frequency distribution with ( $sd = 0.659$ ). Torque and RFC data is left skewed. RMC is also showing a normal distribution with some exceptions.

### 4.3.4.1 Penetration Rate Prediction Model

Penetration rate (PR) is always a major parameter while discussing the optimization or performance of a TBM. After multidimensional analysis, PR was predicted by SPSS linear regression analysis. Model summary, effects and coefficients of the input variables are shown in tables 4.14-4.16 respectively.

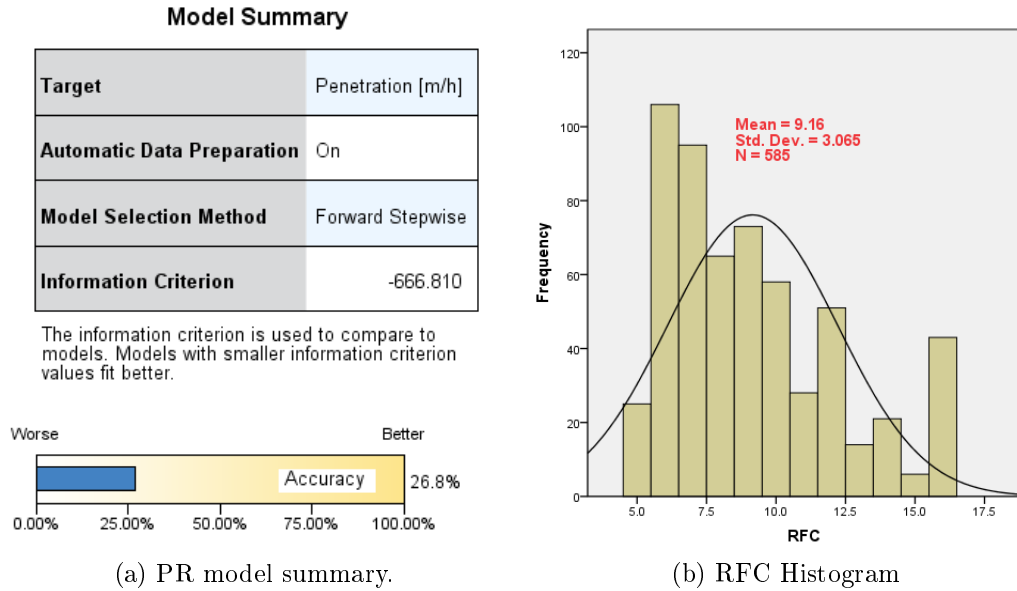


Table 4.14: Model summary and coefficients.

Effects		Target: Penetration [m/h]				
Source	Sum of Squares	df	Mean Square	F	Sig.	Importance
<b>Corrected Model ▼</b>	69.295	5	13.859	43.782	.000	
<b>MomentKNm_transformed</b>	51.974	1	51.974	164.193	.000	0.233
<b>Thrust_transformed</b>	26.307	1	26.307	83.108	.000	0.208
<b>RMC_transformed</b>	7.905	1	7.905	24.972	.000	0.190
<b>mday_transformed</b>	4.489	1	4.489	14.180	.000	0.186
<b>RFC_transformed</b>	1.869	1	1.869	5.904	.015	0.184
<b>Residual</b>	183.278	579	0.317			
<b>Corrected Total</b>	252.573	584				

Table 4.15: PR model effects.

There were five predictors used to establish a model for ROP table. 4.15. Torque and thrust have more influence on model forming and RFC have a least effect to model. Similarly in step forward process torque was the first and most important parameter to involve in iteration process and RFC is last and least important parameter.

Coefficients		Target: Penetration [m/h]					
Model Term	Coefficient ▼	Std.Error	t	Sig.	95% Confidence Interval		Importance
					Lower	Upper	
Intercept	1.388	0.864	1.606	.109	-0.309	3.086	
MomentKNm_transformed	0.000	0.000	12.814	.000	0.000	0.000	0.233
Thrust_transformed	-0.001	0.000	-9.116	.000	-0.001	-0.001	0.208
RMC_transformed	-0.202	0.040	-4.997	.000	-0.281	-0.122	0.190
mday_transformed	0.520	0.138	3.766	.000	0.249	0.792	0.186
RFC_transformed	-0.028	0.012	-2.430	.015	-0.052	-0.005	0.184

(a) Model coefficients.

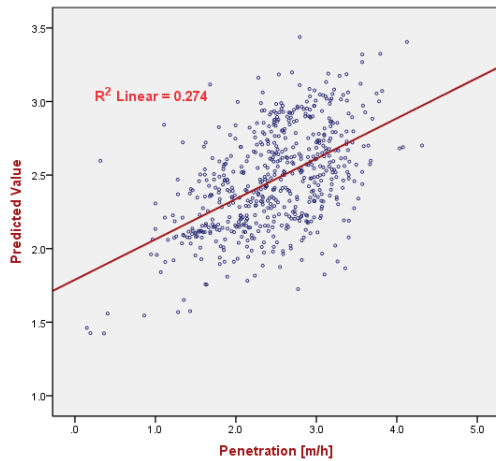
Relation of Property with ROP	Empirical Equation	Corr. Coeff. R
ROP vs Thrust	$ROP = 0.0003Thrust + 2.15$	0.13
ROP vs RMC	$ROP = 0.297RMC + 5.193$	0.13
ROP vs RFC	$ROP = -0.865RFC + 11.29$	0.24
ROP vs (meters/day)	$ROP = 0.159 + 5.68$	0.24

(b) Table of linear equations between input and target variable.

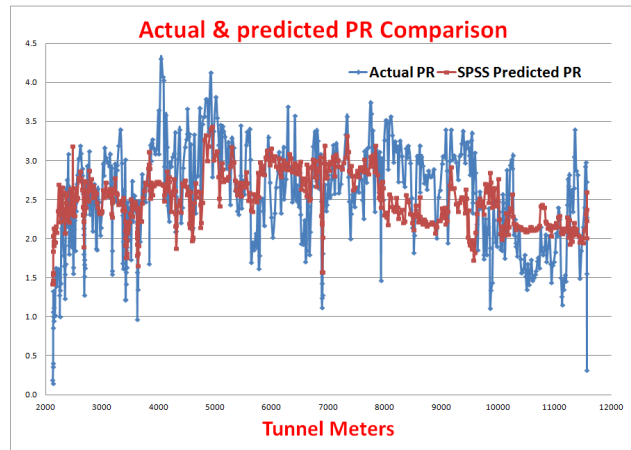
Table 4.16: Table of PR model coefficients and linear equations.

Table 4.16 shows a model coefficients. Standard deviation of predicted value ROP is ( $R^2 = 0.658$ ) and ( $R = 0.811$ ). After using all of these variables, coefficients, residuals and linear equations from table 4.16b, the ROP model was predicted, that is shown below in eq. 4.5;

$$ROP(m/h) = 1.388 - 0.001Thrust + 0.52(m/day) - 0.202RMC - 0.028RFC \quad (4.5)$$



(a) Scattered plot for PR model.



(b) Line plot for PR model.

Figure 4.45: Prediction model plot.

The model obtained is plotted and compared in Figs. 4.45(a, b) respectively, predicted values are plotted versus actual ROP. A good correlation between the two values is found with  $R = 0.52$ . and a good coincidence is found between actual and predicted ROP.

#### 4.3.4.2 Prediction Models for RMC and RFC

Rock mass class was also predicted by Fuzzy logic. Here for the counter check and comparison, RMC is analysed and an empirical prediction model with SPSS19 is formulated.

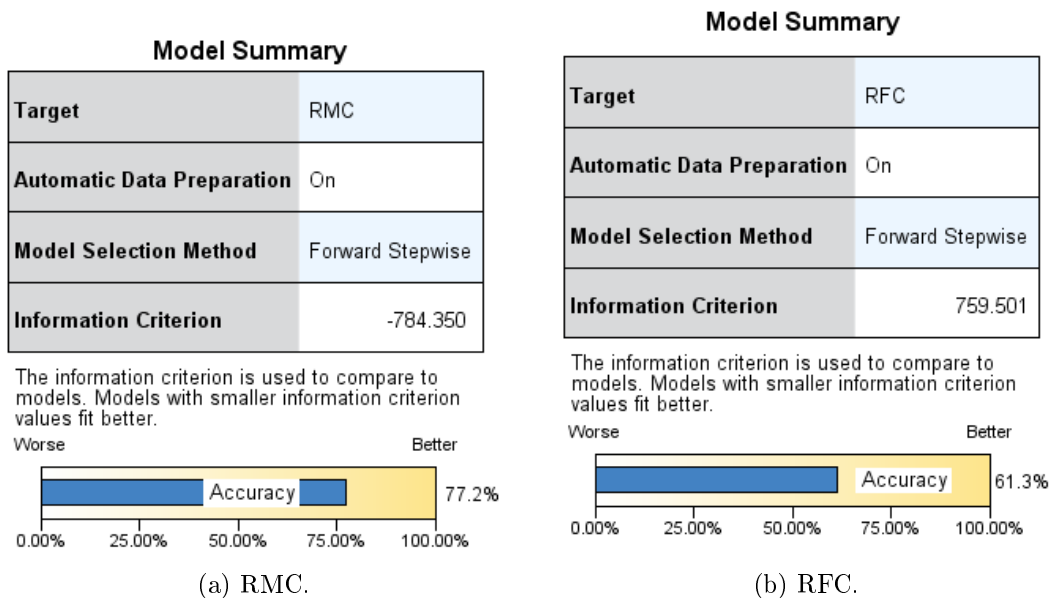


Table 4.17: Model summary.



Effects Target: RMC						
Source	Sum of Squares	df	Mean Square	F	Sig.	Importance
Corrected Model ▼	511.889	5	102.378	395.397	.000	
Thrust_transformed	101.126	1	101.126	390.564	.000	0.274
Petrographie_transformed	40.971	1	40.971	158.234	.000	0.209
MomentKNm_transformed	12.501	1	12.501	48.281	.000	0.178
RFC_transformed	5.374	1	5.374	20.754	.000	0.170
Penetrationmh_transformed	5.220	1	5.220	20.160	.000	0.170
Residual	149.917	579	0.259			
Corrected Total	661.806	584				

(a) RMC.

Effects Target: RFC						
Source	Sum of Squares	df	Mean Square	F	Sig.	Importance
Corrected Model ▼	3,379.349	4	844.837	232.651	.000	
Petrographie_transformed	756.889	1	756.889	208.432	.000	0.292
Thrust_transformed	584.058	1	584.058	160.838	.000	0.275
RMC_transformed	22.035	1	22.035	6.068	.014	0.217
Penetrationmh_transformed	10.011	1	10.011	2.757	.097	0.216
Residual	2,106.182	580	3.631			
Corrected Total	5,485.532	584				

(b) RFC.

Table 4.18: Model effects.

Rock fractured class (RFC) was also an important parameters to analyse. First of all RFC value was calculated by adding different numbers available in data. Then an empirical prediction model for RFC was formulated. Table 4.17(a,b) shows model summary for RMC and RFC linear regression models. RMC model shows a higher accuracy as compare to RFC model. Both prediction model are based upon "step forward" calculation methods. Table 4.18 shows effects of predictors (input variables) upon output variables (RMC and RFC). For RMC linear regression model, thrust plays the most important role, while in the RFC model, petrography is the most important input variable. Five predictors in RMC and four predictors in RFC are used to formulate linear regression model.

Coefficients				Target: RMC			
Model Term	Coefficient ▼	Std.Error	t	Sig.	95% Confidence Interval		Importance
					Lower	Upper	
Intercept	5.012	0.216	23.151	.000	4.587	5.437	
Thrust_transformed	-0.002	0.000	-19.763	.000	-0.002	-0.002	0.274
Petrographie_transformed	0.536	0.043	12.579	.000	0.452	0.620	0.209
MomentKNm_transformed	0.000	0.000	6.948	.000	0.000	0.000	0.178
RFC_transformed	0.050	0.011	4.556	.000	0.029	0.072	0.170
Penetrationmh_transformed	-0.167	0.037	-4.490	.000	-0.240	-0.094	0.170

(a) RMC.

Coefficients				Target: RFC			
Model Term	Coefficient ▼	Std.Error	t	Sig.	95% Confidence Interval		Importance
					Lower	Upper	
Intercept	6.346	0.788	8.051	.000	4.798	7.894	
Petrographie_transformed	2.109	0.146	14.437	.000	1.822	2.396	0.292
Thrust_transformed	-0.003	0.000	-12.682	.000	-0.004	-0.003	0.275
RMC_transformed	0.308	0.125	2.463	.014	0.062	0.554	0.217
Penetrationmh_transformed	-0.206	0.124	-1.660	.097	-0.451	0.038	0.216

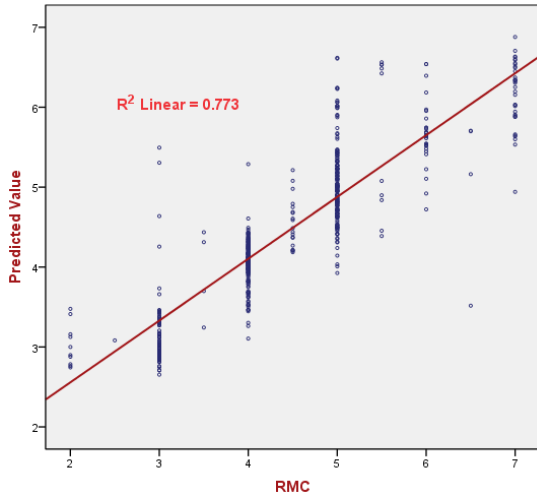
(b) RFC.

Table 4.19: Model coefficients.

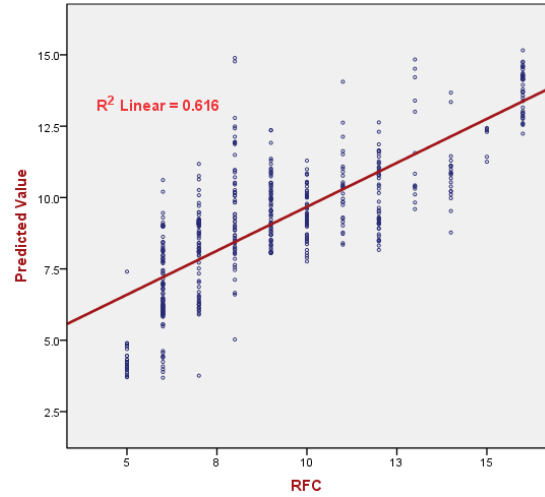
From these coefficients (table 4.19), following linear regression models for RMC and RFC are formulated and shown in Eqs. 4.6 and 4.7 respectively. Resultant output from these models are plotted and shown in Figs. 4.46(a,b). It is clear from the plot that RMC model ( $R^2 = 0.773$ ) is more accurate than RFC model ( $R^2 = 0.616$ ).

$$RMC = 5.012 - 0.002Thrust + 0.536Petrography - 0.001Torque - 0.05RFC \quad (4.6)$$

$$RFC = 6.346 - 0.003Thrust + 2.11Petrography - 0.206ROP + 0.308RMC \quad (4.7)$$



(a) RMC scattered plot.



(b) RFC scattered plot.

Figure 4.46: RMC and RFC models scattered plots.

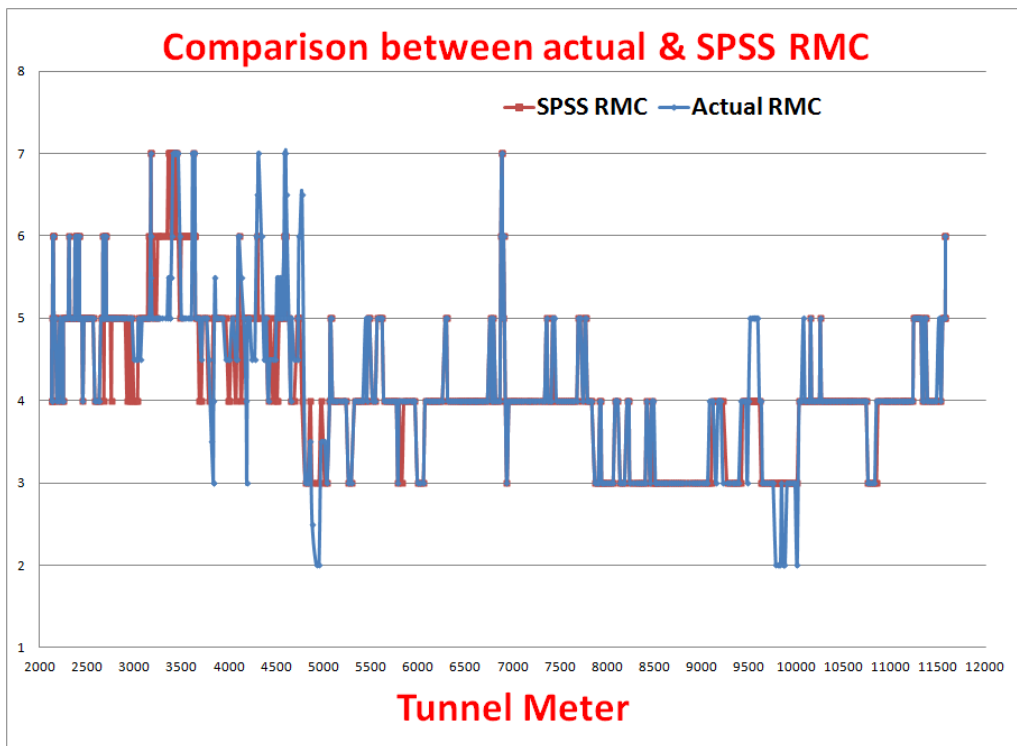


Figure 4.47: Comparison of RMC.

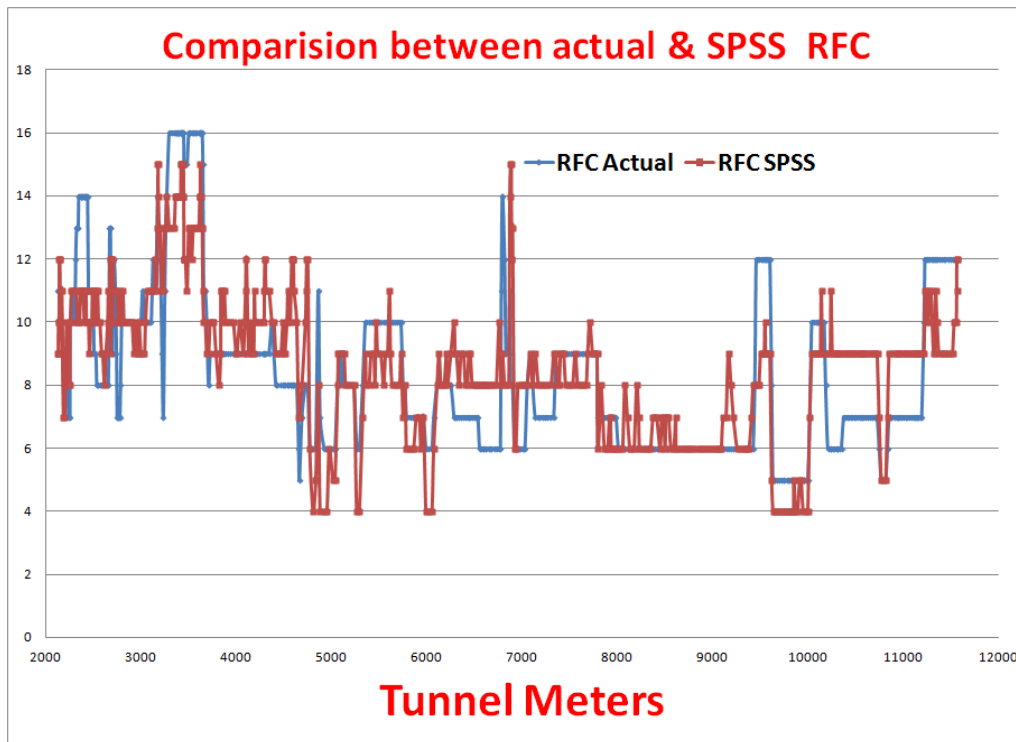


Figure 4.48: Comparison between actual and predicted RFC.

Figures 4.47 and 4.48 shows a comparison between actual (field) RMC, Fuzzy logic predicted and SPSS predicted RMC values. In the case of RMC (Fig. 4.47) SPSS gives a reasonably good prediction, except for few values at the start of tunnel chainage, most of the predicted values coincides with field RMC values. However RFC predicted values at start of chainage, at the end section of tunnel length, SPSS predicted values contradict with field RFC values.

### 4.3.4.3 Correlation and Correlation Coefficient

		Correlations						
		Thrust (t)	Moment[kNm]	m/day	Penetration [m/h]	RFC	RMC	Petrographe
Thrust (t)	Pearson Correlation	1	.612**	.354**	.133**	-.594**	-.690**	-.424**
	Sig. (2-tailed)		.000	.000	.001	.000	.000	.000
	N	585	585	585	585	585	201	585
Moment[kNm]	Pearson Correlation	.612**	1	.233**	.398**	-.312**	-.329**	-.109**
	Sig. (2-tailed)	.000		.000	.000	.000	.000	.009
	N	585	585	585	585	585	201	585
m/day	Pearson Correlation	.354**	.233**	1	.244**	.009	-.217**	-.114**
	Sig. (2-tailed)	.000	.000		.000	.834	.002	.006
	N	585	585	585	585	585	201	585
Penetration [m/h]	Pearson Correlation	.133**	.398**	.244**	1	-.186**	-.257**	-.172**
	Sig. (2-tailed)	.001	.000	.000		.000	.000	.000
	N	585	585	585	585	585	201	585
RFC	Pearson Correlation	-.594**	-.312**	.009	-.186**	1	.723**	.701**
	Sig. (2-tailed)	.000	.000	.834	.000		.000	.000
	N	585	585	585	585	585	201	585
RMC	Pearson Correlation	-.690**	-.329**	-.217**	-.257**	.723**	1	.765**
	Sig. (2-tailed)	.000	.000	.002	.000	.000		.000
	N	201	201	201	201	201	201	201
Petrographe	Pearson Correlation	-.424**	-.109**	-.114**	-.172**	.701**	.765**	1
	Sig. (2-tailed)	.000	.009	.006	.000	.000	.000	
	N	585	585	585	585	585	201	586

\*\* . Correlation is significant at the 0.01 level (2-tailed).

Table 4.20: Pearson correlation coefficient table.

Table 4.20 shows correlation coefficient between different variables. First row of the table shows correlation between thrust ( $t$ ) and all other parameters, like AR ( $m/hr$ ), torque ( $kNm$ ), Petrography, RMC and RFC. It is clear from the table that thrust have a good correlation with all above mentioned parameters except the penetration rate. Moreover, machine parameters are strongly correlated with rock mass properties, e.g thrust-RMC correlation coefficient is  $R^2 = 0.690$ , thrust-RFC correlation coefficient is  $R^2 = 0.594$  and the value for thrust-petrography is  $R^2 = 0.424$ . Penetration ( $m/hr$ ) has greater influence from torque and RMC rather than thrust.

### 4.3.5 Conclusions

Deep tunnels have their specific problems in regard to geo-technical and rock mechanics. The Vereina tunnel is 19.05 km long with an overburden of 1500 m which mainly comprises gneiss and amphibolites the latter being extremely hard and tough rocks. All these formations are bedded horizontally or sub-horizontally, like the sedimentary formations lying underneath and tunnel was excavated by an open TBM. Due to the high water pressures deep tunnels are normally drained tunnels, it is neither technically feasible nor economically reasonable to try to seal off entirely deep tunnels [33]. So for TBM performance prediction, all rock mass properties like rock strength, RFC, RMC, water pressure and overburden must be kept in calculations, for the calculation for machine advance rate. But unfortunately here in Vereina tunnel data analysis, no data was available regarding

presence of water and effect of overburden. Moreover underground temperature increases rigorously with depth.

Linear relation between thrust and penetration shows a little increase in penetration with thrust, but when we plot a 3-D surface, to see the effect of third variable, it is clearly observed that penetration is only maximum, when TBM thrust has moderate values. This is valid for both high and low RFC, RMC and petrography values. Fuzzy logic is another tool here, that was applied for prediction of penetration and RMC and shows acceptable results. RMC, RFC and penetration rate were also predicted by using SPSS19 software packages and give very efficient and accurate result for RMC prediction model  $R^2 = 0.773$ . Last part of analysis consists of correlation between machine and rock mass parameters. Here in Vereina tunnel data, a very good linear correlation between TBM parameters and rock mass properties (thrust-RMC,  $R = 0.831$ ) is observed. Correlation between between thrust and torque  $R = 0.78$  is found. But there is no significant correlation between thrust and penetration  $R = 0.364$ .

## 4.4 Hemerwald Tunnel

### 4.4.1 Preparation for Excel Data Sheets

Hemerwald tunnel data was received as print form (hard copy) of bore logging table as shown in Fig. 4.49. Excel sheets were generated by picking each data point manually.

		3000	3050	3100	3150
DATUM		3.5.78	4.5.78	5.5.78	6.5.78
STATION					
GESTEIN				SCHIEFERGNEIS MIT GÜMMERSCHIEFERLAG	
GEBIRGSKLASSE					
VORTRIEB (lfm)		45,60	39,60	34,80	49,40
NETTOBOHRZEIT (Std)		16,67	16,00	12,50	16,42
AUSLASTUNG % (Theoret. 20 Std. 100%)		77,53	75,04	58,14	77,56
VORTRIEBSGESCHWINDIGKEIT (lfm/Std)		2,74	2,48	2,78	2,99
VORSCHUBDRUCK (PSI) (PSI - 0,07031 kg/cm²)		413,45	405,63	441,77	395,27
LEISTUNGSRAUFNAHME (Kw)		355,55	334,20	336,46	338,45
MEISELWECHSEL					
FELS -	SPRITZBETON				
SICHER -	NRGELUNG				
UNG	STAHLINBAU				
ANMERKUNG					

Figure 4.49: Original data sample pdf. file.

First of all data for rock mass were analyzed for thrust, advance rate (AR), degree of disintegration (DoD), rock mass class (RMC) and excavation velocity. Then data

were segregated for all three rock types (Muscovite-Granite-Gneiss, Micaschists, Schistose-Gneis) and same analysis were done as for rock mass.

## 4.4.2 Rock Mass Data

### 4.4.2.1 2-D Data Analysis with Microsoft Excel

Here data analysis for rock mass are shown, all rock properties and machine parameters plotted versus tunnel meters (TM).

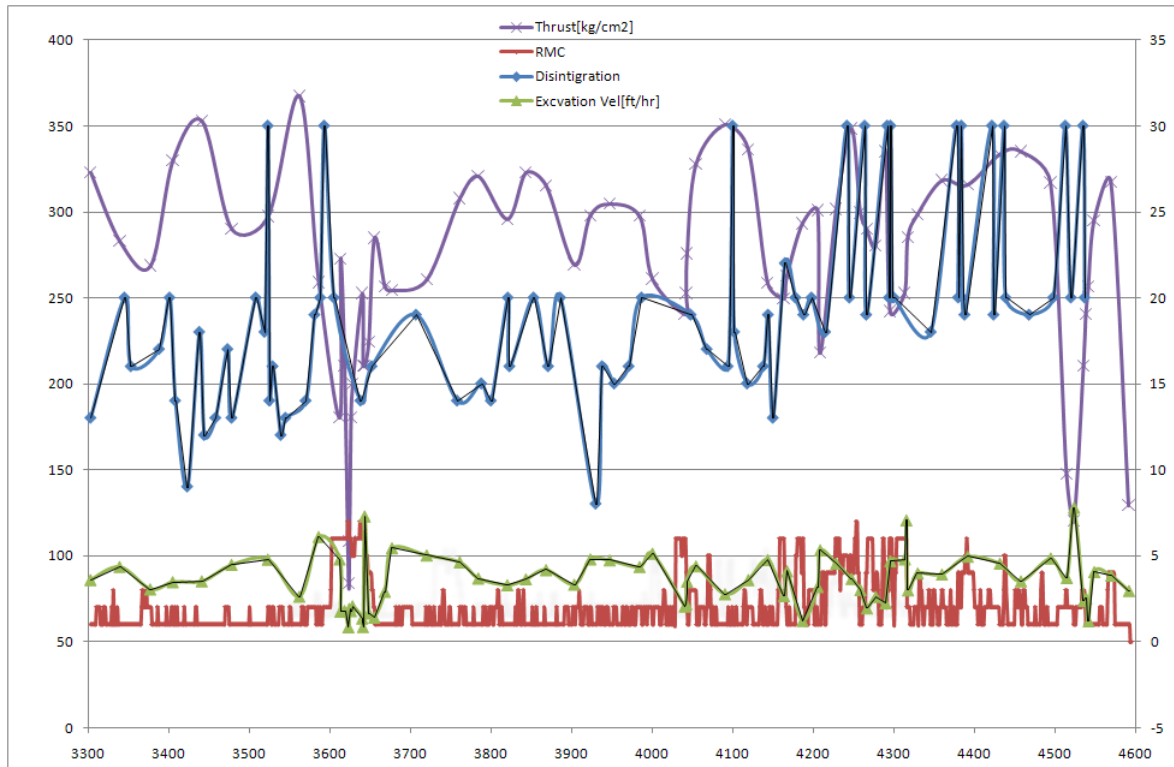
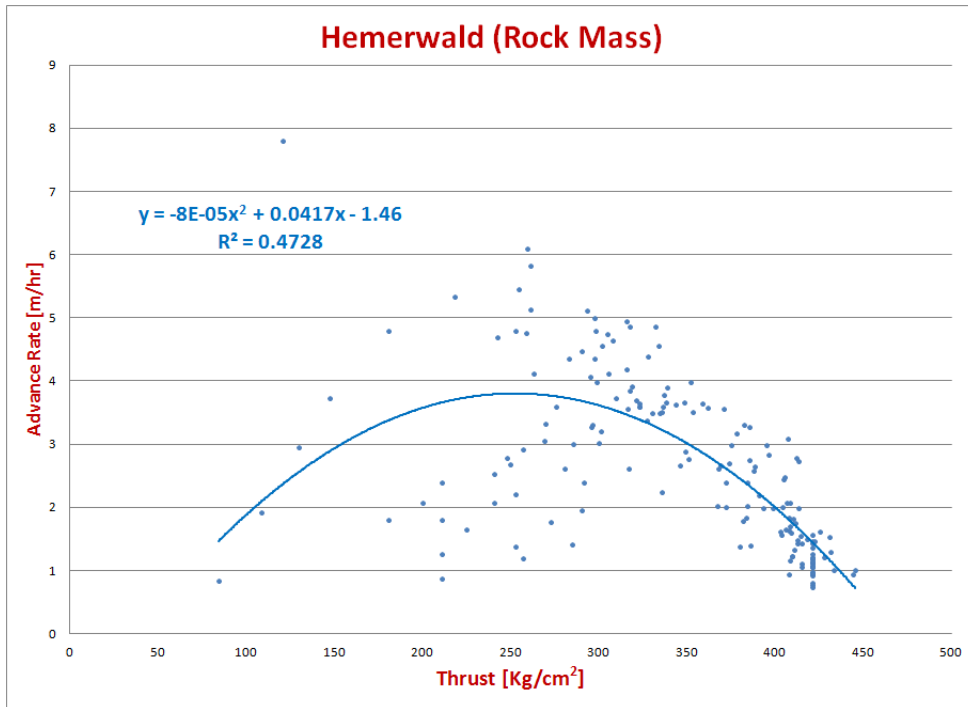
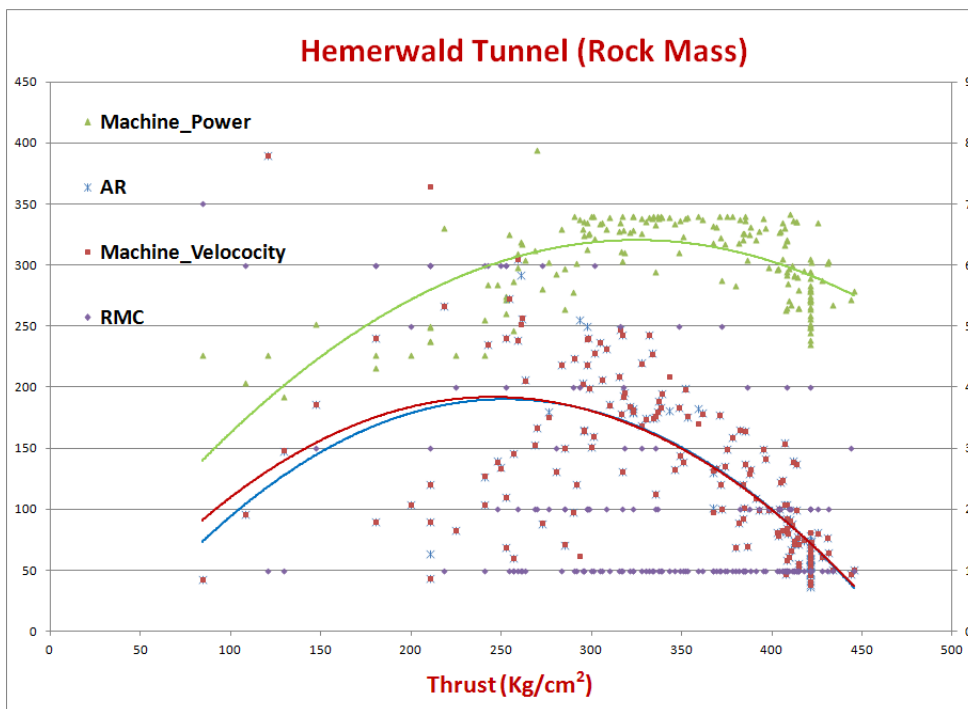


Figure 4.50: TM versus thrust, RMC, excavation velocity, disintegration.

Fig. 4.50 shows variation of different variables along the tunnel meter. Thrust and excavation velocity have almost similar variation. Rock mass class (RMC) and degree of disintegration varies quite similarly along the tunnel length. Variation of thrust and advance rate is shown in Figs. 4.51(a,b), that display AR, RMC, machine velocity against thrust variation. Only RMC have an inverse proportion to thrust, all other have a quadratic relation with thrust. TBM rpm and AR entirely coincide with each other. But at low values of RMC, a high thrust is observed which shows low RMC rock needs more machine thrust for the same AR. This may be due to low values of disintegration machine cutter-head is unable to form chip formation at low thrust.



(a) Thrust versus AR.



(b) Thrust versus AR, power, velocity and RMC.

Figure 4.51: Thrust versus AR power, velocity and RMC (Rock mass).

#### 4.4.2.2 3-D Analysis with “R”

Statistical software “R” is very useful for plotting 3-D surfaces for different parameters to see the variation of three variables simultaneously.



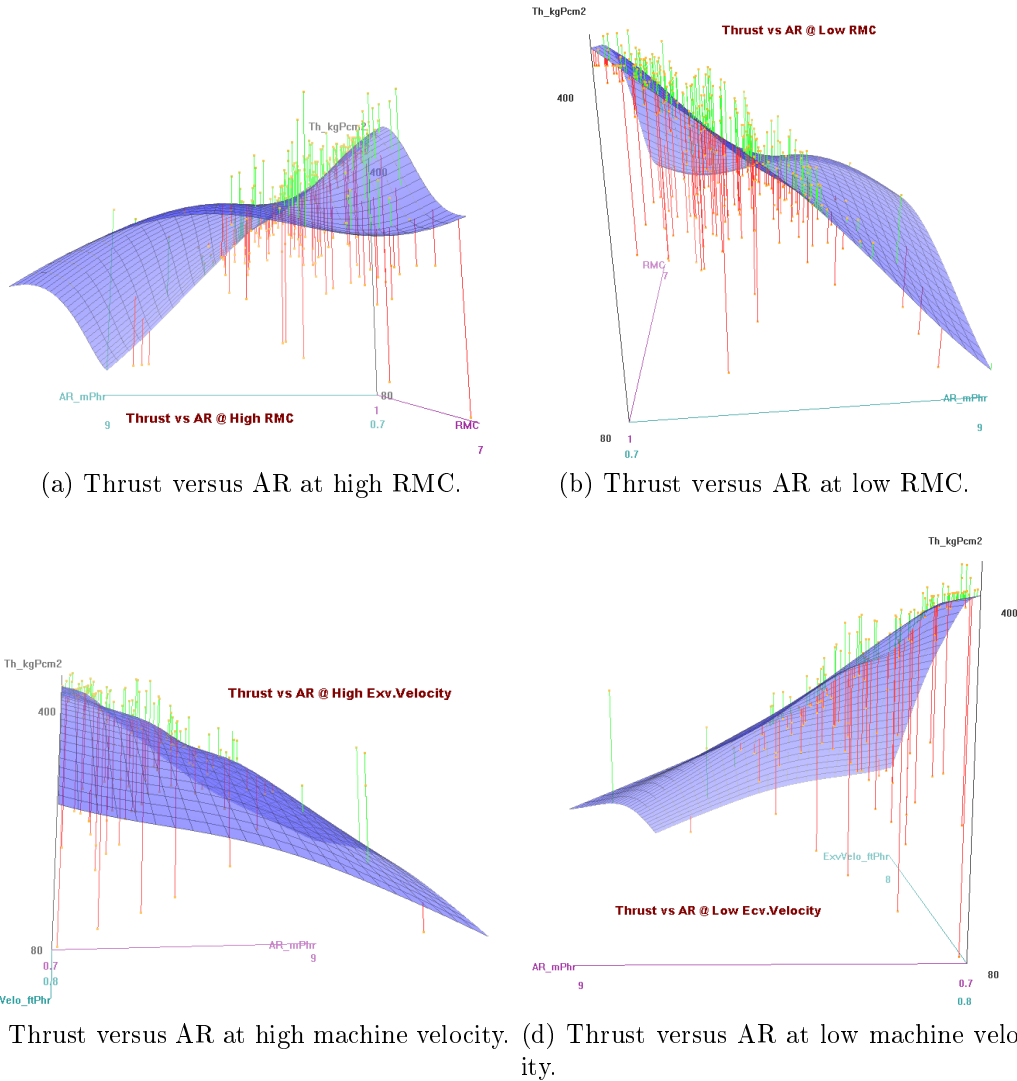
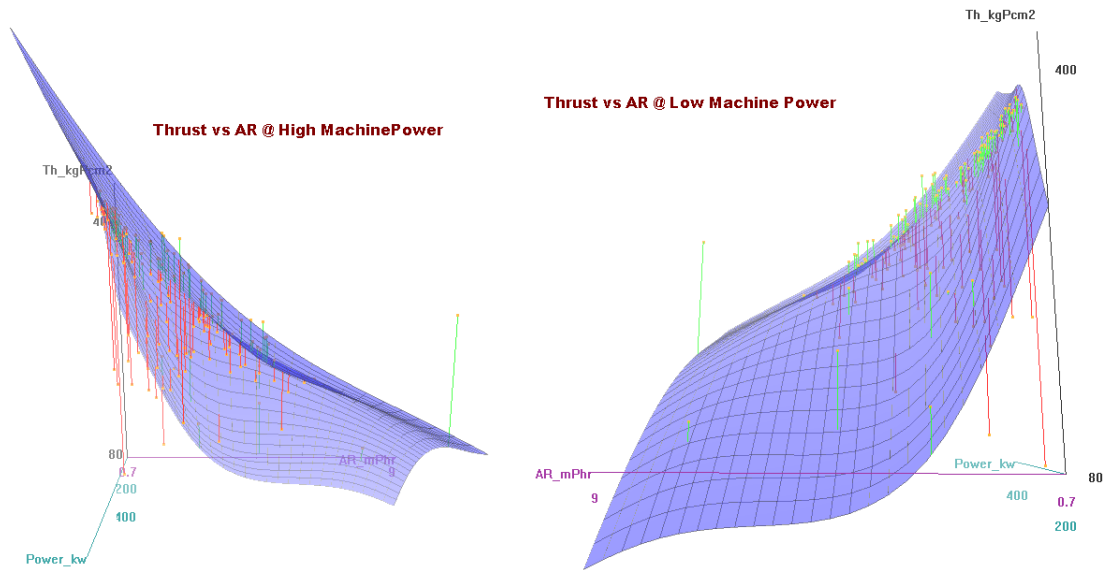


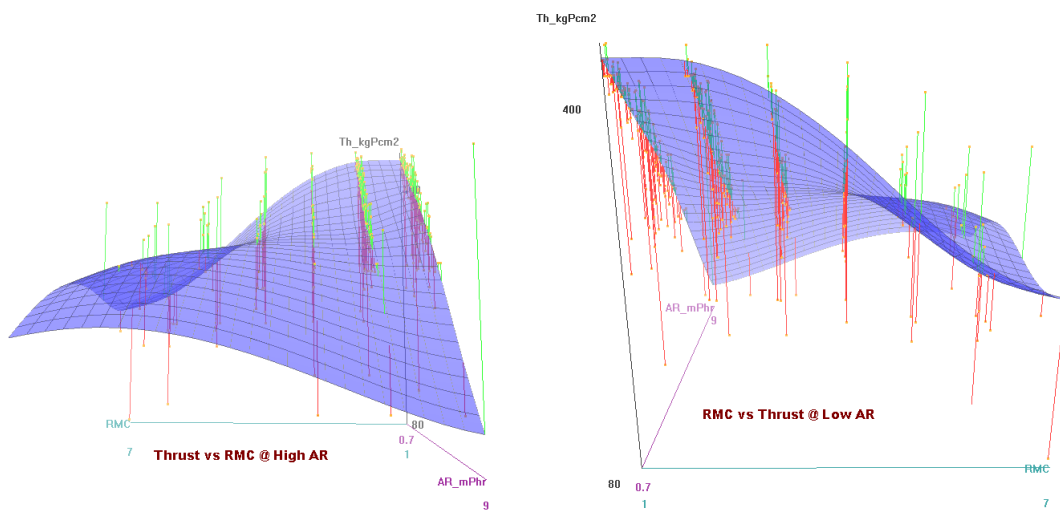
Figure 4.52: 3-D surfaces for thrust, AR, power and RMC (Rock mass).

AR is inversely proportional to thrust at low RMC Figs. 4.52(a,b), while it has a sinusoidal trend with thrust at high values of RMC showing that in poor to medium rock advance rate increase with increase of thrust but when RMC is very low or in other words rock strength is very high, advance rate decreases with increase of thrust values. Reason may be due to low RMC, very strong rock, AR doesn't depends upon thrust above a critical value necessary for chip formation, whereas at high RMC values, AR linearly increases with thrust up-to a specific point, beyond which increase in AR is not possible by simple increase of thrust. Figures 4.52(c,d) shows AR variation against thrust at low and high machine velocity. Machine velocity doesn't play any role for AR, as in both cases (i.e. at high and low machine velocity), AR is inversely proportional to thrust.



(a) Thrust versus AR at high machine power. (b) Thrust versus AR at low machine power.

Figure 4.53: 3-D surfaces thrust versus AR (Rock mass).



(a) Thrust versus RMC at high AR. (b) Thrust versus RMC at low AR.

Figure 4.54: 3-D surfaces thrust versus AR (Rock mass).

Figures 4.53(a,b) shows AR against thrust at high and low machine power. Here again AR and thrust have quadratic relation with each other, both on high and low machine power. Whereas Figs. 4.54(a,b) shows variation of thrust and RMC, at low and high AR. It is clear from the 3-D surface that at high AR, more thrust is required at lower values of RMC, on the other hand low thrust needed at high RMC and vice versa, This trend is sinusoidal.

### 4.4.2.3 Prediction Model With Fuzzy Logic

A Mat-Lab code was written to predict the RMC values taking, thrust, advance rate (AR) and machine power into account as input variables and RMC as output variable. Rule base is formulated for the Math-Lab code after keeping in view all trends and behaviors of all parameters versus RMC.

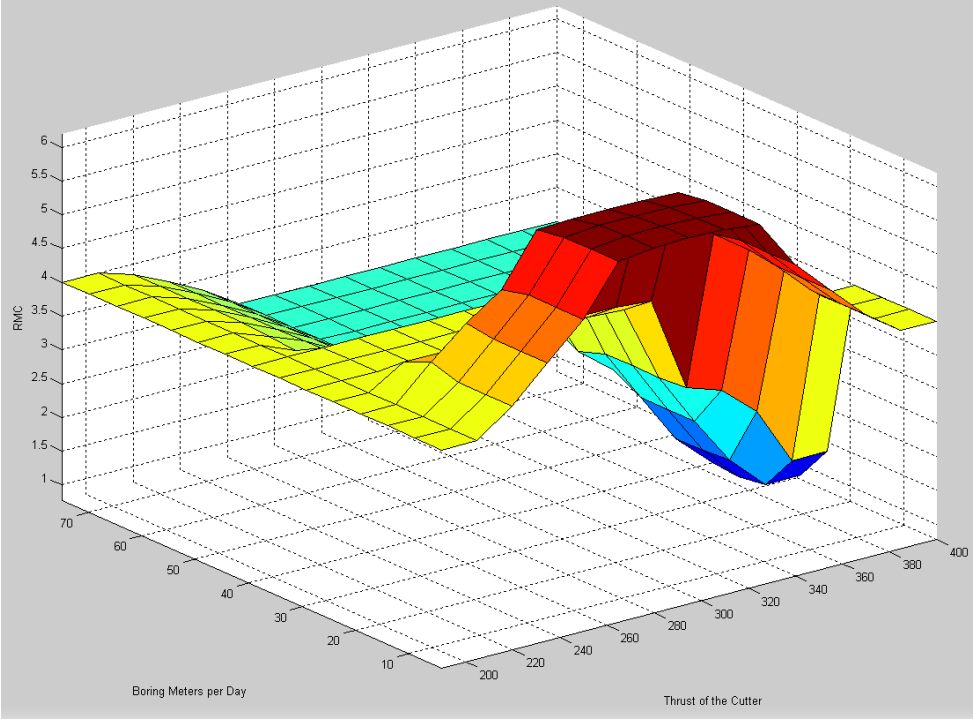
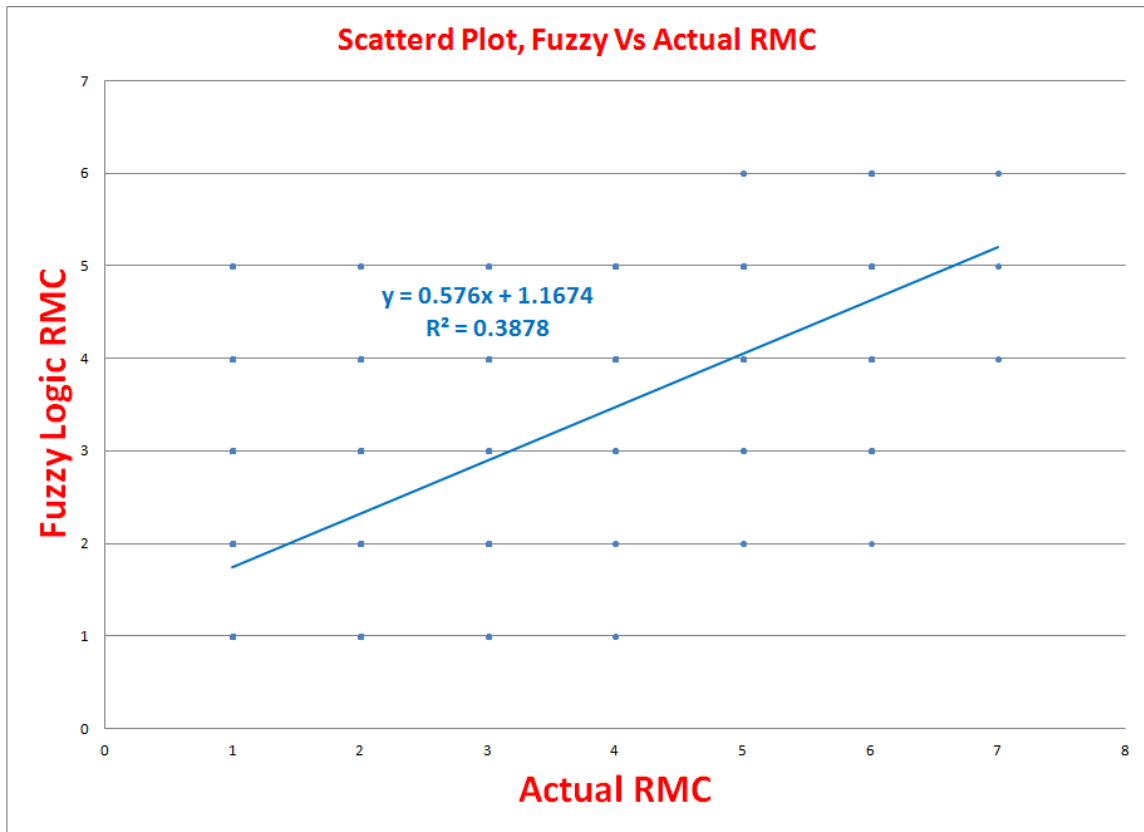
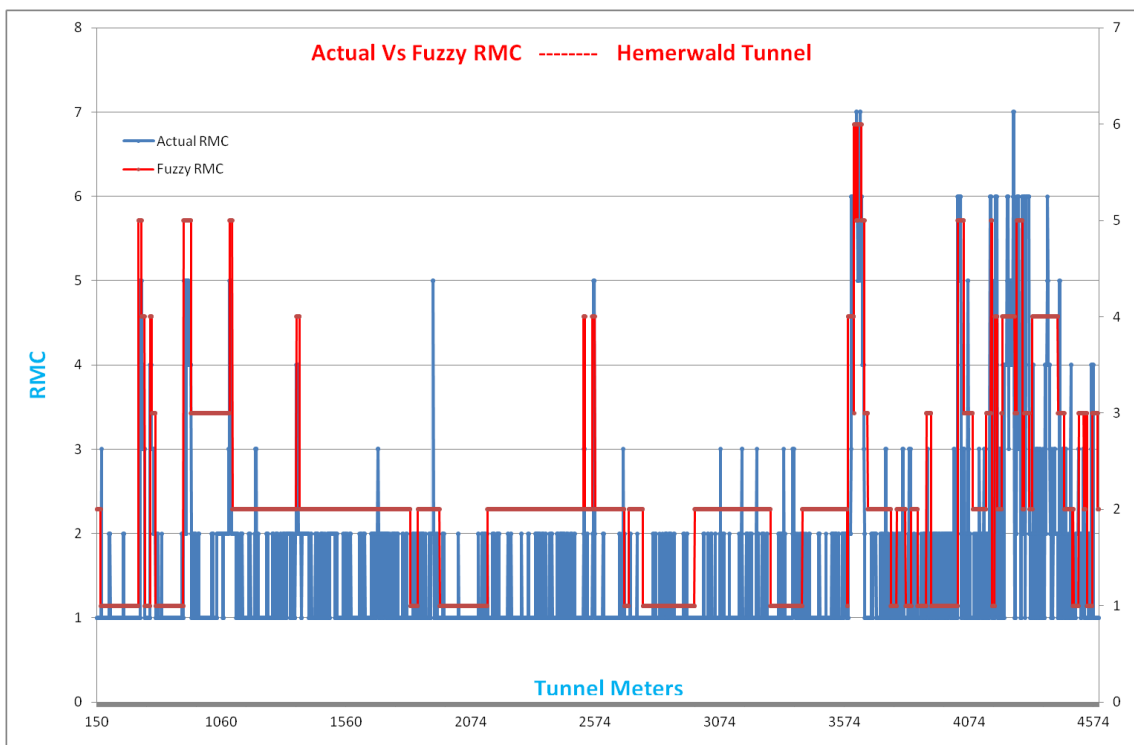


Figure 4.55: 3-D surface by Fuzzy logic.

Plot between actual and Fuzzy RMC shows  $R^2 = 0.39$ , fair correlation between actual and Fuzzy RMC. Fuzzy RMC has a little bit higher values than actual. But improvement can be made by re-formulating the rule base and taking more rock mass properties like presence of water, overburden etc. into account.



(a) Scattered plot Fuzzy versus actual RMC.



(b) Fuzzy versus actual RMC.

Figure 4.56: Fuzzy versus actual RMC.

#### 4.4.2.4 Statistical Modeling with SPSS

For rock mass data, SPSS19 modeling was carried out and histograms for all machine parameters and rock mass properties were generated. After multidimensional analysis, a linear prediction equation (model) was formulated for rock mass data.

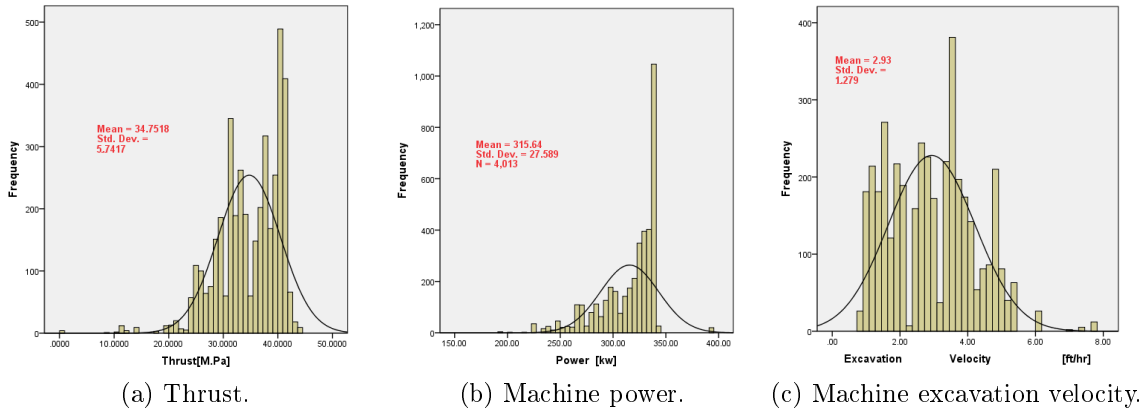


Figure 4.57: Histograms for thrust, power and excavation velocity.

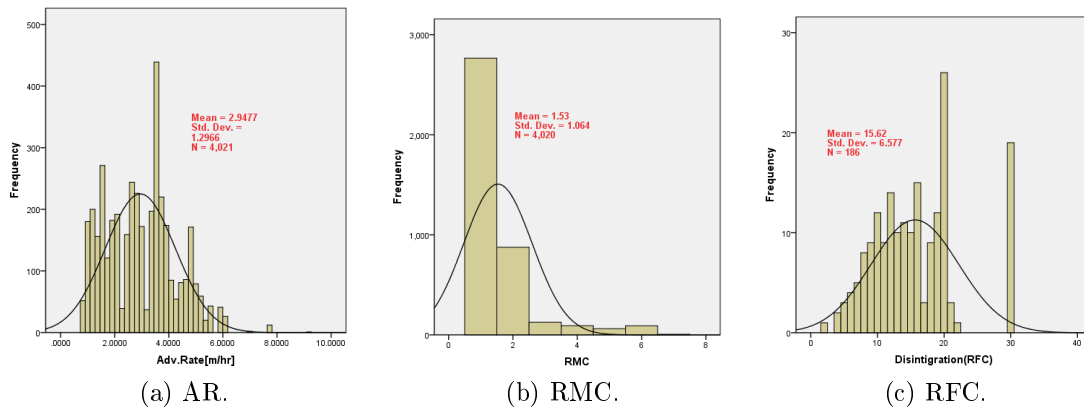


Figure 4.58: Histograms for AR, RMC and RFC.

Figures 4.57-4.58 show that, thrust and excavation velocity have normal frequency distributions, AR have very good normal distributions, and RMC have a left skewed frequency distribution. According to SPSS regression analysis assumptions, AR, RMC and RFC fulfill the required condition for regression modeling.

Model Summary		Effects						Target: Adv.Rate[m/hr]
Target	Adv.Rate[m/hr]	Source	Sum of Squares	df	Mean Square	F	Sig.	Importance
Automatic Data Preparation	On	Corrected Model	6,273.335	4	1,568.334	12,980.375	.000	
Model Selection Method	None (All Predictors Entered)	Exc.v.Vfthr_transformed	1,216.695	1	1,216.695	10,070.026	.000	0.529
Information Criterion	-8,493.069	Thrustkgcm2_transformed	34.959	1	34.959	289.337	.000	0.162
The information criterion is used to compare to models. Models with smaller information criterion values fit better.		Powerkw_transformed	22.653	1	22.653	187.485	.000	0.158
Worse Accuracy Better		RMC_transformed	0.153	1	0.153	1.270	.260	0.151
0.00% 25.00% 50.00% 75.00% 100.00%		Residual	485.227	4,016	0.121			
92.8%		Corrected Total	6,758.562	4,020				

(a) Model summary and effects.

Coefficients		Target: Adv.Rate[m/hr]					
Model Term	Coefficient	Std.Error	t	Sig.	95% Confidence Interval		Importance
					Lower	Upper	
Intercept	0.331	0.092	3.596	.000	0.151	0.512	
Exc.v.Vfthr_transformed	0.849	0.008	100.350	.000	0.832	0.865	0.529
Thrustkgcm2_transformed	-0.003	0.000	-17.010	.000	-0.003	-0.003	0.162
Powerkw_transformed	0.004	0.000	13.693	.000	0.003	0.004	0.158
RMC_transformed	-0.009	0.008	-1.127	.260	-0.026	0.007	0.151

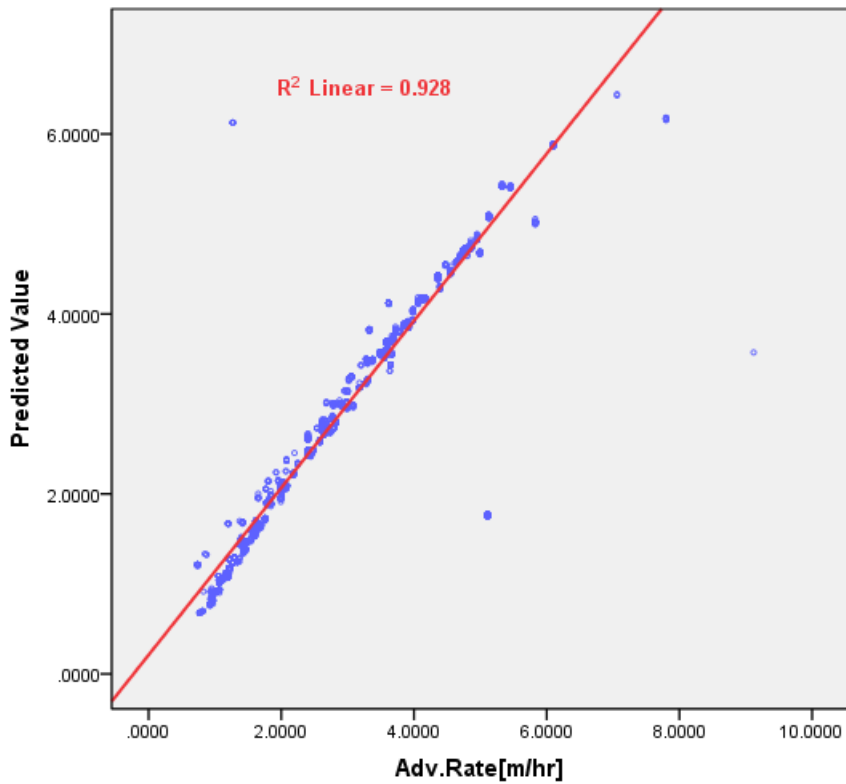
(b) Model coefficients.

Relation of Property with AR	Empirical Equation	Corr. Coeff. R
AR vs Thrust	AR = -0.017Thrust + 8.889	0.744
AR vs Machine RPM	AR = 4.46 RPM + 17.658	0.80
AR vs RMC	AR = 0.165RMC + 2.695	0.135
AR vs Machine Power	AR = 0.025Power + 4.937	0.53
AR vs RFC	AR = 0.013RFC + 0.787	0.60

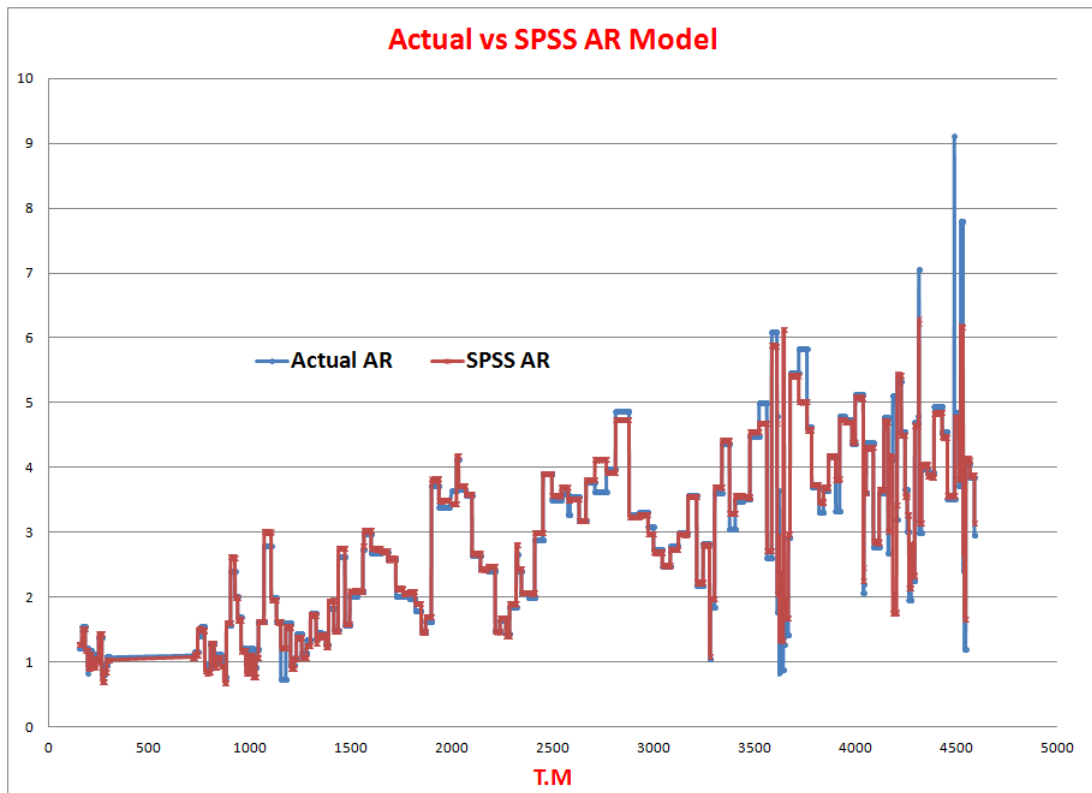
(c) Table of linear equations between input and out variables.

Table 4.21: AR model summary, effects and coefficients.

Using linear equations (table 4.21c) and coefficients matrix (table 4.21b), prediction of AR model with the help of SPSS-19 linear regression modeling, a formula for predicted advance rate was achieved. Model has very high accuracy of 92.8% and excavation velocity was the most important parameter among the predictors.



(a) AR model plot.



(b) Comparison actual and SPSS AR.

Figure 4.59: Actual and SPSS AR comparison.

From the coefficient matrix obtained from table 4.21, following prediction model was

formulated and shown in Eq. 4.8.

$$AR(m/hr) = 0.331 + 0.849Exc.v_{vel} - 0.003Thrust + 0.004Power - 0.009RMC \quad (4.8)$$

Prediction model ( $R^2 = 0.928$ ) for AR is plotted in Fig. 4.59a as scattered plot and Fig. 4.59b shows the comparison between actual and SPSS advance rate as a line plot, where 95% predicted values coincide with actual values.

#### 4.4.2.5 Correlation and Correlation Coefficient

Table 4.22 shows Pearson correlation between machine parameters and rock mass properties. Machine parameters have a good correlation with rock mass properties e.g thrust and AR ( $R^2 = 0.745$ ) and thrust and excavation velocity ( $R^2 = 0.740$ ). This shows a strong correlation between machine and rock mass parameters. Table 4.23 shows Spearman and Kendall correlation coefficients. Again thrust is strongly correlated with excavation velocity and AR with correlation coefficient of  $R^2 = 0.786$  and  $R^2 = 0.799$  respectively. These result also show that the data is not perfectly normally distributed. Otherwise Pearson correlation coefficient should not be less than Kendall correlation coefficient.

		<b>Correlations</b>				
		RMC	Exc.v.[ft/hr]	Thrust [kg/cm <sup>2</sup> ]	Power [kw]	Adv.Rate [m/hr]
RMC	Pearson Correlation	1	.144**	-.369**	-.200**	.135**
	Sig. (2-tailed)		.000	.000	.000	.000
	N	4020	4018	4018	4012	4020
Exc.v.[ft/hr]	Pearson Correlation	.144**	1	-.740**	.511**	.959**
	Sig. (2-tailed)	.000		.000	.000	.000
	N	4018	4019	4019	4013	4019
Thrust [kg/cm <sup>2</sup> ]	Pearson Correlation	-.369**	-.740**	1	-.112**	-.745**
	Sig. (2-tailed)	.000	.000		.000	.000
	N	4018	4019	4019	4013	4019
Power [kw]	Pearson Correlation	-.200**	.511**	-.112**	1	.532**
	Sig. (2-tailed)	.000	.000	.000		.000
	N	4012	4013	4013	4013	4013
Adv.Rate[m/hr]	Pearson Correlation	.135**	.959**	-.745**	.532**	1
	Sig. (2-tailed)	.000	.000	.000	.000	
	N	4020	4019	4019	4013	4021

\*\* . Correlation is significant at the 0.01 level (2-tailed).

Table 4.22: Correlation coefficients for rock mass.



			Correlations				
			RMC	Exc.v.[ft/hr]	Thrust [kg/cm2]	Power [kw]	Adv.Rate [m/hr]
Kendall's tau_b	RMC	Correlation Coefficient	1.000	.086**	-.215**	-.127**	.092**
		Sig. (2-tailed)	.	.000	.000	.000	.000
		N	4020	4018	4018	4012	4020
	Exc.v.[ft/hr]	Correlation Coefficient	.086**	1.000	-.621**	.425**	.962**
		Sig. (2-tailed)	.000	.	.000	.000	.000
		N	4018	4019	4019	4013	4019
	Thrust [kg/cm2]	Correlation Coefficient	-.215**	-.621**	1.000	-.193**	-.635**
		Sig. (2-tailed)	.000	.000	.	.000	.000
		N	4018	4019	4019	4013	4019
	Power [kw]	Correlation Coefficient	-.127**	.425**	-.193**	1.000	.430**
		Sig. (2-tailed)	.000	.000	.000	.	.000
		N	4012	4013	4013	4013	4013
	Adv.Rate[m/hr]	Correlation Coefficient	.092**	.962**	-.635**	.430**	1.000
		Sig. (2-tailed)	.000	.000	.000	.000	.
		N	4020	4019	4019	4013	4021
Spearman's rho	RMC	Correlation Coefficient	1.000	.109**	-.270**	-.158**	.117**
		Sig. (2-tailed)	.	.000	.000	.000	.000
		N	4020	4018	4018	4012	4020
	Exc.v.[ft/hr]	Correlation Coefficient	.109**	1.000	-.786**	.569**	.971**
		Sig. (2-tailed)	.000	.	.000	.000	.000
		N	4018	4019	4019	4013	4019
	Thrust [kg/cm2]	Correlation Coefficient	-.270**	-.786**	1.000	-.271**	-.799**
		Sig. (2-tailed)	.000	.000	.	.000	.000
		N	4018	4019	4019	4013	4019
	Power [kw]	Correlation Coefficient	-.158**	.569**	-.271**	1.000	.581**
		Sig. (2-tailed)	.000	.000	.000	.	.000
		N	4012	4013	4013	4013	4013
	Adv.Rate[m/hr]	Correlation Coefficient	.117**	.971**	-.799**	.581**	1.000
		Sig. (2-tailed)	.000	.000	.000	.000	.
		N	4020	4019	4019	4013	4021

\*\* . Correlation is significant at the 0.01 level (2-tailed).

Table 4.23: Spearman and Kendall correlation coefficients.

### 4.4.3 Muskowit-Granite-Gneis

#### 4.4.3.1 2-D Data Analysis with Microsoft Excel

Figure 4.60 shows a plot between thrust and advance rate, AR is inversely proportional to thrust. This may be due to TBM driver who tried to push more thrust to achieve more AR, but due to rock strength of Muskovite-Granite-Gneis and low degree of disintegration (DoD), AR is decreasing with more thrust applied.

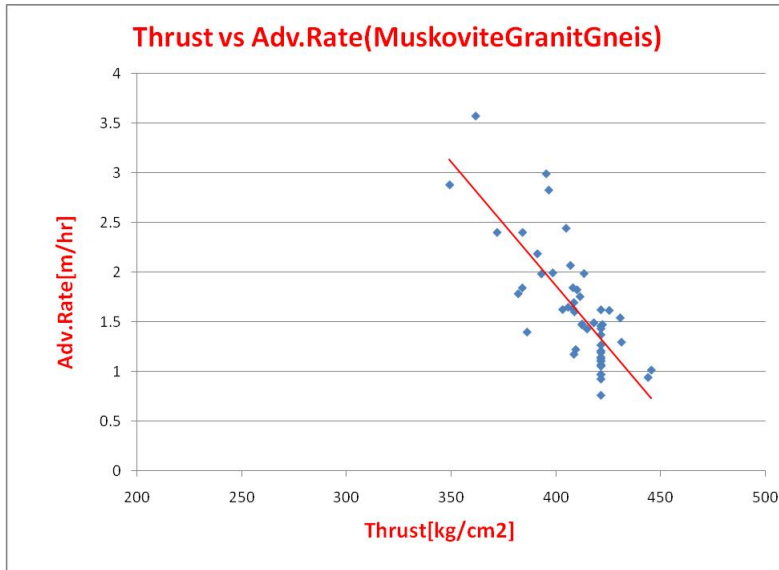


Figure 4.60: Thrust versus AR.

Figure 4.61 shows variation of all parameters along tunnel length, AR and degree of disintegration (DoD) are increasing along tunnel length while thrust drops along TM.

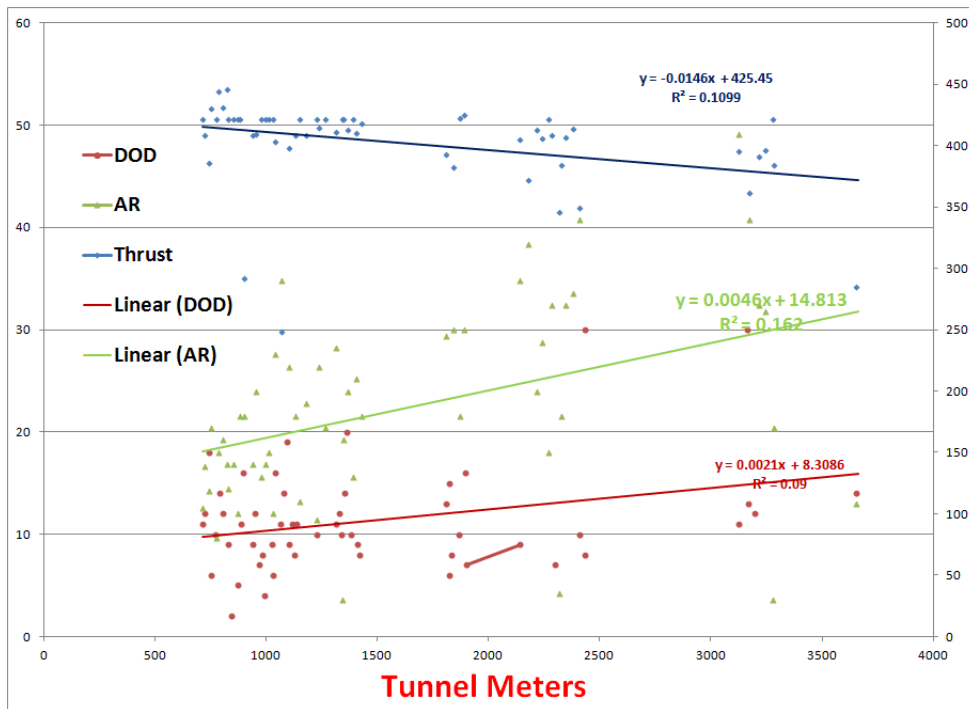


Figure 4.61: Thrust versus AR.

#### 4.4.3.2 3-D Data Analysis With “R”

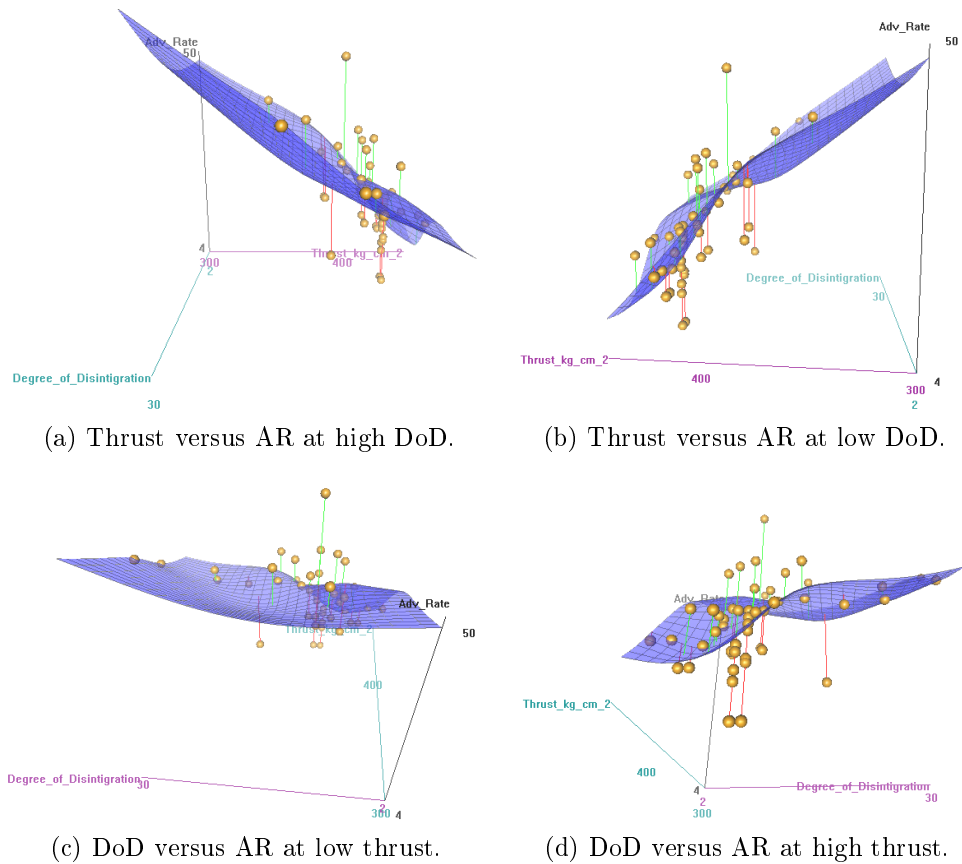


Figure 4.62: 3-D surfaces for Muskovite-Granite-Gneis.

Statistical software “R” was used to plot 3-D surfaces for thrust, advance rate (AR) and degree of disintegration (DoD). Figures 4.62(a,b) shows thrust versus AR at high and low DoD respectively. Both graph shows almost similar behaviour, i.e linear increase in AR with increase of thrust. Figures 4.62(c,d) shows DoD versus AR at low and high thrust respectively. At low thrust AR is almost independent of DoD, while at high thrust values the advance rate increases at start and then its level to a constant value, showing that no further thrust can enhance the AR.

#### 4.4.3.3 Statistical Modeling With SPSS19

Figures 4.63(a-d) shows frequency distributions for thrust, DoD, AR and RMC. Advance rate and DoD data are normally distributed, while thrust data is right skewed and RMC left skewed. Frequency distribution (histograms) for DoD and AR show that, SPSS prediction modeling can be performed on these set of data.

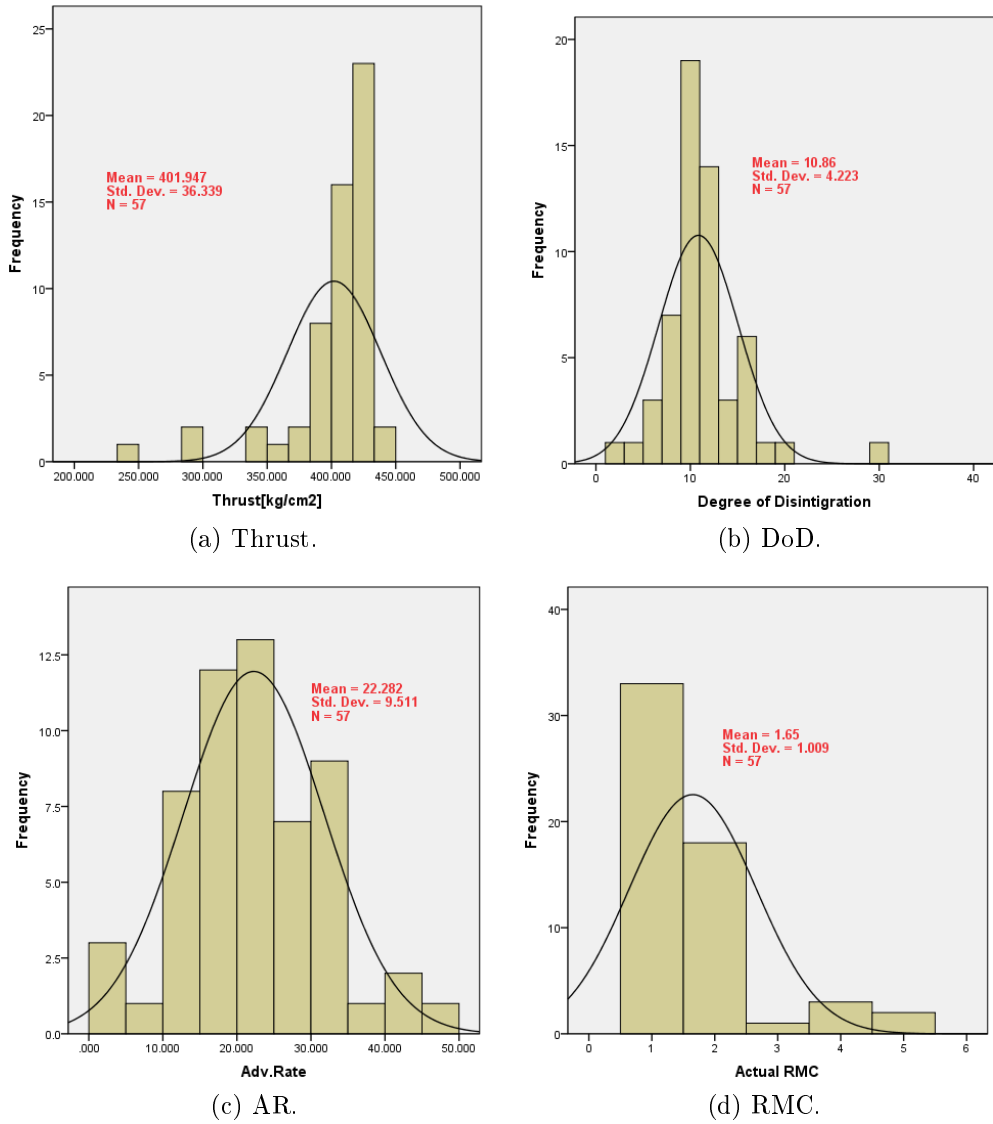


Figure 4.63: Histograms for thrust, DoD, AR and RMC.

	Effects		Target: Adv.Rate			
Source	Sum of Squares	df	Mean Square	F	Sig.	Importance
Corrected Model ▼	749.239	2	374.619	4.686	.013	
DegreeofDisintigration_ transformed	379.068	1	379.068	4.742	.034	0.511
Thrustkgcm2_transformed	179.467	1	179.467	2.245	.140	0.489
Residual	4,316.663	54	79.938			
Corrected Total	5,065.902	56				

Table 4.24: Predictor effects for AR model.

Model Term	Coefficients		Target: Adv.Rate				
	Coefficient ▼	Std.Error	t	Sig.	95% Confidence Interval		Importance
					Lower	Upper	
Intercept	36.771	16.635	2.211	.031	3.407	70.136	
DegreeofDisintigration_ transformed	0.796	0.349	2.277	.027	0.095	1.497	0.349
Thrustkgcm2_ transformed	-0.052	0.038	-1.367	.178	-0.128	0.024	0.329
ActualRMC_ transformed	-1.258	1.383	-0.910	.367	-4.031	1.516	0.323

Table 4.25: Coefficients matrix for AR model.

After multidimensional analysis, different models are predicted using available data. Normal frequency analysis shows that penetration, thrust and DoD are in good normal distribution with very low standard deviation and RMC does not follow any normal distribution. Model selection method was “forward stepwise” and default combining method “mean” at 95% confidence level was used. From coefficients matrix (table 4.25) using coefficients from input variables and intercept, following linear prediction model can be formulated:

$$AR(m/hr) = 37.771 + 0.796DoD - 0.052Thrust - 1.258RMC \quad (4.9)$$

Only the advance rate frequency is normally distributed, so SPSS regression analysis model were applied to these data sets, out put result is plotted and shown in Fig. 4.64 with  $R^2 = 0.148$ .

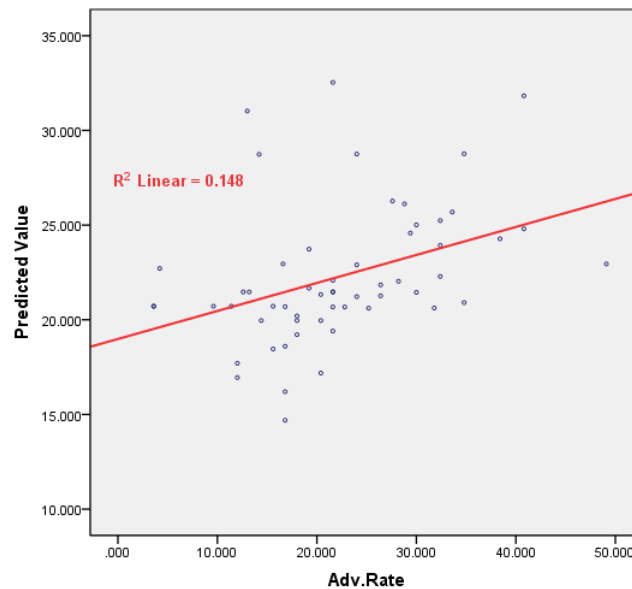


Figure 4.64: AR model for Muscovite-Granite-Gneiss.

#### 4.4.3.4 Correlation and Correlation Coefficients

**Correlations**

		Thrust [kg/cm <sup>2</sup> ]	Degree of Disintegration	Adv.Rate	Actual RMC
Thrust[kg/cm <sup>2</sup> ]	Pearson Correlation	1	-.254	-.270*	.071
	Sig. (2-tailed)		.057	.043	.599
	N	57	57	57	57
Degree of Disintegration	Pearson Correlation	-.254	1	.365**	.039
	Sig. (2-tailed)	.057		.005	.776
	N	57	57	57	57
Adv.Rate	Pearson Correlation	-.270*	.365**	1	-.095
	Sig. (2-tailed)	.043	.005		.482
	N	57	57	57	57
Actual RMC	Pearson Correlation	.071	.039	-.095	1
	Sig. (2-tailed)	.599	.776	.482	
	N	57	57	57	57

\*. Correlation is significant at the 0.05 level (2-tailed).  
 \*\*. Correlation is significant at the 0.01 level (2-tailed).

Table 4.26: Pearson correlation coefficients for Muscovite-Granite-Gneiss.

**Correlations**

			Thrust [kg/cm <sup>2</sup> ]	Degree of Disintegration	Adv.Rate	Actual RMC
Kendall's tau_b	Thrust[kg/cm <sup>2</sup> ]	Correlation Coefficient	1.000	-.176	-.379**	.007
		Sig. (2-tailed)		.074	.000	.949
		N	57	57	57	57
	Degree of Disintegration	Correlation Coefficient	-.176	1.000	.247*	.086
		Sig. (2-tailed)	.074		.010	.438
		N	57	57	57	57
	Adv.Rate	Correlation Coefficient	-.379**	.247*	1.000	-.005
		Sig. (2-tailed)	.000	.010		.962
		N	57	57	57	57
	Actual RMC	Correlation Coefficient	.007	.086	-.005	1.000
		Sig. (2-tailed)	.949	.438	.962	
		N	57	57	57	57
Spearman's rho	Thrust[kg/cm <sup>2</sup> ]	Correlation Coefficient	1.000	-.242	-.498**	.014
		Sig. (2-tailed)		.069	.000	.916
		N	57	57	57	57
	Degree of Disintegration	Correlation Coefficient	-.242	1.000	.347**	.106
		Sig. (2-tailed)	.069		.008	.432
		N	57	57	57	57
	Adv.Rate	Correlation Coefficient	-.498**	.347**	1.000	-.002
		Sig. (2-tailed)	.000	.008		.986
		N	57	57	57	57
	Actual RMC	Correlation Coefficient	.014	.106	-.002	1.000
		Sig. (2-tailed)	.916	.432	.986	
		N	57	57	57	57

\*\* . Correlation is significant at the 0.01 level (2-tailed).  
 \* . Correlation is significant at the 0.05 level (2-tailed).

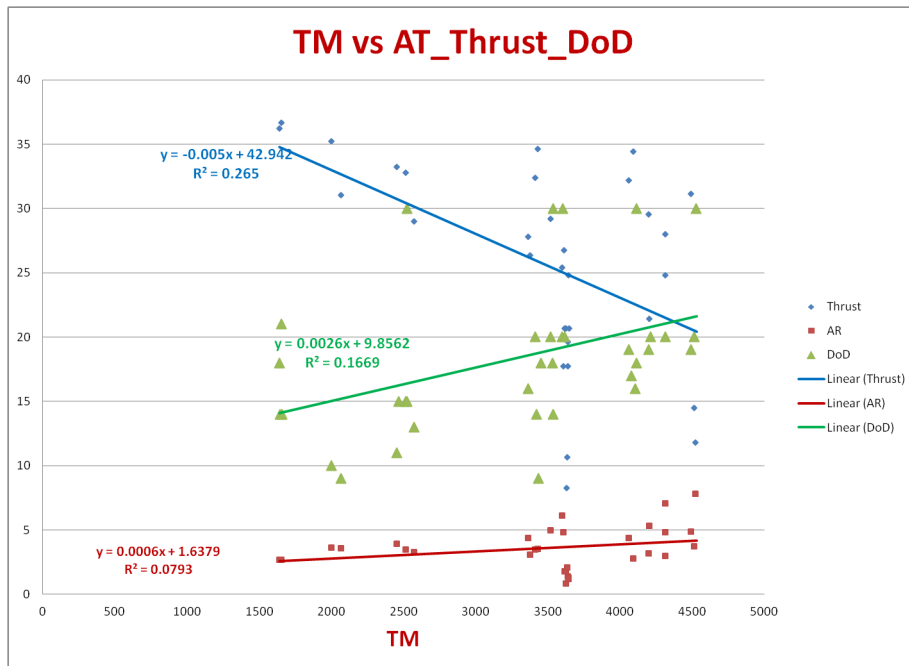
Table 4.27: Spearman's correlation coefficients Muscovite-Granite-Gneiss.

Table 4.26 shows Pearson correlation coefficients for different machine and rock parameters. There is no significant correlation between machine parameters and rock mass properties. Even rock mass properties are not well correlated with themselves. In table 4.27, Spearman and Kendall's correlations are shown. Thrust and advance rate are reasonably good correlated ( $R^2 = 0.498$ ), other all parameters shows correlation less than  $R^2 = 0.40$ .

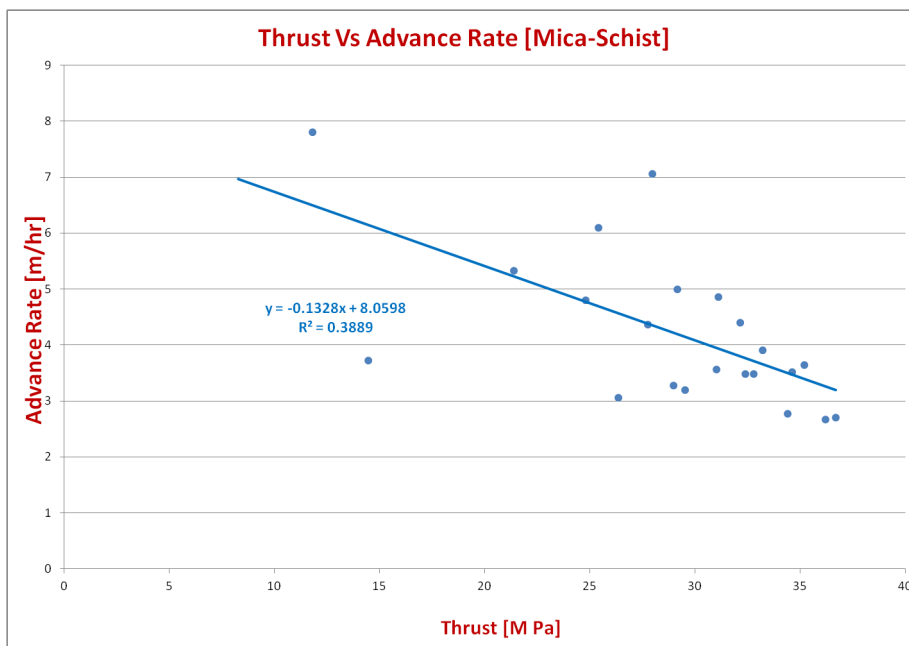
#### **4.4.4 Mica-Schist**

##### **4.4.4.1 Data Analysis with Excel**

Figure 4.65a displays variation of thrust AR and DoD along tunnel length, thrust required for excavation is reducing while tunnel meters goes forward, whereas advance rate and DoD increase along with tunnel meters. Thrust and advance rate, linear curve fit with  $R^2 = 0.39$  shows that AR is going to decreased with increasing thrust, which is due to involvement of other factors like DoD and rock strength.



(a) TM versus thrust, AR and DoD.



(b) Thrust versus AR.

Figure 4.65: TM and thrust versus AR and DoD.



**Correlations**

		Thrust[M-Pa]	Degree of Disintegration	Adv-Rate [m/hr]
Thrust[M-Pa]	Pearson Correlation	1	-.623**	.043
	Sig. (2-tailed)		.001	.828
	N	32	24	28
Degree of Disintegration	Pearson Correlation	-.623**	1	.440*
	Sig. (2-tailed)	.001		.031
	N	24	35	24
Adv-Rate[m/hr]	Pearson Correlation	.043	.440*	1
	Sig. (2-tailed)	.828	.031	
	N	28	24	31

\*\* .Correlation is significant at the 0.01 level (2-tailed).  
 \* .Correlation is significant at the 0.05 level (2-tailed).

Table 4.28: Pearson correlation for Micaschists.

Tables 4.28-4.29 shows different correlations between machine parameters and rock mass properties. In table 4.28 Pearson correlations are shown, thrust and DoD have a negative correlation ( $R^2 = -0.623$ ), whereas thrust and AR, are positively correlated ( $R^2 = 0.828$ ).

**Correlations**

			Thrust[M-Pa]	Degree of Disintegration	Adv-Rate [m/hr]
Kendall's tau_b	Thrust[M-Pa]	Correlation Coefficient	1.000	-.375*	.021
		Sig. (2-tailed)		.013	.874
		N	32	24	28
	Degree of Disintegration	Correlation Coefficient	-.375*	1.000	.234
		Sig. (2-tailed)	.013		.124
		N	24	35	24
	Adv-Rate[m/hr]	Correlation Coefficient	.021	.234	1.000
		Sig. (2-tailed)	.874	.124	
		N	28	24	31
Spearman's rho	Thrust[M-Pa]	Correlation Coefficient	1.000	-.476*	.067
		Sig. (2-tailed)		.019	.736
		N	32	24	28
	Degree of Disintegration	Correlation Coefficient	-.476*	1.000	.325
		Sig. (2-tailed)	.019		.121
		N	24	35	24
	Adv-Rate[m/hr]	Correlation Coefficient	.067	.325	1.000
		Sig. (2-tailed)	.736	.121	
		N	28	24	31

\*. Correlation is significant at the 0.05 level (2-tailed).

Table 4.29: Spearman's correlation coefficients for Micaschists.

On the other hand in table 4.29 Spearman's and Kendall's correlations are shown.

There is no significant correlation between machine and rock mass properties found, except only between thrust and DoD ( $R^2 = 0.476$ ) a good correlation found.

**4.4.4.2 Fuzzy Logic RMC Prediction Model**

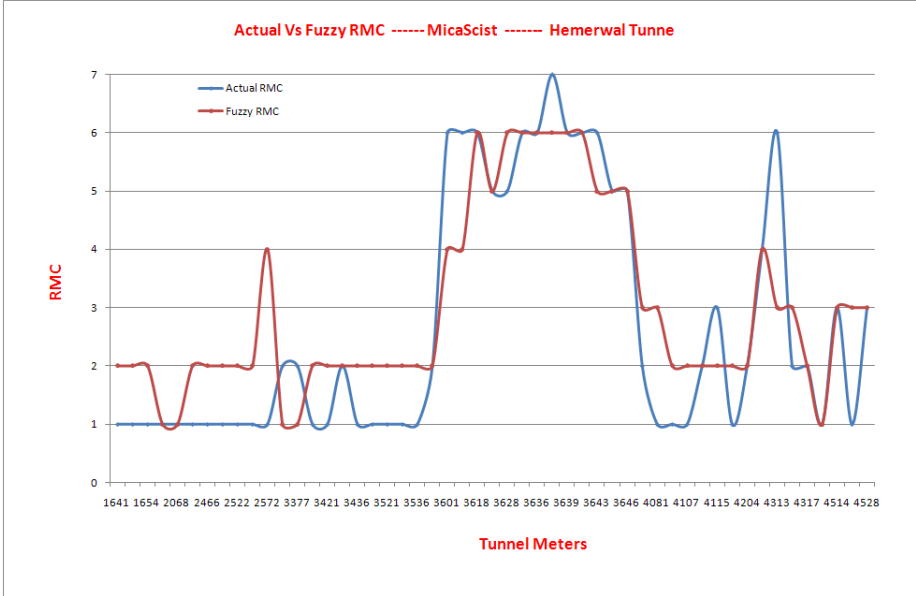


Figure 4.66: Comparison of RMC for Micaschists.

Figure 4.66 shows a comparison between actual and Fuzzy logic RMC, overall a good correlation between actual and Fuzzy RMC is seen. In first portion of TM and at the last part of tunnel meters, Fuzzy logic doesn't match well with actual results, but from TM 3500 to 400 almost a good matching of RMC is observed.

**4.4.4.3 3-D Analysis with “R”**

In Figs. 4.67(a-d) there are 3-D surfaces plotted for more detailed analysis of three variables dependency upon each other. Figures. 4.67(a,b) shows thrust versus AR at low and high DoD, it is clear from figure that both plots at low and high values of DoD are mirror image of each other, and showing constant values of AR at low thrust and a steep increase in AR at medium and high thrust force. Figures 4.67(c,d) shows AR variation with DoD at low and high thrust, AR varies sinusoidal with DoD both at low and high thrust.

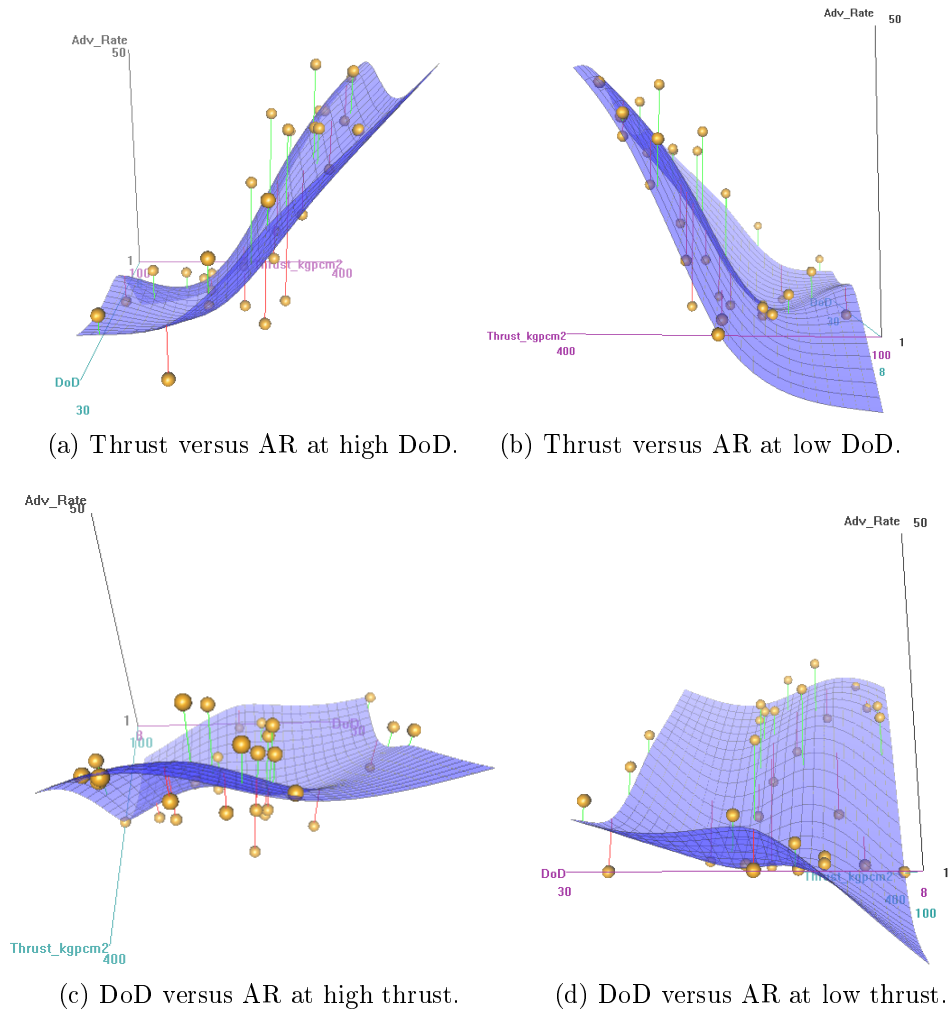
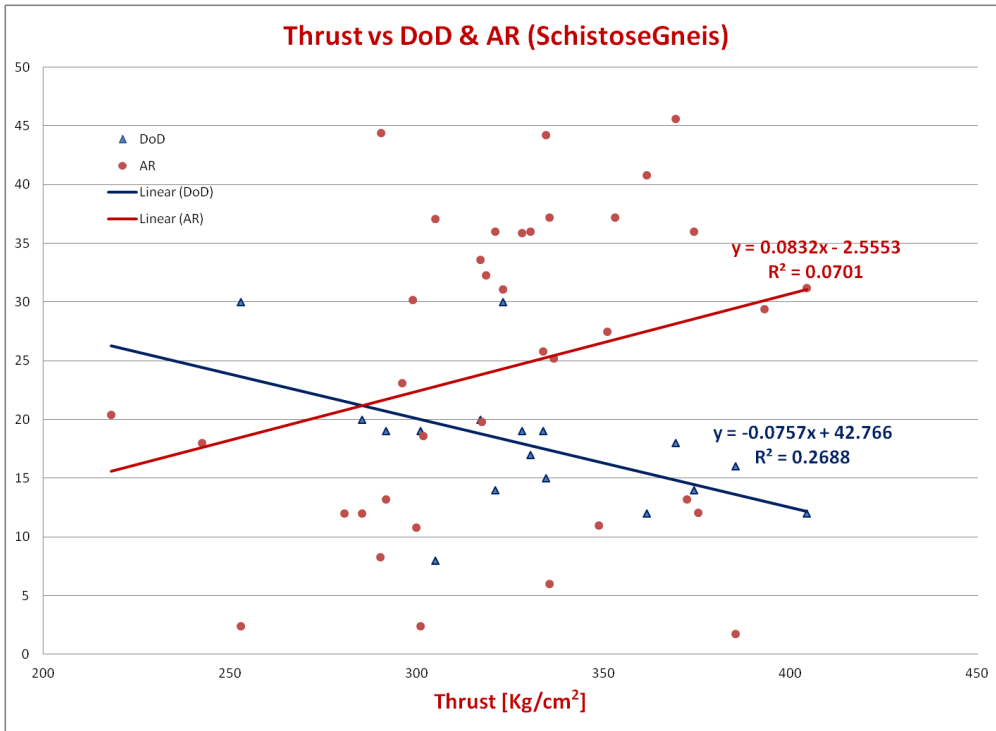


Figure 4.67: 3-D surfaces for Micaschists.

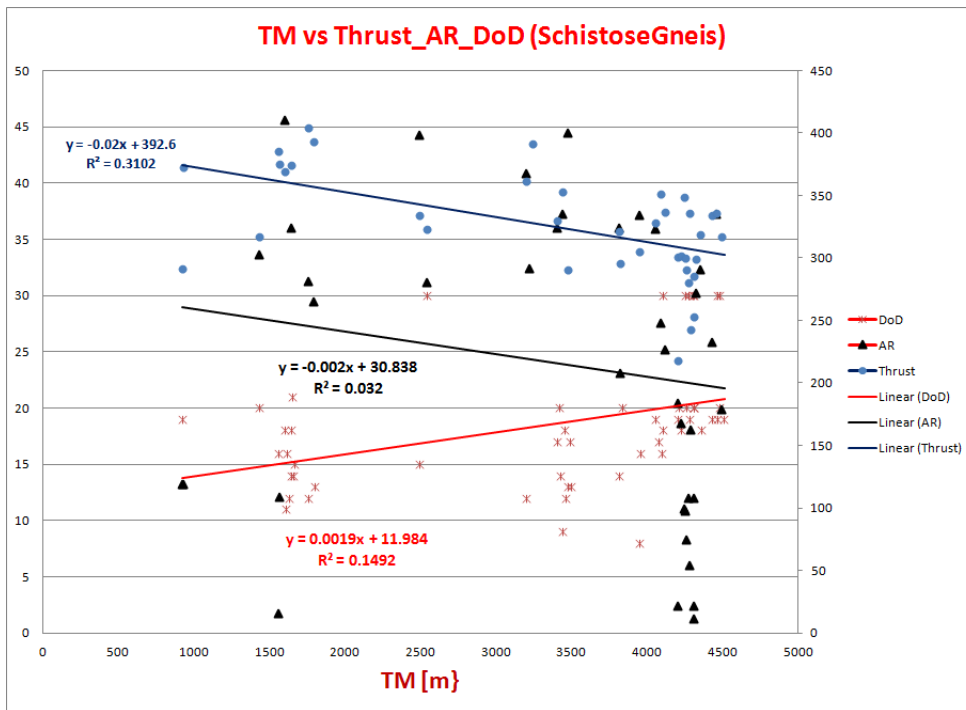
## 4.4.5 Schistose-Gneis

### 4.4.5.1 Data Analysis with Excel

Figure 4.68a shows relation between thrust, AR and DoD. Advance rate is linearly increasing with thrust with the same rate as DoD decreases. From this graph it is clear that more thrust is needed to achieve high advance rate provided that degree of disintegration is very low. In other words rock type, strength and DoD play a key role for TBM performance. In Fig. 4.68b shows variation of DoD, AR and thrust along with chainage. DoD is increasing with tunnel length whereas thrust and AR is slightly on lower side with chainage.



(a) Thrust versus AR and DoD.



(b) TM versus thrust, AR and DoD.

Figure 4.68: Thrust versus AR and DoD.

4.4.5.2 Fuzzy RMC Model

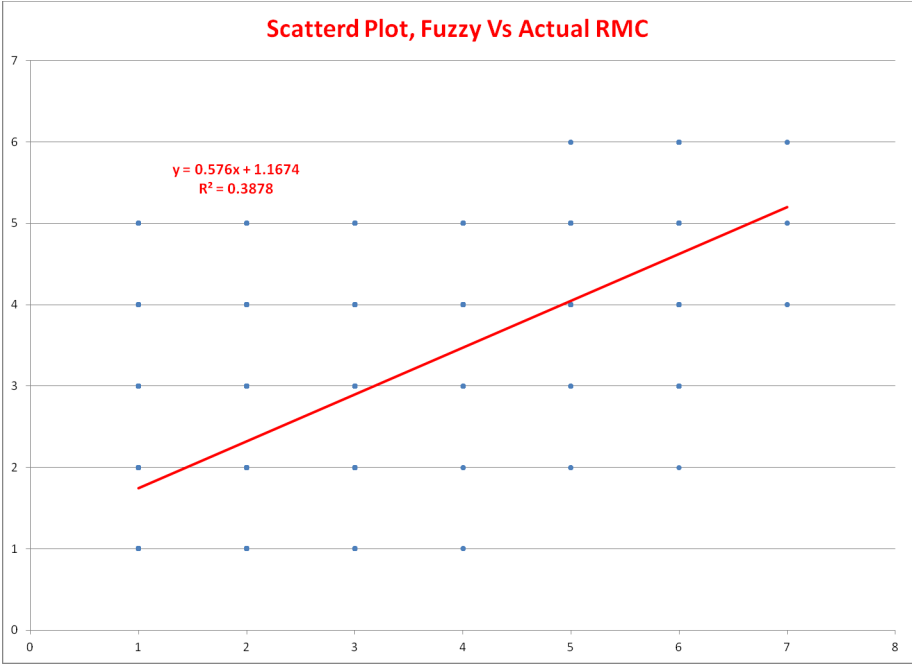
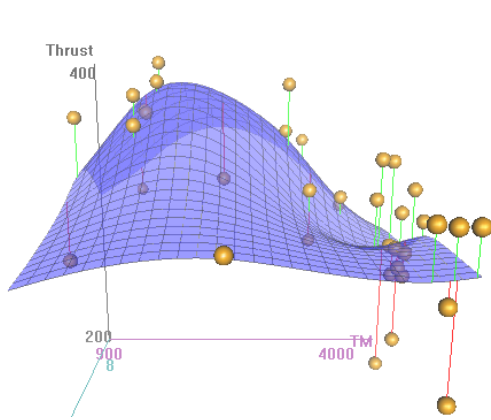


Figure 4.69: Fuzzy versus actual RMC.

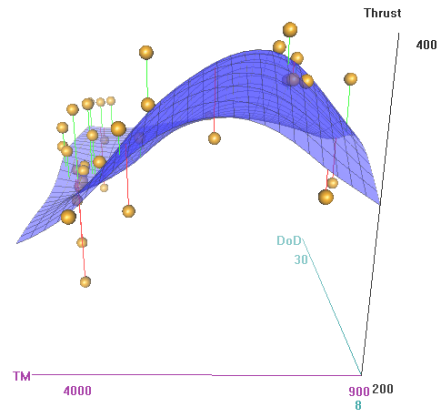
Fuzzy prediction model for RMC ( $R^2 = 0.39$ ) using machine and rock mass data of Schistos-Gneis rock is formulated and plotted Fig. 4.69, it seems not a fairly good model.

4.4.5.3 3-D Surface Plot and Analysis With “R”

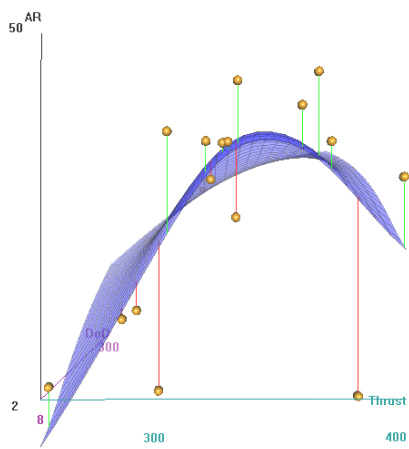
Figures 4.70(a-d) show 3-D surfaces for different variables in Schistose-Gneis rock, which revealed that higher DoD values AR is directly proportional to thrust, quadratic relation is found at high values of DoD, which shows that at stronger rock, the behaviour of TBM excavation is not as simple as in week rock i.e. more thrust more advance rate is not a rule of thumb. But there involve many factors for chip formation, rock breakage and cushioning effect and TBM cutter wear, that play important role in machine’s overall performance.



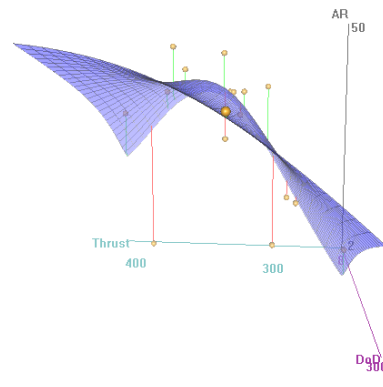
(a) TM versus thrust at low DoD.



(b) TM versus thrust at high DoD.



(c) Thrust versus AR at low DoD.

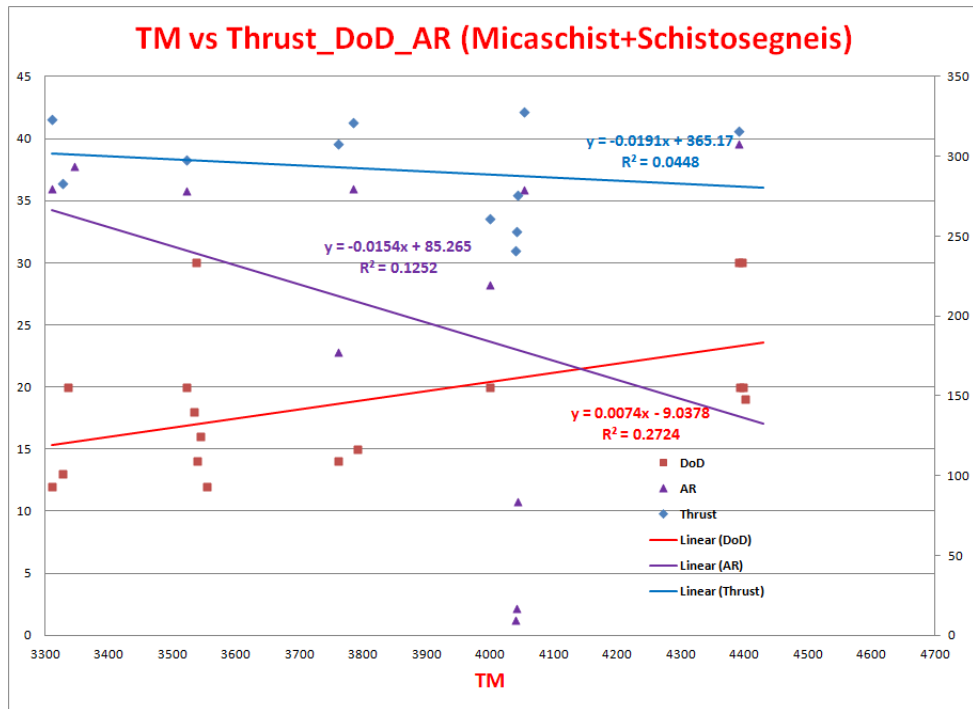


(d) Thrust versus AR at high DoD.

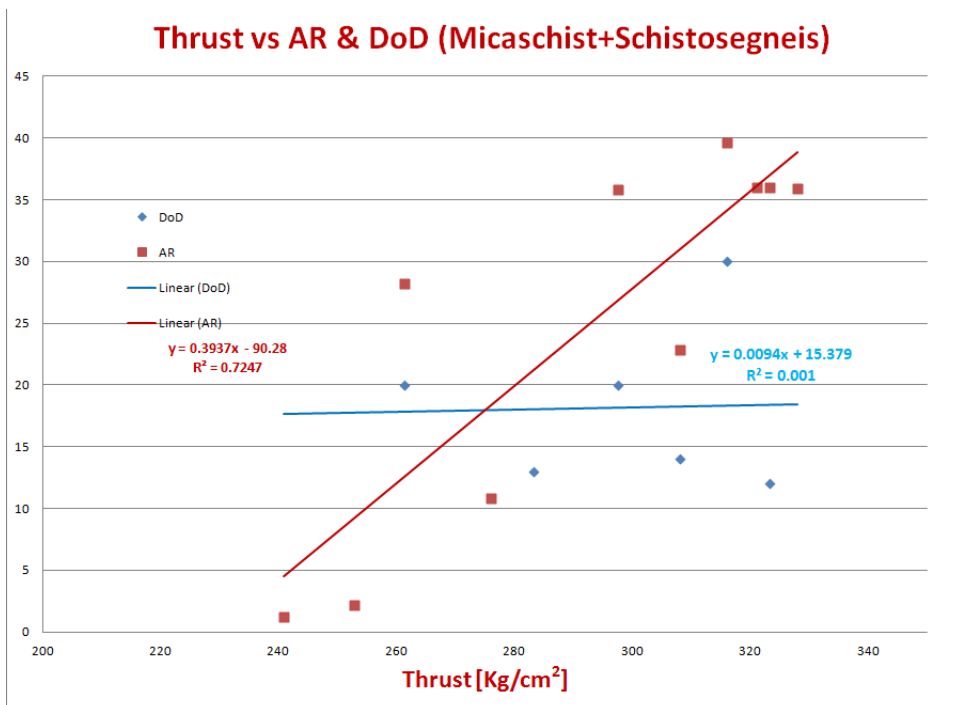
Figure 4.70: Schistose-Gneiss 3-D surface plots.

## 4.4.6 Mica-schist+Schistose-Gneis

### 4.4.6.1 Data Analysis with Excel



(a) TM versus thrust, AR and DoD.



(b) Thrust versus AR and DoD.

Figure 4.71: 2-D plots with Excel.

Figures 4.71(a,b) shows a linear plots for Mica-Schist+Schistose-Gneis rock. In Fig. 4.71a variation of all parameters along with chainage is shown, while in Fig. 4.71b variation of thrust against AR and DoD is plotted. It is clear from the figure that thrust is independent of DoD, whereas AR increases linearly with thrust.

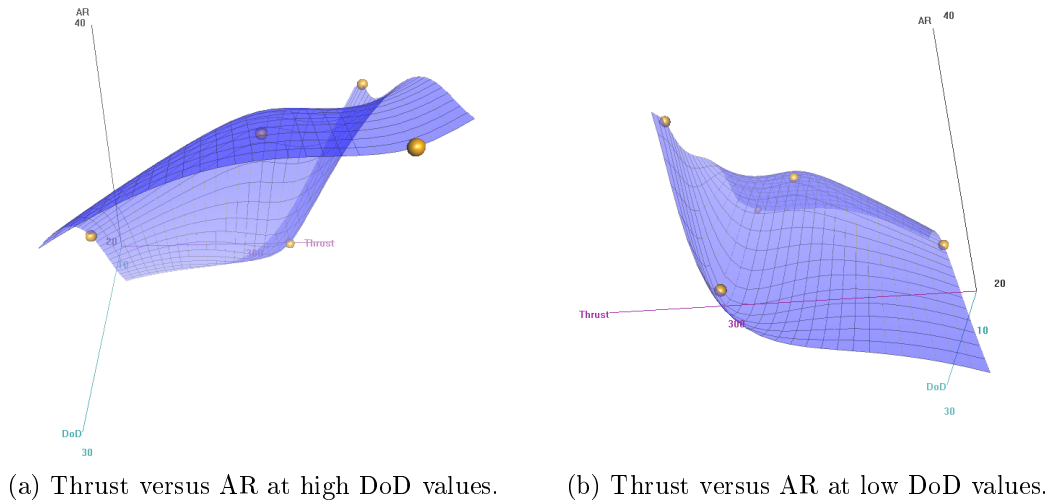


Figure 4.72: 3-D surface plots.

Figures 4.72(a,b) shows variation of AR with thrust at low and high values of DO D. both graphs are almost mirror image of each other. At start AR is constant with increase of thrust up to a medium thrust values, but at very high thrust AR increase drastically.

#### 4.4.7 Conclusions

Hemerwald hydro tunnel was excavated by Robbins Series 120,  $\phi = 3.90\text{ m}$  started in 1977, in Kühtai area of Tirol, Austria. For rock mass data (all rocks), trend of thrust, excavation velocity and degree of disjuncting varies almost in same way when plotted against tunnel meters. Advance rate increases quadratically with thrust, having a peak of  $6\text{ m/hr}$  at  $250\text{ kg/cm}^2$ , and then decreases rapidly. RMC and DoD have a major role in machine performance. Fuzzy logic generated 3-D surfaces for rock mass data, also show a maximum ROP at moderate thrust values and medium RMC. Linear regression model for advance rate shows a very accurate estimation model ( $R^2 = 0.928$ ) and there was a significant correlation between machine parameters and rock mass properties e.g. thrust-AR correlation ( $R^2 = -0.745$ ).

For Muskowit-Granite-Gneis data, no correlation between machine parameters and rock properties was found. ROP decreases sharply with increase of thrust, showing adverse effect of rock behaviour against application of more thrust than required. In Micaschists rock, same behaviour of thrust and ROP is seen, but a significant correlation between thrust and DoD is observed. Moreover a good Fuzzy logic prediction model is obtained for RMC, that shows a credible results. Same analysis, when performed on Schistos-Gneis,



ROP is linearly increases with thrust. Reason behind this trend is clear, when we plot a 3-D surface between thrust, ROP and DoD, shown in this section, ROP directly increases with thrust as DoD here have a moderate values throughout the section. When data for rock mass were analysed and plotted for different correlations, it is observed that, thrust and advance rate correlation follow a second degree polynomial. Maximum advance rate is observed at medium thrust rate values. Both extremes of thrust values i.e too low and too high thrust results in a very low advance rate. On the other hand, when data for separated individual rocks were analysed and plotted, it revealed that, advance rate is always directly proportional to thrust. This may be due to presence of favorable degree of disintegration in these section of tunnel.

## 4.5 Tunnels (Maen, Pieve and Varzo) in the Italian Alps

Data for TBM performance analysis have been obtained from three tunnels excavated in hard metamorphic rocks for hydraulic purposes in northern Italy. Three tunnels are located in the northwestern Alps (Italy) and consists of one inclined tunnel for the installation of a penstock (Maen) and two horizontal diversion tunnels (Pieve and Varzo). A total of 14 *km* of tunnel was surveyed almost continually, yielding over 700 sets of data featuring rock mass characteristics and TBM performance. The empirical relations between rock mass rating and penetration rate clearly show that TBM performance reaches a maximum in the rock mass rating (RMR) range 40–70 while slower penetration is experienced in both too bad and too good rock masses. However, different rocks gives different penetrations for the same RMR and use of the Bieniawski's classification for predictive purpose is only possible provided one uses a normalized RMR index with reference to the basic factors affecting TBM tunneling [37].

### 4.5.1 Maen Tunnel

These rock units consist of meta-ophiolites (Serpentinite, Metagabbro, Metabasite, Chlorite Schist and Talc Schist) and meta-sediments (Calc Schist and Silicate marble) belonging to the Zermatt-Saas Zone of the Penninic Domain [37]. The parent rocks were carbonate pelagic sequences and mafic crystalline rocks that underwent high-pressure low-temperature metamorphism during the early phases of the alpine orogenesis. Schists and serpentinite show a foliated texture while metagabbro and metabasite are generally weakly foliated. The attitude of rock units is more or less uniform throughout the tunnel, at  $N220-2701E/35-451$  (dip direction/dip), so that the longitudinal axis of the inclined tunnel (plunging direction  $N1281E$ ) is almost normal to the schistosity [42, 43].

#### 4.5.1.1 Data Analysis by Excel

Data from Maen tunnel was analysed and different parameters were compared by Excel. When thrust is plotted against advance rate and penetration rate, it gives interesting results. Performance prediction of TBM requires the estimation of both penetration rate (PR) and advance rate (AR). Penetration rate is defined as the distance excavated divided by the operating time during a continuous excavation phase, while advance rate is the actual distance mined and supported divided by the total time and it includes downtime for TBM maintenance, machine breakdown, and tunnel failure [42]. In Maen tunnel advance rate increases linearly with thrust but it is inversely proportional to penetration rate. Figure 4.73 shows that there is drastic difference between penetration rate and advance rate, which ultimately revealed that high downtime, machine breakdown and maintenance time for the TBM is present, that shows very low utilization factor of TBM. RMR and Bieniawski RMR (BRMR) Fig. 4.74 have almost same trend i.e linearly increasing with a small step difference.

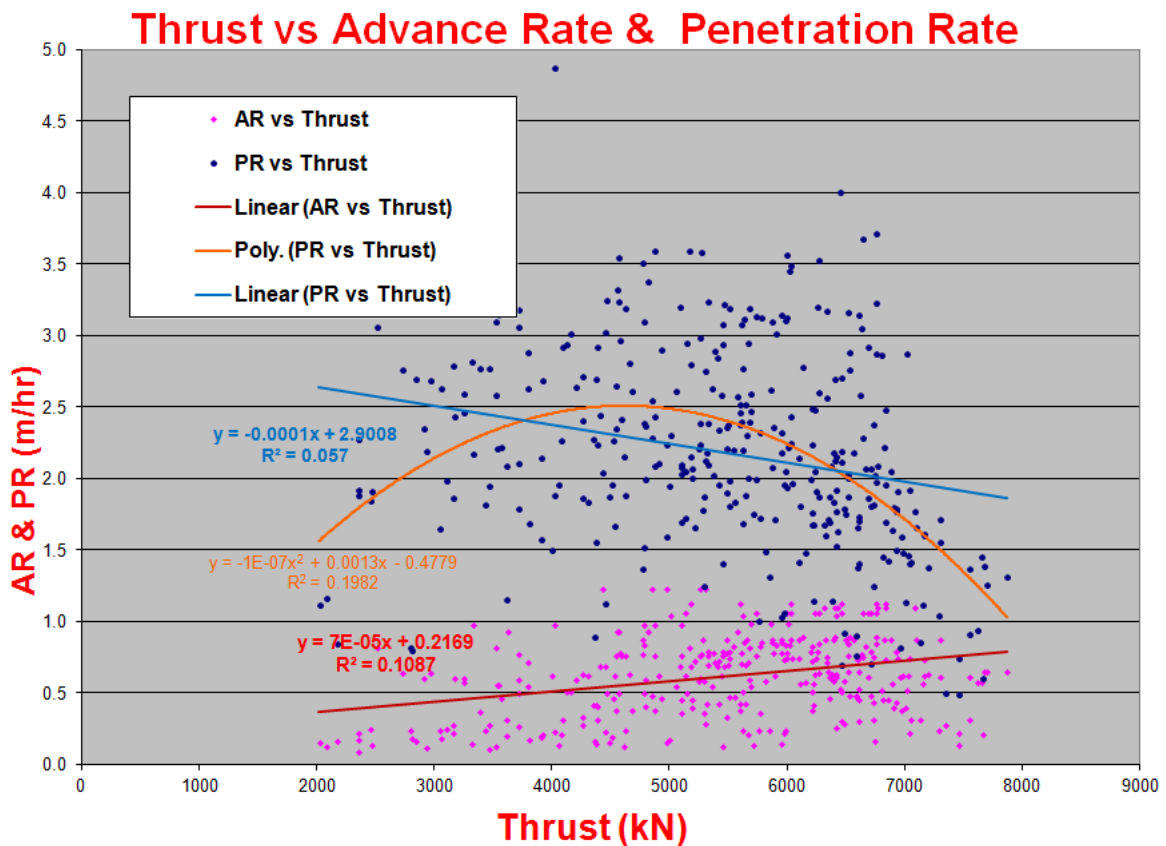


Figure 4.73: Thrust versus AR and PR.

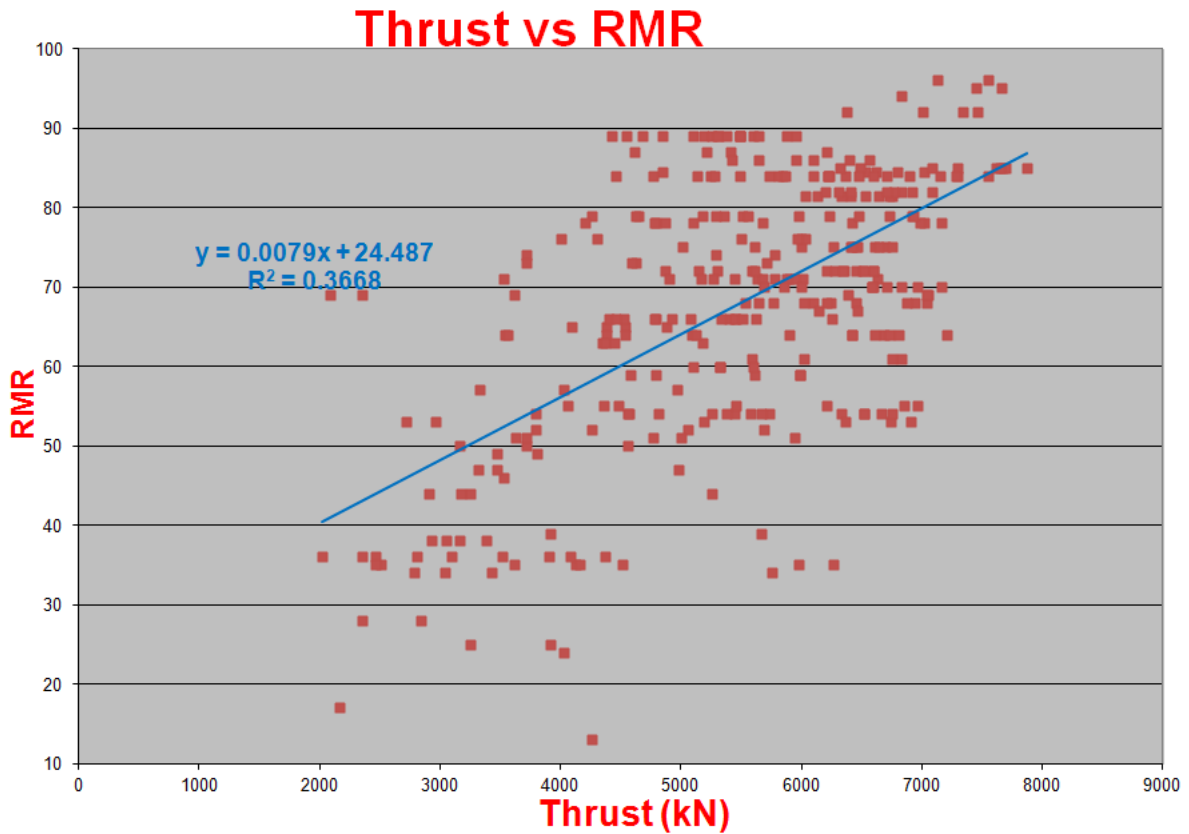


Figure 4.74: Thrust versus RMR.

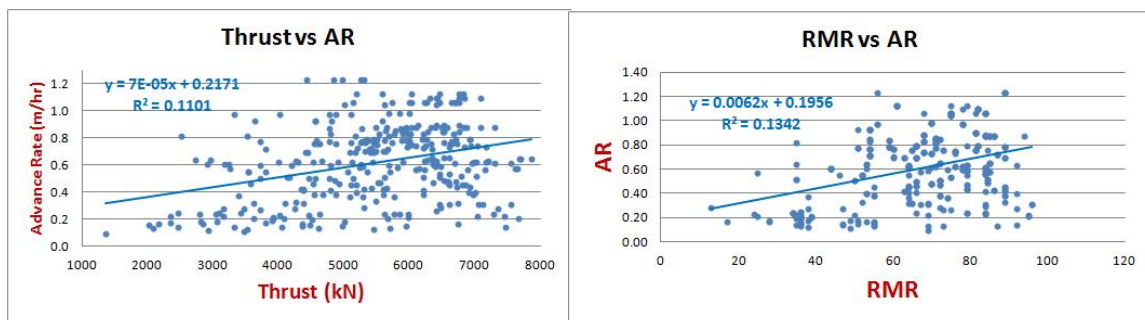


Figure 4.75: AR versus thrust and RMR.

In Fig. 4.75 advance rate increases linearly with same rate both against thrust and RMR, from this relation it is obvious that thrust and RMR are also directly proportional to each other. RMR versus AR plot shows that there is more penetration in weak rock, i.e poor and medium rocks are favorable for TBM when there is very low degree of disjuncting.

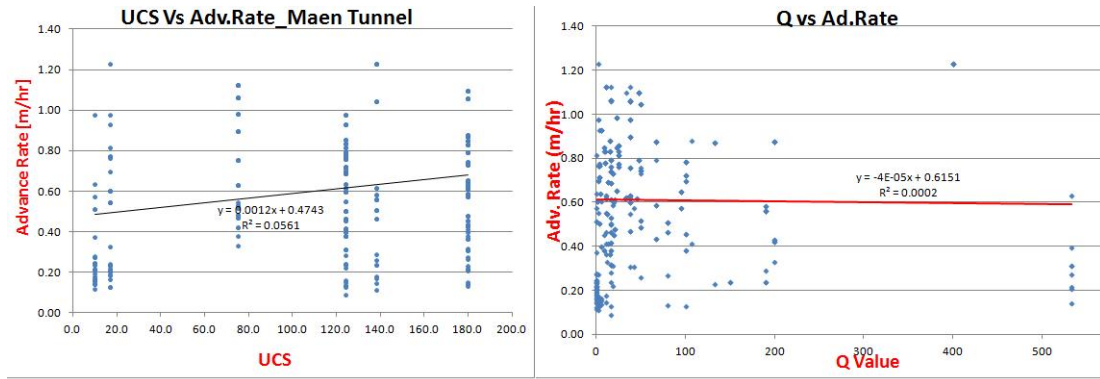


Figure 4.76: UCS and Q-value versus AR.

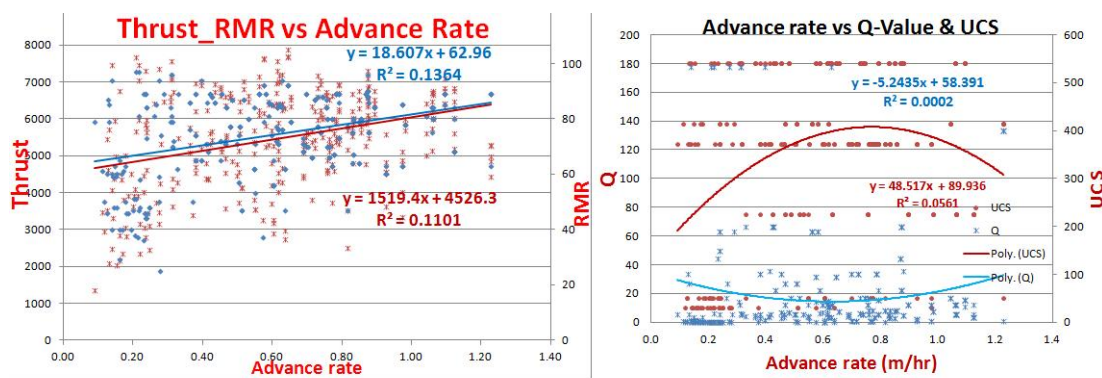


Figure 4.77: AR versus thrust and RMR.

Figure 4.76 displays UCS and Q value plot against advance rate. UCS have almost similar behaviour as RMR and Fig. 4.76b displayed that there is no influence of Q value upon AR and a constant horizontal line is observed. At low Q-values frequency of points is almost 90%, that shows in this tunnel area, rock strata posses medium and low Q-values. In Fig. 4.77 different parameters shows their influence upon AR. Q-value and UCS have a totally mirror image behaviour against AR, that shows, medium values of AR are observed at high UCS and low Q-values. But there are other factors too, that effect the behaviour of these parameters.

#### 4.5.1.2 Data Analysis With Fuzzy Logic

Rule base for this tunnel was established and by giving three input parameters, AR was predicted and compared with actual AR. Rule base for Maen tunnel is shown below in table. 4.30.

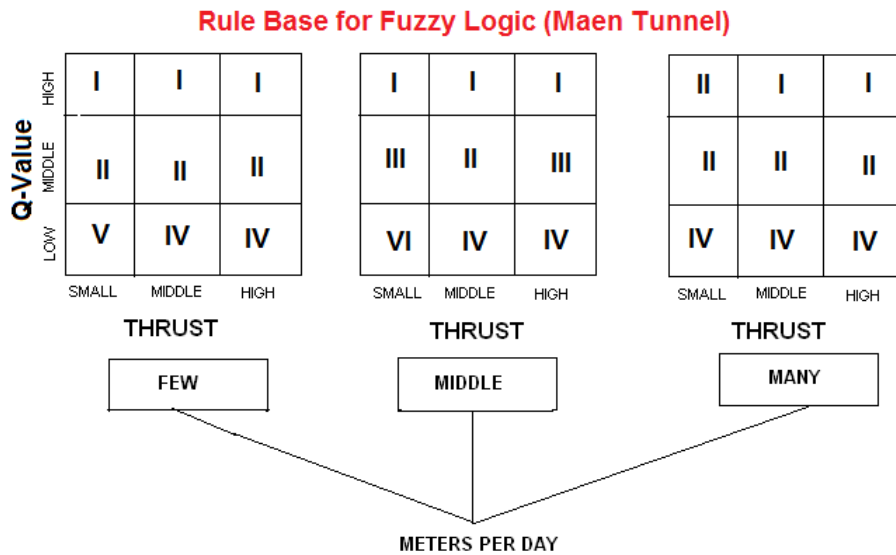


Table 4.30: Fuzzy rule base for Maen tunnel.

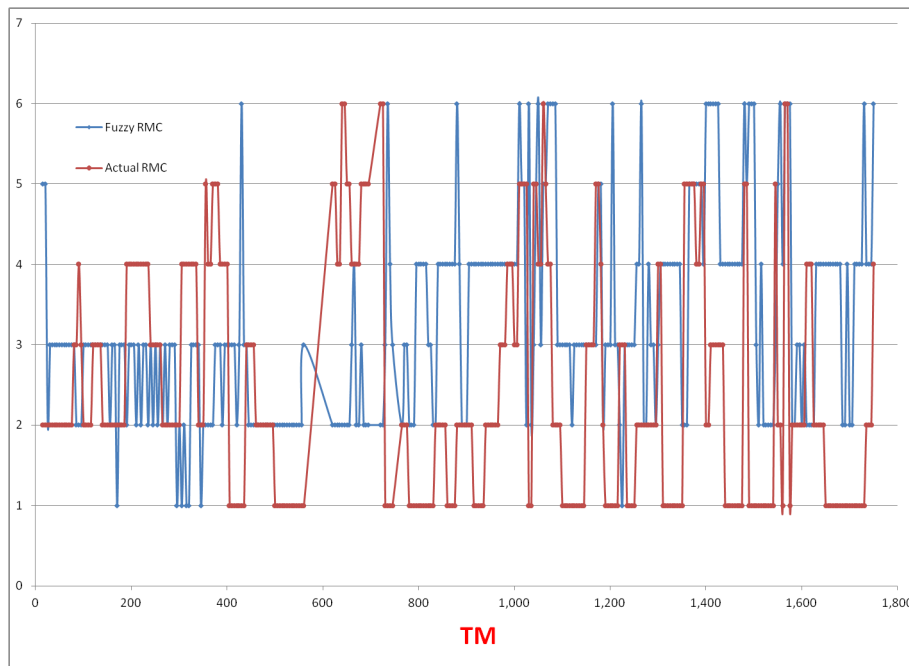


Figure 4.78: Fuzzy versus actual RMC plot.

Figures 4.78 and 4.79 show comparison between actual, Fuzzy logic and SPSS RMC. In Fig. 4.78 Fuzzy and actual RMC is compared, and it rarely matches each other that shows poor accuracy of the Fuzzy model. Comparison between SPSS and actual RMC, shows almost 90% predicted values coincides with corresponding actual values, showing a very good prediction model by SPSS.

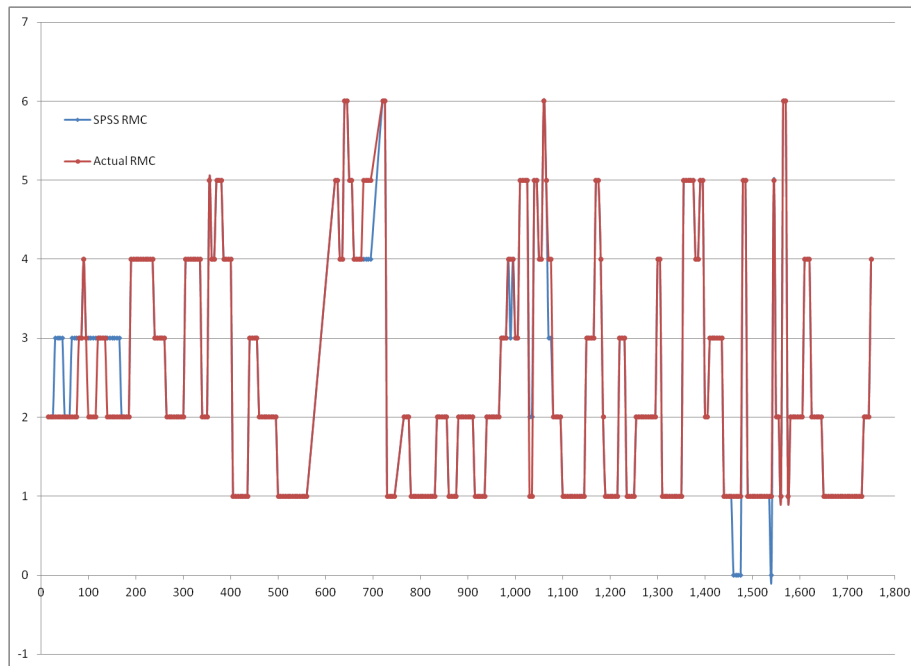


Figure 4.79: Fuzzy versus SPSS RMC.

#### 4.5.1.3 Data Analysis by Statistical Software “R”

Statistical software R has been used to plot 3-D surfaces and to see different sides of the picture. 3-D surface also shows the intensity of the data points at specific location and helps to visualize the effect of three different parameters on each other in a broader way. Here only two views were captured and shown with respect to high and low values of third variable, when the remaining two variables were compared.

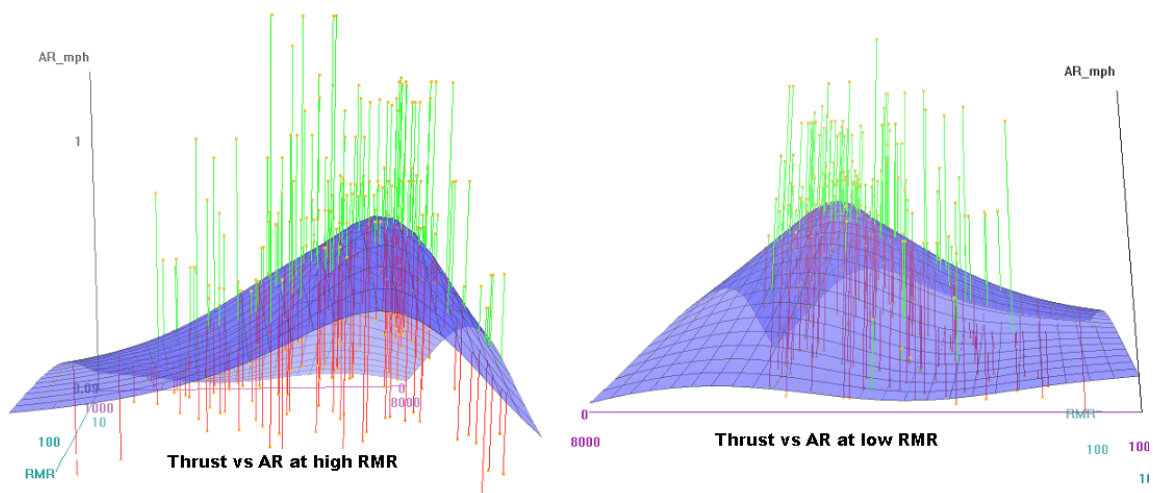


Figure 4.80: Thrust versus AR at low and high RMR.

Figure 4.80 shows at lower values of RMR, AR is uniform with respect to thrust, but at high values of RMR, trend is quadratic and maximum AR is obtained at moderate

values of thrust. Reason may be that a very good rock (with medium rock strength) and average disintegration, is easy to chip formation for the TBM.

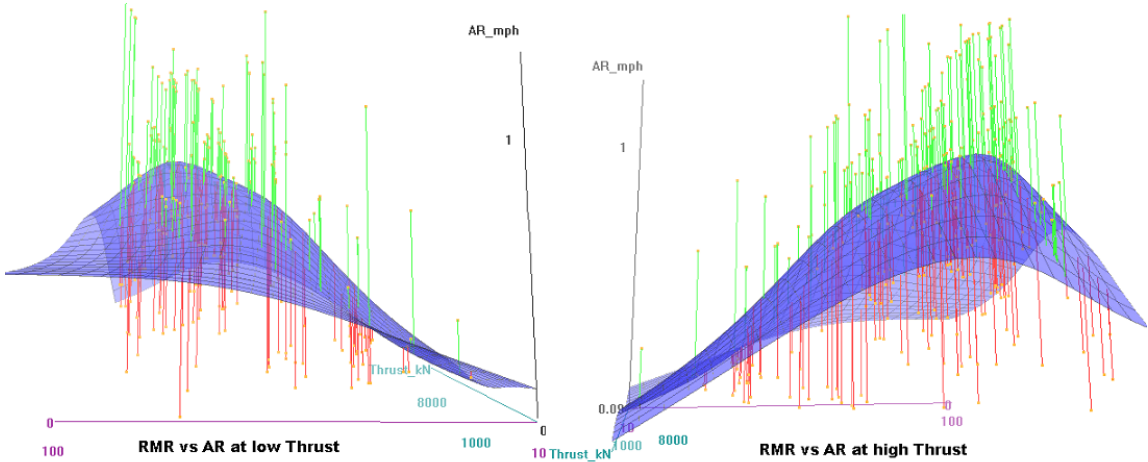


Figure 4.81: RMR versus AR at low and high thrust.

In Fig. 4.81, 3-D surface is plotted for RMR versus AR at low and high machine thrust. At low thrust advance rate increase linearly with RMR, but at high values of machine thrust again a quadratic behaviour is found. It revealed that like UCS, RMR also plays an important role in machine advance. Medium to moderate rock strength is always good for the TBM to get a better advance rate, even at medium machine thrust. Figure 4.82 displays effect of UCS, which shows maximum advance rate at medium strength of rock. Reason may be that at low thrust, chip formation is not possible when thrust is below the critical value necessary for chip formation, at high values of UCS.

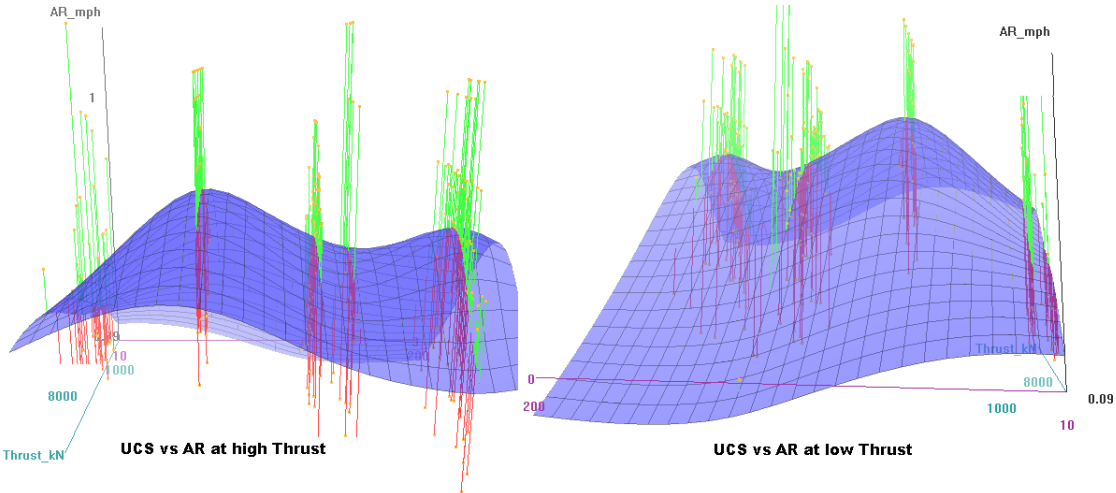


Figure 4.82: Thrust versus AR at the rate of UCS.

**4.5.1.4 Statistical Modeling with SPSS 19**

IBM SPSS19 was used for statistical analysis of the data taken from Maen tunnel. In order to obtain a penetration prediction model, multidimensional regression analysis were

carried out for rock properties and machine parameters. Effect of each parameter was separately discussed on rate of penetration (ROP). Separate equation was developed for each rock parameter against the ROP, to see the weight and importance of that parameter in overall model.

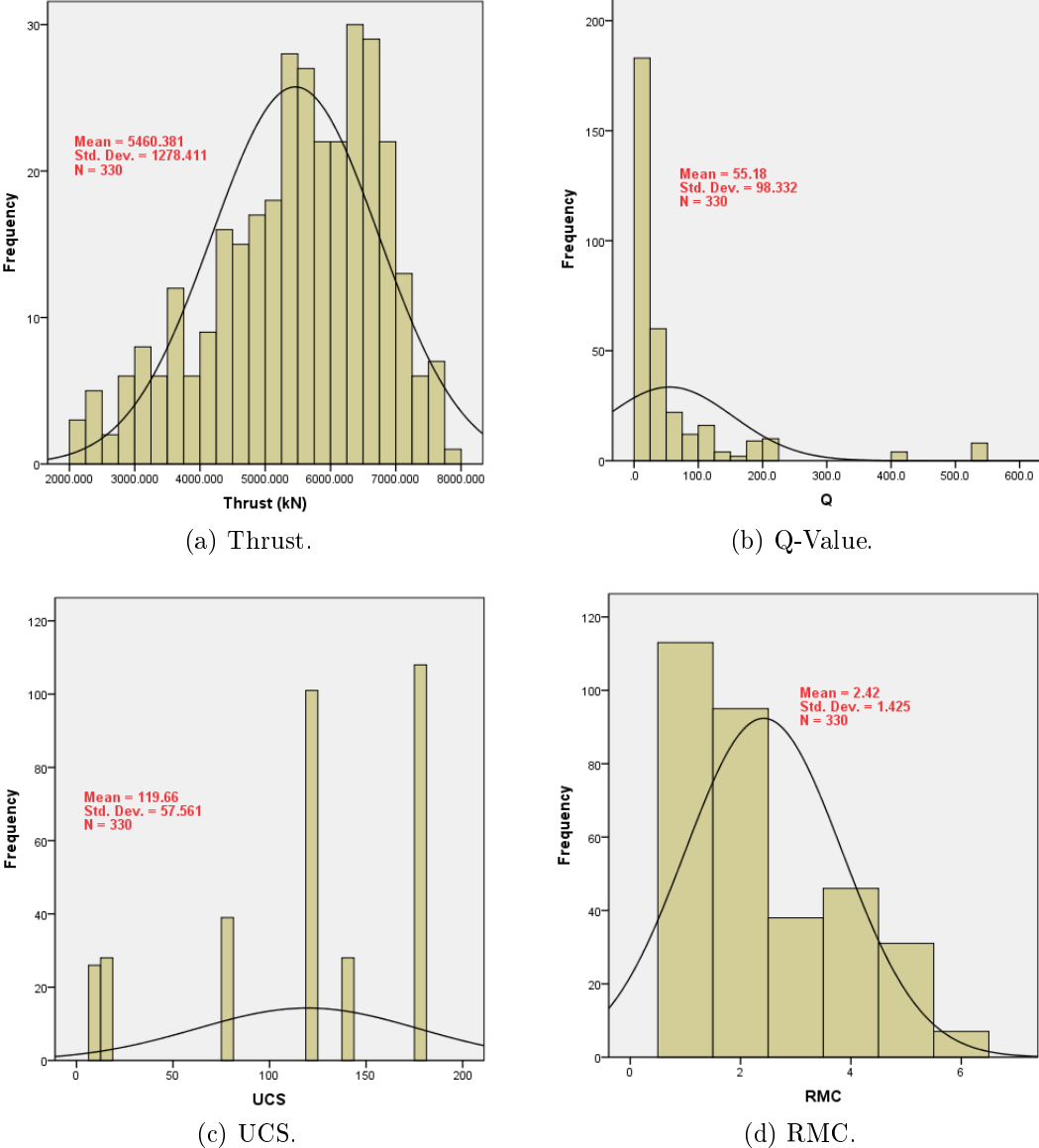


Figure 4.83: Histograms for Maen tunnel 1.

Histograms in Fig. 4.83 shows that there is normal distribution and very low standard deviation in thrust frequency distribution. But in UCS, frequency distribution, it is skewed right and shows a step function as its step values are repeating at specific interval. Frequency distribution of Q-value and RMC are skewed left and are not normally distributed. In Fig. 4.84 frequency distribution of four parameters is shown, penetration rate (PR) has a perfect normal distribution with a standard deviation  $SD = 0.7$ . Where as AR, RMR have also a good normal distribution. Frequency distribution of BRMR is



skewed right and shows some discrepancy as compare with RMR.

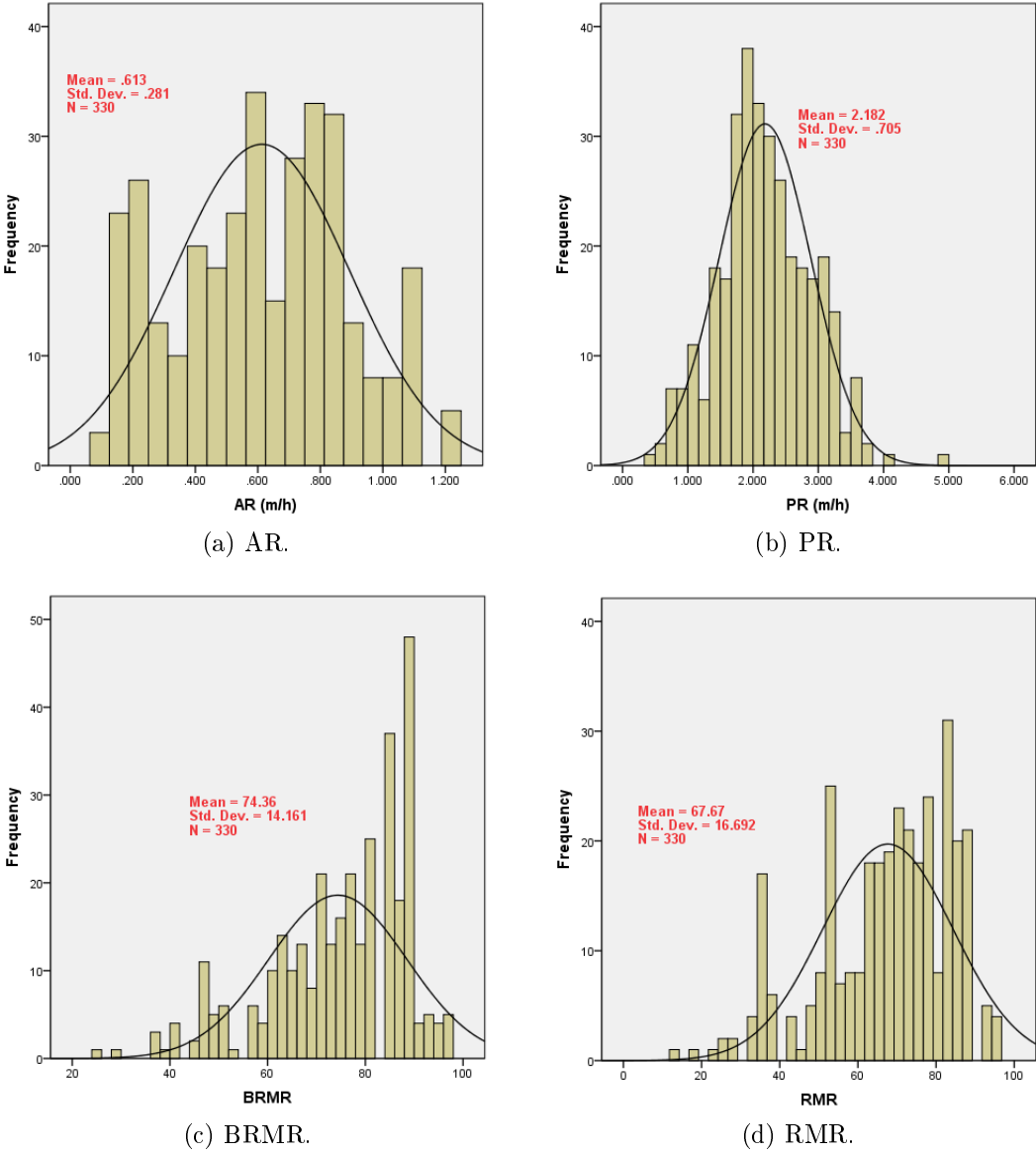


Figure 4.84: Histograms for Maen tunnel 2.

**Advance Rate (AR) Prediction Model:** Table 4.31 shows a model summary for Maen tunnel advance rate model with an accuracy of 37.8% and its a “forward stepwise model”. There were seven predicted i.e Q-value, Thrust, RMC, UCS, PR and RMR and one target variable i.e advance rate (AR) were used. Q-value shows most importance in the model where as RMC has least importance.

### Model Summary

<b>Target</b>	AR (m/h)
<b>Automatic Data Preparation</b>	On
<b>Model Selection Method</b>	None (All Predictors Entered)
<b>Information Criterion</b>	-986.105

The information criterion is used to compare to models. Models with smaller information criterion values fit better.

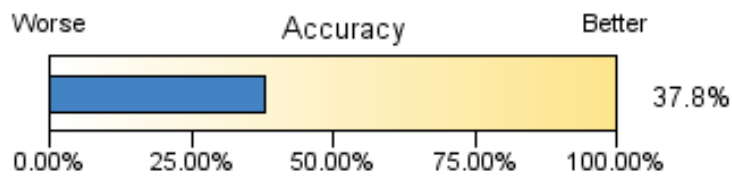


Table 4.31: AR model summary.

Effects		Target: AR (m/h)				
Source	Sum of Squares	df	Mean Square	F	Sig.	Importance
<b>Corrected Model ▼</b>	10.178	7	1.454	29.602	.000	
<b>PRmh_transformed</b>	3.827	1	3.827	77.918	.000	0.170
<b>ThrustkN_transformed</b>	0.674	1	0.674	13.728	.000	0.143
<b>Q_transformed</b>	0.228	1	0.228	4.649	.032	0.139
<b>UCS_transformed</b>	0.066	1	0.066	1.351	.246	0.137
<b>RMC_transformed</b>	0.046	1	0.046	0.932	.335	0.137
<b>BRMR_transformed</b>	0.007	1	0.007	0.135	.714	0.137
<b>RMR_transformed</b>	0.003	1	0.003	0.059	.808	0.137
<b>Residual</b>	15.816	322	0.049			
<b>Corrected Total</b>	25.995	329				

Table 4.32: AR model effects.

Table 4.32 shows importance of the predictors, here for this AR model, thrust and PR

are most important input variables and RMC is least important. On the other hand table 4.33 shows the list of coefficients, which are used to formulate a linear regression model shown in Eq. 4.10.

		Coefficients			Target: AR (m/h)		
Model Term	Coefficient ▼	Std.Error	t	Sig.	95% Confidence Interval		Importance
					Lower	Upper	
Intercept	-0.195	0.362	-0.540	.590	-0.906	0.516	
PRmh_transformed	0.182	0.021	8.827	.000	0.142	0.223	0.170
ThrustkN_transformed	0.000	0.000	3.705	.000	0.000	0.000	0.143
Q_transformed	-0.001	0.000	-2.156	.032	-0.001	-0.000	0.139
UCS_transformed	0.000	0.000	1.162	.246	-0.000	0.001	0.137
RMC_transformed	-0.039	0.040	-0.965	.335	-0.118	0.040	0.137
BRMR_transformed	0.002	0.005	0.367	.714	-0.008	0.012	0.137
RMR_transformed	0.001	0.005	0.243	.808	-0.009	0.012	0.137

Table 4.33: AR model coefficients.

The model can be written in the form of a linear equation as in Eq. 4.10

$$AR(m/hr) = -0.148 - 0.002Q_{value} + 0.001Thrust + 0.010RMR - 0.001UCS - 0.011RMC \quad (4.10)$$

By applying this model on the data available from Maen tunnel, following predicted values are obtained and the plot between actual AR and predicted values is shown in Fig. 4.85 ( $R = 0.62$ ).

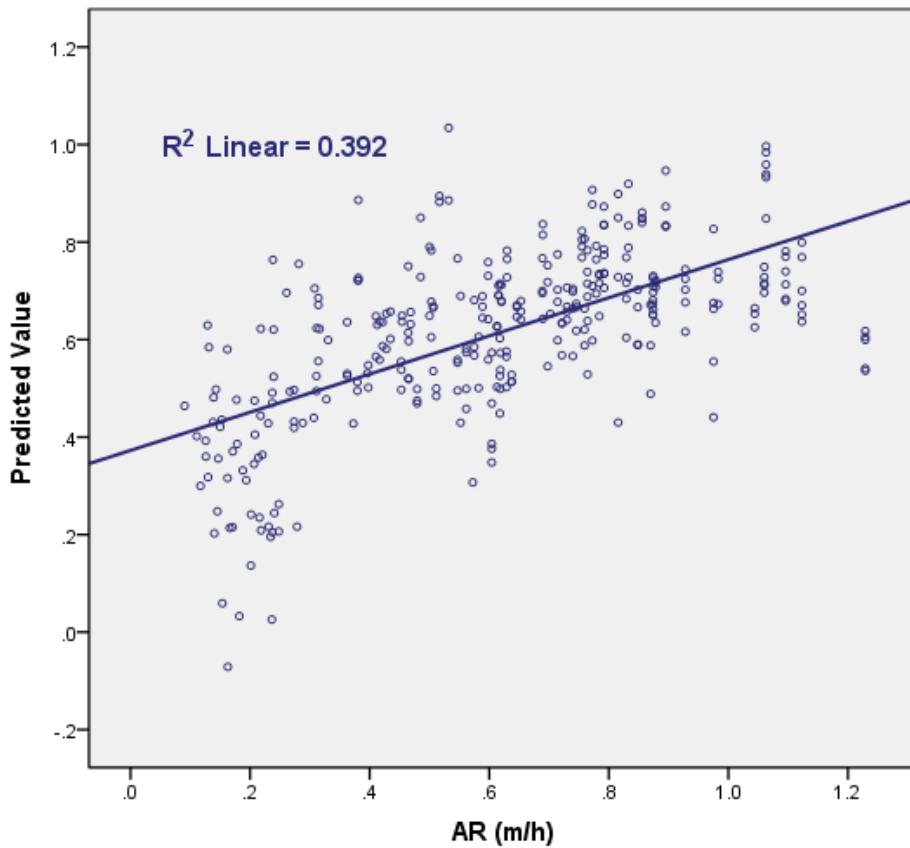


Figure 4.85: AR linear regression model.

**Penetration Rate (PR) Prediction Model:** Penetration rate (PR) model summary (Table 4.34) shows that model has an accuracy of 40.8%.

**Model Summary**

<b>Target</b>	PR (m/h)
<b>Automatic Data Preparation</b>	On
<b>Model Selection Method</b>	None (All Predictors Entered)
<b>Information Criterion</b>	-395.591

The information criterion is used to compare to models. Models with smaller information criterion values fit better.

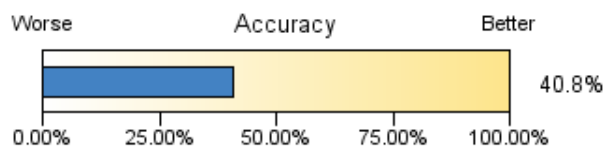


Table 4.34: Model summary for PR.

Q-values and UCS plays important role in model prediction. Using coefficients from table 4.36, a linear regression model for PR is formulated and shown in Eq. 4.11.

Effects			Target: PR (m/h)			
Source	Sum of Squares	df	Mean Square	F	Sig.	Importance
Corrected Model ▼	68.716	7	9.817	33.386	.000	
ARmh_transformed	23.079	1	23.079	78.491	.000	0.165
Q_transformed	10.321	1	10.321	35.102	.000	0.147
UCS_transformed	9.786	1	9.786	33.283	.000	0.146
ThrustkN_transformed	4.169	1	4.169	14.180	.000	0.139
RMR_transformed	2.323	1	2.323	7.901	.005	0.136
RMC_transformed	0.752	1	0.752	2.556	.111	0.134
BRMR_transformed	0.284	1	0.284	0.967	.326	0.133
Residual	94.678	322	0.294			
Corrected Total	163.395	329				

Table 4.35: Predictors effects for PR model.

Coefficients		Target: PR (m/h)					
Model Term	Coefficient ▼	Std.Error	t	Sig.	95% Confidence Interval		Importance
					Lower	Upper	
Intercept	0.929	0.884	1.051	.294	-0.809	2.668	
ARmh_transformed	1.084	0.122	8.860	.000	0.843	1.325	0.165
Q_transformed	-0.005	0.001	-5.925	.000	-0.007	-0.003	0.147
UCS_transformed	-0.004	0.001	-5.769	.000	-0.006	-0.003	0.146
ThrustkN_transformed	-0.000	0.000	-3.766	.000	-0.000	-0.000	0.139
RMR_transformed	0.037	0.013	2.811	.005	0.011	0.063	0.136
RMC_transformed	0.157	0.098	1.599	.111	-0.036	0.351	0.134
BRMR_transformed	-0.012	0.012	-0.983	.326	-0.036	0.012	0.133

Table 4.36: Predictors coefficients for PR model.

$$PR(m/hr) = 0.929 + 1.08AR - 0.005Q_{-value} - 0.004UCS - 0.157RMC - 0.037RMR - 0.001Thrust \tag{4.11}$$

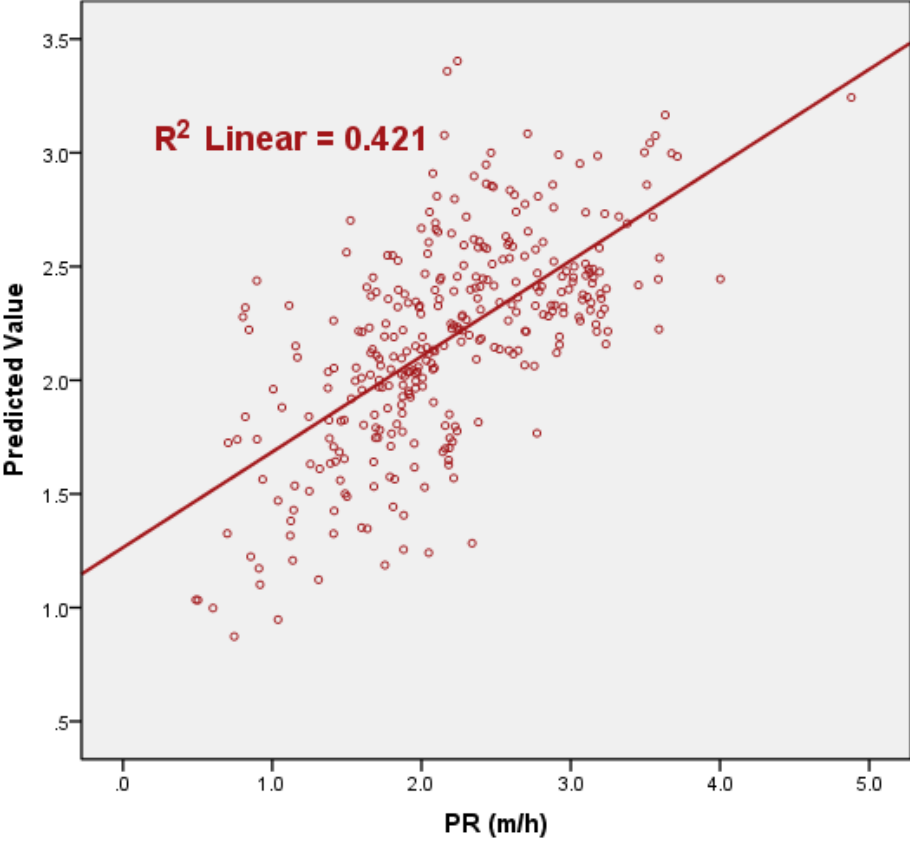


Figure 4.86: PR regression model .

**Rock Mass Class (RMC) Prediction Model** Prediction model for RMC is also obtained by multidimensional analysis. thrust, UCS, Q-value and penetration rate were used as predictors. RMR was excluded as UCS values were calculated from RMR by an excel formula. Model has a good accuracy (66.4%), model summary, predictors effects and coefficients are shown in tables 4.37-4.39 respectively. Q-values and UCS play important role in model prediction and PR was least important.

### Model Summary

<b>Target</b>	RMC
<b>Automatic Data Preparation</b>	On
<b>Model Selection Method</b>	None (All Predictors Entered)
<b>Information Criterion</b>	-119.980

The information criterion is used to compare to models. Models with smaller information criterion values fit better.

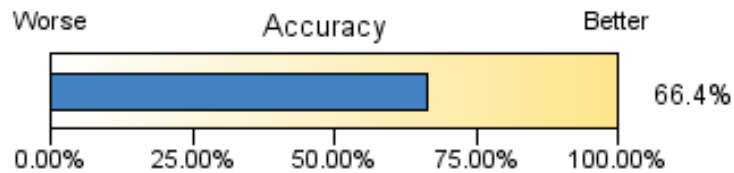


Table 4.37: Model summary for RMC.

Effects		Target: RMC				
Source	Sum of Squares	df	Mean Square	F	Sig.	Importance
<b>Corrected Model ▼</b>	447.246	5	89.449	131.112	.000	
<b>Q_transformed</b>	116.599	1	116.599	170.907	.000	0.260
<b>UCS_transformed</b>	39.729	1	39.729	58.234	.000	0.201
<b>ThrustkN_transformed</b>	15.592	1	15.592	22.854	.000	0.183
<b>ARmh_transformed</b>	14.033	1	14.033	20.568	.000	0.181
<b>PRmh_transformed</b>	5.377	1	5.377	7.881	.005	0.175
<b>Residual</b>	221.045	324	0.682			
<b>Corrected Total</b>	668.291	329				

Table 4.38: RMC model effects.

Coefficients		Target: RMC					
Model Term	Coefficient ▼	Std.Error	t	Sig.	95% Confidence Interval		Importance
					Lower	Upper	
Intercept	6.215	0.290	21.421	.000	5.644	6.786	
Q_transformed	-0.012	0.001	-13.073	.000	-0.014	-0.010	0.260
UCS_transformed	-0.008	0.001	-7.631	.000	-0.010	-0.006	0.201
ThrustkN_transformed	-0.000	0.000	-4.781	.000	-0.000	-0.000	0.183
ARmh_transformed	-0.913	0.201	-4.535	.000	-1.308	-0.517	0.181
PRmh_transformed	-0.234	0.083	-2.807	.005	-0.399	-0.070	0.175

Table 4.39: RMC model coefficients.

RMC linear regression model with a reasonable accuracy ( $R^2 = 0.669$ ), formulated from above predictors, coefficients and analysis, is given in Eq. 4.12

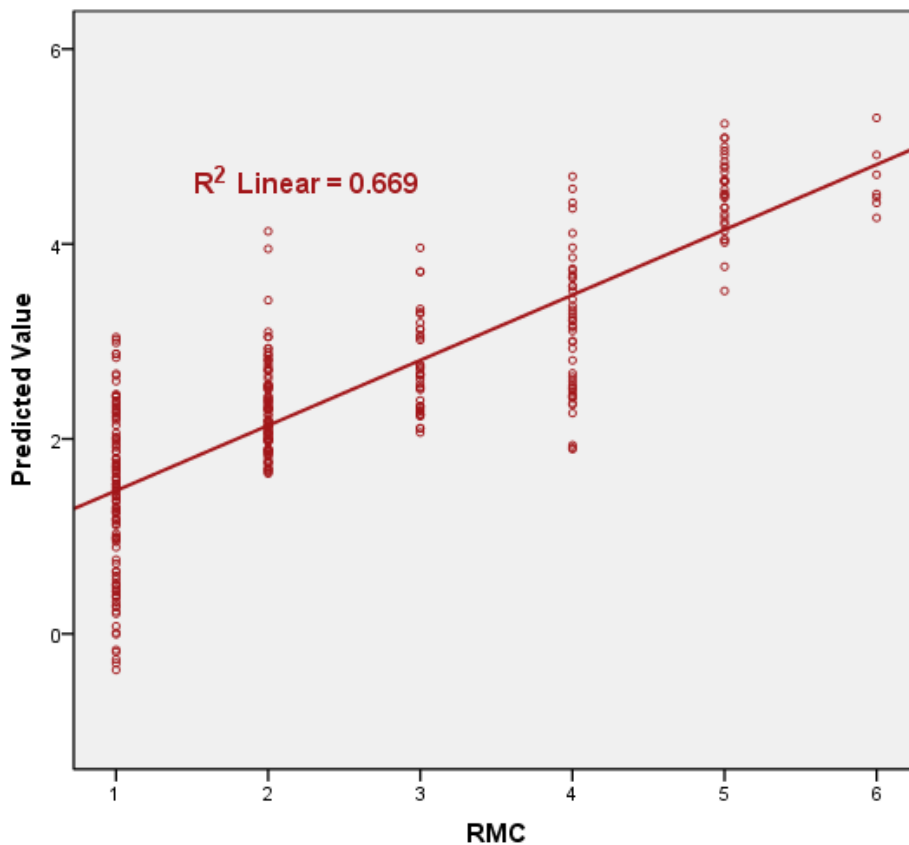


Figure 4.87: RMC linear regression model.

$$RMC = 5.645 - 0.011Q - 0.007UCS - 1.202AR - 0.0001Thrust \quad (4.12)$$



RMC regression model values are plotted against the actual RMC and shown in Fig. 4.87.

#### 4.5.1.5 Correlation and Correlation Coefficients

		Correlations						
		BRMR	Q	Thrust (kN)	PR (m/h)	UCS	AR (m/h)	RMC
BRMR	Pearson Correlation	1	.529**	.633**	-.174**	.680**	.369**	-.957**
	Sig. (2-tailed)		.000	.000	.002	.000	.000	.000
	N	330	330	330	330	330	330	330
Q	Pearson Correlation	.529**	1	.304**	-.360**	.308**	-.015	-.465**
	Sig. (2-tailed)	.000		.000	.000	.000	.786	.000
	N	330	330	330	330	330	330	330
Thrust (kN)	Pearson Correlation	.633**	.304**	1	-.239**	.599**	.330**	-.584**
	Sig. (2-tailed)	.000	.000		.000	.000	.000	.000
	N	330	330	330	330	330	330	330
PR (m/h)	Pearson Correlation	-.174**	-.360**	-.239**	1	-.339**	.371**	.131*
	Sig. (2-tailed)	.002	.000	.000		.000	.000	.017
	N	330	330	330	330	330	330	330
UCS	Pearson Correlation	.680**	.308**	.599**	-.339**	1	.237**	-.624**
	Sig. (2-tailed)	.000	.000	.000	.000		.000	.000
	N	330	330	330	330	330	330	330
AR (m/h)	Pearson Correlation	.369**	-.015	.330**	.371**	.237**	1	-.380**
	Sig. (2-tailed)	.000	.786	.000	.000	.000		.000
	N	330	330	330	330	330	330	330
RMC	Pearson Correlation	-.957**	-.465**	-.584**	.131*	-.624**	-.380**	1
	Sig. (2-tailed)	.000	.000	.000	.017	.000	.000	
	N	330	330	330	330	330	330	330

\*\* Correlation is significant at the 0.01 level (2-tailed).

\* Correlation is significant at the 0.05 level (2-tailed).

Table 4.40: Pearson correlation coefficients for Maen tunnel.

Table 4.40 shows good correlation between TBM parameters and rock mass properties, thrust-RMR ( $R^2 = 0.633$ ), UCS-thrust-RMC ( $R^2 = 0.589$ ). Moreover rock mass properties are strongly correlated e.g. RMR-RMC ( $R^2 = 0.957$ ), shows a strong linear dependence of TBM parameters upon rock mass properties and also among themselves too. On the other hand table 4.41 shows Spearman's and Kendall's correlation coefficients. It is clear from the table that there is no significant correlation between machine and rock properties, although rock properties are very well inter-correlated (e.g. RMR-Q-Value  $R^2 = 0.94$ ).

			Correlations							
			BRMR	Q	Thrust (kN)	PR (m/h)	UCS	AR (m/h)	RMC	
Kendall's tau_b	BRMR	Correlation Coefficient	1.000	.814**	.392**	-.190**	.445**	.196**	-.852**	
		Sig. (2-tailed)	.	.000	.000	.000	.000	.000	.000	
		N	330	330	330	330	330	330	330	
	Q	Correlation Coefficient	.814**	1.000	.343**	-.178**	.417**	.146**	-.812**	
		Sig. (2-tailed)	.000	.	.000	.000	.000	.000	.000	
		N	330	330	330	330	330	330	330	
	Thrust (kN)	Correlation Coefficient	.392**	.343**	1.000	-.218**	.449**	.191**	-.384**	
		Sig. (2-tailed)	.000	.000	.	.000	.000	.000	.000	
		N	330	330	330	330	330	330	330	
	PR (m/h)	Correlation Coefficient	-.190**	-.178**	-.218**	1.000	-.366**	.243**	.139**	
		Sig. (2-tailed)	.000	.000	.000	.	.000	.000	.001	
		N	330	330	330	330	330	330	330	
	UCS	Correlation Coefficient	.445**	.417**	.449**	-.366**	1.000	.135**	-.415**	
		Sig. (2-tailed)	.000	.000	.000	.000	.	.001	.000	
		N	330	330	330	330	330	330	330	
	AR (m/h)	Correlation Coefficient	.196**	.146**	.191**	.243**	.135**	1.000	-.231**	
		Sig. (2-tailed)	.000	.000	.000	.000	.001	.	.000	
		N	330	330	330	330	330	330	330	
	RMC	Correlation Coefficient	-.852**	-.812**	-.384**	.139**	-.415**	-.231**	1.000	
		Sig. (2-tailed)	.000	.000	.000	.001	.000	.000	.	
		N	330	330	330	330	330	330	330	
	Spearman's rho	BRMR	Correlation Coefficient	1.000	.942**	.548**	-.271**	.565**	.286**	-.943**
			Sig. (2-tailed)	.	.000	.000	.000	.000	.000	.000
			N	330	330	330	330	330	330	330
Q		Correlation Coefficient	.942**	1.000	.492**	-.265**	.540**	.223**	-.919**	
		Sig. (2-tailed)	.000	.	.000	.000	.000	.000	.000	
		N	330	330	330	330	330	330	330	
Thrust (kN)		Correlation Coefficient	.548**	.492**	1.000	-.315**	.581**	.281**	-.498**	
		Sig. (2-tailed)	.000	.000	.	.000	.000	.000	.000	
		N	330	330	330	330	330	330	330	
PR (m/h)		Correlation Coefficient	-.271**	-.265**	-.315**	1.000	-.495**	.359**	.192**	
		Sig. (2-tailed)	.000	.000	.000	.	.000	.000	.000	
		N	330	330	330	330	330	330	330	
UCS		Correlation Coefficient	.565**	.540**	.581**	-.495**	1.000	.187**	-.490**	
		Sig. (2-tailed)	.000	.000	.000	.000	.	.001	.000	
		N	330	330	330	330	330	330	330	
AR (m/h)		Correlation Coefficient	.286**	.223**	.281**	.359**	.187**	1.000	-.311**	
		Sig. (2-tailed)	.000	.000	.000	.000	.001	.	.000	
		N	330	330	330	330	330	330	330	
RMC		Correlation Coefficient	-.943**	-.919**	-.498**	.192**	-.490**	-.311**	1.000	
		Sig. (2-tailed)	.000	.000	.000	.000	.000	.000	.	
		N	330	330	330	330	330	330	330	

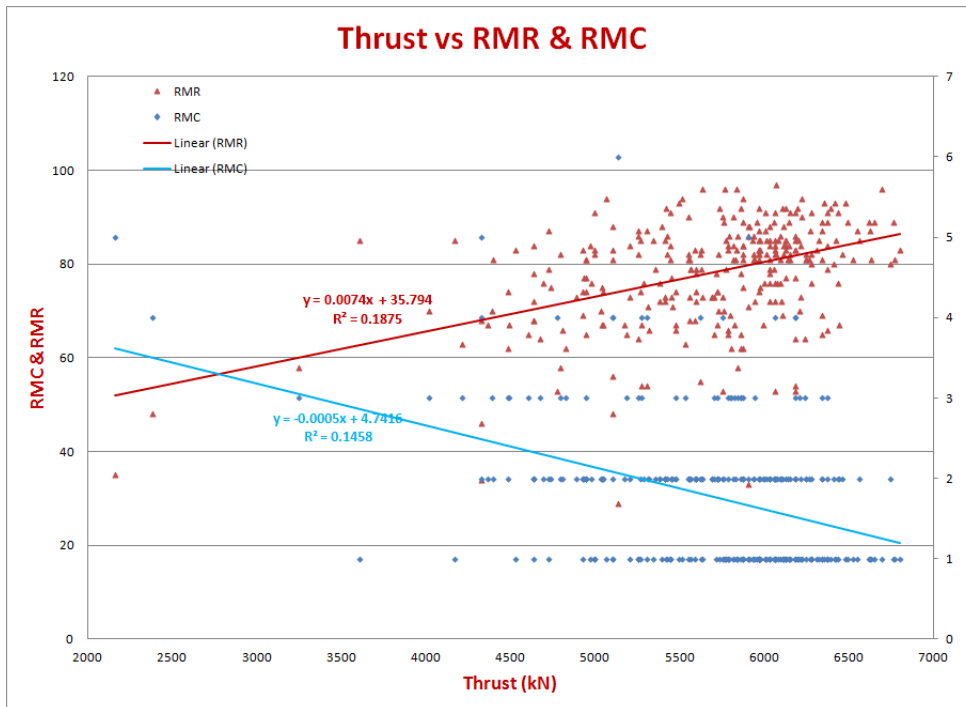
\*\* Correlation is significant at the 0.01 level (2-tailed).

Table 4.41: Spearman correlation coefficients for Maen tunnel.

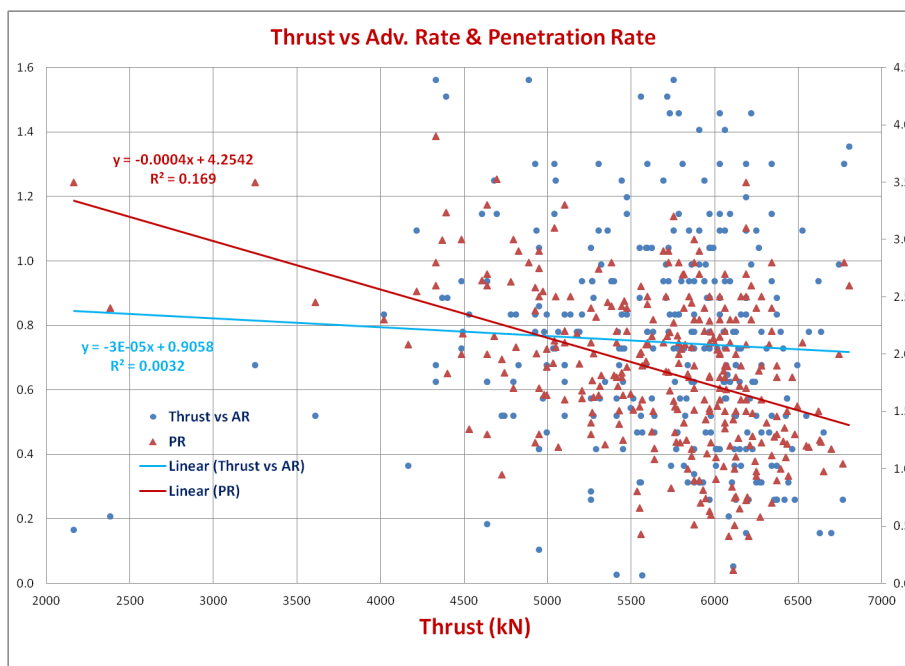
## 4.5.2 Pieve Vergonate Tunnel

Most area of the Pieve Vergonate tunnel is located in the Sesia-Lanzo zone of the Austroalpine domain [44, 45]. Excavated rocks consists of two metamorphic complexes made up of gneiss and micaschists separated by a metadiorite intrusive body with minor masses of metaquartzdiorite and metagabbro. The geological structure is complicated by multiple folding associated with shear zones and brittle fault zones, but the general attitude of rock units forms a monocline dipping at  $N140-1801E/30-601$  (dip direction/ dip), so that the longitudinal axis of the tunnel (direction  $N070-050E$ ) is mainly parallel to the schistosity.

#### 4.5.2.1 2-D Analysis by Excel



(a) Thrust versus RMR and RMC.

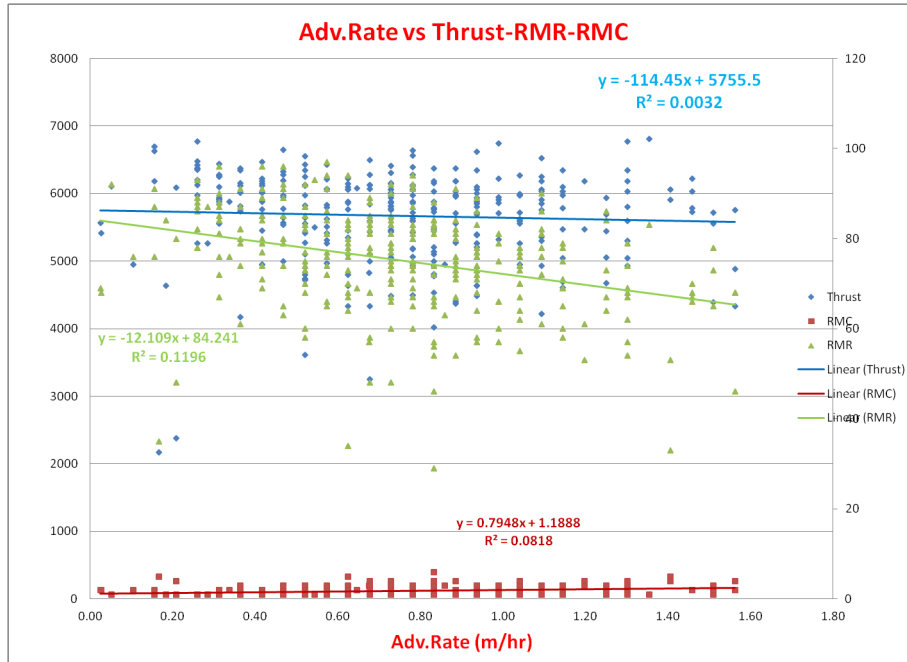


(b) Thrust versus AR and PR.

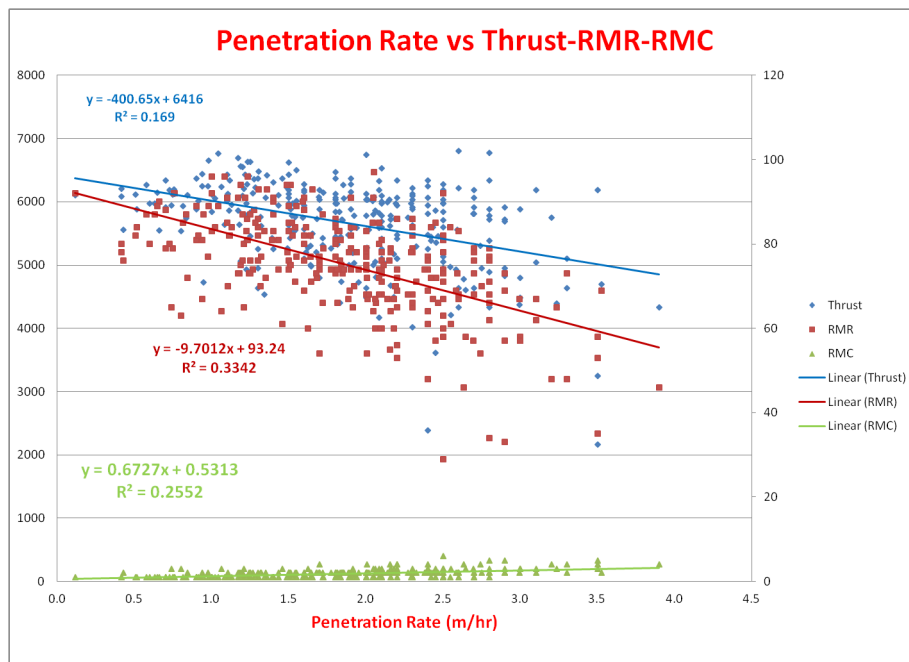
Figure 4.88: Thrust versus RMR, RMC, AR and PR.

Figure 4.88a shows a simple 2-D plot between thrust and RMC and RMR. In first trend line between thrust and BRMR, its a linear relation and quite simple, reveals that more thrust is required for a rock mass having low RMR. Trend between thrust and RMR shows that low thrust is required for harder rock (Having less RMR). This might be due

to that RMR was originally formulated for civil engineering problems and calculations, Bieniawski formulated RMR known as BRMR in 1973 and he reformulate them in 1989 specially for mining purposes. Figure 4.88b shows a relationship between thrust, advance rate and penetration rate, both AR and PR are going to decrease with increase of thrust, but with a different rate.



(a) AR versus thrust, RMR and RMC.



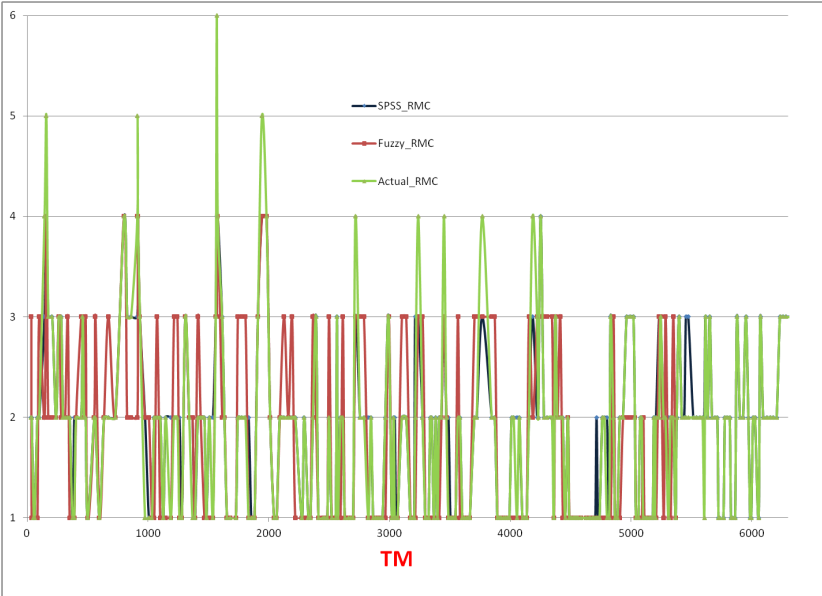
(b) PR versus thrust, RMR and RMC.

Figure 4.89: AR and PR versus RMC and RMR.

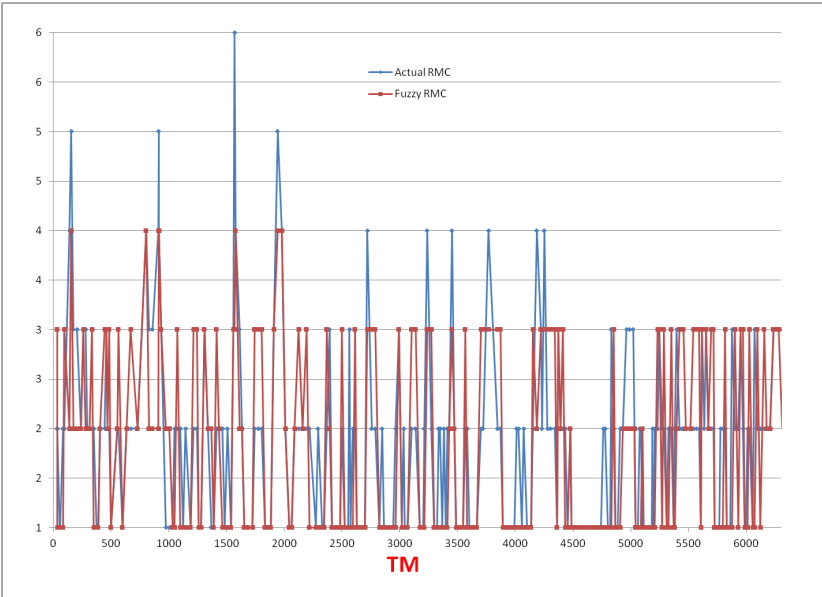
In Fig. 4.89a advance rate is plotted against thrust, RMC and RMR. Thrust and RMC

shows almost no effect on AR, but AR is decreasing with increasing RMR. Simply it is revealed that advance rate is low in harder rocks. Figure 4.89b show the same parameters trend against penetration rate. Slightly more penetration rate is observed at high RMC values, reason is that in more stable rock having more standup time PR is more. Whereas PR is inversely proportional to both thrust and RMR. This is the combined effect of many unknown and hidden parameters due to which increasing thrust resulted in low advance rate. High RMR gives low penetration, which is quite normal.

**4.5.2.2 Fuzzy Logic Prediction Model**



(a) Comparison of Fuzzy logic, SPSS and actual RMC.



(b) Comparison between Fuzzy logic and actual RMC.

Figure 4.90: Actual versus Fuzzy RMC comparison.

Figure 4.90a shows a three value comparison between, actual, Fuzzy and SPSS RMC. Here we see that Fuzzy RMC, comparatively better coincide with actual RMC as compare to corresponding values of SPSS predicted RMC. In Fig. 4.90b Fuzzy and actual RMC is compared separately. Again a reasonably good agreement is observed here.

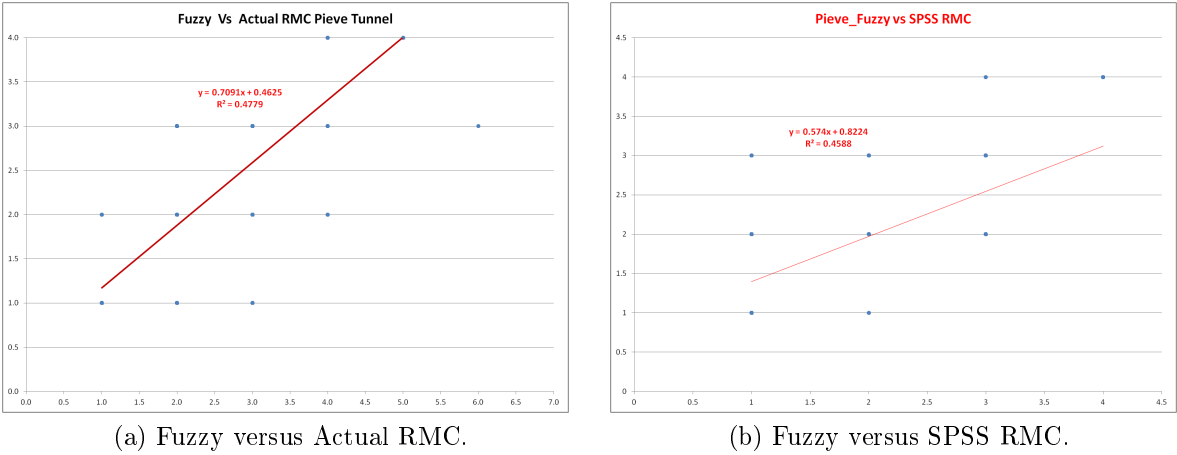


Figure 4.91: Actual versus Fuzzy and SPSS RMC.

4.5.2.3 3-D Analysis with “R”

Statistical software “R” was used to analyze different variables for the Pieve tunnel.

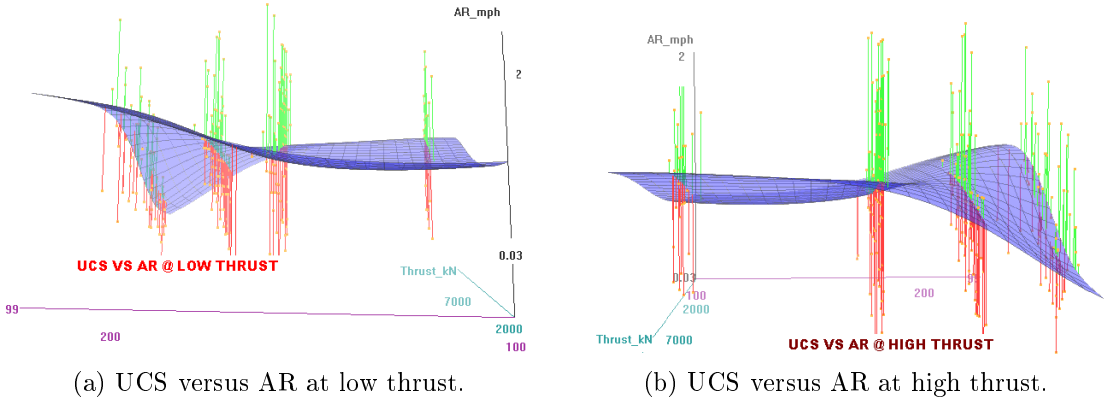


Figure 4.92: USC versus AR at low and high thrust.

Figure 4.92 shows a 3-D surface for thrust, AR and UCS. In Fig. 4.92a variation of AR against UCS at low thrust is shown. At low thrust we see no variation of AR against USC till  $UCS = 150MPa$ . that shows a turning point, after that a slight increase in AR with high values of UCS is observed. On the other hand in Fig. 4.92b, variation of AR with UCS at high thrust values, shows a mirror image of Fig. 4.92a, after a critical value of  $UCS = 150MPa$ , AR decreasing sharply. This trend shows that UCS plays an important role in thrust-AR relation.

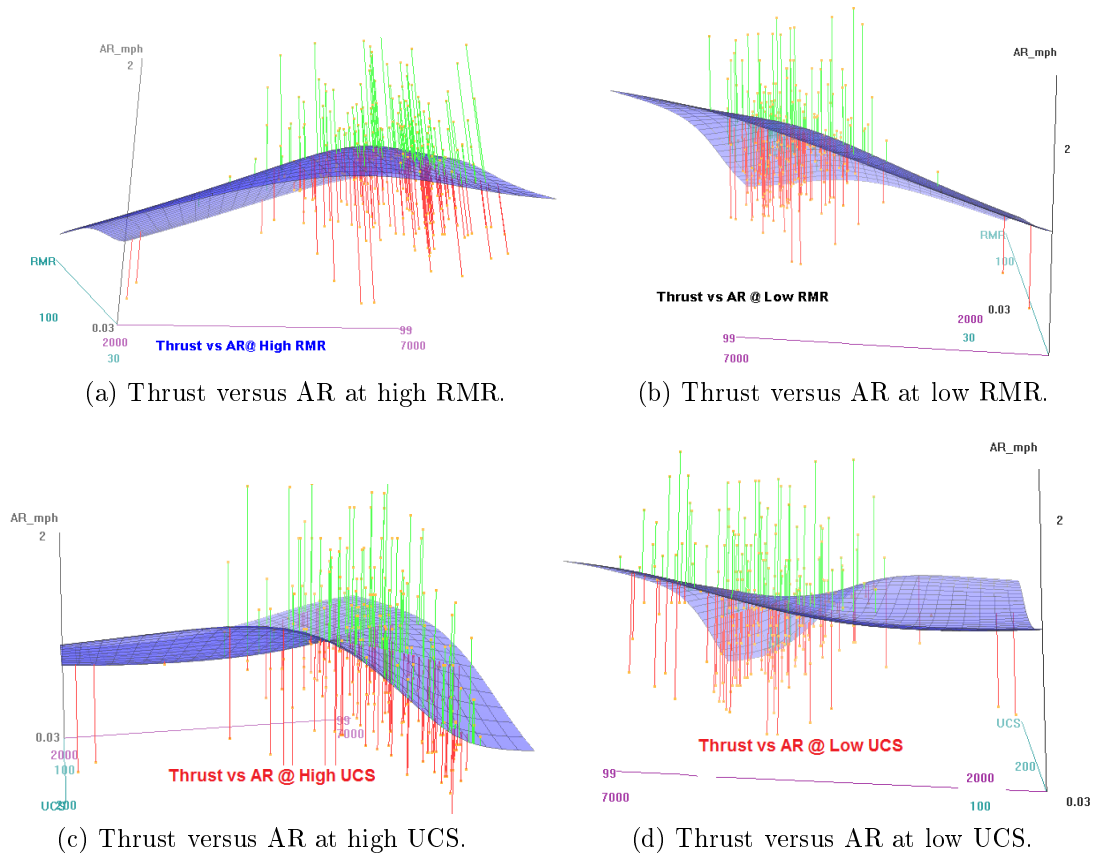


Figure 4.93: Thrust versus AR.

Figures 4.93(a-d) shows a behaviour of advance rate w.r.t thrust at low and high values of RMR and UCS. It can be seen from Fig. 4.93a, AR increases curvi-linear with thrust and then stabilize at very high values of thrust. This relation shows, for a very good rock, thrust beyond a moderate value is not advisable to get more advance rate. Figure 4.93b show a direct linear proportional between AR and thrust at low RMR. Figures 4.93(c,d) shows thrust and advance rate relation at high and low UCS values. Again after a certain value of thrust, AR drastically reduces even at high thrust, that shows UCS is a critical parameter in TBM performance and advance rate.

#### 4.5.2.4 Statistical Modeling with SPSS (Pieve)

First of all histograms of all parameters were drawn and shown in Figs. 4.94 and 4.95. Frequency distribution of advance rate and penetration rate are normally distributed with a standard deviation  $SD = -0.324$  and  $SD = -0.676$  respectively. The rest of frequency distributions of thrust, BRMR and RMR are right skewed and that of UCS is left skewed.

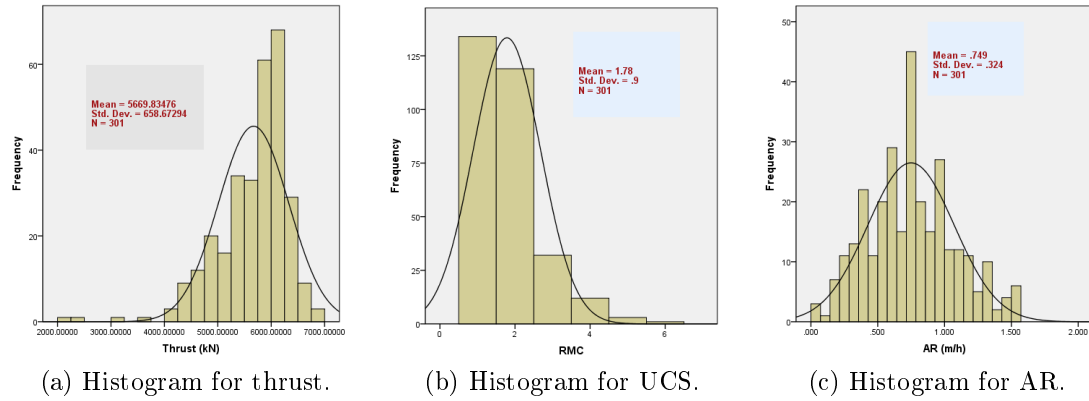


Figure 4.94: Histograms for Pieve tunnel.

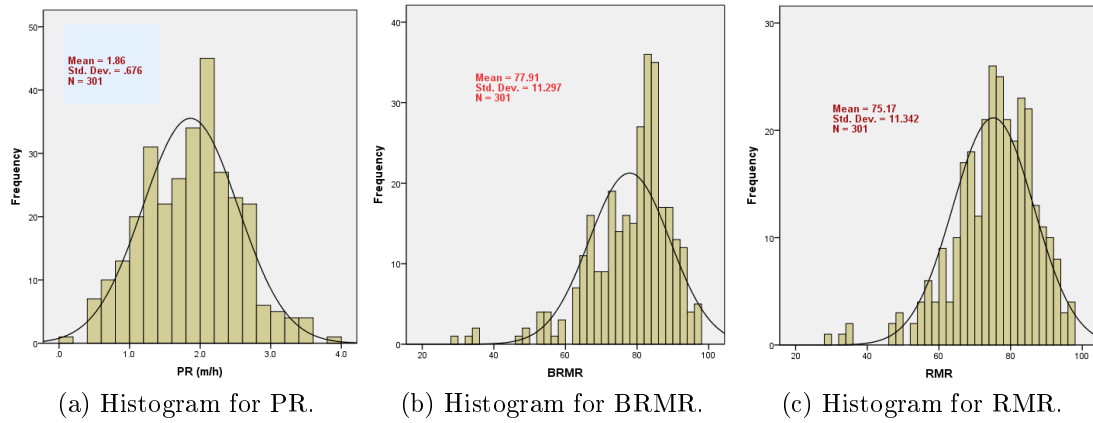


Figure 4.95: Histograms for Pieve tunnel.

Different models parameters and models summaries are shown in table 4.42 and 4.43. Models accuracy for AR and PR is reasonably good i.e 38.6% and 55.1% respectively.

Model Summary		Coefficients Target: AR (m/h)							
Target	AR (m/h)	Model Term	Coefficient ▼	Std.Error	t	Sig.	95% Confidence Interval		Importance
Automatic Data Preparation	On	Intercept	0.547	0.377	1.452	.148	Lower	Upper	
Model Selection Method	Forward Stepwise	PRmh_transformed	0.290	0.027	10.556	.000	0.236	0.344	0.308
Information Criterion	-820.167	ThrustkN_transformed	0.000	0.000	3.736	.000	0.000	0.000	0.235
The information criterion is used to compare to models. Models with smaller information criterion values fit better.		BRMR_transformed	-0.010	0.004	-2.830	.005	-0.017	-0.003	0.230
Worse <span style="float:right">Better</span>		RMC_transformed	-0.084	0.040	-2.116	.035	-0.162	-0.006	0.228
Accuracy 38.6%									

Table 4.42: AR linear regression model summary for Pieve tunnel.



Model Summary		Coefficients		Target: PR (m/h)					
Target	PR (m/h)	Model Term	Coefficient ▼	Std.Error	t	Sig.	95% Confidence Interval	Importance	
				Lower	Upper				
Automatic Data Preparation	On	Intercept	4.207	0.297	14.164	.000	3.622	4.791	
Model Selection Method	Forward Stepwise	ARmh_transformed	0.945	0.087	10.885	.000	0.774	1.116	0.380
Information Criterion	-472.406	RMR_transformed	-0.021	0.003	-7.287	.000	-0.026	-0.015	0.321
		ThrustkN_transformed	-0.000	0.000	-5.452	.000	-0.000	-0.000	0.299

The information criterion is used to compare to models. Models with smaller information criterion values fit better.

Worse  Better

Accuracy 55.1%

0.00% 25.00% 50.00% 75.00% 100.00%

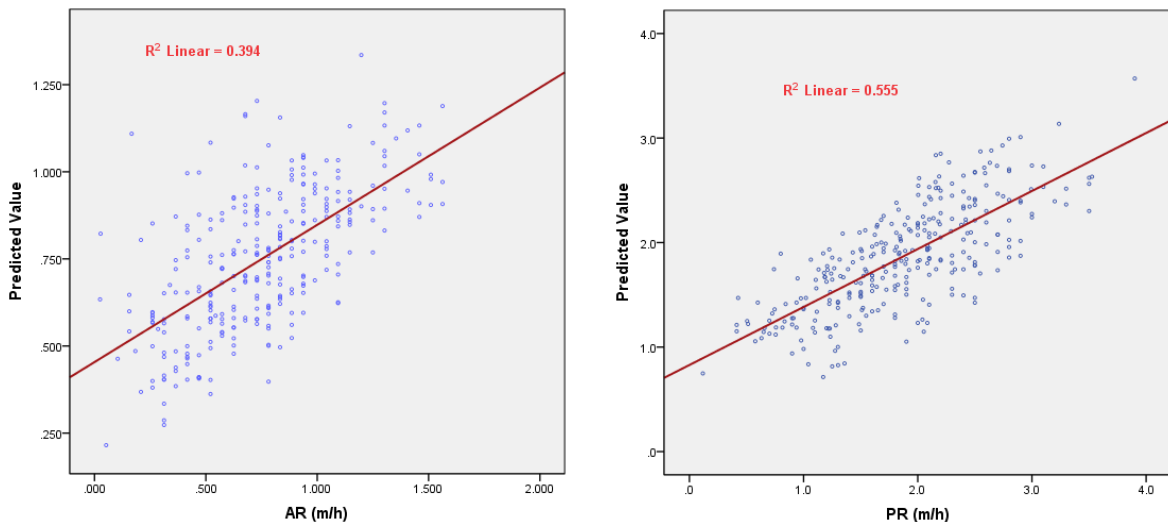
Table 4.43: PR linear regression model summary for Pieve tunnel.

From these tables of parameters and target variable, following AR and PR models equation are deducted and shown in eqs. 4.13 and 4.14. AR prediction model have four parameters, whereas PR prediction model have only three parameters.

$$AR(m/hr) = 0.547 + 0.290PR - 0.0001Thrust - 0.010RMR - 0.084RMC \quad (4.13)$$

$$PR(m/hr) = 4.207 + 0.945AR - 0.021RMR - 0.0001Thrust \quad (4.14)$$

Model plot having a  $R^2 = 0.394 \rightarrow R = 0.628$  and  $R^2 = 0.555 \rightarrow R = 0.745$  respectively are shown in Fig. 4.96 below.



(a) AR model for Pieve tunnel.

(b) PR model for Pieve tunnel.

Figure 4.96: Linear regression model plot for AR and PR.

#### 4.5.2.5 Correlation and Correlation Coefficient

		Correlations					
		BRMR	RMR	Thrust (kN)	PR (m/h)	AR (m/h)	RMC
BRMR	Pearson Correlation	1	.961**	.433**	-.574**	-.356**	-.915**
	Sig. (2-tailed)		.000	.000	.000	.000	.000
	N	301	301	301	301	301	301
RMR	Pearson Correlation	.961**	1	.419**	-.578**	-.346**	-.932**
	Sig. (2-tailed)	.000		.000	.000	.000	.000
	N	301	301	301	301	301	301
Thrust (kN)	Pearson Correlation	.433**	.419**	1	-.411**	-.056	-.382**
	Sig. (2-tailed)	.000	.000		.000	.330	.000
	N	301	301	301	301	301	301
PR (m/h)	Pearson Correlation	-.574**	-.578**	-.411**	1	.596**	.505**
	Sig. (2-tailed)	.000	.000	.000		.000	.000
	N	301	301	301	301	301	301
AR (m/h)	Pearson Correlation	-.356**	-.346**	-.056	.596**	1	.286**
	Sig. (2-tailed)	.000	.000	.330	.000		.000
	N	301	301	301	301	301	301
RMC	Pearson Correlation	-.915**	-.932**	-.382**	.505**	.286**	1
	Sig. (2-tailed)	.000	.000	.000	.000	.000	
	N	301	301	301	301	301	301

\*\* . Correlation is significant at the 0.01 level (2-tailed).

Table 4.44: Pearson correlation for Pieve tunnel.

Pearson and Spearman correlation coefficients are shown in tables 4.44 and 4.45 respectively. In Pearson correlation, we found no correlation between thrust and advance rate. But machine parameter thrust have a fairly good correlation with rock properties like RMR and RMC ( $Avg.R^2 = 0.4$ ). On the other hand table 4.45 shows Spearman and Kendall's correlation coefficients. Here we found no correlation neither between machine parameters and rock mass properties nor between the rock mass properties themselves. This shows that data of Pieve tunnel is randomly distributed and no fix correlation exist between any two parameters, except the RMC and RMR.

			Correlations						
			BRMR	RMR	Thrust (kN)	PR (m/h)	AR (m/h)	RMC	
Kendall's tau_b	BRMR	Correlation Coefficient	1.000	.839**	.264**	-.421**	-.302**	-.765**	
		Sig. (2-tailed)	.	.000	.000	.000	.000	.000	
		N	301	301	301	301	301	301	
	RMR	Correlation Coefficient	.839**	1.000	.263**	-.409**	-.277**	-.808**	
		Sig. (2-tailed)	.000	.	.000	.000	.000	.000	
		N	301	301	301	301	301	301	
	Thrust (kN)	Correlation Coefficient	.264**	.263**	1.000	-.260**	-.100*	-.266**	
		Sig. (2-tailed)	.000	.000	.	.000	.012	.000	
		N	301	301	301	301	301	301	
	PR (m/h)	Correlation Coefficient	-.421**	-.409**	-.260**	1.000	.447**	.401**	
		Sig. (2-tailed)	.000	.000	.000	.	.000	.000	
		N	301	301	301	301	301	301	
	AR (m/h)	Correlation Coefficient	-.302**	-.277**	-.100*	.447**	1.000	.264**	
		Sig. (2-tailed)	.000	.000	.012	.000	.	.000	
		N	301	301	301	301	301	301	
	RMC	Correlation Coefficient	-.765**	-.808**	-.266**	.401**	.264**	1.000	
		Sig. (2-tailed)	.000	.000	.000	.000	.000	.	
		N	301	301	301	301	301	301	
	Spearman's rho	BRMR	Correlation Coefficient	1.000	.945**	.381**	-.583**	-.421**	-.877**
			Sig. (2-tailed)	.	.000	.000	.000	.000	.000
			N	301	301	301	301	301	301
		RMR	Correlation Coefficient	.945**	1.000	.379**	-.572**	-.391**	-.922**
			Sig. (2-tailed)	.000	.	.000	.000	.000	.000
			N	301	301	301	301	301	301
Thrust (kN)		Correlation Coefficient	.381**	.379**	1.000	-.378**	-.143*	-.338**	
		Sig. (2-tailed)	.000	.000	.	.000	.013	.000	
		N	301	301	301	301	301	301	
PR (m/h)		Correlation Coefficient	-.583**	-.572**	-.378**	1.000	.606**	.500**	
		Sig. (2-tailed)	.000	.000	.000	.	.000	.000	
		N	301	301	301	301	301	301	
AR (m/h)		Correlation Coefficient	-.421**	-.391**	-.143*	.606**	1.000	.331**	
		Sig. (2-tailed)	.000	.000	.013	.000	.	.000	
		N	301	301	301	301	301	301	
RMC		Correlation Coefficient	-.877**	-.922**	-.338**	.500**	.331**	1.000	
		Sig. (2-tailed)	.000	.000	.000	.000	.000	.	
		N	301	301	301	301	301	301	

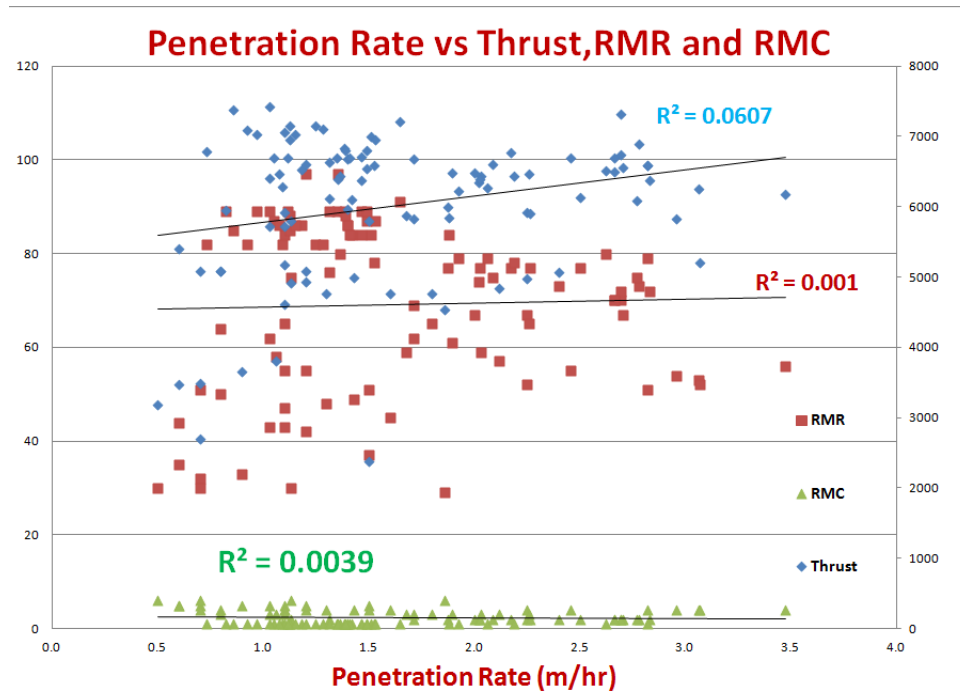
\*\* . Correlation is significant at the 0.01 level (2-tailed).  
\* . Correlation is significant at the 0.05 level (2-tailed).

Table 4.45: Spearman correlation table for Pieve tunnel.

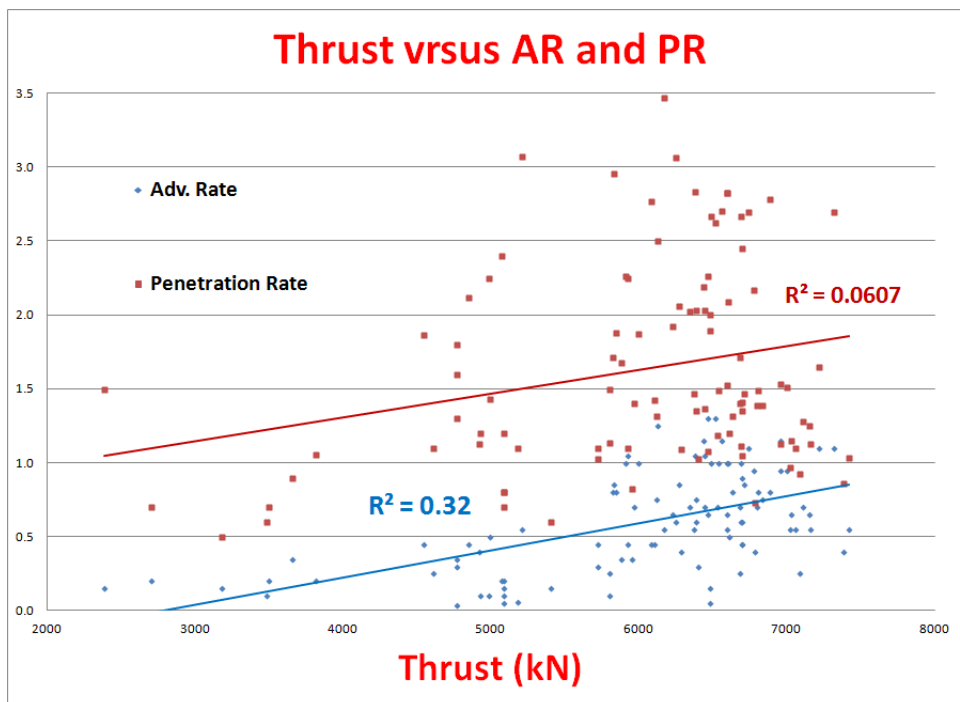
### 4.5.3 Varzo Tunnel

The Varzo tunnel is excavated entirely in the Antigorio Gneiss formation, a massive or weakly foliated rock generated by high-grade metamorphism of granite and Granodiorite rocks [46]. Metaaplite and metabasite dikes locally traverse the tunnel axis, but the area may be considered essentially homogeneous. The geological structure is a monocline gently dipping ( $10 - 20^\circ$ ) in a southerly direction, slightly complicated by folds and minor fault zones related to the Sempione- Centovalli fault, a major tectonic structure located 2 km to the south [47]. In general, the schistosity follows the attitude of the overall structure and, is therefore, mainly parallel to the longitudinal axis of the tunnel (plunging direction  $N080E-N070E$ ) [37].

### 4.5.3.1 2-D Data Analysis with Excel



(a) PR versus thrust, RMR and RMC.

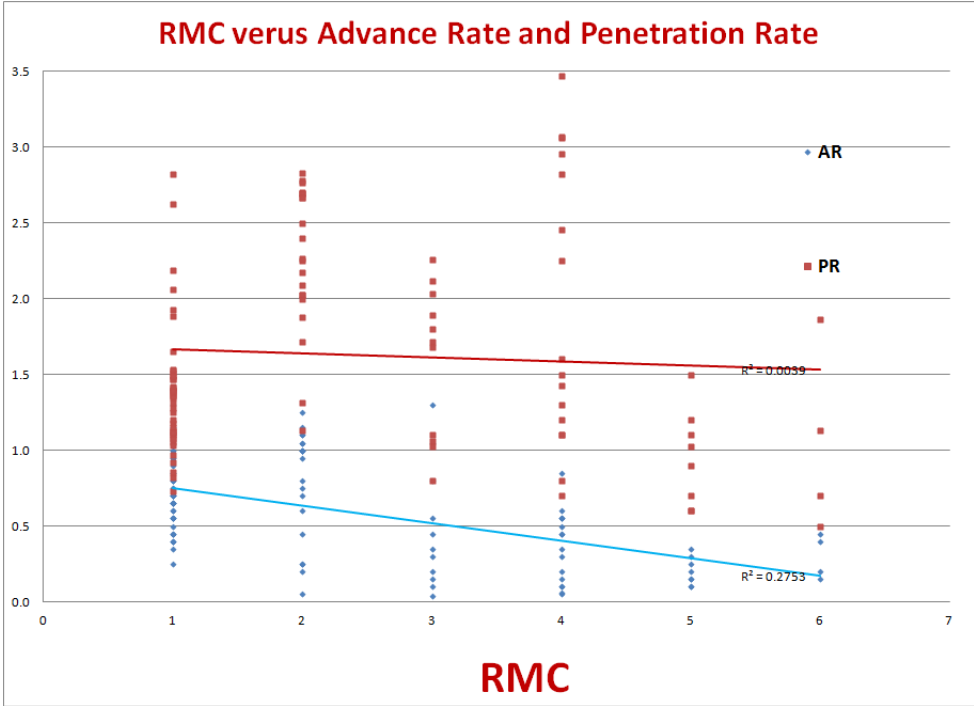


(b) Thrust versus AR and PR.

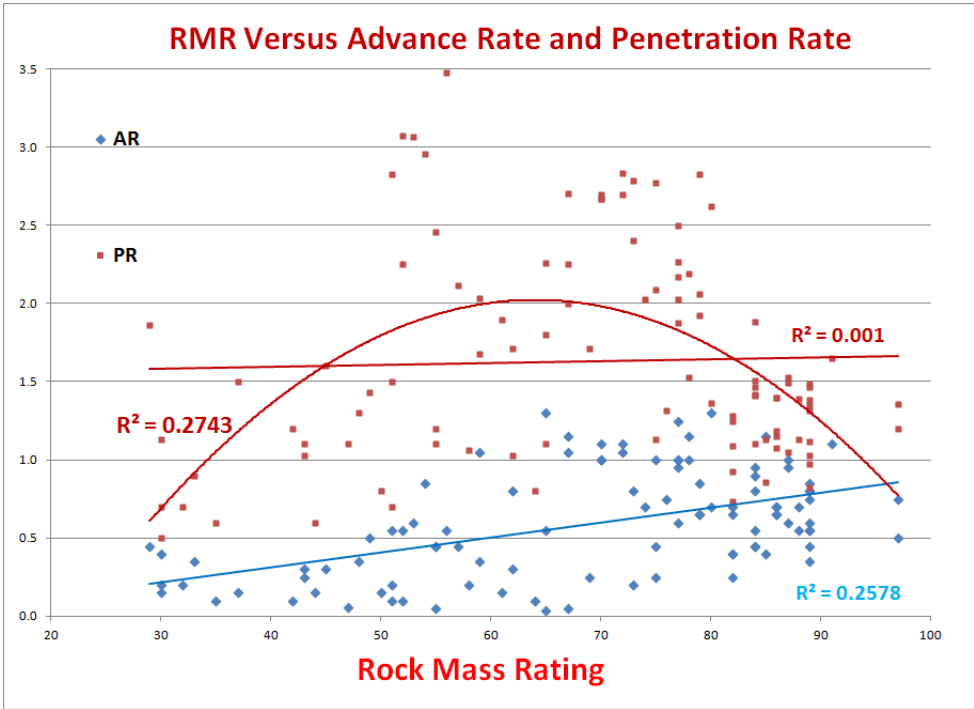
Figure 4.97: Varzo tunnel 2-D plots.

Figure 4.97 show different plots between thrust vs AR, PR and RMC. In Fig. 4.97a variation of penetration rate is plotted against thrust, RMR, RMC, that shows increase in PR with increase of thrust and RMR. Penetration rate slightly decrease with increase of

RMC, reason is that with increase of rock hardness, its difficult to perform chip formation. But actual reason can be find only when we plot a 3-D surface between PR, thrust and RMC (given in next section). Figure 4.97b shows variation of AP and PR with thrust, and both penetration rate and advance rate are linearly increasing with thrust.



(a) RMC versus AR and PR.

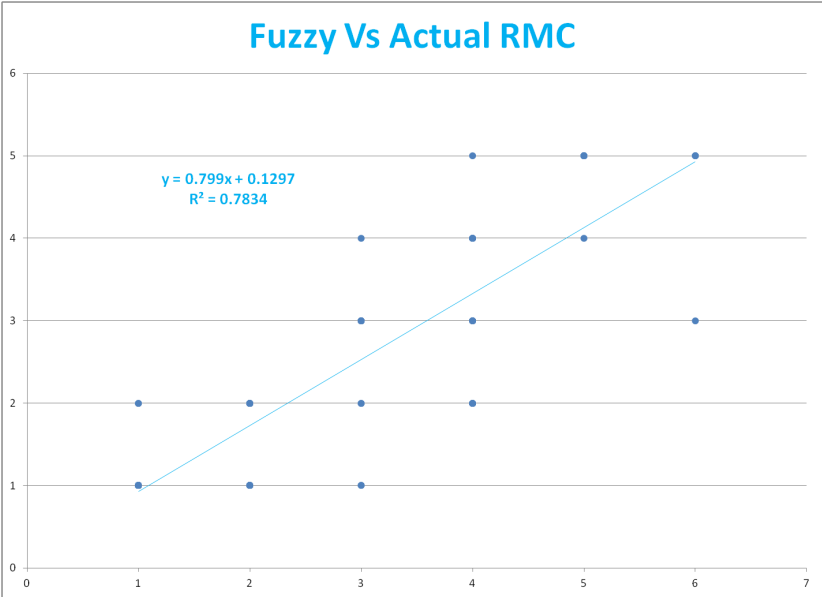


(b) RMR versus AR and PR.

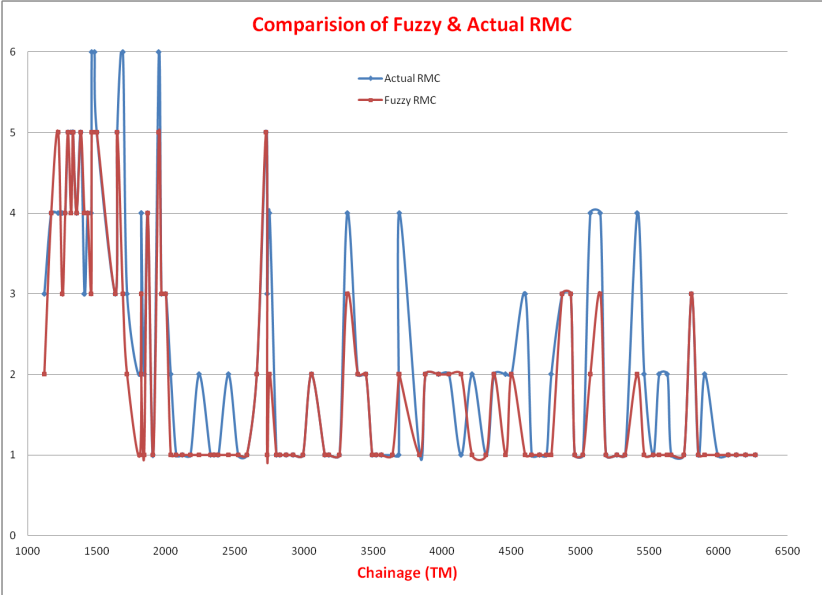
Figure 4.98: Varzo tunnel 2-D plots.

In Fig. 4.98a RMC is plotted against PR and AR, both decreasing with RMC, reason is same as described in Figs. 4.97a and 4.98b describes variation between RMR and PR-AR, that shows an increase in both AR and PR. This is entirely opposite to RMC behaviour, reason here again will be found when a 3-D surface will be plotted between thrust, RMR and AR-PR.

**4.5.3.2 RMC Prediction Model by Fuzzy Logic Varzo Tunnel**



(a) Fuzzy versus actual RMC.



(b) Fuzzy versus actual RMC.

Figure 4.99: Fuzzy versus actual RMC.

Fuzzy logic is largely used to predict different variations in mining, civil and almost all other engineering problems. Here for this data a Mat-Lab subroutine was written and

applied to predict future RMC, keeping the previous rock and machine (TBM) data in input parameters. Figure 4.99b shows comparison between actual and Fuzzy logic RMC. A good coincidence between the two values is found, showing good Fuzzy logic power to predict/forecast unknown rock mass properties. Figure 4.100 shows a three value comparison between actual, Fuzzy and SPSS RMC. It is clear from the figure that Fuzzy RMC is more closer to the actual as compare to SPSS corresponding values.

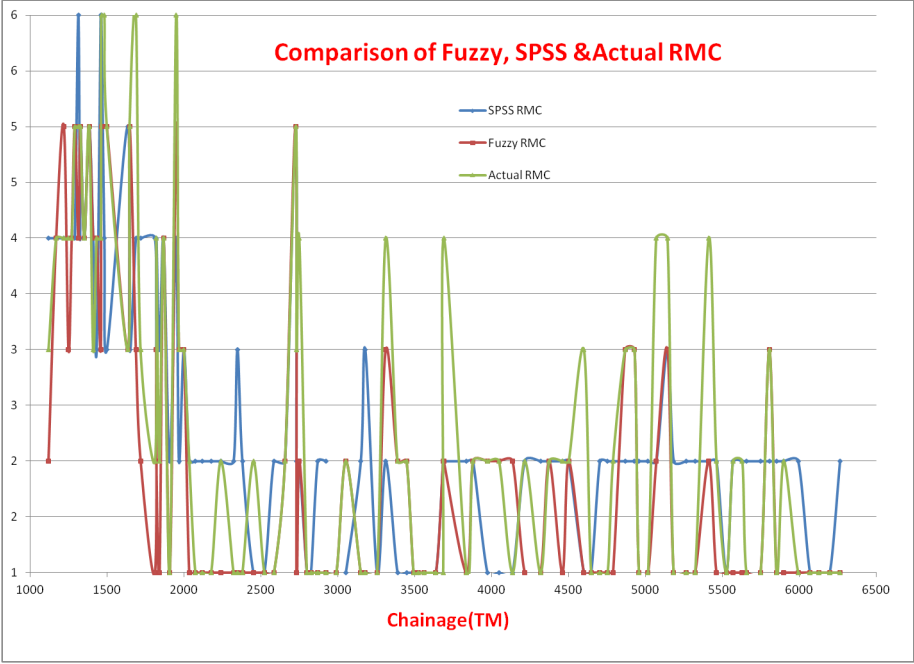


Figure 4.100: Comparison of RMC for Varzo tunnel.

**4.5.3.3 3-D Analysis with “R”**

Statistical software “R” was used to analyze different variables for the Pieve tunnel. 3-D surfaces were plotted both for penetration rate (PR) and advance rate (AR) to see what factors are involved in machine dead time and what is the effect of utilization factor of the TBM. 3-D surfaces plotted by “R” clearly elaborate variation and influence of one variable upon other, keeping third variable constant.

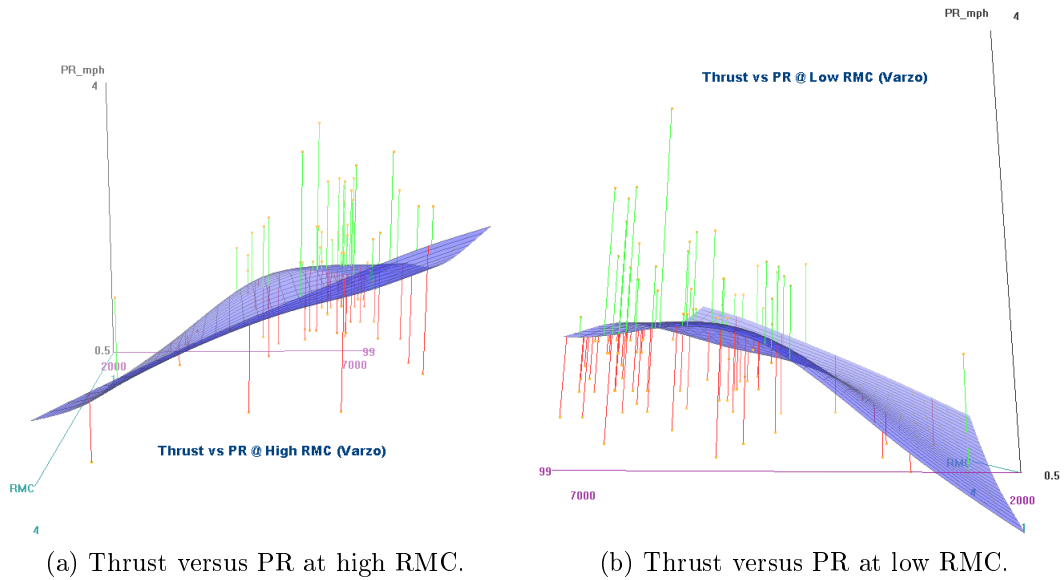


Figure 4.101: 3-D surfaces penetration rate.

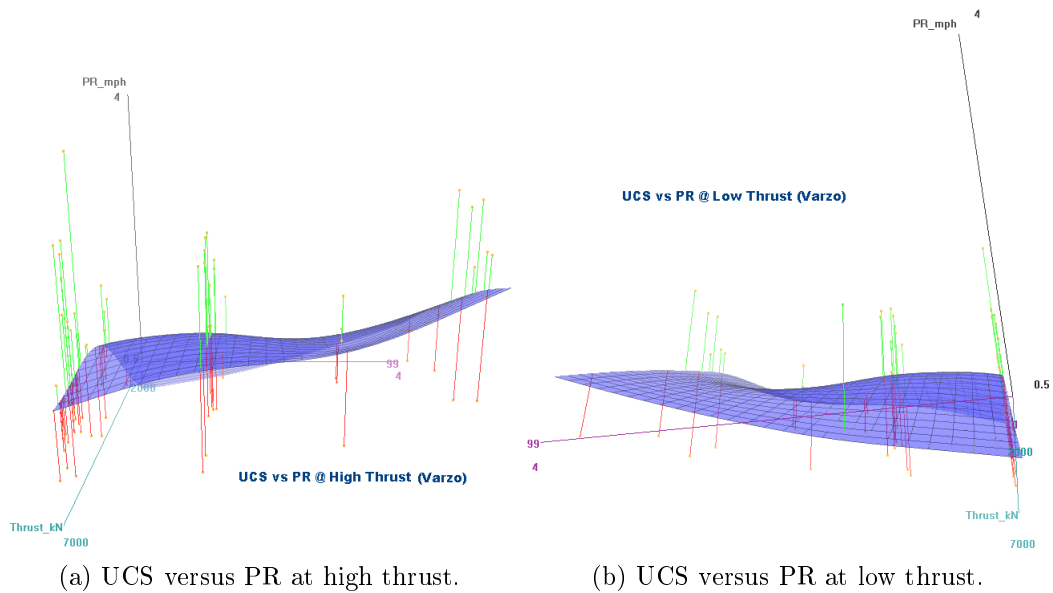


Figure 4.102: 3-D surfaces for Varzo tunnel.

Figure 4.101 shows a 3-D pictures of variations of penetration rate (PR) with thrust and UCS at high and low values of RMC and thrust respectively. In Fig. 4.101a PR varies linearly with thrust at high values of RMC. On the other hand same trend in Fig. 4.101b is plotted at low RMC, that shows a curvi-linear trend. Reason from this trend may be that a low values of RMC, PR cannot be increased by increasing simply the thrust. But at high values of RMC, when there is good rock, machine efficiency can be enhanced by applying more thrust than an average value required for chip formation. Figures 4.102(a,b) shows surfaces between UCS vs PR at high and low thrust. We see



that there is no effect of thrust values on PR, i.e same trend at both high and low thrust.

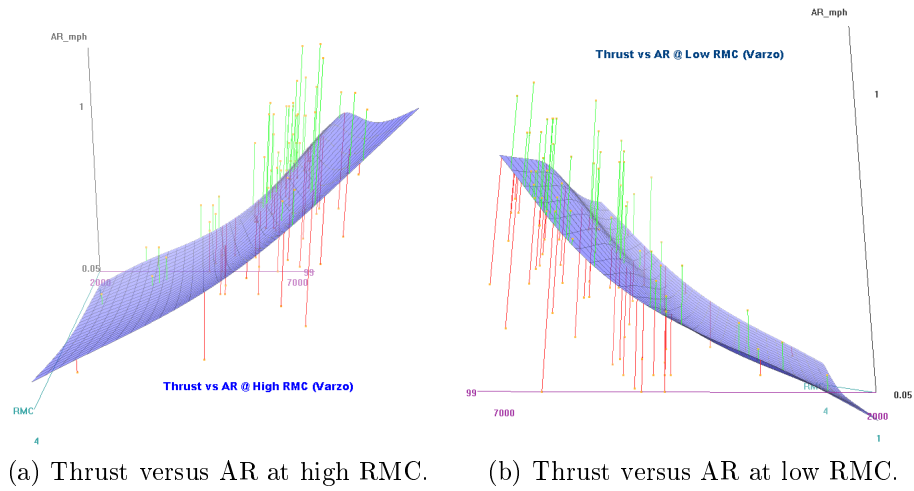


Figure 4.103: 3-D surfaces AR.

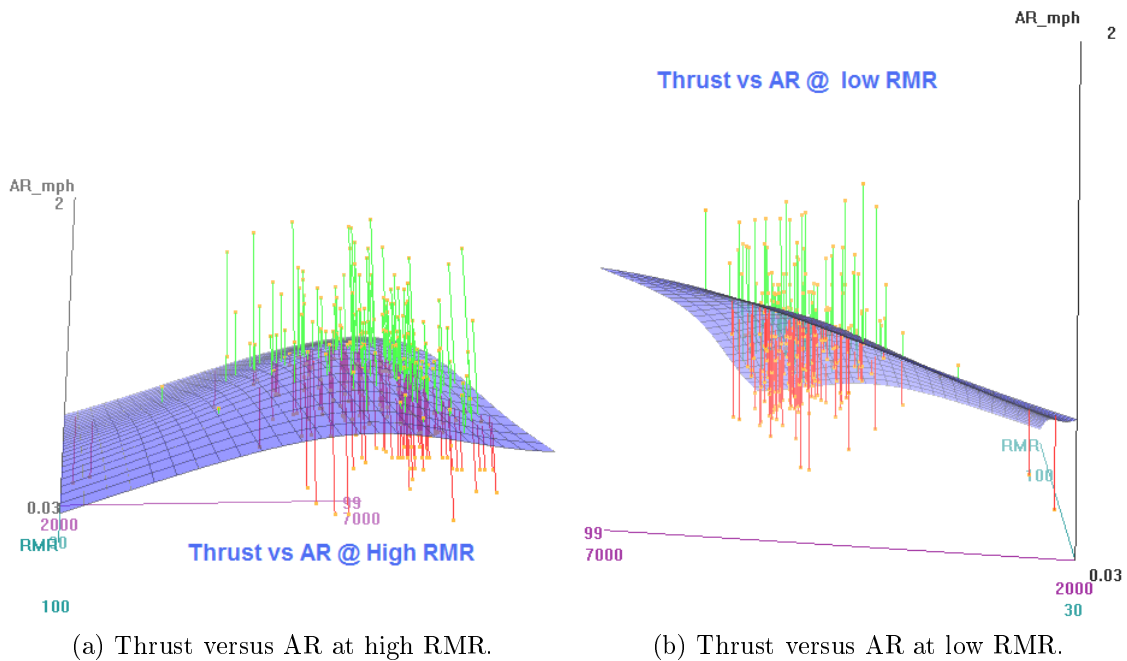


Figure 4.104: 3-D Surfaces generated by R software.

Figures 4.103 and 4.104 shows four 3-D surfaces, that are between thrust and AR at high and low values of RMC and RMR respectively. In figure. 4.103(a,b) shows thrust-AR relation at high and low RMC, it is clear from figure. that there is no effect of RMC on thrust-AR trend. Figures 4.104(a,b) shows thrust-AR trend at low and high values of RMR. Again thrust-AR trend is same at both for good and poor rock.

#### 4.5.3.4 Statistical Modeling with SPSS, Varzo Tunnel

SPSS statistical software was used to analyze Varzo tunnel data. Figures 4.105 and 4.106 shows frequency distribution of different variables. Figures 4.105(a-c) shows frequency distribution of BRMR, RMR and thrust. All distributions are right skewed and with  $SD > 10$ . But in Figs. 4.106(a-c), frequency distribution of advance rate (AR) is normal with  $SD = 0.337$ , while others of RMC and PR are left skewed and having more standard deviation.

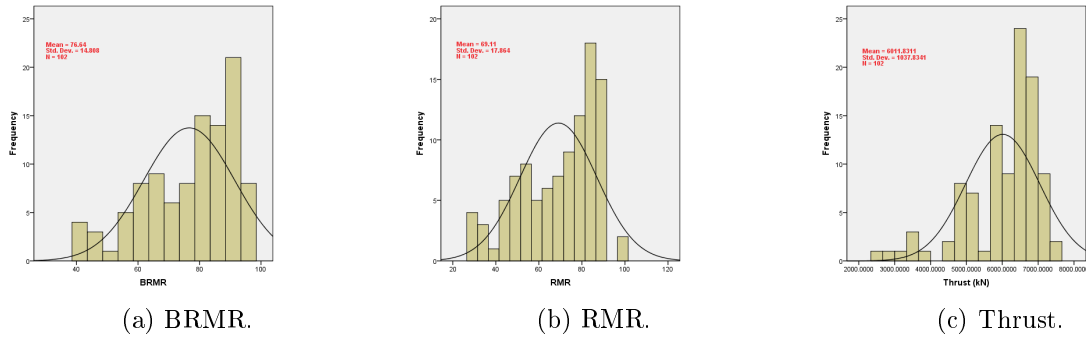


Figure 4.105: Histograms for Varzo tunnel.

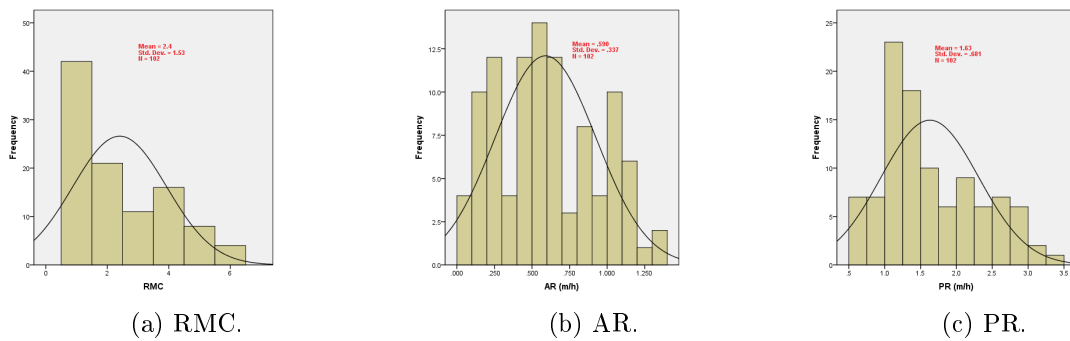


Figure 4.106: Histogram Varzo tunnel.

Table 4.46(a,b) show the model summary for AR and PR models with accuracy of 49.7% and 32.7% respectively. RMR plays most important role in model prediction for AR and PR, where as RMC was the least important input parameter.

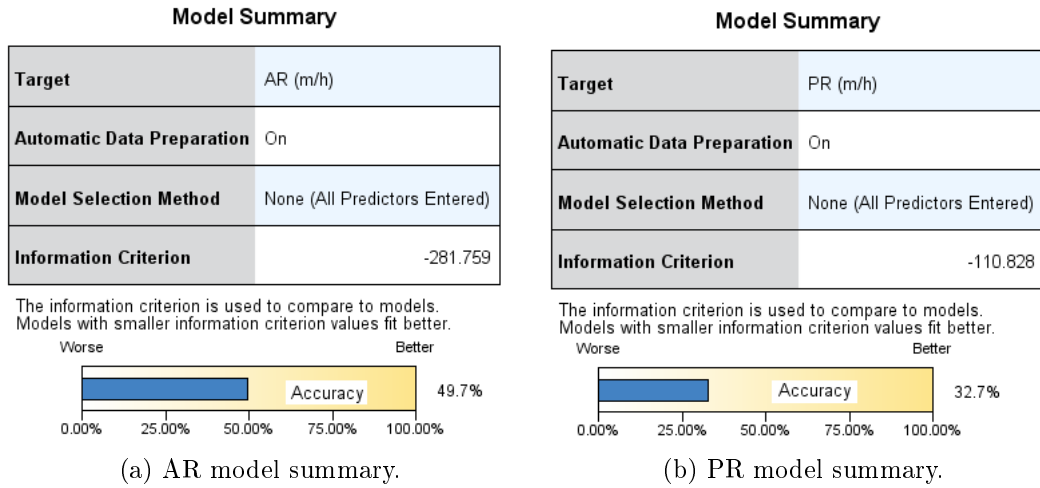


Table 4.46: Model summary.

Coefficients		Target: PR (m/h)					
Model Term	Coefficient ▼	Std.Error	t	Sig.	95% Confidence Interval		Importance
					Lower	Upper	
Intercept	0.638	1.602	0.399	.691	-2.541	3.818	
ARmh_transformed	1.136	0.209	5.439	.000	0.721	1.550	0.239
RMR_transformed	-0.059	0.021	-2.789	.006	-0.101	-0.017	0.197
ThrustkN_transformed	0.000	0.000	2.102	.038	0.000	0.000	0.191
BRMR_transformed	0.043	0.022	1.945	.055	-0.001	0.088	0.190
RMC_transformed	-0.064	0.174	-0.369	.713	-0.411	0.282	0.183

(a) PR model coefficients.

Coefficients		Target: AR (m/h)					
Model Term	Coefficient ▼	Std.Error	t	Sig.	95% Confidence Interval		Importance
					Lower	Upper	
Intercept	0.566	0.685	0.826	.411	-0.795	1.926	
PRmh_transformed	0.209	0.038	5.439	.000	0.133	0.285	0.240
BRMR_transformed	-0.019	0.010	-2.027	.046	-0.038	-0.000	0.192
ThrustkN_transformed	0.000	0.000	1.967	.052	-0.000	0.000	0.192
RMR_transformed	0.013	0.009	1.433	.155	-0.005	0.032	0.188
RMC_transformed	-0.100	0.074	-1.351	.180	-0.247	0.047	0.188

(b) AR model coefficients.

Table 4.47: Varzo AR and PR linear model coefficients.

		Coefficients			Target: RMC		
Model Term	Coefficient ▼	Std.Error	t	Sig.	95% Confidence Interval		Importance
					Lower	Upper	
Intercept	8.533	0.658	12.968	.000	7.227	9.839	
ThrustkN_transformed	-0.001	0.000	-8.720	.000	-0.001	-0.001	0.448
PRmh_transformed	0.508	0.161	3.159	.002	0.189	0.827	0.278
ARmh_transformed	-1.127	0.384	-2.933	.004	-1.890	-0.364	0.274

Table 4.48: RMC model coefficients.

From tables 4.46 - 4.48, the coefficients leads towards the AR, PR and RMC Linear regression Model Eq. 4.15, 4.16 and 4.17 shown below.

$$AR(m/hr) = 0.566 - 0.209PR - 0.019BRMR - 0.0001Thrust - 0.010RMC \quad (4.15)$$

$$PR(m/hr) = 0.638 + 1.36AR - 0.059RMR - 0.0001Thrust - 0.064RMC \quad (4.16)$$

$$RMC = 8.533 - 0.001Thrust + 0.508PR - 1.127AR \quad (4.17)$$

Advance rate and penetration rate models are plotted in Fig. 4.107(a,b) and RMC model and comparison are plotted in Fig. 4.108. AR model has a  $R = 0.723$ , where the PR model has a  $R = 0.60$  and RMC model has  $R = 0.788$ .

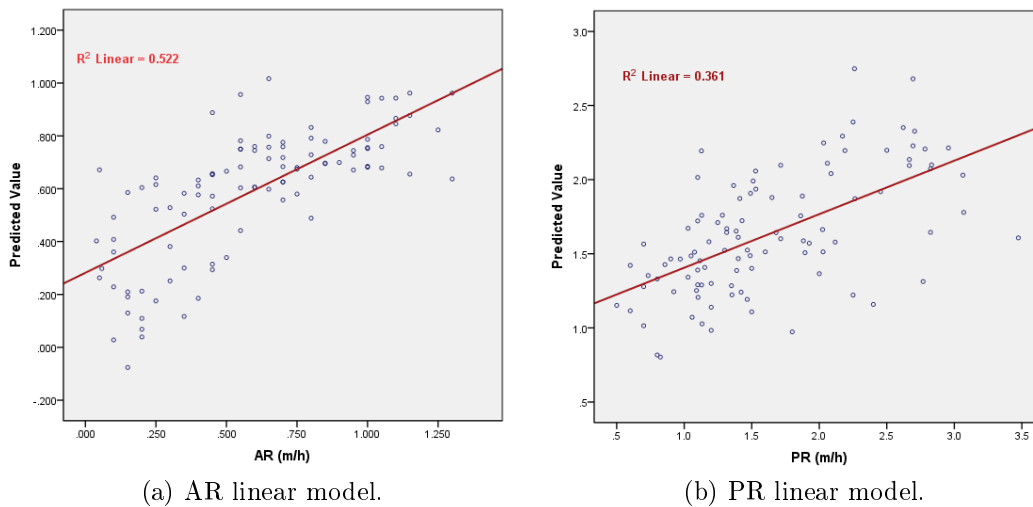


Figure 4.107: AR linear regression model plot for Varzo tunnel.

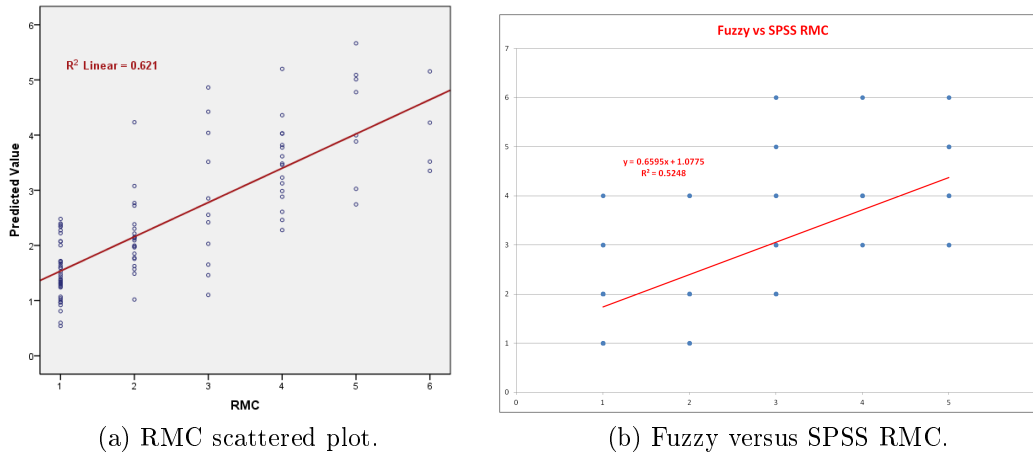


Figure 4.108: RMC linear regression model Varzo tunnel.

#### 4.5.3.5 Bi-variant Correlations and Correlation Coefficient

		Correlations					
		BRMR	RMR	Thrust (kN)	PR (m/h)	AR (m/h)	RMC
BRMR	Pearson Correlation	1	.985**	.760**	.058	.491**	-.969**
	Sig. (2-tailed)		.000	.000	.565	.000	.000
	N	102	102	102	102	102	102
RMR	Pearson Correlation	.985**	1	.762**	.032	.508**	-.976**
	Sig. (2-tailed)	.000		.000	.751	.000	.000
	N	102	102	102	102	102	102
Thrust (kN)	Pearson Correlation	.760**	.762**	1	.246*	.566**	-.745**
	Sig. (2-tailed)	.000	.000		.013	.000	.000
	N	102	102	102	102	102	102
PR (m/h)	Pearson Correlation	.058	.032	.246*	1	.486**	-.062
	Sig. (2-tailed)	.565	.751	.013		.000	.534
	N	102	102	102	102	102	102
AR (m/h)	Pearson Correlation	.491**	.508**	.566**	.486**	1	-.525**
	Sig. (2-tailed)	.000	.000	.000	.000		.000
	N	102	102	102	102	102	102
RMC	Pearson Correlation	-.969**	-.976**	-.745**	-.062	-.525**	1
	Sig. (2-tailed)	.000	.000	.000	.534	.000	
	N	102	102	102	102	102	102

\*\* . Correlation is significant at the 0.01 level (2-tailed).  
 \* . Correlation is significant at the 0.05 level (2-tailed).

Table 4.49: Pearson correlation for Varzo tunnel.

Table 4.49 shows Pearson correlation between all machine and rock mass parameters. In the table at line no. 3 we see correlation between thrust and all rock mass parameters, thrust have a very good correlation with, RMR, RMC and AR. On the other hand RMC has a good correlation with AR ( $R^2 = -0.525$ ), which shows that AR strongly depends upon machine parameters and rock mass properties. RMC and RMR has a Bi-Variant correlation of  $R^2 = -0.98$  which shows that we can use RMR and RMC alternatively, wherever we need it.

In table 4.50 Spearman's and Kendall's correlations. Table shows that machine and rock mass have a little bit better Spearman's rho correlations as compare to Kendall's tau\_b corresponding values. Here one thing is clear that, machine (TBM) data is linearly correlated with rock mass data. Otherwise table. 4.49 would have better corresponding correlations. Advance rate can be better predicted by using Pearson or Spearman's rho correlations.

			Correlations					
			BRMR	RMR	Thrust (kN)	PR (m/h)	AR (m/h)	RMC
Kendall's tau_b	BRMR	Correlation Coefficient	1.000	.899**	.511**	-.043	.300**	-.856**
		Sig. (2-tailed)	.	.000	.000	.524	.000	.000
		N	102	102	102	102	102	102
	RMR	Correlation Coefficient	.899**	1.000	.533**	-.051	.300**	-.877**
		Sig. (2-tailed)	.000	.	.000	.450	.000	.000
		N	102	102	102	102	102	102
	Thrust (kN)	Correlation Coefficient	.511**	.533**	1.000	.079	.365**	-.566**
		Sig. (2-tailed)	.000	.000	.	.240	.000	.000
		N	102	102	102	102	102	102
	PR (m/h)	Correlation Coefficient	-.043	-.051	.079	1.000	.392**	.017
		Sig. (2-tailed)	.524	.450	.240	.	.000	.820
		N	102	102	102	102	102	102
	AR (m/h)	Correlation Coefficient	.300**	.300**	.365**	.392**	1.000	-.351**
		Sig. (2-tailed)	.000	.000	.000	.000	.	.000
		N	102	102	102	102	102	102
	RMC	Correlation Coefficient	-.856**	-.877**	-.566**	.017	-.351**	1.000
		Sig. (2-tailed)	.000	.000	.000	.820	.000	.
		N	102	102	102	102	102	102
Spearman's rho	BRMR	Correlation Coefficient	1.000	.970**	.702**	-.027	.469**	-.943**
		Sig. (2-tailed)	.	.000	.000	.789	.000	.000
		N	102	102	102	102	102	102
	RMR	Correlation Coefficient	.970**	1.000	.720**	-.040	.485**	-.958**
		Sig. (2-tailed)	.000	.	.000	.692	.000	.000
		N	102	102	102	102	102	102
	Thrust (kN)	Correlation Coefficient	.702**	.720**	1.000	.119	.540**	-.714**
		Sig. (2-tailed)	.000	.000	.	.232	.000	.000
		N	102	102	102	102	102	102
	PR (m/h)	Correlation Coefficient	-.027	-.040	.119	1.000	.517**	-.001
		Sig. (2-tailed)	.789	.692	.232	.	.000	.991
		N	102	102	102	102	102	102
	AR (m/h)	Correlation Coefficient	.469**	.485**	.540**	.517**	1.000	-.505**
		Sig. (2-tailed)	.000	.000	.000	.000	.	.000
		N	102	102	102	102	102	102
	RMC	Correlation Coefficient	-.943**	-.958**	-.714**	-.001	-.505**	1.000
		Sig. (2-tailed)	.000	.000	.000	.991	.000	.
		N	102	102	102	102	102	102

\*\* Correlation is significant at the 0.01 level (2-tailed).

Table 4.50: Spearman's correlations for Varzo tunnel.

#### 4.5.4 Conclusions

Analysis for Maen tunnel data shows that, there is drastic difference between trends and behaviour of penetration rate and advance rate. This ultimately shows high downtime, machine breakdown and maintenance time for the TBM, which indicates very low utiliza-

tion factor of TBM (Fig. 4.73). More over machine performance is strongly dependent upon rock mass strength. RMC values were predicted by Fuzzy and SPSS both, shows a weak prediction model by Fuzzy and an accurate and efficient prediction model by SPSS. Advance rate (AR) and penetration rate (PR) prediction models were also formulated with a reasonably good accuracy.

Pieve tunnel data shows inverse relation between penetration rate and thrust. SPSS 19 gives a very accurate PR linear regression model ( $R^2 = 0.555$ ). In Varzo tunnel data, AR and thrust have linear correlation, and RMR plays a major role in machine performance. SPSS19 gives here a good prediction model for AR, PR and RMC. Moreover in all three tunnel sites, a significant positive correlation is found between machine parameters and rock mass properties.

# Chapter 5

## Discussion and Conclusions

### 5.1 Comparison Between Case Histories

After analyzing the data from seven tunnel sites, based on rock strength, fracture class and behaviour of thrust versus advance rate (AR), seven case histories have been divided into two major groups. Group one consists of Hieflau, Hemerwald, Maen and Pieve tunnels. Rock mass strata mainly comprises Limestone, Schistos-Gneis, Micaschists and Meta-granite. For group one rock strength (UCS) of intact rocks ranges from 162 – 226 *MPa*, that contains high strength rocks. In this group AR decreases linearly with increase of thrust (Figs. 4.3a, 4.51a, 4.73 and 4.88b). Reason for this trend is very clear from data analysis, that is due to very high strength, presence of less joints and very low fracture class. So it is concluded that for high strength rocks following prediction model for AR may be used with slight variation from case to case.

$$AR(m/hr) = 0.33 + 0.849RPM - 0.003Thrust + 0.004Power - 0.009RMC \quad (5.1)$$

If seismic data is available, then model can be reformulated as:

$$AR(mph) = 4.51 - 0.29Thr + 0.396rpm - 23.49Amp_{ref} - 0.001P_{seve} - 0.001Torq - 0.008RMC \quad (5.2)$$

On other hand group two comprises Queens water tunnel (QWT), Vereina and Varzo tunnels. Rock mass strata mainly consists of Micaschists and Gneiss. Rock strength (UCS) of intact rocks, varies between 55 – 162 *MPa*, that is low to medium strength rocks. Rock strata is highly fractured. In group two AR linearly increases with increase of TBM thrust (Figs. 4.17a, 4.32a and 4.97b). Reason is low rock strength and presence of medium to high frequency of joints and a high rock fracture class. For the low strength rocks, following AR prediction model is suggested.



$$AR(m/hr) = 0.566 - 0.0001Thrust - 0.019RMR - 0.010RMC \quad (5.3)$$

If data for rock fracture class and rock joints is available then model can be modified as:

$$AR(m/hr) = 1.022 + 0.029Thrust + 0.475Log(\alpha) - 0.217DPW - 0.003USC \quad (5.4)$$

## 5.2 Discussion

Machine (TBM) data and rock mass data were analyzed using Microsoft excel, Origin pro 8.1, statistical software R and IBM SPSS19, Kaleida Graph and Fuzzy logic tools in Mat-Lab. In 2-D analysis for Hieflau tunnel data, interesting trend between thrust and advance rate is found. AR decreases with increase of thrust (Fig. 4.3a). This result is verified by finding the correlation between these two parameters ( $R^2 = -0.647$ ). Same trend is repeated in case of UCS and AR, illustrating the reason behind this divergent relation. After detailed 3-D analysis of the data from Hieflau tunnel, it is concluded that, advance rate is inversely proportional to thrust and UCS at high torque, when we analyse the same relation at low torque, the trend reverses. This is due to the limestone rock mass having a moderate strength and a medium degree of fracture, low torque cannot produce chip formation required for a good advance. Additionally in Hieflau expansion tunnel, seismic data was available (recorded by Geo-physicist TU-Wien), was also coupled and analysed with machine and rock mass data. Machine thrust and amplitude of erestizeit when plotted against each other, maximum amplitudes was found at the thrust values ranging from 8000 to 10,000  $kN$ . There is no significant correlation between thrust and seismic parameters, between AR and seismic parameters. At maximum value of amplitude of reflexion, a depression in AR value is found, that shows rock brittleness and hardness are key parameters in TBM performance. At low torque and too low and too high thrust, tool wear is maximum, TBM cannot achieve maximum AR only by applying more thrust. However when data for cutter wear for Hieflau tunnel is analyzed, it is obvious that cutter wear can be economized and cutter life can be maximized when TBM thrust is kept at a moderate value of 7900 to 8100  $kN$ , but at the same time maximum number of cutter changes are found at that thrust range. After multidimensional analysis, advance rate linear regression prediction models for mix data, TBM data and TBM+seismic data, were formulated with the help of SPSS19 software, which shows a good significance of the model. Other reason for this trend between thrust and AR, may be the learning effect of the TBM operator's conduct who tries to push the thrust to the limit of admissible values, or even beyond, when the penetration rate is deemed to be unsatisfactory [48].

Queens water tunnel, New York's city tunnel *No. 3* is one of the most complex and

intricate engineering projects in the world [31]. Real field data for TBM and rock mass is analysed by different ways using different software. 2-D data analysis shows that AR linearly increases with, thrust, UCS, BTS and RFC. Even more AR is observed at high values of UCS. This ambiguity is clarified when AR, UCS and thrust are plotted all together in a 3-D surface (Figs. 4.21a,b). Here it is clear that due to low values of UCS, AR linearly increased with thrust, but when rock strength is more than a critical value (200 MPa), AR decreased with applying further thrust. Whereas the rock mass have high UCS and low brittleness (BTS) then obtained AR is relatively lower than expected. Maximum AR are observed as the alpha angle ranges from 50 – 65 degrees. As DPW ranges from about 20–40 cm, the obtained AR is also rather high. UCS plays a major rule in TBM performance, at low UCS, a linear correlation of AR with thrust, whereas at high USC thrust make a curvi-linear correlation with AR (Fig. 4.21). Advance rate (AR) and RFC models has accuracy of 64.4% and 57.1% respectively. AR linear regression model when plotted against the actual AR values gives a significant correlation ( $R^2 = 0.655$ ). Similarly a linear regression model for rock fracture class (RFC) was formulated and give accuracy of 57% and comparison of predicted and actual RFC values give  $R^2 = 0.588$ . Only one rock property i.e UCS is in good correlation with machine thrust ( $R^2 = 0.629$ ). Moreover machine thrust and AR have a positive linear correlation of  $R^2 = 0.577$ .

Vereina tunnel is a 19 km long traffic tunnel. Vereina is a tunnel in hard rocks having a high overburden, excavated with open TBM [36]. At high RMC, lowest values of thrust and momentum (Fig. 4.31) shows that rock strength is key parameters for machine performance, where low AR is observed against highest RMC value. Linear relation between thrust and penetration shows a little increase in penetration with thrust. But when we plot a 3-D surface, to see the effect of third variable, it is clearly observed that penetration is only maximum, when machine thrust is in the range of medium values. This result/conclusion is valid for both high and low RFC, RMC and petrography values. Fuzzy logic gives a reasonably good results for RMC prediction. RMC, RFC and ROP, were also predicted by using SPSS19 software packages, shows a very efficient and accurate result for RMC prediction model ( $R^2 = 0.773$ ). Penetration rate and RFC prediction model shows a medium to low accuracy in their predicted models respectively. Last part of analysis consists of correlation between machine and rock mass parameters. Here in Vereina tunnel data, we observed a very good linear correlation between TBM parameters and rock mass properties (thrust-RMC,  $R=0.831$ ). Correlation between between thrust and torque ( $R= 0.78$ ) is found. But there is no significant correlation between thrust and penetration ( $R=0.364$ ).

Hemerwald is another hydro-power project expansion tunnel excavated by Robbins series 120-TBM by Tiroler water power company [49]. Data was received as hard copy, that was converted into excel files for rock mass data and then segregated in different rocks data. Most of the tunnel strata consists of Granite Gneiss, Muscovite, Micaschists

and Schistos-Gneiss gneiss, tunnel was under a high overburden and 69% of the rock mass belong to RMC-I. Lowest values of thrust and excavation velocity is found at  $TM = 3640$ , where the maximum value of RMC is observed. Rock mass class (RMC) looks to be independent of degree of disintegration (DoD). Advance rate increases quadratically with thrust, having a peak of  $6 \text{ m/hr}$  at  $250 \text{ kg/cm}^2$ , and then decreases rapidly. RMC have a major role in machine performance (Figs. 4.52(a,b)), as obvious from the 3-D surface, up to a critical  $UCS=40 \text{ MPa}$ , advance rate increase and then sharply fall down even with high thrust applied. Fuzzy logic generated 3-D surface for rock mass data, also shows a maximum ROP at moderate thrust values and medium RMC. Frequency distribution of actual field data shows, thrust, RFC and ROP data is normally distributed and fulfill the condition for SSS19 prediction models. Linear regression model for advance rate shows a very accurate estimation model ( $R^2 = 0.928 \rightarrow R = 0.963$ ) and there was a significant correlation between machine parameters and rock mass properties e.g. thrust-AR correlation ( $R^2 = -0.745$ ). On the other hand, rock mass data was segregated into separate rock sections, Muskowite-Granite-Gneiss, Micaschists and Schistos-Gneiss. In Muskowit-Granite-Gneiss, there founds to be no correlation between machine parameters and rock properties. ROP decreases sharply with increase of thrust, showing adverse effect of rock behaviour against application of more thrust than required. In Mica-Schist rock, same behaviour of thrust and ROP is seen, but here a significant behaviour between thrust and DoD is observed. Moreover a good Fuzzy logic prediction model is obtained for RMC, that shows a credible results. Same analysis, when performed on Schistos-Gneiss, ROP is linearly increases with thrust. Reason behind this trend is clear, when we plot a 3-D surface between thrust, ROP and DoD, that shows in this section, ROP directly increases with thrust as DoD here have a moderate values throughout the section. At very high value of thrust, the low advance rate in Hemerwald tunnel, may be due to learning effect of TBM driver [48].

The three tunnels (Maen, Pieve and Varzo) are located in the northwestern Italian alps and consists of one inclined tunnel for the installation of a penstock (Maen) and two horizontal diversion tunnels (Pieve and Varzo). A total of  $14 \text{ km}$  of tunnel was surveyed almost continually, yielding over 700 sets of data featuring rock mass characteristics and TBM performance [37]. Performance prediction of TBM requires the estimation of both penetration rate (PR) and advance rate (AR). Analysis for Maen tunnel data shows that, there is drastic difference between trends and behaviour of penetration rate and advance rate, which ultimately shows high downtime, machine breakdown and maintenance time for the TBM, that shows very low utilization factor of TBM (Fig. 4.73). Moreover machine performance shows a strong dependence upon rock mass strength. RMC values were predicted by Fuzzy and SPSS both, shown a week prediction model by Fuzzy and an accurate and efficient prediction model by SPSS. Advance rate (AR) and penetration rate (PR) prediction models were also formulated with a reasonably good accuracy. Pieve

tunnel data shows inverse relation between penetration rate and thrust. SPSS-19 gives a very accurate PR linear regression model ( $R^2 = 0.55$ ). Pieve tunnel rocks consist of two metamorphic complexes made up of gneiss and micaschists separated by a metadiorite intrusive body with minor masses of metaquartzdiorite and metagabbro [37]. Both AR and PR have inverse linear correlation with thrust and PR decreasing with increase of USC and RMR. At medium UCS both AR and PR shows a turning point in machine performance (Figs. 4.92(a,b), showing that rock mass strength plays an important role in machine efficiency. Data from Pieve tunnel shows a good normal distribution and fulfill conditions for SPSS19 prediction modeling. RMC model predicted by Fuzzy logic shows a poor accuracy, while SPSS19 predict a good RMC model for Maen tunnel. AR and PR predicted model by SPSS-19 also shows a good empirical formulas. In Varzo tunnel data, AR and thrust have linear correlation, and RMR plays a major role in machine performance. SPSS-19 gives here a good prediction model for AR, PR and RMC. Moreover in all three tunnel sites, a significant positive correlation is found between machine parameters and rock mass properties. In general the penetration rate increases with decreasing rock mass quality until RMR values of about 50 – 70. The performance below that ranges reflect bad boreability in adverse rock mass due to mucking problem and face instability [50]. On the contrary, low PR recorded in very good rock masses  $RMR > 80 - 90$  depend upon high strength of intact rock. Correlation between thrust and advance rate highly depends upon the strength (UCS) of the rock. TBM performance reaches a maximum in the  $RMR 40 - 70 (UCS = 100MPa)$ , while slower penetration is experienced in both too good and too bad rock masses.

### 5.3 Conclusions

Geological conditions and rock mass characterizations in the field should be investigated before selecting the TBM, since the machine specification including thrust, cutter-head power and both diameter and number of disc cutters heavily influence the ROP. Hence geology and the best estimation of unknown rock mass properties, including orientation, condition and frequency of discontinuities together with rock strength and brittleness provide the major control on the penetrability of tunnel boring machine. These factors should be known before the start of excavation with a good accuracy. Due to high water pressures deep tunnels are normally drained tunnels, it is neither technically feasible nor economically reasonable to try to seal off entirely deep tunnels. So for TBM performance prediction, all rock mass properties like rock strength, RFC, RMC, water pressure and overburden must be the part of input parameters and predictors, for the calculation for machine advance rate. But unfortunately here in all available tunnels data analysis, no data was available regarding presence of water and effect of overburden. Moreover underground temperature increases rigorously with depth, so in deep tunnel temperature

and hydraulic pressure should be a part and parcel of the influential variables. In Hieflau, assuming rock strength to follow Gausion's distribution, UCS versus AR plot revealed that rock strength is major consequential parameter for TBM performance. Moreover this behavior is possibly due to the fact that machine operator tries to improve the low penetration rate in very hard rock by pushing the thrust near or above the recommended level, whereas he reduces the thrust when the penetration rate (ROP) is considered to be acceptable. In Hieflau tunnel, trends resembles with that of Hemerwald tunnel data.

Empirical relations between rock mass rating and penetration rate clearly show that TBM performance reaches a maximum in the rock mass rating (RMR) range 40–70 while slower penetration is experienced in both too bad and too good rock masses [37]. Different rocks give different penetrations for the same RMR, the use of Bieniawski classification for predictive purpose is only possible provided one uses a normalized RMR index with reference to the basic factors affecting TBM tunneling [2]. In Hemerwald tunnel AR has a quadratic correlation with thrust, above 24.56 MPa advance rate rapidly decreases. The simplest explanation for this divergent phenomenon is that at low thrust, the cutter action for the chip formation is different than at higher thrust. Perhaps this is the critical thrust above which more consistent chip formation occurs. Disc cutter performance depends upon the cutter head being totally engaged with the rock. Hence it revealed that, correlation between thrust and advance rate highly depends upon the strength, orientation and type of rock. Energy transferred and energy dissipation into the rock by the cutter head is a localized and time dependent phenomenon. Experience and skill of the TBM operator plays a major role in tunnel excavation efficiency. TBM performance predictive law has been also applied verifying a scarce gap between the predicted and actual values of the net advance rate, hence predicted models by SPSS-19, for RMC, RMR and AR are comparable to many empirical models available in literature.

# Bibliography

- [1] Spencer M. et al. , *"Tunnel Boring Machines"*, IMIA Conference Istanbul, 2009.
- [2] Khademi J. et al. , *"Performance prediction of hard rock TBM using RMR system"*, 2010.
- [3] Fred H. , *"The Underground Cutting Edge. The innovators who made digging tunnels high-tech"*, *Invention and Technology* vol. 20, no. 2, 2004.
- [4] Bernhard M. et al. , *"Hardrock Tunnel Boring Machines"*, Ernst and Sohn. , 2008.
- [5] Gary S. , *"Finding aid for the hoosac tunnel collection"*, North Adams Public Library, 2011.
- [6] Howes M. , *"Hoosac Tunnel History Abridged Time line"*, July 2011.
- [7] Herrenknecht AG, *www.herrenknecht.com*.
- [8] Robbins, *www.robbinstbm.com*.
- [9] Levent Z. , *"North American Tunneling 2006"*, Washington, DC: Taylor and Francis, pp. 246, 2006.
- [10] Karakus M. , Fowell R.J. , *Regional Rock Mechanics Symposium, Sivas, Turkiye, Invention and Technology* vol. 20, no. 2, 2004 VII.
- [11] Samuel A. E. , *"Disc force measurements on a full-face tunnelling machine"*, 1984.
- [12] Gehring K. , *"The influence of TBM design and machine features on performance and tool wear in rock"*, *Geomechanics and Tunnelling* vol. 2, no. 2, April 2009.
- [13] Gong Q. M. , *"In situ TBM penetration tests and rock mass boreability analysis in hard rock tunnels"*, *Tunnelling and Underground Space Technology* vol. 22, pp. 303-316, 2007.
- [14] Balci C. , *"Correlation of rock cutting tests with field performance of a TBM in a highly fractured rock formation: A case study in Kozyatagi Kadikoy metro tunnel"*, Turkey, 2009.

- [15] Ribacchi R. , *"Influence of Rock Mass Parameters on the Performance of a TBM in a Gneissic Formation"*, *Rock Mech. Rock Engng.* vol. 38, no. 2, pp. 105-127, 2005.
- [16] Cardu M. , *"Analysis of the Tunnel Boring Machine Advancement on the Bologna-Florence Railway Link"*, *American J. of Engineering and Applied Sciences* vol. 2, no. 2, pp. 416-420, 2009.
- [17] Poisel R. et al. , *"Rock Mass Rating based on Tunnel Boring Machine Data"*, *FELS-BAU* 17, no. 3, 1999.
- [18] Berti M. , *"TBM performance estimation using rock mass classifications"*, *International Journal of Rock Mechanics and Mining Sciences* vol. 39, pp. 771-788, 2002.
- [19] Yagiz S. , *"Utilizing rock mass properties for predicting TBM performance in hard rock condition"*, *Tunnelling and Underground Space Technology*, no. 23, pp. 326-339, 2008.
- [20] KaleidaGraph, [www.msg.ucsf.edu](http://www.msg.ucsf.edu).
- [21] MatLab, *"GettingStartedwithMATLAB.html"*, 2008.
- [22] R, *"A Programming Environment for Data Analysis and Graphics Version 2.13.2"*, 2011.
- [23] R-Software, [www.r.project.org](http://www.r.project.org).
- [24] IBM, [www.unileon.es/english.spss.IBMSPSS](http://www.unileon.es/english.spss.IBMSPSS).
- [25] Indiana State University, [www.indstate.edu.cirt.spss.spss13.correlation.pdf](http://www.indstate.edu.cirt.spss.spss13.correlation.pdf).
- [26] Walter A. et al. , *"Extension Hieflau HEP Economical Solutions for the Headrace Tunnel"*, *Geomechanics and Tunnelling*, vol. 1, no. 6, pp. 534-607, December 2008.
- [27] Jaegerbau Strabag, [www.jaegerbau.com](http://www.jaegerbau.com).
- [28] Bitschnau M. et al. , *"Hieflau power station extension mechanical tunnelling with innovative solutions"*, *Geomechanics and Tunnelling* vol. 2, no. 1, pp. 85-93, February 2009.
- [29] Verbund Austrian Hydro Power AG, [www.jaegerbau.com](http://www.jaegerbau.com).
- [30] Water Technology, [www.water-technology.net](http://www.water-technology.net).
- [31] Merguerian C. , *"Tunnel Vision Subterranean Paradise or Name That Quake"*, *Hofstra University Distinguished Faculty Lecture Series*, 2000.
- [32] DEP, [www.nyc.gov](http://www.nyc.gov).

- [33] Brian B. et al. , "*High performance tunnel boring machine for Queen water tunnel no. 3*", *Atlas Copco Robbins Inc. and Grow Tunneling Corp.* , 1997.
- [34] Berti M. , "*TBM performance estimation using rock mass classifications*", *International journal of Rock mechanics*, vol. 39 pp. 771- 788, 2002.
- [35] Leica Geosystems, *www.rhb.ch.index*.
- [36] Amberg F. , "*Tunnelling in High Overburden with Reference to Deep Tunnels in Switzerland*", *Tunneling and underground space technology*, vol. 19, no. 45, 2004.
- [37] Sapigni M. et al. , "*TBM performance estimation using rock mass classifications*", *International Journal of Rock Mechanics and Mining Sciences* vol. 39, pp. 771-788, 2002.
- [38] Chwatal W. et al. , "*Exploration Ahead of a Tunnel Face by TSWD, Tunnel Seismic While Drilling*", *Geomechanics and Tunneling*, vol. 1, no. 5, 2008.
- [39] Rummel, R. J. , "*Understanding Correlations*", *Honolulu: Department of Political Science University of Hawaii*, 1976.
- [40] Wikipedia, *wikipedia.org.wiki.Petrography*.
- [41] Ans.com, *www.answers.com.topic.petrography*.
- [42] Piazz DGV. , "*Revised setting of the piedmont zone in the northern Aosta valley, Western Alps*", *Ophioliti*, no. 13, pp. 157-62, 1988.
- [43] Reinecke T. , "*Very high pressure metamorphism and uplift of coesite bearing metasediments from the Zermatt Saas zone, Western Alps*", *Eur J Mineral*, vol. 3, pp. 7-17, 1991.
- [44] Reinhardt B. , "*Geologie und Petrographie der Monte Rosa Zone, der Sesia Zone und des Canavese im Gebiet zwischen Valle Ossola und Valle Loana (Prov. Di Novara, Italien)*", 1996.
- [45] Compagnoni R. et al. , "*The Sesia Lanzo Zone, a slice of continental crust with alpine high pressure low temperature assemblages in the Western Italian Alps.*", *Rend Soc Ital Mineral Petrol*, vol. 33, pp. 281-334, 1977.
- [46] Milnes AG. , "*Structural reinterpretation of the classic Simplon Tunnel Section of the Central Alps*", *Journal of the Geological Society*, vol. 142, no. 1, pp. 129-136, February 1, 1985.
- [47] Mancktelow N. , "*The Simplon line: a major displacement zone in the western Lepontine Alps*", *Eclogae Geol Helv*, no. 78, pp. 73-96, 1985.



- [48] Wais, A. , Wachter, R. , *"Predicting the learning Curve in TBM Tunnelling"*, Institut für Baubetrieb, Bauwirtschaft und Baumanagement Universität Innsbruck, 2005.
- [49] Tirolerwasserkraft, *www.tirolerwasserkraft.at*.
- [50] Yagis S. et al. , *"Geological controls on the breakthrough of TBM in hard rock crystalline terrains"*, *Rock Mechanics in Civil and Environmental Engineering* Zhao, Labiouse, Dudt and Mathier Taylor and Francis Group, London, 2010.

# List of Abbreviations and Notations

ABM: Auger boring machine

Ampl<sub>erste</sub>: Amplitude of ersteinsatz (amplitude of first arrival) of seismic wave

Ampl<sub>reflex</sub>: Amplitude of reflexion of seismic wave

AR: Advance rate

BRMR: Bieniawski rock mass rating

BTS: Brazilian tensile strength

DEP: Department of environmental protection

DoD: Degree of disintegration

DPW: Distance between plane of weakness

EPBM: Earth pressure balance machine

HPP: Hydro power plant

MPa: Megapascal

NATM: The new Austrian tunneling methods

Pseu<sub>vel</sub>: Pseudo velocity

QWT: Queens water tunnel

RFC: Rock fracture class

RMC: Rock mass classification

RMR: Rock mass rating

ROP: Rate of penetration

PR: Penetration rate

TBM: Tunnel boring machine

TM: tunnel meters

TSWD: Tunnel seismic while drilling

UCS: Uniaxial compressive strength

$\alpha$  : Angle between tunnel axis and plane of weakness

# List of Figures

- 1.1 First tunnelling shield [1]. . . . . 2
- 1.2 Gripper machine [7]. . . . . 4
- 1.3 Single shield machine [7]. . . . . 4
- 1.4 Double shield TBM [7]. . . . . 5
- 1.5 Mix-shield TBM [7]. . . . . 6
- 1.6 Slurry machine [7]. . . . . 7
- 1.7 Earth pressure balance machine [7]. . . . . 8
- 1.8 Auger boring machine [8]. . . . . 9
- 1.9 Thrust versus penetration [12]. . . . . 12
- 1.10 Thrust versus penetration [13]. . . . . 13
- 1.11 Relationship between thrust and penetration [14]. . . . . 13
- 1.12 Thrust versus advance rate [15]. . . . . 14
- 1.13 Applied thrust versus net advance rate [16]. . . . . 15
- 1.14 Rock mass class predicted by Fuzzy logic [17]. . . . . 16
- 1.15 RMR versus rock mass quality [18]. . . . . 17
- 1.16 ROP versus PSI and UCS [19]. . . . . 17
  
- 2.1 Kaleida GUI and scattered plot. . . . . 19
- 2.2 Fuzzy logic tools [21]. . . . . 20
- 2.3 Fuzzy logic tools. . . . . 21
- 2.4 Fuzzy rule base. . . . . 21
- 2.5 Fuzzy 3-D surface. . . . . 22
- 2.6 Linear regression method description. . . . . 25
- 2.7 SPSS model coefficients. . . . . 25
- 2.8 Automatic linear modeling. . . . . 26
- 2.9 Model summary. . . . . 26
- 2.10 Effects of input parameters. . . . . 27
- 2.11 Table of coefficients. . . . . 27
- 2.12 Scattered plot between actual and SPSS predicted value. . . . . 27
- 2.13 SPSS predicted AR line plot. . . . . 28
- 2.14 Spearman’s and Kendall’s correlation coefficients. . . . . 29

3.1	Hieflau expansion tunnel layout [26]. . . . .	30
3.2	Geology of Hieflau headrace tunnel [26]. . . . .	32
3.3	The Hieflau hydro power project, TBM and lining segments. . . . .	32
3.4	Queen water tunnel [32]. . . . .	35
3.5	TBM for Queens water tunnel [31], [33]. . . . .	36
3.6	Vereina tunnel east portal [35]. . . . .	38
3.7	Vereina tunnel X-section [36]. . . . .	38
3.8	Geological longitudinal X-section of Vereina tunnel [36]. . . . .	39
3.9	Hemerwald tunnel TBM [courtesy, Ewald Tentschert]. . . . .	40
3.10	Geological profile and X-section of Hemerwald tunnel [?]. . . . .	41
3.11	Original data file. . . . .	42
3.12	Tunnel log map. . . . .	43
3.13	Maen-Pieve-Varzo layout [37]. . . . .	45
4.1	Seismic data recording procedure [38]. . . . .	47
4.2	Chainage versus thrust, torque and AR. . . . .	48
4.3	2-D graphs for TM, thrust, AR and torque. . . . .	49
4.4	Thrust versus amplitude of ersteinsatz and reflexion. . . . .	50
4.5	3-D surfaces. . . . .	50
4.6	3-D surfaces. . . . .	51
4.7	3-D surfaces. . . . .	52
4.8	Thrust versus tool wear. . . . .	53
4.9	Chainage versus tool wear. . . . .	54
4.10	Tool wear. . . . .	54
4.11	Histograms of TBM data 1. . . . .	55
4.12	Histograms of TBM data 2. . . . .	56
4.13	Histograms of seismic data 1. . . . .	56
4.14	Histogram of seismic data 2. . . . .	57
4.15	AR regression models. . . . .	61
4.16	AR model comparison. . . . .	61
4.17	Thrust and UCS versus AR. . . . .	66
4.18	2-D plots. . . . .	67
4.19	2-D plots. . . . .	68
4.20	3-D surfaces. . . . .	69
4.21	3-D surfaces. . . . .	69
4.22	3-D surfaces. . . . .	70
4.23	3-D surfaces. . . . .	70
4.24	Histograms for UCS and BTS. . . . .	71
4.25	Histograms thrust and ROP. . . . .	71

4.26	Histograms for alpha angle and DPW. . . . .	72
4.27	Predicted ROP model scattered plot. . . . .	75
4.28	AR model comparison. . . . .	75
4.29	Predicted RFC model. . . . .	77
4.30	Comparison of RFC. . . . .	77
4.31	TM versus ROP, RMC, RFC and torque. . . . .	80
4.32	Thrust versus PR and torque. . . . .	80
4.33	Penetration versus RMC, RFC, torque and petrography. . . . .	81
4.34	Thrust versus RMC and RFC. . . . .	82
4.35	Fuzzy rule-base for Vereina tunnel data. . . . .	83
4.36	Fuzzy 3-D surface. . . . .	85
4.37	Comparison of actual and Fuzzy RMC. . . . .	85
4.38	Thrust versus penetration, RMC, torque 9000-10000 TM. . . . .	86
4.39	3-D surface by Fuzzy logic. . . . .	87
4.40	Comparison of RMC. . . . .	87
4.41	Thrust versus ROP at low and high torque. . . . .	88
4.42	Thrust versus ROP at high and low RMC. . . . .	89
4.43	Histograms for thrust and torque. . . . .	90
4.44	Histograms for ROP and RMC. . . . .	90
4.45	Prediction model plot. . . . .	93
4.46	RMC and RFC models scattered plots. . . . .	96
4.47	Comparison of RMC. . . . .	96
4.48	Comparison between actual and predicted RFC. . . . .	97
4.49	Original data sample pdf. file. . . . .	99
4.50	TM versus thrust, RMC, excavation velocity, disintegration. . . . .	100
4.51	Thrust versus AR power, velocity and RMC (Rock mass). . . . .	101
4.52	3-D surfaces for thrust, AR, power and RMC (Rock mass). . . . .	102
4.53	3-D surfaces thrust versus AR (Rock mass). . . . .	103
4.54	3-D surfaces thrust versus AR (Rock mass). . . . .	103
4.55	3-D surface by Fuzzy logic. . . . .	104
4.56	Fuzzy versus actual RMC. . . . .	105
4.57	Histograms for thrust, power and excavation velocity. . . . .	106
4.58	Histograms for AR, RMC and RFC. . . . .	106
4.59	Actual and SPSS AR comparison. . . . .	108
4.60	Thrust versus AR. . . . .	111
4.61	Thrust versus AR. . . . .	111
4.62	3-D surfaces for Muscovite-Granite-Gneiss. . . . .	112
4.63	Histograms for thrust, DoD, AR and RMC. . . . .	113
4.64	AR model for Muscovite-Granite-Gneiss. . . . .	114

4.65	TM and thrust versus AR and DoD. . . . .	117
4.66	Comparison of RMC for Micaschists. . . . .	119
4.67	3-D surfaces for Micaschists. . . . .	120
4.68	Thrust versus AR and DoD. . . . .	121
4.69	Fuzzy versus actual RMC. . . . .	122
4.70	Schistose-Gneiss 3-D surface plots. . . . .	123
4.71	2-D plots with Excel. . . . .	124
4.72	3-D surface plots. . . . .	125
4.73	Thrust versus AR and PR. . . . .	127
4.74	Thrust versus RMR. . . . .	128
4.75	AR versus thrust and RMR. . . . .	128
4.76	UCS and Q-value versus AR. . . . .	129
4.77	AR versus thrust and RMR. . . . .	129
4.78	Fuzzy versus actual RMC plot. . . . .	130
4.79	Fuzzy versus SPSS RMC. . . . .	131
4.80	Thrust versus AR at low and high RMR. . . . .	131
4.81	RMR versus AR at low and high thrust. . . . .	132
4.82	Thrust versus AR at the rate of UCS. . . . .	132
4.83	Histograms for Maen tunnel 1. . . . .	133
4.84	Histograms for Maen tunnel 2. . . . .	134
4.85	AR linear regression model. . . . .	137
4.86	PR regression model . . . . .	139
4.87	RMC linear regression model. . . . .	141
4.88	Thrust versus RMR, RMC, AR and PR. . . . .	144
4.89	AR and PR versus RMC and RMR. . . . .	145
4.90	Actual versus Fuzzy RMC comparison. . . . .	146
4.91	Actual versus Fuzzy and SPSS RMC. . . . .	147
4.92	USC versus AR at low and high thrust. . . . .	147
4.93	Thrust versus AR. . . . .	148
4.94	Histograms for Pieve tunnel. . . . .	149
4.95	Histograms for Pieve tunnel. . . . .	149
4.96	Linear regression model plot for AR and PR. . . . .	150
4.97	Varzo tunnel 2-D plots. . . . .	153
4.98	Varzo tunnel 2-D plots. . . . .	154
4.99	Fuzzy versus actual RMC. . . . .	155
4.100	Comparison of RMC for Varzo tunnel. . . . .	156
4.101	3-D surfaces penetration rate. . . . .	157
4.102	3-D surfaces for Varzo tunnel. . . . .	157
4.103	3-D surfaces AR. . . . .	158

4.1043-D Surfaces generated by R software. . . . .	158
4.105Histograms for Varzo tunnel. . . . .	159
4.106Histogram Varzo tunnel. . . . .	159
4.107AR linear regression model plot for Varzo tunnel. . . . .	161
4.108RMC linear regression model Varzo tunnel. . . . .	162



# List of Tables

2.1	Bi-variant correlation. . . . .	28
3.1	Technical data of the Hieflau TBM. . . . .	31
3.2	Hieflau TBM data logger [27]. . . . .	33
3.3	Specification of TBM for Queens water tunnel [34]. . . . .	36
3.4	Vereina TBM technical data. . . . .	39
3.5	Technical data of Hemerwald tunnel TBM. . . . .	40
3.6	Description of three tunnels and TBM technical data. . . . .	44
4.1	Rock mass plus machine and seismic data versus AR. . . . .	55
4.2	Model summaries. . . . .	58
4.3	Model effects. . . . .	59
4.4	Model effects. . . . .	60
4.5	Partial correlation coefficients. . . . .	62
4.6	Bi-variant correlation coefficients. . . . .	63
4.7	Bi-variant correlation coefficients. . . . .	64
4.8	Table of rock properties versus ROP. . . . .	73
4.9	AR model summary. . . . .	73
4.10	Effects and parameters of AR model. . . . .	74
4.11	RFC model summary and effects. . . . .	76
4.12	RFC model coefficients. . . . .	76
4.13	Bi-variant correlation. . . . .	78
4.14	Model summary and coefficients. . . . .	91
4.15	PR model effects. . . . .	91
4.16	Table of PR model coefficients and linear equations. . . . .	92
4.17	Model summary. . . . .	93
4.18	Model effects. . . . .	94
4.19	Model coefficients. . . . .	95
4.20	Pearson correlation coefficient table. . . . .	98
4.21	AR model summary, effects and coefficients. . . . .	107
4.22	Correlation coefficients for rock mass. . . . .	109
4.23	Spearman and Kendall correlation coefficients. . . . .	110

4.24	Predictor effects for AR model. . . . .	113
4.25	Coefficients matrix for AR model. . . . .	114
4.26	Pearson correlation coefficients for Muscovite-Granite-Gneiss. . . . .	115
4.27	Spearman's correlation coefficients Muscovite-Granite-Gneiss. . . . .	115
4.28	Pearson correlation for Micaschists. . . . .	118
4.29	Spearman's correlation coefficients for Micaschists. . . . .	118
4.30	Fuzzy rule base for Maen tunnel. . . . .	130
4.31	AR model summary. . . . .	135
4.32	AR model effects. . . . .	135
4.33	AR model coefficients. . . . .	136
4.34	Model summary for PR. . . . .	137
4.35	Predictors effects for PR model. . . . .	138
4.36	Predictors coefficients for PR model. . . . .	138
4.37	Model summary for RMC. . . . .	140
4.38	RMC model effects. . . . .	140
4.39	RMC model coefficients. . . . .	141
4.40	Pearson correlation coefficients for Maen tunnel. . . . .	142
4.41	Spearman correlation coefficients for Maen tunnel. . . . .	143
4.42	AR linear regression model summary for Pieve tunnel. . . . .	149
4.43	PR linear regression model summary for Pieve tunnel. . . . .	150
4.44	Pearson correlation for Pieve tunnel. . . . .	151
4.45	Spearman correlation table for Pieve tunnel. . . . .	152
4.46	Model summary. . . . .	160
4.47	Varzo AR and PR linear model coefficients. . . . .	160
4.48	RMC model coefficients. . . . .	161
4.49	Pearson correlation for Varzo tunnel. . . . .	162
4.50	Spearman's correlations for Varzo tunnel. . . . .	163

# List of Algorithms

- 2.1 Algorithm for R software. . . . . 23
- 4.1 I/O subroutine for Vereina. . . . . 84

# Curriculum Vitae

## Personal Informations:

Name: Ghulam Dastgir  
Date of Birth: 22-04-1976  
Sex: Male  
Nationality: Pakistan

## Academic Profile:

Successfully completed 18-years of education with excellent grades (A+) throughout;

1992: Matriculation (SSC) from Govt. Jamia Saddiquia High School Chak No. 316/G.B, Toba Tek Sing, Pakistan.

1993-1994: FSc. (Pre-Engg., HSSC) From Govt. M.D College Toba Tek Singh, Pakistan.

1995-1999: Bsc. Mining Engineering from University of Engineering & Technology (UET), Lahore, Pakistan.  
Bachelor Thesis: Description and Implementation of Mine Safety Instruments.

2001-2003: M.S (N.E) from Pakistan Institute of Engineering & Applied Sciences (PIEAS), Islamabad, Pakistan.  
Master Thesis: Optimization of Froth Flotation Column.

2008-Present PhD Student at the Institute of Geotechnical, Department of Engineering Geology, Technical University Vienna (TU WIEN), Austria.  
PhD. Thesis: Prediction of Tunnel Boring Machine Performance Using Machine and Rock Mass Data.

## Professional Experience:

2003- Present: Senior Engineer (S.E) in a public sector organization involved in geotechnical analysis and Tunneling.